Proceedings of the

15th Working Meeting on European VLBI for Geodesy and Astrometry

September 7-8, 2001

Barcelona, Spain

Edited by

Dirk Behrend and Antonio Rius

IEEC

Institut d'Estudis Espacials de Catalunya

Consejo Superior de Investigaciones Científicas

Preface

This volume is the proceedings of the **15th Working Working on European VLBI for Geodesy and Astrometry** which was organized by the Institut d'Estudis Espacials de Catalunya (IEEC) and took place in Barcelona, Spain, in September 2001. In addition to the main event, several side and splinter meetings were held: (1) final meeting of the EU-TMR project "Measurement of Vertical Crustal Motion in Europe by VLBI"; (2) IVS (International VLBI Service for Geodesy and Astrometry) Working Group 2 meeting; (3) "6th IVS Directing Board Meeting". Taking all these meetings together, the VLBI specialists spent some four days (September 6-9) under perfect weather conditions in late summer Barcelona.

Photo: The participants of the 15th European VLBI Meeting in front of the premises of the Delegation of the Spanish Research Council in Barcelona.

About 40 scientists from three different continents (Europe, North America and Asia) came together in Barcelona. The topics covered go from reports of the different facilities and IVS components, over data analysis and new delopments to reference frames and astrometric results. Other points of special interest were the local surveys performed at several observatories and the modelling of the tropospheric parameters. The meeting culminated in an interesting and, at times, controversial discussion which marked the end of a very successful event. We hope that these proceedings reflect the enthusiasm and pleasure in doing VLBI that were noticeable during the meeting.

Electronic version. The content of this volume also appears on the web site of the IEEC at:

`http://www.ieec.fcr.es/hosted/15wmevga/proceedings/toc.html`

The online version also provides ps and pdf files for easy (colour) printing.

Citation. These proceedings were published by the Institut d'Estudis Espacials de Catalunya (IEEC), Barcelona, Spain, in December 2001.

The papers of this publication should be cited as:

> {*name of author(s)*}*:* {*title*}*.* In: D. Behrend and A. Rius (Eds.): Proceedings of the 15th Working Meeting on European VLBI for Geodesy and Astrometry, Institut d'Estudis Espacials de Catalunya, Consejo Superior de Investigaciones Científicas, Barcelona, Spain, 2001.

Acknowledgements

The editors would like to thank the IVS Coordinating Center (with special thanks to Nancy Vandenberg and Karen Baver) for providing the necessary scripts and templates in order to be able to create this volume. Without this help the proceedings would not have been finished so fast and definitely not in this form.

Thanks also to all the authors for preparing and submitting their papers in such a short time facilitating a rapid publication of the excellent results of the different groups.

Thanks to the staff of the Residència d'Investigadors of the Consejo Superior de Investigaciones Científicas (CSIC) for their great help and support during the meeting.

The working meeting has been organized under the auspices of the Training and Mobility (TMR) network project FMRX-CT96-0071 "Measurement of Vertical Crustal Motion in Europe by VLBI" of the European Union. The financial support is gratefully acknowledged.

Dirk Behrend and Antonio Rius
Editors, 15th European VLBI Meeting Proceedings
Barcelona, in December 2001

Table of Contents

Preface ..... **iii**

Acknowledgements ..... **v**

Session 1: IVS and Facility Reports **1**

Harald Schuh: IVS Working Group 2 for Product Specification and Observing Programs — Status Report of the Chairman **3**

Volkmar Thorandt, Dieter Ullrich, Reiner Wojdziak: Technological Processes at BKG Data and Analysis Center **4**

Gerald Engelhardt, Volkmar Thorandt, Dieter Ullrich: The Current Status of the IVS Analysis Center at BKG **8**

Cristina García Miró, Jose F. Gómez, Dirk Behrend, Antonio Rius, Antxon Alberdi, Elena Jiménez Bailón, Itziar de Gregorio Monsalo: MDSCC Radio Astronomy Report **14**

Richard W. Porcas: Effelsberg Station Report - September 2001 ..... **22**

Francisco Colomer: The New 40 Meter Radiotelescope of OAN at Yebes **23**

Hayo Hase: Status of the TIGO-Project in Concepción **24**

Giuseppe Colucci, Pippo Bianco, Domenico Del Rosso, Luciano Garramone, Eustachio Lunalbi: Matera CGS VLBI Station **28**

Alessandro Orfei, Franco Mantovani, Gino Tuccari, Giancarlo Stanghellini: Medicina and Noto Stations Report **32**

Rüdiger Haas, Sten Bergstrand, Gunnar Elgered, Lubomir Gradinarsky, Boris Stoew, Harald Bouma, Martin Lidberg: Geodetic Very Long Baseline Interferometry at the Onsala Space Observatory 2000–2001: Observations **36**

Robert M. Campbell: The EVN MkIV Data Processor at JIVE **40**

Walter Alef and Arno Müskens: Status of the MPIfR-BKG MK IV correlator **46**

Arno Müskens: Improvements of the Geodesy MK IV Correlation during the Last Year **50**

Zinovy Malkin: On Computation of Combined IVS EOP Series **55**

Session 2: Data Analysis and New Developments **63**

J. Campbell and B. Richter: Towards a stable European vertical velocity reference system using VLBI, GPS and absolute gravity measurements **65**

W. Schwegmann: Automatic VLBI Data Analysis using Calc/Solve and a Knowledge-Based System **75**

Volker Tesmer, Hansjörg Kutterer, Burghard Richter, Harald Schuh: Reassessment of Highly Resolved EOP Determined with VLBI **83**

Yasuhiro Koyama, Tetsuro Kondo, Junichi Nakajima, Mamoru Sekido, Moritaka Kimura: Internet VLBI system and 1 Gbps VLBI System Based on the VSI **91**

Erwan Gueguen, Paolo Tomasi, Hans-Georg Scherneck, Rüdiger Haas, James Campbell: Recent Crustal Movements: Geological Meaning of European Geodetic VLBI Network Observations **99**

Machiel Simon Bos and Rüdiger Haas: Observing Long-period Tides in Gravity and VLBI Observations at Ny-Ålesund (Svalbard) – A Progress Report **108**

Zinovy Malkin, Natalia Panafidina, Elena Skurikhina: Length Variations of European Baselines Derived from VLBI and GPS Observations **116**

Elena Skurikhina: On Computation of Antenna Thermal Deformation in VLBI Data Processing **124**

Session 3: Atmospheric Modelling **131**

Arthur E. Niell: An a priori Hydrostatic Gradient Model for Atmospheric Delay **133**

Axel Nothnagel: On the Effects of Solution Types on Clock and Atmosphere Parameters **137**

Johannes Böhm and Harald Schuh: Spherical Harmonics as a Supplement to Global Tropospheric Mapping Functions and Horizontal Gradients **143**

María J. Rioja, Paolo Tomasi: External tropospheric calibration for VLBI observations **149**

Alexander A. Stotskii and Irina M. Stotskaya: Structure Analysis of Wet Path Delays in IRIS-S Experiments **154**

Session 4: Local Surveys **159**

Luca Vittuari, Pierguido Sarti, Paolo Tomasi: 2001 GPS and Classical Survey at Medicina Observatory: Local Tie and VLBI Antenna's Reference Point Determination **161**

Axel Nothnagel, Christoph Steinforth, Bernd Binnenbruck, Lars Bockmann, Leif Grimstveit: Results of the 2000 Ny-Ålesund Local Survey **168**

Rüdiger Haas and Michael Kirchner: Local survey activities at the Onsala Space Observatory 1999–2001 .... **177**

Session 5: Reference Frames and Astrometric Results **185**

Chopo Ma: Extension of the ICRF **187**

Patrick Charlot, Robert Campbell, Walter Alef, Kazimierz Borkowski, John Conway, Anthony Foley, Simon Garrington, Alexander Kraus, Axel Nothnagel, Ojars Sovers, Corrado Trigilio, Tiziana Venturi, Huang Xinyong: ITRF2000 Positions of Non-geodetic Telescopes in the European VLBI Network **194**

Richard W. Porcas: Finding astrometric reference sources using the NVSS Survey **201**

Eduardo Ros and Andrei P. Lobanov: Opacity in the Jet of 3C 309.1 .... **208**

Splinter Meeting: IVS Working Group 2 217

Harald Schuh, Patrick Charlot, Hayo Hase, Ed Himwich, Kerry Kingham, Calvin Klatt, Chopo Ma, Zinovy Malkin, Arthur Niell, Axel Nothnagel, Wolfgang Schlüter, Kazuhiro Takashima, Nancy Vandenberg: IVS Working Group 2 for Product Specification and Observing Programs — Final Report (1st of November 2001) **219**

Annex **249**

Participants **251**

Programme **252**

Session 1

IVS and Facility Reports

Harald Schuh: IVS Working Group 2 for Product Specification and Observing Programs — Status Report of the Chairman, Proceedings of the 15th Working Meeting on European VLBI for Geodesy and Astrometry, p.3–3
http://www.ieec.fcr.es/hosted/15wmevga/proceedings/schuh

IVS Working Group 2 for Product Specification and Observing Programs — Status Report of the Chairman

Harald Schuh

Institute of Geodesy and Geophysics, TU Vienna
e-mail: `hschuh@luna.tuwien.ac.at`

Abstract

An important part of the IVS efforts is to provide the best products for the user community and to optimize the use of available global resources. During the 5th IVS Directing Board meeting on Feb 15th, 2001 the IVS products and related programs were discussed. It was decided to set up an IVS Working Group (WG2) for Product Specification and Observing Programs. Members of WG2 were chosen from among experts in the field of geodetic/astrometric VLBI. The charter to WG2 is:

- Review the usefulness and appropriateness of the current definition of IVS products and suggest modifications.
- Recommend guidelines for accuracy, timeliness, and redundancy of products.
- Review the quality and appropriateness of existing observing programs with respect to the desired products.
- Suggest a realistic set of observing programs which should result in achieving the desired products, taking into account existing agency programs.
- Set goals for improvements in IVS products and suggest how these may possibly be achieved in the future.
- Present a written report to the IVS Directing Board at its next meeting.

An overview about the activities of Working Group 2 and the results achieved so far will be given.

Please find the final report of the IVS Working Group 2 for "Product Specification and Observing Programs" in the splinter meeting section of this volume.

Volkmar Thorandt et al.: Technological Processes at BKG Data and Analysis Center, Proceedings of the 15th Working Meeting on European VLBI for Geodesy and Astrometry, p.4–7
http://www.ieec.fcr.es/hosted/15wmevga/proceedings/thorandt

Technological Processes at BKG Data and Analysis Center

Volkmar Thorandt, Dieter Ullrich, Reiner Wojdziak

Bundesamt für Kartographie und Geodäsie (BKG)
Contact author: Volkmar Thorandt, e-mail: vt@leipzig.ifag.de

Abstract

The VLBI group at Federal Agency for Cartography and Geodesy (BKG) established an integrated technological process to manage data flow and analysis tasks at IVS Data and Analysis Center in an automatic manner.

1. Introduction

The BKG VLBI group is one of three primary IVS Data Centers and together with the VLBI group at the Bonn University an IVS Analysis Center. To guarantee a high level of Data Center reliability and high quality of analysis products it is essential to integrate data flow and analysis activities in a homogeneous technological process (see figure 1). The established technological process is subdivided in four sub processes (mi_and_in, pre_solve, int_solve, post_solve) which are working together and a monitoring process (monitor).

2. The sub-processes

(a) Program mi_and_in is running in automatic mode eight times per day and is responsible for the following tasks:

- Mirror CDDIS and OPAR (Observatoire de Paris) IVS Data Centers. For this purpose a PERL script is running.
- Watch the incoming area of BKG IVS Data Center and verify the syntax of appearing files against the IVS syntax rules as described in IVS documents. This task is managed by an incoming script, maintained by GSFC. The incoming area is available for selected users and it is password protected.
- Watch BKG IVS Data Center for new databases, copied by mirror, incoming script or dserver (another data transfer program, similar to the incoming script). Program mi_and_in delivers new databases into the Interface Area which is established between IVS Data Center and Operational Data Center (ODC).
- Get miscellaneous analysis files (aprioris etc.) from GSFC.
- Set up input information for the next step (pre_solve). For this purpose mi_and_in interprets the status information for the databases in the Interface Area. This information consists of "availability" and "special cases" status which is collected by monitor (see below) permanently. The result is a database input information for the next technological step pre_solve. Program mi_and_in hands over control to pre_solve.
- Send mail with protocol information to selected users.

(b) Program pre_solve is running automatically and is started by mi_and_in. It is responsible for the following tasks:

- Inspect the Interface Area whether there are any new databases delivered by mi_and_in.

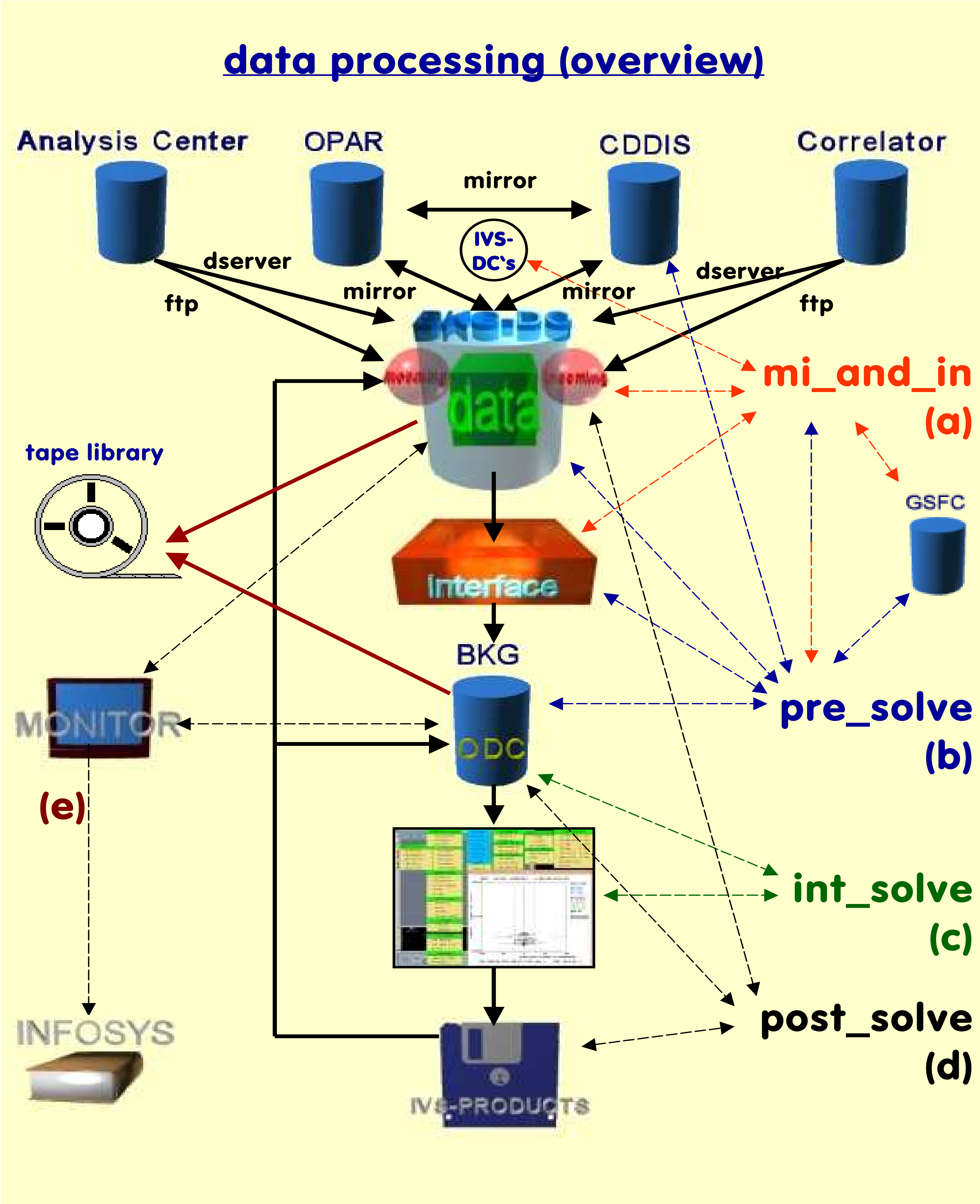

Figure 1. Data processing - overview

- Get databases from GSFC if necessary. If mi_and_in made available higher database versions then pre_solve tries to get version 1 databases from GSFC because the BKG Analysis Center prefers to analyse databases beginning with version 1.
- Import masterfiles from IVS and make one overall masterfile.
- Send and import databases to proper catalog areas after accepting them.
- Import logfiles, schedule and reports for the available databases from CDDIS and/or IVS.
- Import RINEX meteorological files from CDDIS for selected stations if there are no meteorological data in the logfiles. Merge logfiles with RINEX data.
- Establish the weather and cable calibration files.
- Run CALC/SOLVE programs apriori, calc and dbcal (Ref. [1]).
- Send mail with protocol information to selected users.

(c) Program int_solve is the interactive part of the analysis process. It covers the elimination of ambiguities and outliers, ionosphere calibration and weighting of data. For this purpose the well known CALC/SOLVE package is used.

(d) Program post_solve runs after int_solve in an automatic mode. It is responsible for the following tasks:

- Make superfiles of the latest databases.
- Make NGS files if BKG is the submitting IVS Analysis Center.
- Submit databases, NGS files, logfiles, schedules, weather and cable calibration files to IVS (if BKG is responsible).
- Update superfile catalog and BATCH control files with new databases.
- BATCH run in eops-, eopr- or eopi-mode. Merge solutions with previous solutions in IVS-EOP format. The files bkg00001.eops and bkg0002.eops are two EOP time series made of 24h VLBI experiments since 1984 with two different parameter sets. The file bkgint01.eops is a UT1-UTC time series made of Intensive experiments since 1999. These three files are available at IVS web sites, i.e. at ftp://ftp.leipzig.ifag.de/pub/vlbi/ivsproducts.
- Send new EOP solutions to IVS and into the ODC (see figure 1).
- Send mail with protocol information to selected users.

(e) Program monitor is watching permanently the IVS Data Center and the Operational Data Center (see figure 1). It establishes a text file which serves as source of information about the status of databases for all parts of technological process as described above. It includes in it‘s attention the ODC (database catalog, superfile catalog, analysis spoolfiles and, if necessary, manual input) and the IVS Data Center (databases and masterfiles). Additionally the text file is suitable to be imported into a database management system like INFORMIX or MS-ACCESS. The analyst can query and filter the system and benefits by faster information like data availability in IVS Data Center and Operational Data Center, analysis status, analysis quality, special problems with databases and superfiles. Program monitor also cleans the database catalog (purge, delete S-Band keys after analysis, move databases to proper catalog areas) and superfile catalog automatically.

3. Technical environment

For VLBI purposes an HP9000/D280 computer with 190 GByte Raid disc space is available. For automatic safety copies a tape library TLZ894 is in use. The Internet rate is 2 Mbit/sec. To increase the data security a new network configuration is under construction (see figure 2). In the future the IVS server will reside behind a fire wall in the so called Secure Server Network, but publicly accessible. The Operational Data Center will be established in the Local Area Network. It will not be possible to access it from the Wide Area Network. That means, all public activities will happen only in the Secure Server Network.

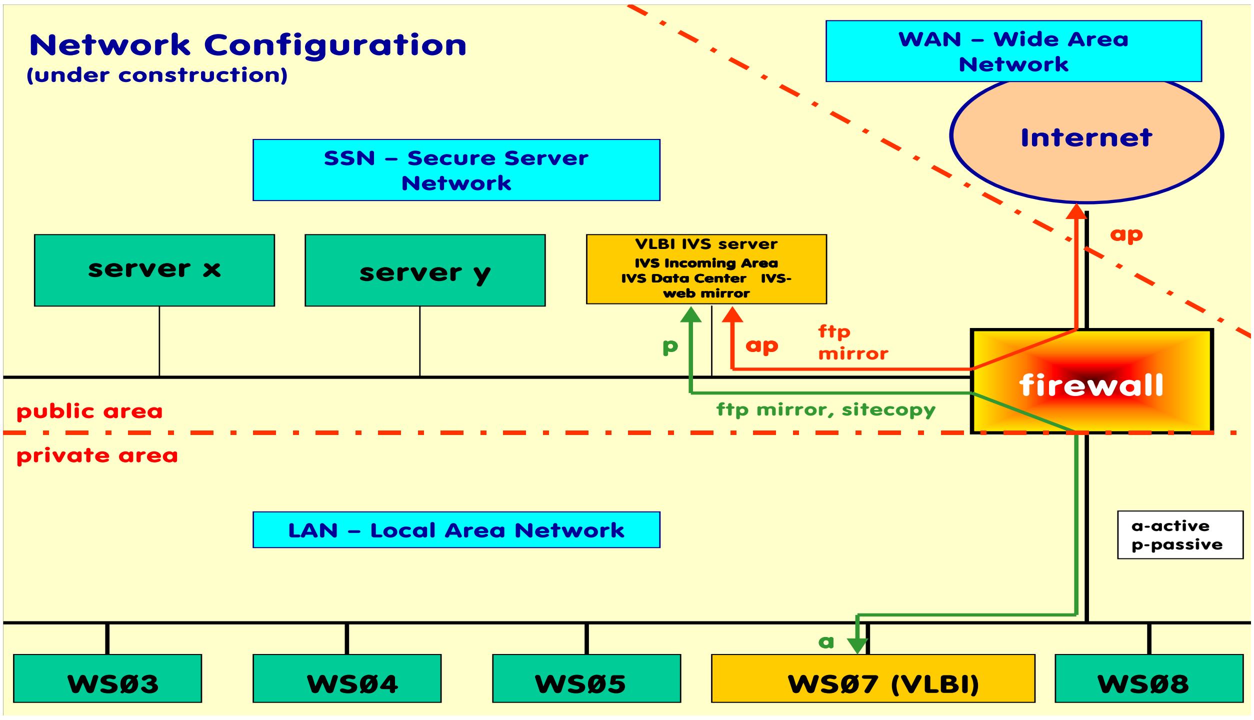

Figure 2. Network configuration

References

[1] GSFC, NASA (2001), Release of Mark-IV VLBI Analysis Software CALC/SOLVE from June 05, 2001 (web-reference: http://gemini.gsfc.nasa.gov/solve_root/release).

Gerald Engelhardt et al.: The Current Status of the IVS Analysis Center at BKG, Proceedings of the 15th Working Meeting on European VLBI for Geodesy and Astrometry, p.8–13
http://www.ieec.fcr.es/hosted/15wmevga/proceedings/engelhardt

The Current Status of the IVS Analysis Center at BKG

Gerald Engelhardt, Volkmar Thorandt, Dieter Ullrich

Bundesamt für Kartographie und Geodäsie (BKG)
Contact author: Gerald Engelhardt, e-mail: `engelhardt@leipzig.ifag.de`

Abstract

The analysis activities at the IVS Analysis Center at BKG can be divided in the processing of the correlator output, the producing of three EOP time series for submission to the IVS and the computation of repeated annual solutions for submission to IERS. The main features of these works are explained and the results are compared with the official IERS products. The processing and managing of the VLBI databases are maintained by using the CALC/SOLVE software and self-developed program environment around it.

1. Introduction

The Leipzig branch of the Bundesamt für Kartographie und Geodäsie (BKG) and the Geodetic Institute of the University of Bonn (GIUB) cooperate in geodetic VLBI for several years. Both institutions are operating the BKG/GIUB VLBI Analysis Center. The BKG is responsible for the establishment of the Earth Orientation Parameter (EOP) time series and the annual solutions for the International VLBI Service (IVS) and the International Earth Rotation Service (IERS). The GIUB gives scientific assistance for that.

The Mark-IV Data Analysis Software System CALC/SOLVE, release of June 5, 2001 (Ref. [1])is currently used for the VLBI data processing at BKG. Besides there is an own program environment around the CALC/SOLVE software for the pre- and post-interactive part of the EOP series establishment. At BKG the CALC/SOLVE software is installed on a HP9000/280/1 workstation with the operating system HP-UX10.20.

2. The processing of correlator output

The BKG is responsible for the further processing of correlator output from the Bonn correlator at Max Planck Institut für Radioastronomie (MPIfR). The correlator files cover so-called VLBI databases version 1 from X- and S-band and related log files for the VLBI experiments IRIS-S, EUROPE, and COHIG. From the beginning of 1999 up to now altogether 54 VLBI experiments were processed, that means in detail 31 IRIS-S, 13 EUROPE, and 10 COHIG VLBI experiments.

After the generation of calibrated databases with higher version numbers they are submitted together with related files to the IVS Data Centers for distribution. The VLBI data processing steps include the program runs of APRIORI, CALC, SOLVE, XLOG, DBCAL, i.e.:

- Providing of a priori information.
- Calculation of theoretical values.
- Group delay ambiguity resolution for X- and S-band.
- Adding of the ionosphere correction.
- Calibration of the databases with meteorological and cable data.
- Inspection of the residuals in the least squares solution.
- Weighting of observations.

3. The main features of the EOP time series computation from 24 hour sessions

All available individual VLBI experiments (NEOS, CORE, COHIG, IRIS-S, EUROPE, ...) are the basis for the final processing, but 96 sessions among them were excluded because of not suitable station configuration. The EOP time series from BKG named bkg00001.eops was generated from altogether 2358 24 hours VLBI sessions between 1984 and August 7, 2001. The time delay is only less than one day from appearing of a new VLBI experiment in the IVS Data Center and the final EOP series results. The BKG EOP time series from 24 hours VLBI experiments is also a contribution to the Bulletin B (Ref. [2]).

The main program options for the computation of the 24 hours session series are:

- Group delays with 5 degrees elevation cutoff are processed.
- The estimated parameter types are the EOP (x-pole, y-pole, ut1-utc and rate, dpsi, deps), station clocks (every hour), zenith troposphere (every hour), troposphere gradients (east and north offset).
- The a priori Terrestrial Reference Frame (TRF) is defined by the Navy 1998-10 frame (Ref. [3]) and the a priori Celestial Reference Frame (CRF) is defined by the ICRF-Ext.1 frame (Ref. [4]). Both reference frames are fixed.

The BKG IVS Analysis Center also generates a second EOP time series for 24 hours VLBI sessions. This series, named bkg00002.eops includes in contrast to the official series bkg00001.eops the additional estimation of the x- and y-pole rates.

4. The main features of the EOP time series computation from the UT1 intensive sessions

VLBI UT1 intensive sessions consist of only one baseline in east-west direction with a measurement duration of about one hour. They are measured around five times per week, generally from Monday to Friday. At present the stations Wettzell (Germany, Europe) and Kokee (Hawaii, Pacific) form this baseline. All available individual VLBI UT1 intensive sessions (XT, XU databases version 1) are the basis for the final processing. The UT1 time series named bkgint01.eops was computed from altogether 634 VLBI UT1 sessions between 1999 and August 8, 2001. The time delay is less than one day from appearing of a new VLBI intensive experiment in the IVS Data Center and the final UT1 series results too. Furthermore the results contribute to the issue of Bulletin B as well.

The main program options for the computation of the UT1 intensive session series are:

- Group delays with 5 degrees elevation cutoff are processed.
- Only the relevant UT1-UTC parameter type is estimated on the epoch of the middle of session. Together with that are the estimation of station clock parameters at one station and zenith troposphere offsets at both stations of the baseline for each session.
- The a priori TRF and CRF are fixed with the same values as in the described analysis procedure of the EOP time series computation from 24 hours VLBI sessions.

5. The BKG annual solution for submission to IVS/IERS

In addition to the described session solutions a combined global solution is computed each year. The last global solution comprises VLBI experiments with a data span from January 1984 to December 2000. Two solution types named bkgira00 for EOP and CRF and bkgtra00 for TRF are the basis for the annual submission to the IVS resp. IERS.

The main features of the solution bkgira00 are:

- The estimated parameter types include the EOP, the CRF, the TRF, and others.
- There is a no net rotation condition for 209 defining sources from the ICRF-Ext.1.
- There are no net rotation and translation conditions for 12 station positions related to the ITRF97 (Ref. [5]).
- There are no net rotation and translation conditions for 5 station velocities related to the ITRF97.
- The station HRAS (Fort Davis, USA) is piece-wise modeled with an interval of one month.
- The results of the EOP- and CRF estimations were submitted to the IVS and to the IERS.

The main features of the solution bkgtra00 are:

- Use of the same program options as in solution type bkgira00 with one exception: station HRAS is not modelled piece-wise but as one global estimation for coordinates and velocities.
- At present the TRF solution is available in SINEX format (coordinates, velocities, covariance matrix) and as normal equations including the global source parameters with an own arbitrarily defined format.

6. Comparisons and assessment of the accuracy of the BKG EOP series

Some comparisons within the computed BKG EOP series and comparisons to the official IERS C04 series (Ref. [6]) were carried out to assess the accuracy of the BKG EOP series.

A: Statements refer to the difference to C04 for solution bkgira00 (see point 5.).

A decreasing of scattering from 1984 to 2000 is obvious but there are remaining systematic deviations especially from 1984 to 1988. Figure 1 is an example for the EOP component x-pole.

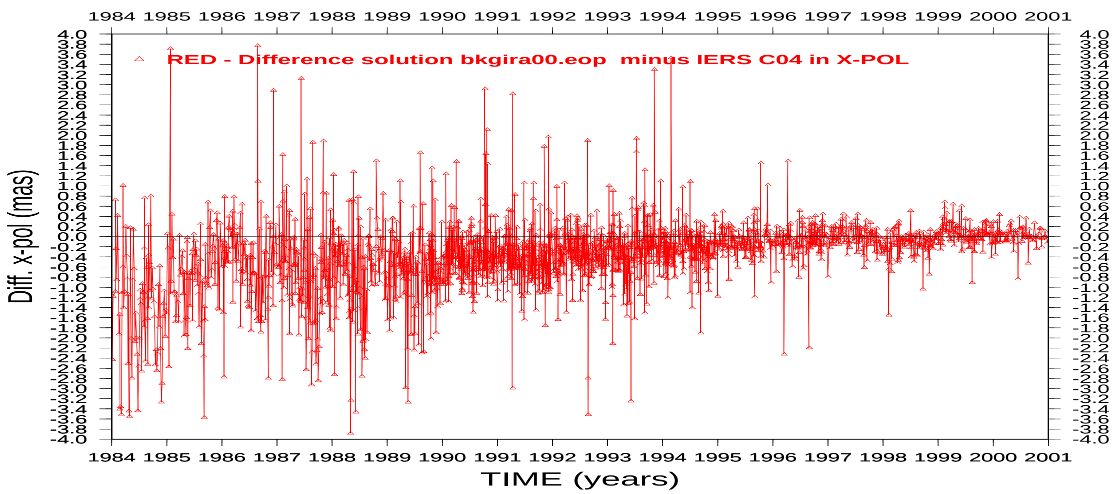

Figure 1. Difference of the BKG annual solution bkgira00 and c04

B: Statements refer to the comparison between the solutions bkg00001 and bkg00002 (see point 3.) from 1999 up to present time.

Most differences in the EOP are smaller than their formal standard deviations. The mean formal standard deviations are: sigma(x-pole)=0.23 masec, sigma(y-pole)=0.15 masec, sigma(ut1-utc)=12 microsec. Figure 2 is an example for the EOP component y-pole for both solutions.

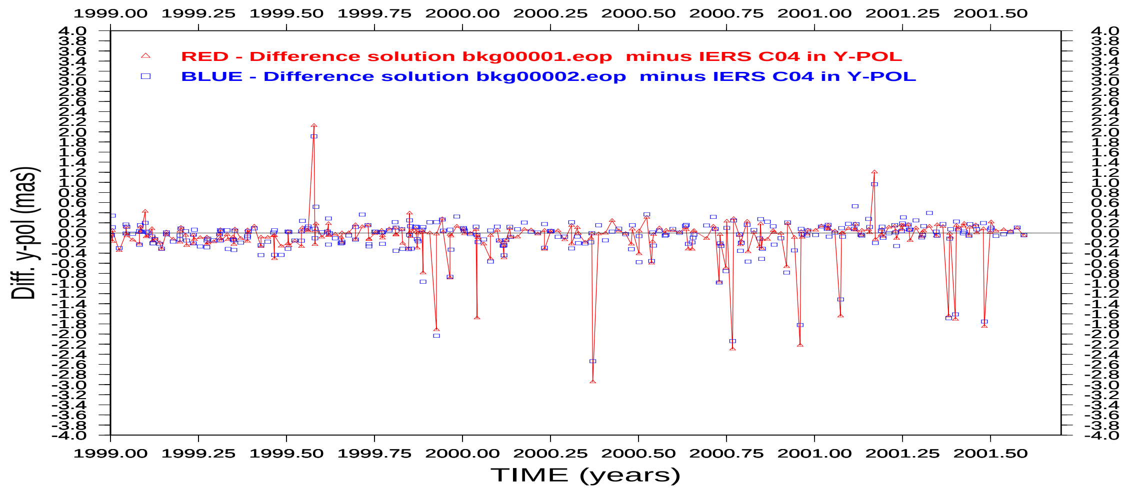

Figure 2. Difference of the BKG solutions bkg00001 and bkg00002

C: Statements refer to the comparison between the solutions bkg00001 (see point 3.) and bkgint01 (see point 4.) in UT1-UTC from 1999 up to present time.

The scattering of the intensive UT1 series till June 2000 is higher than afterwards. This fact corresponds with the change in the baseline configuration in the middle of the year 2000 from baseline Wettzell (Germany) to Greenbank (East coast USA) to the longer baseline Wettzell to Kokee (Hawaii, Pacific). The substitution of the station Greenbank by the station Kokee also causes a jump of about 20 microseconds (see figure 3).

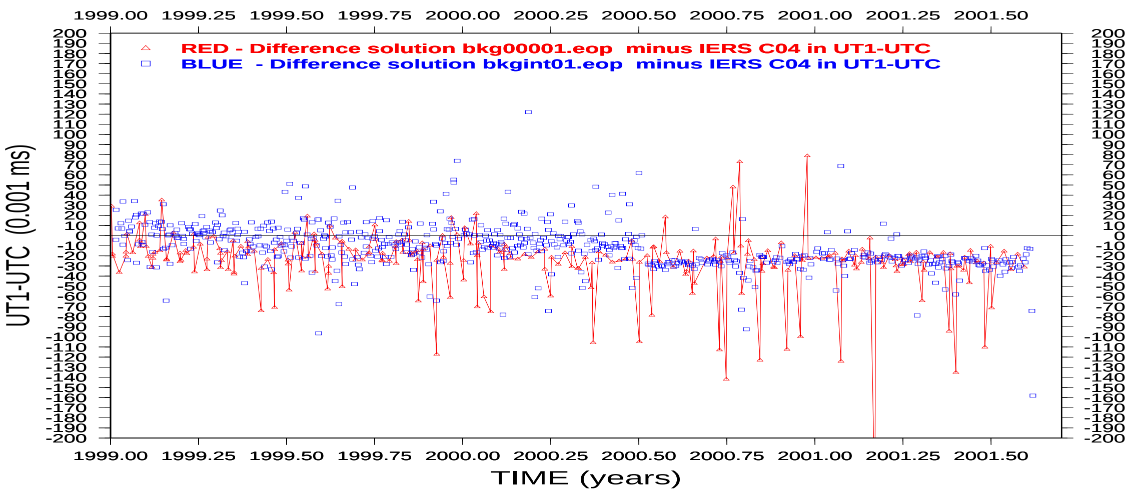

Figure 3. Comparison of the BKG solutions bkg00001 and bkgint01 with a priori TRF Navy 1998-10

A new test computation of the two BKG EOP series with a new a priori TRF ITRF2000 (Ref. [7]) shows interesting results. The former jump of about 20 microseconds disappears and furthermore the EOP series bkg00001 appears more homogeneously (see figure 4).

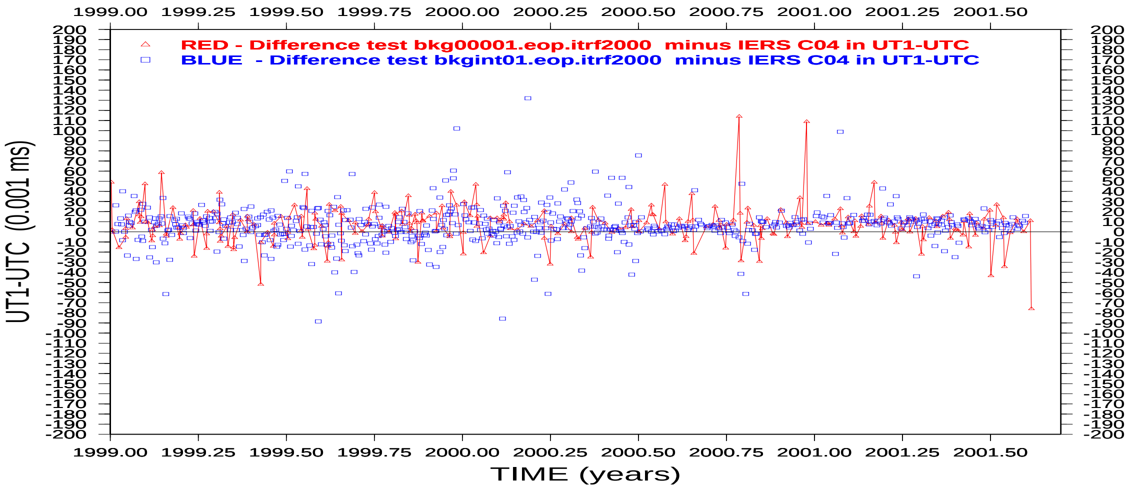

Figure 4. Comparison of the BKG test solutions bkg00001 and bkgint01 with a priori ITRF2000

D: Statements refer to the comparison between the VLBI experiments NEOS and CORE observed on the same day of the series bkg00001 (see point 3.) from 1999 to the middle of 2000.

Both VLBI experiment series NEOS and CORE are characterized by a comparably global station distribution, by the same periods of time of measurements, and by the same processing steps. So the processing results should be theoretically the same. Assuming the difference of the determined EOP results from both experiment series has to be zero, the accuracy derived from double measurements can be estimated by

$$s1 = \sqrt{\frac{[dd]}{2n}} \qquad \text{and} \tag{1}$$

s1: standard deviation of the EOP component

d: difference between the EOP component form NEOS and CORE

n: number of the data points (32 double measurements).

In addition to the values from equation (1) the mean formal standard deviations s2 of the EOP components are used to compute a factor s1/s2 for each EOP component (ut1-utc, x-pole, y-pole, dpsi, deps). So the reliability of the formal standard deviations can be checked. The conclusion from this is a too optimistic estimation of the mean formal standard deviations of the EOP by a mean factor of 2.5.

A second computation of the factor s1/s2 with the same data points but with a new determined EOP series bkg00001 on the basis of a new a priori TRF ITRF2000 yields a better agreement with the formal standard deviations. Now the mean factor amounts to 1.6 with constant s2 in both computations. These results confirm the higher accuracy of the ITRF2000 in contrast to the TRF Navy 1998-10. The standard deviations s1, s2 and the corresponding factors of the EOP components for both calculations are given in table 1.

7. Outlook

On the basis of our test computations (see point 6.) for the EOP time series a revision of the procedures with regard to an optimum choice of the parameter set is planned. Furthermore we

Table 1. Mean standard deviations for EOP components derived from NEOS and CORE on the same day

EOP component	s1	s1.itrf2000	s2	s2.itrf2000	s1/s2	s1.itrf2000/s2.itrf2000
x-pole	0.32 mas	0.23 mas	0.15 mas	0.15 mas	2.1	1.5
y-pole	0.38 mas	0.15 mas	0.12 mas	0.12 mas	3.2	1.3
ut1-utc	23.8 μs	12.5 μs	6.8 μs	6.8 μs	3.5	1.8
$d\psi$	0.36 mas	0.29 mas	0.18 mas	0.17 mas	2.0	1.7
$d\epsilon$	0.13 mas	0.13 mas	0.07 mas	0.07 mas	1.9	1.9
					mean 2.5	mean 1.6

intend to produce the IVS TRF solution four times per year according to the IVS instructions.

To maintain the BKG IVS Data and Analysis Center further improvements of automated analysis processes are under construction.

The BKG will participate in the second IVS Pilot Project (Ref. [8]).

References

[1] GSFC, NASA (2001), Release of Mark-IV VLBI Analysis Software CALC/SOLVE from June 05, 2001 (web-reference: http://gemini.gsfc.nasa.gov/solve_root/release).

[2] Bulletin B, web-reference: http://hpiers.obspm.fr/eop-pc.

[3] USNO (1997), U.S. Naval Observatory IERS Annual Report for 1997.

[4] ICRF-Ext.1, web-reference: http://hpiers.obspm.fr/webiers/results/icrf.

[5] Boucher, C. et al., (1999), The 1997 International Terrestrial Reference Frame (ITRF97), IERS Technical Note 27, Observatoire de Paris.

[6] C04 EOP, web-reference: http://hpiers.obspm.fr/eoppc/eop/eopc04.

[7] ITRF2000, web-reference: http://lareg.ensg.ign.fr/ITRF/ITRF2000.

[8] Call for 2nd IVS Analysis Pilot Project, IVS mail no. 00360 (17-JUL-01), web-reference: http://ivscc.leipzig.ifag.de/mhonarc/ivsmail/maillist.

Cristina García Miró et al.: MDSCC Radio Astronomy Report, Proceedings of the 15th Working Meeting on European VLBI for Geodesy and Astrometry, p.14–21
http://www.ieec.fcr.es/hosted/15wmevga/proceedings/garcia

MDSCC Radio Astronomy Report

Cristina García Miró [1], *Jose F. Gómez* [2], *Dirk Behrend* [3], *Antonio Rius* [3], *Antxon Alberdi* [4], *Elena Jiménez Bailón* [2], *Itziar de Gregorio Monsalo* [2]

1) *Madrid Deep Space Communications Complex, INTA/NASA*
2) *Laboratorio de Astrofísica Espacial y Física Fundamental, INTA*
3) *Institut d'Estudis Espacials de Catalunya*
4) *Instituto de Astrofísica de Andalucía*

Contact author: Cristina García Miró, e-mail: `cgmiro@lrid.mdscc.nasa.gov`

Abstract

This report reviews the radio astronomy and geodetic activities, in which MDSCC is involved, as well as the operational philosophy. A summary of the observations performed in the years 2000–2001 and a reliability and performance study of the operations are given. News about MDSCC and future plans concude the report.

1. Radio Astronomy and Geodesy Operations in MDSCC

The Radio Astronomy and Development Control (RDC) System has been designed to simplify R&D operations for DSN personnel and to enable remote directing and monitoring by investigators. The system is being continuously improved towards high automation and rapid reconfiguration. This will allow the use of short blocks of antenna time and use of unanticipated antenna availability on very short notice.

The RDC integrates both DSN Operations subsystems and experimental subsystems. Some key elements of the system are (see figure 1):

- the Equipment Activity Controller (EAC), which performs the same functions as a DSN operator's console but has the additional capability of controlling R&D equipment,
- the Radio Astronomy Controller (RAC), which controls much of the radio astronomy and other R&D equipment, and
- the PC Field System (PCFS), which controls the VLBI recorders and the MarkIV Acquisition Terminal.

2. VLBI and non-VLBI Radio Astronomy and Geodetic Activities

During the reported period a total of 69 VLBI observations have been performed, representing a total time of 696 hours. Tables 1 and 2 summarize the VLBI observations performed from August to December 2000 and from January to August 2001. MDSCC has been involved in the following projects:

- DSN Flight Projects: Clock Synchronization (Clock Sync) and Catalog Maintenance and Enhancement (CATM&E) (37 observations). Clock Sync uses VLBI techniques to study the instantaneous Earth rotation angle, polar motion, source positions and difference between two Deep Space Network (DSN) station clocks. These results are required by different JPL projects in order to be able to measure the frequency rate offset of the H_2 maser frequency standards within the DSN. It is performed once every two weeks. The purpose of the CatM&E project is the development and maintenance of a high accuracy position radio source catalog

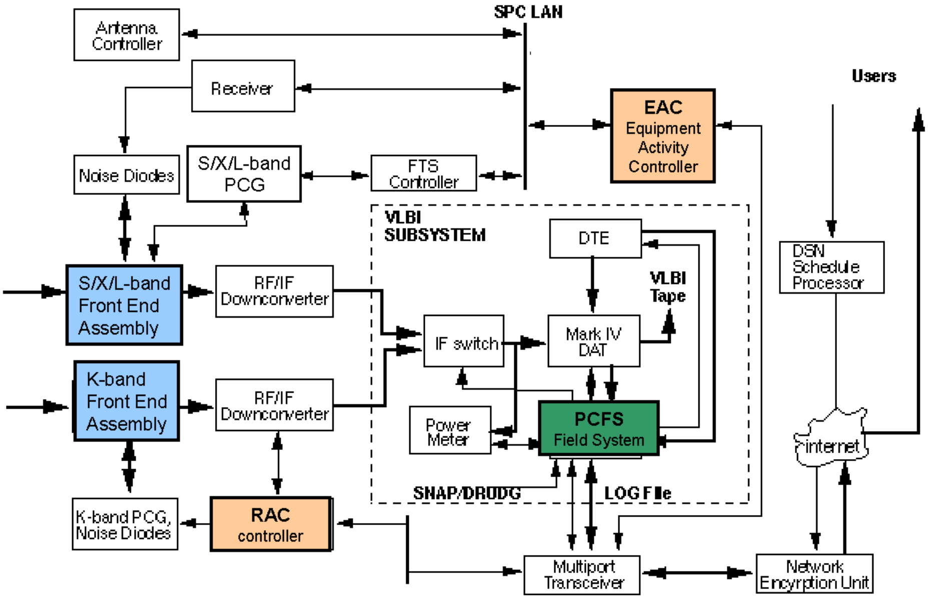

Figure 1. MDSCC Radio Astronomy Operational Diagram. The diagram shows the interconnection between the RA control systems and the antenna.

(within $0\farcs001$ error). This stellar reference frame is used as a reference for JPL missions navigation purposes. It is performed once a month.

- NASA Projects: OSSA (1 observation).
- SVLBI Co-observing Program (5 observations). L-Band observations participating in the space VLBI observations carried out with the space antenna VSOP and other terrestrial radio observatories.
- Stanford University: Gravity Probe B Mission (4 observations). This project intends to test predictions of the General Theory of Relativity about the curvature of space-time. It will use a precise orbit and pointing, accurate gyroscopes and sensitive detectors to measure extremely small variations in the spin of the onboard gyroscopes.
- Goddard Space Flight Center: Space Geodesy Program (SGP) — Europe and CORE (6 observations). SGP has the objective to establish, maintain and distribute to the US and international community a high accuracy terrestrial reference frame (TRF). This frame gives location and velocities of different sites around the world (accuracy 2cm in position, 1mm/yr in velocity).
- EVN + VLBA: Global Observations (8 observations). The purpose of these projects is the observation and study of the radio emission of astronomical objects.
- EVN Calibrations (2 observations).
- Others: Radio Stars (7 observations). Study of stars similar to the Sun in order to detect Jupiter-like planets, applying phase reference techniques.

Most common failures experienced during the reported period are:

- DSS65 Pre-limits problem. While moving from one source to the following, the 34m High Efficiency antenna (DSS65) starts an erroneous movement reaching elevation or azimuth

Table 1. VLBI observations in the August-December 2000 period. In the comments columnn, the completely successful observations are labeled as 'OK'. In contrast, observations that completely failed (100% data loss) are labeled as 'FAIL'. Problems that caused the data to be lost (partially or completely), or degraded are specified. Most common problems are described in the running text. PCG stands for phase calibration signal, REC#N is the VLBI recorder number N, OE stands for operator error, APA is the Antenna Pointing Assembly and VC#N is the video converter number N. Deep Space Antennas used for VLBI are DSS63 and DSS65.

Code	**Project**	**DOY**	**Antenna**	**Band**	**Comments**
BR067B	GPB	220	63	XDUAL	OK
00CS234	Clock Sync	234	65	S/X	OK, PCG low
W329A	SVLB	236	63	L	FAIL
W327C	SVLB	243	63	L	FAIL: formatter not in sync
00CS243	Clock Sync	243	65	S/X	REC#1 problems
EURO58	Europe SGP	248	65	S/X	DSS65 Prelimits, Drudg problem, REC#1 problems
00CS256	Clock Sync	256	65	S/X	OK, PCG low
00CS270	Clock Sync	270	65	S/X	OK
00CS277	Clock Sync	277	65	S/X	OK
00281	CatM&E	281	65	S/X	REC#2 problems
28800	RA stars	288	63	X	Drudg problem
00289	CatM&E	288	65	S/X	DSS65 Prelimits
CB702	CORE SGP	290	65	S/X	DSS65 Prelimits, Drudg problem
00CS292	Clock Sync	292	65	S/X	OK
29600	RA stars	296	63	X	FAIL: Drudg problem
30200	RA stars	302	63	X	FAIL: Drudg problem
BR067C	GPB	310	63	XDUAL	Subreflector problem
00CS315	Clock Sync	315	65	S/X	OK
GB037	GLOBAL	316	63	XDUAL	OK
GB038A	GLOBAL	317	63	S/X DUAL	OK
00CS319	Clock Sync	319	65	S/X	DSS65 Prelimits
00330	CatM&E	330	65	S/X	Sources lost problem
GM043B	GLOBAL	331	63	KDUAL	OE (antenna misconfiguration)
00CS338	Clock Sync	338	65	S/X	OK
EURO59	Europe SGP	342	65	S/X	OK
00CS350	Clock Sync	350	65	S/X	OK
W023B4	SVLB	357	63	L	No noise diodes control
00CS363	Clock Sync	363	65	S/X	OK

Table 2. VLBI observations in the January-August 2001 period.

Code	Project	DOY	Antenna	Band	Comments
01CS008	Clock Sync	8	65	S/X	OK
W308A	SVLB	15	63	L	L-Band RFI, no noise diodes control
01CS023	Clock Sync	23	65	S/X	DSS65 Prelimits, APA#2 problem
01030	CatM&E	30	65	S/X	DSS65 Prelimits, OE (recorder)
01CS035	Clock Sync	35	65	S/X	OK
036-01	RA stars	36	63	XDUAL	OK
048-01	RA stars	48	63	XDUAL	APA#1 problem, OE (antenna misconfiguration)
01CS050	Clock Sync	50	65	S/X	OK
GB036	GLOBAL	54	63	L	Problems REC#1, no noise diodes control
GM038	GLOBAL	54	63	L	Subreflector hung up
N01L1	EVNCAL	54	63	L	VC#3 low, no noise diodes control
W302A	SVLB	64	63	L	No noise diodes control
01CS070	Clock Sync	70	65	S/X	OK
01083	CatM&E	83	65	S/X	Problems REC#2, antenna stopped
01CS084	Clock Sync	84	65	S/X	Sources lost problem
BR071A	GPB	90	63	XDUAL	Xband PCG red, APA#1 problem
01CS093	Clock Sync	93	65	S/X	Sources lost, VC#2 problems
01CS098	Clock Sync	98	65	S/X	Sources lost, VC#2 problems
01CS110	Clock Sync	110	65	S/X	VC#3 problems
01125	CatM&E	125	65	S/X	DSS65 Prelimits, Problems REC#1
01CS126	Clock Sync	126	65	S/X	VC#13 problems
01CS137	Clock Sync	137	65	S/X	Sources lost, VC#13 problems
139-01	RA stars	139	63	XDUAL	VC#2&VC#13 problems
01CS149	Clock Sync	149	65	S/X	Antenna problem (AZ encoder)
GR016C	GLOBAL	153	63	XDUAL	OK
N01X2	GLOBAL	153	63	XDUAL	OK
GG038C	GLOBAL	153	63	XDUAL	OK
01154	CatM&E	154	65	S/X	VC#13 problems
161-01	RA stars	161	63	XDUAL	Subreflector hung up
01CS166	Clock Sync	166	65	S/X	OK
CC201	CORE SGP	162	65	S/X	DSS65 Prelimits, OE (PCG low)
EURO60	Europe SGP	169	65	S/X	Sources lost, OE (subreflector fix 10deg EL)
01174	CatM&E	174	65	S/X	DSS65 Prelimits, antenna problem, OE(recorder)
01CS178	Clock Sync	178	65	S/X	VC#3 problems, OE(recorder)
BR071B	GPB	180	63	XDUAL	Sources lost
CC202	CORE SGP	185	65	S/X	OE (PCG low)
01CS194	Clock Sync	194	65	S/X	VC#3 problems
01CS206	Clock Sync	206	65	S/X	VC#3 problems
01209	CatM&E	209	65	S/X	VC#3 problems
01CS220	Clock Sync	220	65	S/X	Sources lost
01CS232	Clock Sync	232	65	S/X	FAIL (recorder problem and OE)

software and hardware pre-limits. During the antenna recovering process several sources can be lost. The problem is under investigation.

- EAC-antenna communication problems. Due to heavy traffic in the communications between the EAC and the antenna controllers, some of the move commands for next source are lost. This problem can cause up to a 5% of the time to be lost.
- Antenna problem (Antenna pointing assembly problem, Antenna Controllers problems, etc).
- Subreflector problem (subreflector stopped tracking).
- Schedule processing errors. This was the most important cause of data loss during the year 2000. An incorrect Schedule Processing Software (Drudg) version was used.
- VLBI Data Acquisition Terminal failures (formatter, recorders, video converters, etc).
- Operator error. Most common operator errors are configuration errors (signal polarization crossed, antenna and subreflector configuration error). Other errors are related with check neglected during the observation (formatter unsynchronized, subreflector or antenna erroneous status). Deficient managing of VLBI recorders is another cause of data loss (e.g. recorder head not properly cleaned).

Apart from the VLBI Observations, a total of 22 observations have been performed during the Host Country time that is managed by the Laboratorio de Astrofísica Espacial y Física Fundamental -LAEFF/INTA-. This time is scheduled for the Spanish Astronomical Community and represents a 5% of the total. During Host Country time, K-Band spectroscopy and single-dish observations are performed.

Part of the time during this period has been used to complete the installation and calibration of the autocorrelation spectrograph. Also was necessary to develop new software to improve the communications of the spectrometer with the receiver. First successful K-Band spectra (water masers from Cepheus A) were obtained on May 18^{th}, 2001.

Also single-dish observations in S and X Bands were carried out for a study of Blazars emission variability.

Additionally K-Band and X-Band gain curves have been measured.

A study has been done to compare geodetic VLBI observations before and after the track and wheel repair of the DSS65 in 1997 with results from conventional geodetic surveys. The repair work caused small displacements in the horizontal and vertical position of the antenna. Whereas the horizontal displacements derived from the two techniques agree very well, the vertical offset as determined by the conventional geodetic surveys cannot, up to now, be seen in the geodetic VLBI data. This is probably due to the short time series available after the repair work and will hopefully be cured when more geodetic VLBI data become available.

3. MDSCC Reliability and Performance

MDSCC performance results for 2000 and January-August 2001 periods are represented in the figures of this section. Figures 2 and 3 show the amount of data observed, degraded or lost for each different project we have participated in. In the year 2000, the projects most affected by data loss were Radio Stars (100% of data loss) and Space VLBI. During the January-August 2001 period, our performance has improved considerably, diminishing the quantity of data degraded or lost.

Figures 4, 5, 6 and 7 show, for each considered period, the total amount of data observed, degraded or lost as well as the causes of lost time.

Different aspects impact on the MDSCC reliability and performance results:

- VLBI operations are not very frequent compared with other station activities: a given operator may not perform VLBI observations for up to several weeks or even a month.

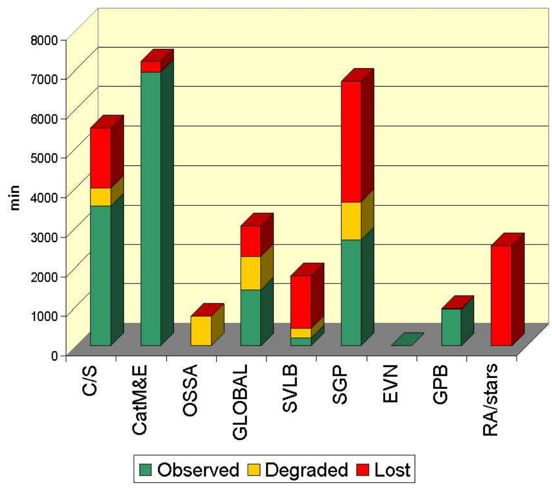

Figure 2. Performance Study: Projects. Year 2000. The plot shows the observed, degraded and lost time in minutes for each project.

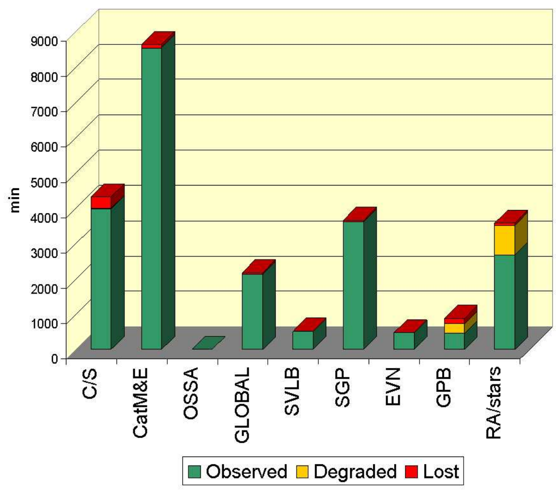

Figure 3. Performance Study: Projects. January-August 2001. The plot shows the observed, degraded and lost time in minutes for each project.

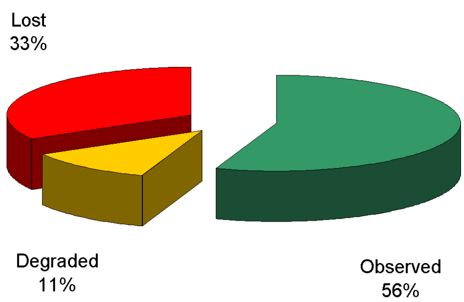

Figure 4. Observed, degraded and lost time (%) during year 2000.

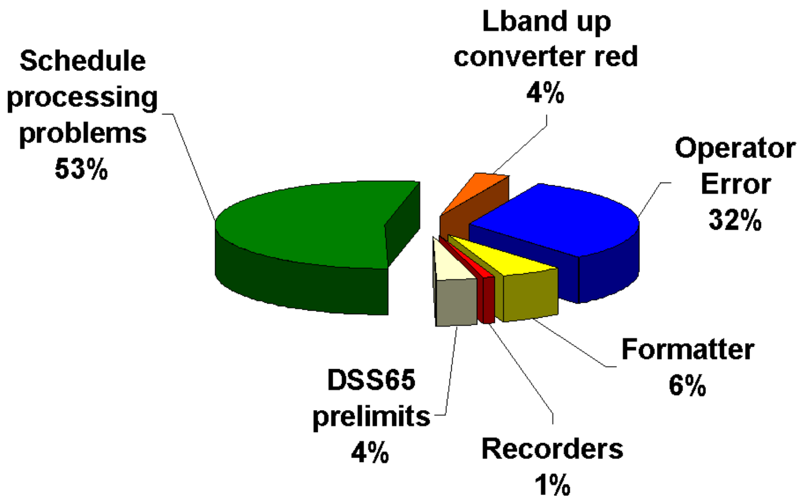

Figure 5. Causes of lost time (%) during year 2000

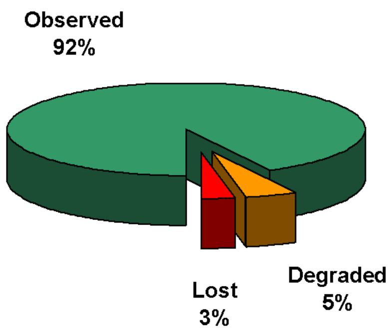

Figure 6. Observed, degraded and lost time (%) during January-August 2001 period.

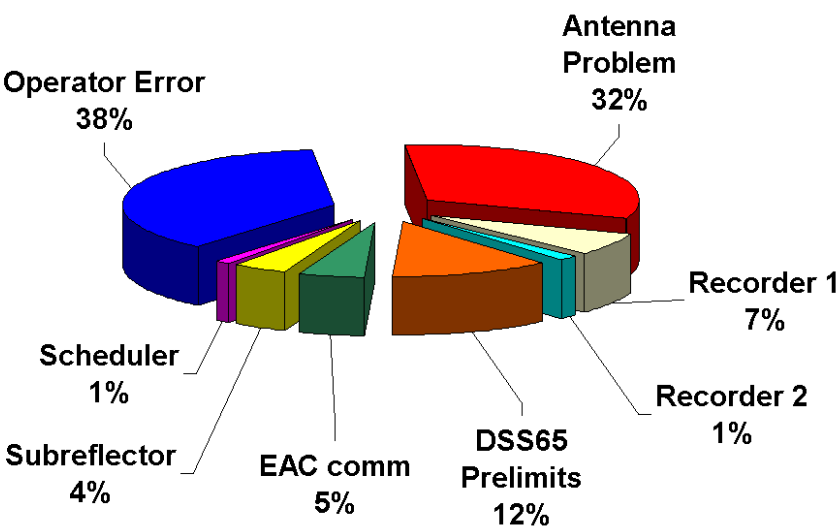

Figure 7. Causes of lost time (%) during January-August 2001 period.

- Most of the VLBI operations are not standard (there are few exceptions, e.g. Clock Sync and CatM&E Projects) and repeated configurations are not very frequent. Non standard observations need the RA Engineer support, providing the required information to configure the equipment and specific instructions to perform the operations.
- Low reliability of the VLBI system: no full automation of the system, old equipment, VLBI magnetic tape recorder/reproducer system has low reliability, etc.
- Complexity of the VLBI control system: EAC-PCFS-RAC complex interaction.

These facts imply the necessity of specialized VLBI operators. A VLBI Operations Training Course has been prepared with the purpose of improving the operators' knowledge of the system and provide sufficient background to the solution of VLBI operations difficulties.

Apart from the efforts to improve the operators' expertise on the VLBI system, it would be convenient to increase the operators' motivation with information about the Scientific Projects they are involved in (scientific goals, etc), as well as the scientific results achieved. Principal investigators of the different projects are encouraged to provide to the station feedback of their results.

4. News and Future Plans

- Cristina Calderón is on leave for one year and Cristina García Miró is the actual Radio Astronomy Engineer (cgmiro@lrid.mdscc.nasa.gov, Tel.: +34-91-867-7130/7000, Fax: +34-91-867-7185).
- The antenna DSS63 (70m) has been down for X-Band up-link upgrade from July to October 15^{th}, 2001. First successful observations were performed in November 2001. X-band Masers have been replaced by a two polarization HEMT with comparable system temperature but improved bandwidth. New gain curves and pointing models have been determined.
- A S2 Data Acquisition Terminal has been installed and the first fringe test will be performed before the end of 2001. PC Field System software has been modified to be able to control the S2 Terminal.
- The K-Band problem in the on-axis RCP path has been determined. The other two paths (on-axis LCP and off-axis LCP) performance are not affected by the problem. A new K-Band HEMT will be purchased and installed in 2002.
- A new Spectrometer developed by the Harvard Smithsonian Institute will be installed at the end of the year 2001.
- A group of MDSCC operators have attended a Radio Astronomy Operations training course during September 2001. The purpose of the course is the improvement of their knowledge and expertise on the VLBI system. It is already scheduled a second training course.
- New software for the Equipment Activity Controller (EAC) and PC Field System (PCFS) is currently being installed. Future hardware upgrades are the gps-fmout, new MarkIV firmware and decoder.
- We have started providing System Temperature Monitoring for the last observations we performed, following the observers requirement. This requirement was not fulfilled since January 2000, when the Quasar Meter System was found to be not year 2000 compliant.
- Future frequency bands upgrades (C-Band and Q-Band) are being studied.
- One of our decommissioned 34m antenna is going to participate in an educational project: PARTNeR (INTA/NASA). The radio telescope is currently in the integration phase.

Richard W. Porcas: Effelsberg Station Report - September 2001, Proceedings of the 15th Working Meeting on European VLBI for Geodesy and Astrometry, p.22–22
http://www.ieec.fcr.es/hosted/15wmevga/proceedings/porcas1

Effelsberg Station Report - September 2001

Richard W. Porcas

Max-Planck-Institut für Radioastronomie
e-mail: porcas@mpifr-bonn.mpg.de

Abstract

This report lists a number of developments at the Effelsberg 100m telescope since the last Working Group meeting which may be of relevance for geodetic VLBI observing.

1. Developments: September 2000 - September 2001

Replacement of the worn gears in the telescope azimuth drives has started. This work should be completed by the end of 2001.

The long-awaited new 8.4 GHz receiver has now been installed in the telescope and is currently being tested by telescope staff. It will be used for an astronomical VLBI experiment at the end of September. (This receiver will support the "R&D" wide frequency range, although Effelsberg does not have an IF3 unit.)

Following completion of development, an upgraded MKIV formatter was installed in December 2000. Bug fixes and new facilities such as barrel roll were successfully tested in a geodetic VLBI experiment correlated in Bonn.

We now have a MKIV decoder in Effelsberg.

In June a second headstack was installed in the MKIV recorder, in preparation for 512 Mb/s recording with the EVN and for mm-VLBI.

The formatter of the VLBA terminal has been upgraded with additional boards (kindly made available from NRAO) in order to make VLBA-compatible 512 Mb/s recording. In this mode, the MKIV recorder will run simultaneously as a second VLBA recorder.

Following the announcement at the EVN TOG meeting last June of a *thin-tape-only* policy for EVN operations, we have changed the Effelsberg policy to *thin-tape-only* for **all** VLBI operations. This applies to both the VLBA and MKIV terminals and includes our occasional **GEODETIC observations**.

Work continues on both the water vapour radiometer and the plans for installing a GPS receiver in Effelsberg, for providing auxiliary phase and delay measurements for VLBI. More information can be found at:

http://www.mpifr-bonn.mpg.de/staff/aroy/wvr.html and
http://www.mpifr-bonn.mpg.de/staff/aroy/gps.html

Francisco Colomer: The New 40 Meter Radiotelescope of OAN at Yebes, Proceedings of the 15th Working Meeting on European VLBI for Geodesy and Astrometry, p.23–23
http://www.ieec.fcr.es/hosted/15wmevga/proceedings/colomer

The New 40 Meter Radiotelescope of OAN at Yebes

Francisco Colomer

Observatorio Astronómico Nacional
e-mail: colomer@oan.es

Abstract

The Observatorio Astronómico Nacional (OAN) of Spain (Instituto Geográfico Nacional – Ministerio de Fomento) is building a new 40 meter parabolic radiotelescope in its premises at Centro Astronómico de Yebes (CAY), near Guadalajara, Spain. The instrument, whose construction is progressing well, is expected to be available for observations in 2004. The new radiotelescope will be equiped with state-of-the-art receivers in the 2 to 115 GHz range (including the geodetic S/X bands), and will join the astronomical and geodetic VLBI networks (EVN and IVS) from the start of its operations.

The National Astronomical Observatory of Spain (OAN) has started the construction of a new 40 meter radiotelescope in the town of Yebes (Guadalajara, Spain), next to the radome-enclosed 14 meter radiotelescope built by ESSCO in 1976. The new instrument will be the most important large scale facility for Radio Astronomy run by the Spanish administration, and become an important partner in the VLBI networks at centimeter and millimeter wavelengths.

The 40 meter radiotelescope will operate in the 13 cm (2.3 Ghz) to 2.6 mm (115 Ghz) range, both as a single antenna and as one element in a VLBI array for astronomical and geodetic studies. The antenna will consist of a homologous parabolic reflector, and a subreflector on a quadrupode, in Nasmyth focus configuration. This system is installed on a concrete pedestal which serves also as control building and workshop (Figure 1). The large receiver cabin will move in azimuth together with the telescope. All receivers will be located in the secondary focus cabin (so that several of them can be used simultaneously), where multibeam receivers at the highest frequencies may also be installed.

Figure 1. Pedestal of the new 40 meter radiotelescope of OAN at Yebes.

The telescope construction started in July 1999. The concrete pedestal was built in 2000, and the telescope structure is expected by 2003. Commissioning and observations could start then with the S/X, K, and Q band receivers.

More information on the construction of the new telescope can be found on the WEB page of the observatory at the URL: http://www.oan.es/cay/40m/.

Hayo Hase: Status of the TIGO-Project in Concepción, Proceedings of the 15th Working Meeting on European VLBI for Geodesy and Astrometry, p.24–27
http://www.ieec.fcr.es/hosted/15wmevga/proceedings/hase

Status of the TIGO-Project in Concepción

Hayo Hase

BKG Wettzell
e-mail: hase@wettzell.ifag.de

Abstract

The Transportable Integrated Geodetic Observatory (TIGO), a fundamental station for geodesy, will be transfered from Wettzell, Germany, to Concepción, Chile. This report gives an overview about the ongoing constructions of the TIGO-platform in Concepción.

1. Introduction

On January 21, 2000, it was decided that BKG's Transportable Integrated Geodetic Observatory will be installed at Concepción in Chile. On June 21, 2000, an Arrangement of the cooperative operation of TIGO was signed between BKG and the Universidad de Concepción (UdeC) on behalf of a Chilean consortium consisting of UdeC, Universidad del Bío Bío (UBB), Universidad de la Santísima Concepción and the Instituto Geográfico Militar of Chile. In 2001 the construction of the necessary infrastructure for TIGO is carried out. This article covers some events until September 7, 2001.

2. Location

The location for TIGO was defined under various aspects:

- **Microwave Noise.** The platform is protected from the urban microwave noise sources such as mobile telephones and wireless networking (2.4GHz) by a natural hill chain between the TIGO-platform and the city of Concepción. An investigation with small S- and X-band horn antennas was carried out in March 2000.
- **Light Noise.** A requirement for good SLR-observations at night are the absence of artificial light sources. The remote location in the unhabited hills adjacent to Concepcón allows good visibility conditions at night.
- **Horizon.** Its location on top of a hill allows in almost all directions observations down to 7 degree of elevation. This is important for common observations (VLBI) since Concepción connects to other observatories mainly with large baselines (> 8000 km).
- **Vibration Noise.** Due to the intended first installation of a super-conducting gravity meter on the Latin-American continent a soil-noise free location is desired. Roads with heavy traffic are not closer than 1 km in all directions. Even local traffic to the observatory approaches not closer than 100 m to the gravity and seismic monument.
- **Operators.** The operation of TIGO requires the support of Chilean institutions which will provide 11 staff. The human resources necessary for TIGO are not available outside cities. The involvement of 3 university opens research oportunities in relation to the data provided by TIGO. The permanent exchange of science and data acquisition also requires a location close to the universities.

With the defined location all of the above conditions could be met.

3. Constructions

3.1. Access Road

The location of the TIGO-platform was remote with respect to its access with heavy container-trucks. Therefore a 2.5km long unpaved forestry road need to be adapted in terms of changing radii of curves and take away high inclinations. This work was carried out during February and March 2001 (fig. 1).

Figure 1. March 23, 2001. The access road to the TIGO-platform is being prepared.

3.2. Constructions at the platform

In addition the platform was realised by plane on top of the selected hill and needed to be enforced with compacted gravel (fig. 2).

Due to the heavy rain falls in Concepción during winter (June, July) it was not possible to continue the constructions before the end of July 2001. The constructions for TIGO consists not only of the installation of monuments for all its instruments (radiotelescope, lasertelescope, GPS, gravity and seismometer), but also of the realisation of infrastructure such as electricity, water, telephone, internet, its cable ducts, security, toilets, office space and deforestration for a good horizon. In the ongoing first phase of the constructions (until mid September 2001) the foundations for the instruments and a middle tension line were realised (fig. 3, 4). The second phase contains the rest of the necessity and will be finished by the end of November 2001.

4. Outlook

The platform for TIGO will be prepared by the end of November 2001, when the observatory will be installed in Chile. Observing data from this fundamental station for geodesy will be produced by eleven Chileans under the supervision of three Germans and can be expected in 2002.

Figure 2. April 4, 2001. The platform is prepared for the foundations of the monuments.

Figure 3. September 7, 2001. TIGO-platform with foundations for 5 containers (left) and the radiotelescope (right). Two of the reference pillars for controlling local site stability by local geodetic surveys can be seen at the far left side and next to camion with concrete at the far right side. In the foreground begins the escarvation for the SLR-monument.

Figure 4. September 7, 2001. Monument for the GPS-permanent station (future IGS-station). The 3 m tall pillar is being filled with concrete. It is located on a block of concrete with the dimensions $2.6 \times 2.6 \times 1.5$ m^3. The center of the pillar contains an empty tube for the later installation of a tiltmeter. The monument can be seen from the SLR-platform and will carry later a retroreflector below the GPS-antenna for direct determination of the excentricity vector between GPS antenna and SLR telescope.

Giuseppe Colucci et al.: Matera CGS VLBI Station, Proceedings of the 15th Working Meeting on European VLBI for Geodesy and Astrometry, p.28–31
http://www.ieec.fcr.es/hosted/15wmevga/proceedings/colucci

Matera CGS VLBI Station

Giuseppe Colucci [1], *Pippo Bianco* [2], *Domenico Del Rosso* [1], *Luciano Garramone* [1], *Eustachio Lunalbi* [1]

[1] *Telespazio S.p.A.*
[2] *Agenzia Spaziale Italiana*
Contact author: Giuseppe Colucci, *e-mail:* `colucci@asi.it`

Abstract

This report summarizes the present status of the operational VLBI activities at the Matera Space Geodesy Center.

1. The system

The Matera VLBI system is operated, on behalf of Italian Space Agency (ASI), by Telespazio S.p.A. at Centro di Geodesia Spaziale (CGS) of Matera.

The CGS came into operation on 1983 in the framework of an agreement with the Basilicata Regional Government and ASI.

A fixed SLR system and a network of permanent GPS receivers (including one at Matera site) are also operated at CGS. Honeywell (formerly ATSC) is now installing a new SLR system: MLRO.

The Matera VLBI system includes:

- X/S bands receiver;
- 20 meter diameter cassegrain antenna;
- MARK-IV DAT and VLBA4 recorder.

2. Status

The Fig 2 summarizes the sessions from September 2000 up to August 2001, while Fig 3 shows the summary of acquisitions from May 1990 up to August 2001.

3. Performed upgrades

Follwing upgrades were performed in order to increase reliability of the system and to upgrade the equipment to the current standards:

- new cryogenic system;
- FS Linux 3 (new Linux Kernel);
- Mark IV Rack power supply 110V to 220V;
- Mark IV Formatter firmware (now 4.1).

4. Maintenance

In April 2001, an azimuth motor reduction unit failed (see Fig. 4). The unit was dismounted and the motors no. 2 and 4 were disabled. Up to now, antenna is moving using only motors no. 1 and 3.

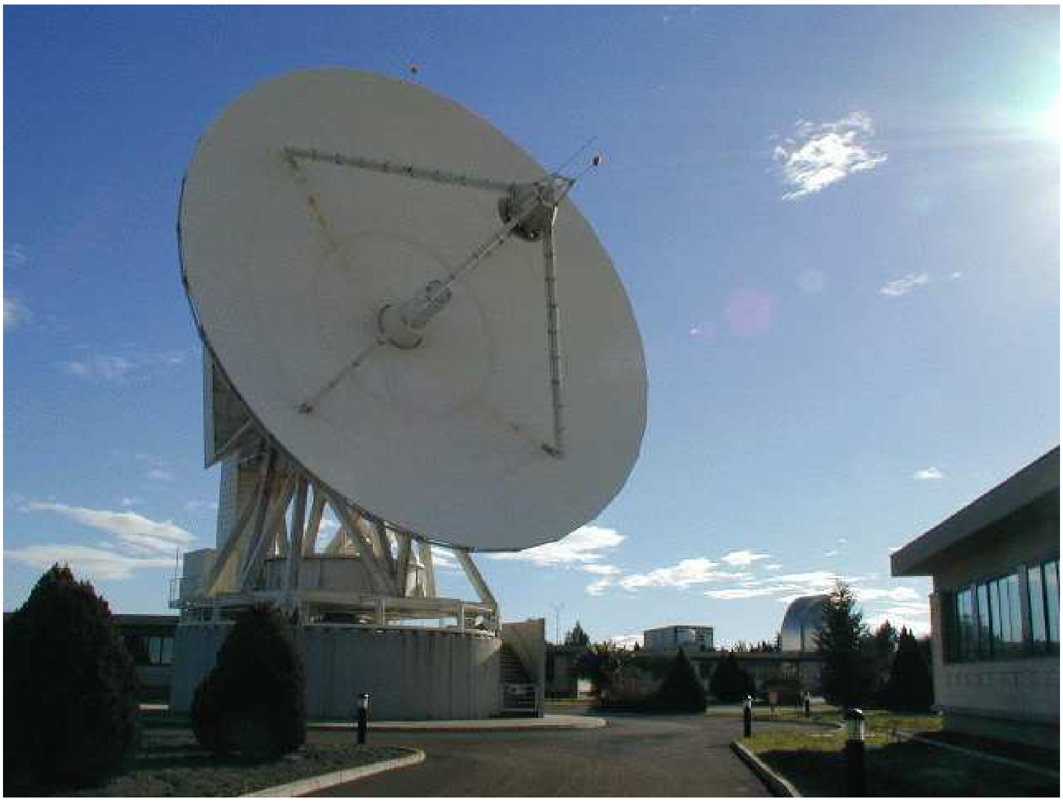

Figure 1. The Matera “Centro di Geodesia Spaziale” (CGS)

	Europe			Core-1			Core-3			RDV			Neos-A			Cont			Other			TOT.		
	#	Tot. [hh]	Lost [hh]	#	Tot. [hh]	Lost [hh]	#	Tot. [hh]	Lost [hh]	#	Tot. [hh]	Lost [hh]	#	Tot. [hh]	Lost [hh]	#	Tot. [hh]	Lost [hh]	#	Tot. [hh]	Lost [hh]	#	Tot. [hh]	Lost [hh]
September 2000	1	24		2	48 (*)		1	24 (*)														4	96	0.0
October				1	24		1	24		1	24											3	72	0.0
November				1	24		1	24					1	24								3	72	0.0
December				1	24		1	24		1	24											3	72	0.0
January 2001				1	24					1	24		1	24								3	72	0.0
February				1	24		2	48					1	24								4	96	0.0
March				1	24					1	24	0.3	3	72	1	2	48					7	168	1.3
April				1	24					1	24		1	24								3	72	0.0
May				1	24 (**)	24	1	24 (**)	24				1	24 (**)	24				1	24 (**)	24	4	96	96.0
June	1	24 (**)	24	1	24 (**)	24	1	24 (**)	24													3	72	72.0
July				1	24		1	24		1	24 (**)	24							2	20		5	92	24.0
August				1	24																	1	24	0.0
Tot.	2	48	24	13	312	48	9	216	48	6	144	24	8	192	25	2	48	0	3	44	24	43	1004	193.3

(*) Uncooled LNA
(**) Motor reduction unit failure

Figure 2. Summary of sessions

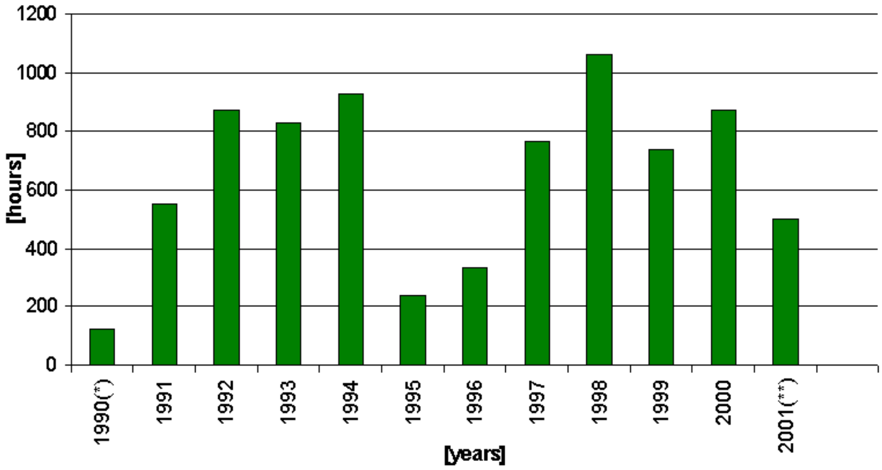

Figure 3. Summary of acquisitions from May 1990 up to August 2001

Figure 4. Motor reduction unit that failed in April

Minor rail maintenance was performed during September while antenna painting is now in progress.

5. Contact points

The list of the VLBI staff members of Matera VLBI station is provided in Table 1.

Table 1. Matera VLBI staff members

Name	Agency	Activity	E-Mail
VLBI Team at CGS	Telespazio		vlbi@asi.it
Dr. Giuseppe Bianco	ASI	VLBI Manager	bianco@asi.it
Domenico Del Rosso	Telespazio	Operations Manager	domenico_delrosso@telespazio.it
Luciano Garramone	Telespazio	Station Engeneer	garramone@asi.it
Giuseppe Colucci	Telespazio	VLBI contact	colucci@asi.it

References

[1] Lunalbi, E., “Matera VLBI Station report on the operational and performance evaluations activities from January to December 2000”, available on-line at this address: http://geodaf.mt.asi.it/html/surv_rep.html

Alessandro Orfei et al.: Medicina and Noto Stations Report, Proceedings of the 15th Working Meeting on European VLBI for Geodesy and Astrometry, p.32–35
http://www.ieec.fcr.es/hosted/15wmevga/proceedings/orfei

Medicina and Noto Stations Report

Alessandro Orfei [1], *Franco Mantovani* [1], *Gino Tuccari* [2], *Giancarlo Stanghellini* [2]

[1] *Istituto di Radioastronomia, Bologna, Italy*
[2] *Istituto di Radioastronomia, Noto, Italy*
Contact author: Alessandro Orfei, e-mail: orfei@ira.bo.cnr.it

Abstract

This report summarizes the activities at the Medicina and Noto Stations in the last year, after the 14th Working Meeting in Castel San Pietro Terme, to improve the station performances,

1. Introduction

The activities at the Medicina and Noto Stations were mainly addressed to improve the data acquisition quality. Most of the upgrading work was done in the electronic hardware and to improve the efficiency of the two 32-m dish. Great care was also taken to increase the reliability of the stations during the VLBI sessions.

2. Main Activities at the Medicina Station

2.1. The upgrade of the Data Acquisition System

a) Main computer and Field System

A new version of the Linux operating system has been installed on the computer driving the antenna and also in charge for the setup of the data acquisition terminal. The computer hardware has also been upgraded. The updated version of the FS (9.5.1) have been implemented. This happened four times in the last year to mantain the FS at the state of the art.

b) MK4 Phase Cal signal

The switch ON/OFF of the 'phase cal' tone is now possible under computer control. An ad hoc FS command can be inserted in the observing schedule to automatically set the switch in the required position.

c) Station Clock

The GPS minus Formatter (Station Clock) difference is now continuosly and automatically acquired in the log file for each VLBI observing project.

d) Two-Heads recording

Two-Heads recording is now available. Two new heads (triple cap) have been mounted. Local playback tests showed that recording is fine at 80 and 135 ips. Problems persist in playback at 160 ips.

e) Formatter

The formatter has been upgraded with new chips.

f) Delay Unit

The Ground Delay Unit has been refurbished following indication from Haystack. It was understood that the cable measurement system was unstable and noisy because of bad capacitors in the antenna unit.

g) Decoder Display The MKIV Decoder Display has been bought. It will be installed as soon as possible.

2.2. The upgrade of the antenna

a) Antenna Pointing

The pointing model has been improved implementing two more parameters. The pointing rms accuracy is now ±10 arcsecond.

b) Azimuth Mount

The special cement which supports the rail azimuth track of the 32-m dish has been completely replaced. A new supporting system for the rail has been introduced. The rail track has been replaced as well.

c) Project Vertex Room

The final design for the new Vertex Room is ready. The replacement has been postponed because of the upgrading of the Noto dish and urgent work on the Azimuth track of the Medicina telescope. The goal of the project is to achieve full frequency agility at both Medicina and Noto 32-m telescopes. The Vertex room will guests 8 receivers which will continuously cover the band 4.3–48 GHz. A wide-band receiver working in the band 4.3–5.8 GHz is under test. The feed system (horn/directional coupler/polarimeter/omt) is under construction by CSELT.

2.3. General information

a) Local Survey

In the period 29 June - 04 July a Local Survey of the antenna has been performed using GPS technique and classical geodesy. The results of those measurements are presented in Vittuari et al. (this conference).

b) Station Reliable Operations

An engineer has been hired thanks to the Infrastructure Cooperation Programme 'Radionet' funded by EC. The main duties for this engineer will be:
1) Check the observing schedules for VLBI projects and the requested data acquisition setup.
2) Work on the completion of the 'frequency agile' system for the antenna.
3) Improve the station calibration information.

2.4. Geodetic VLBI Observations

During 2001, the Medicina 32-m dish has taken part to 28 Geodetic VLBI Observations as follows:
16 CORE projects
6 VLBA projects
3 EUROPE projects
3 CONT projects

3. Main Activities at the Noto Station

3.1. The upgrade of the Data Acquisition System

a) Field System

The updated version of the FS (9.5.1) has been implemented.

b) The MKIV Formatter and Decoder

The MKIV formatter can now be used as standard also for the VLBA DAS. The result of this upgrade consists in an automatic switch between MKIV and VLBA type of observations, i.e. no cabling, nor reboot of the Field System are needed.

The Decoder was also mounted and tested.

c) Data Acquisition Terminal

The second head was mounted and tested.

3.2. The upgrade of the antenna

a) Active Surface for the Noto telescope

The Active Surface of the telescope is now in the implementation phase. New panels, which will allow observations at frequencies up to 43 GHz, and 250 actuators will be mounted. The actuators have been tested and assembled at the Medicina Station. The mechanical interface actuator/panel has been developped in collaboration with the firm in charge for the production of panels. The actuators are under computer control. Ad hoc in-house software has been written for that purpose. The expected efficiency is ~50% at 43 GHz.

b) Tracking System

The SCU interface between encoders and control system of the dish has been changed improving the tracking reliability.

3.3. New Receivers

The primary focus box which will contain the new S/X/L band receivers is under construction. The L and S/X band feeds have been delivered by CSELT. The dewar (cryogenic system) is also under construction. Both feeds will be cooled, together to the front-end LNAs.

3.4. Geodetic VLBI Observations

During 2001, the NOTO 32-m dish has taken part to 3 Geodetic VLBI Observations: CORE-C101, EUROPE-60 AND CORE-C102. Note that the antenna did not observe from August to September due to the maintenance work (which will continue till December 2001) needed to upgrade its performance.

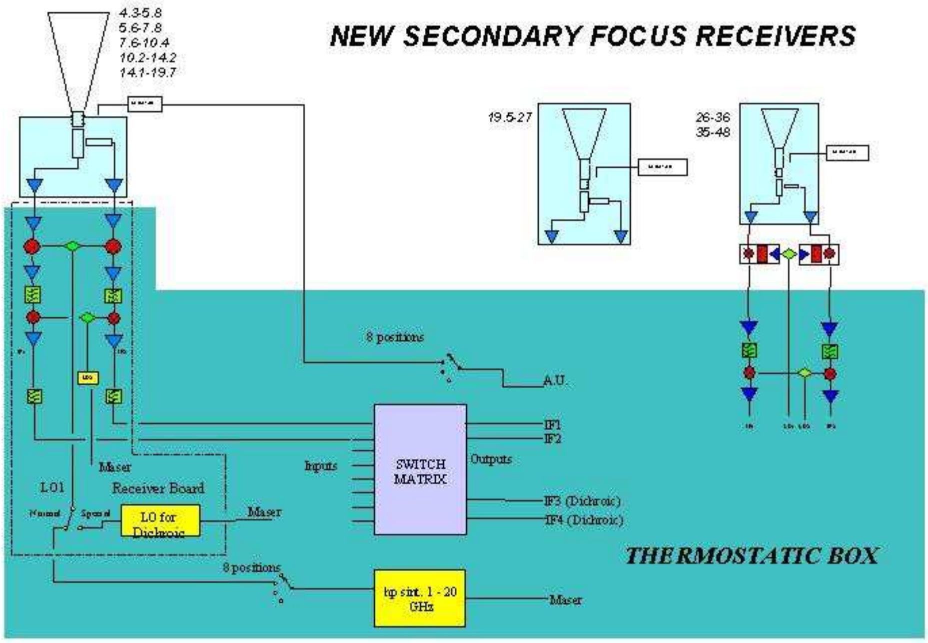

Figure 1. New secondary focus receivers for the Medicina Radio Telescope.

Rüdiger Haas et al.: Geodetic Very Long Baseline Interferometry at the Onsala Space Observatory 2000–2001: Observations, Proceedings of the 15th Working Meeting on European VLBI for Geodesy and Astrometry, p.36–39
http://www.ieec.fcr.es/hosted/15wmevga/proceedings/haas1

Geodetic Very Long Baseline Interferometry at the Onsala Space Observatory 2000–2001: Observations

Rüdiger Haas, Sten Bergstrand, Gunnar Elgered, Lubomir Gradinarsky, Boris Stoew, Harald Bouma, Martin Lidberg

Onsala Space Observatory (OSO), Chalmers University of Technology

Contact author: Rüdiger Haas, *e-mail:* haas@oso.chalmers.se, geo@oso.chalmers.se

Abstract

We give a short overview of the work related to geodetic VLBI experiments at the Onsala Space Observatory for the period 2000–2001. We concentrate on the performance of the VLBI system, recordings and hardware development. Due to limited correlator capacity, in 2000 only 14 geodetic VLBI experiments were observed. In 2001, the number of planned experiments is 25, most of them have already been observed without major problems.

1. VLBI Observations

The Onsala 20 m radio telescope has regularly participated in several different geodetic VLBI series during 2000 and 2001, i.e. EUROPE, CORE-3, and VLBA, see Table 1.

Table 1. Geodetic VLBI experiments at the Onsala Space Observatory 2000–2001. Experiments that were lost due to technical problems are marked with †.

Experiments observed in 2000					
EUROPE-53	EUROPE-56	EUROPE-59	CORE-3001	CORE-3005	VLBA19
EUROPE-54	EUROPE-57		CORE-3002†	CORE-3006	VLBA20
EUROPE-55	EUROPE-58		CORE-3004		
Experiments observed in 2001 up to October 15					
EUROPE-60	CONT-M3	CORE-3007	CORE-3014	CORE-3022	VLBA25
EUROPE-61	CONT-M4	CORE-3008	CORE-3015	CORE-3024†	VLBA26
	CONT-M5	CORE-3011	CORE-3016	CORE-3026	VLBA28
		CORE-3012	CORE-3019	CORE-3028	
		CONT-3013	CORE-3020		
Remaining experiments scheduled for 2001					
EUROPE-62		CORE-3033	CORE-3035		

In 2000, Onsala was scheduled for and has participated in all seven experiments of the EUROPE series. In 2001 initially only two EUROPE experiments were scheduled due to the limited capacity of the Bonn correlator. Fortunately, the situation at the Bonn correlator improved significantly during 2001, so one additional EUROPE experiment was observed in September 2001.

In 2000, Onsala was scheduled for six CORE-3 experiments. Five of them were observed successfully while problems with the pointing of the telescope caused a failure of CORE-3002. In 2001 Onsala has been scheduled to participate in sixteen CORE-3 experiments. Fourteen of these have already been observed and two more are going to be observed during October 2001. The experiment CORE-3024 was lost due to a failure of the recorder brakes.

Two VLBA experiments in 2000 and three in 2001 have been observed. Onsala participated also in three experiments of the CONT-M series in March 2001.

2. Technical development and technical problems during 2000-2001

The overall system performance of the Onsala VLBI system is checked continuously, see e.g. [1], [2]. The hardware component causing the majority of the problems is still the tape recorder. In order to overcome problems related to different type of tapes and different vacuum levels, we decided to run Onsala as a thin-tape-only station from January 2001. Nevertheless, the recording quality is still unstable, producing highly varying parity errors levels.

The readings often give $$$$$ values indicating very high parity errors or maybe problems in the read electronics. Table 2 shows the amount of $$$$$ readings from forward and reverse recordings during the last six CORE-3 experiments observed at Onsala. Figure 1 displays empirical cumulative distribution functions for the forward and reverse parity errors during the last six CORE-3 experiments. For these plots the $$$$$ readings have been neglected.

Table 2. Percentage of $$$$$ readings from parity errors checks during the last six CORE-3 experiments.

	CORE-3016	CORE-3019	CORE-3020	CORE-3022	CORE-3026	CORE-3028
for./rev.	6% / 5%	9% / 3%	41% / 22%	16% / 5%	10% / 6%	6% / 7%

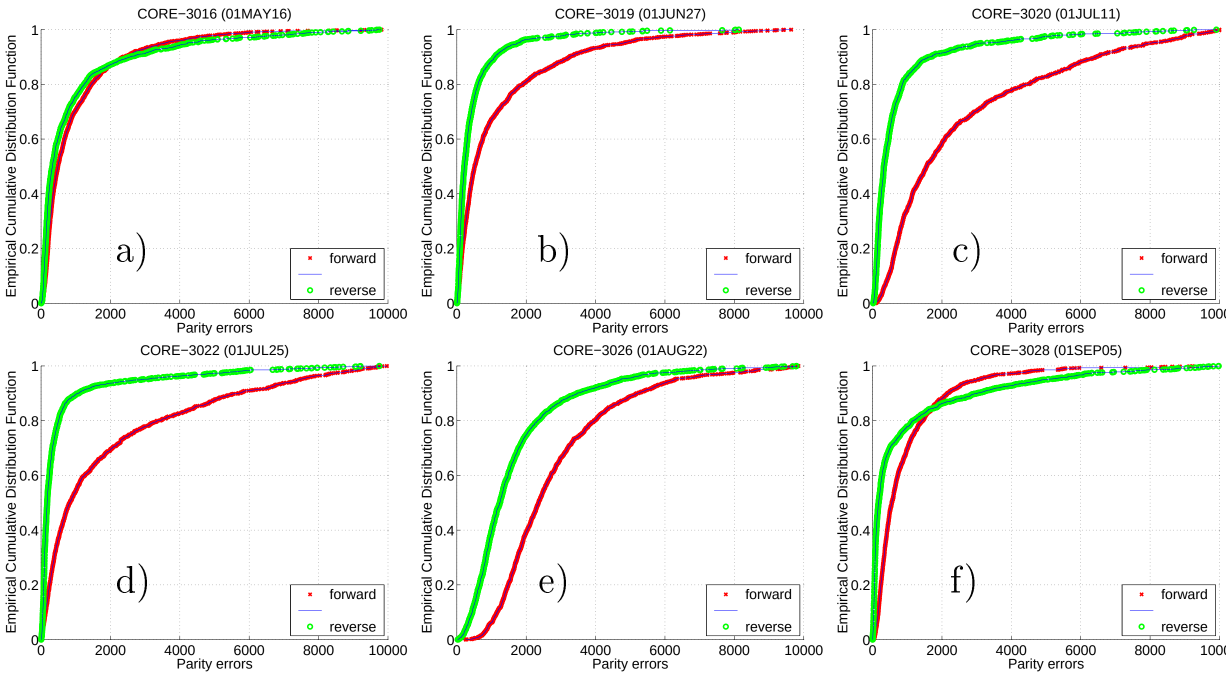

Figure 1. Empirical cumulative distribution functions of the parity errors during CORE-3016 (a), CORE-3010 (b), CORE-3020 (c), CORE-3022 (d), CORE-3026 (e), CORE-3028 (f).

For CORE-3016 more than 70% of the parity errors were below 1000, about 90% were below 2000. Forward and reverse recordings showed similar behaviour. Starting with CORE-3019 the situation got worse, especially for the forward parity errors. In particular CORE-3020 and CORE-3022 showed a drastic difference in the forward and reverse recordings, where the reverse passes gave lower values than the forward passes. During CORE-3026 both recordings gave poor parity error levels and also here forward recording was worse than reverse recording. First for CORE-3028 there seems to be an improvement and forward and reverse recordings performed more similar again and on lower partiy error levels, too.

One possible cause for poor parity error performance was identified during summer 2001, when a leakage at the glass windows of the vacuum chamber was detected. This defect caused small flucuations of the vacuum level by about 5%. After repair, the levels of parity errors stabilised to some extend, compare the plots for CORE-3026 and CORE-3028 in Fig. 1. Another possible explanation for the poor parity error performance is internal interference affecting the read heads. This cause is currently under further investigation.

In Figure 2 we show the median (and mean) parity errors against the track used for forward and reverse recordings during the last nine CORE-3 experiments observed at Onsala. Again, it is clearly visible that for nearly all experiments the forward passes gave worse parity errors than the reverse ones. Besides this, it appears to be some track dependence since some of the tracks, e.g. track 32, seem to perform significantly worse than others.

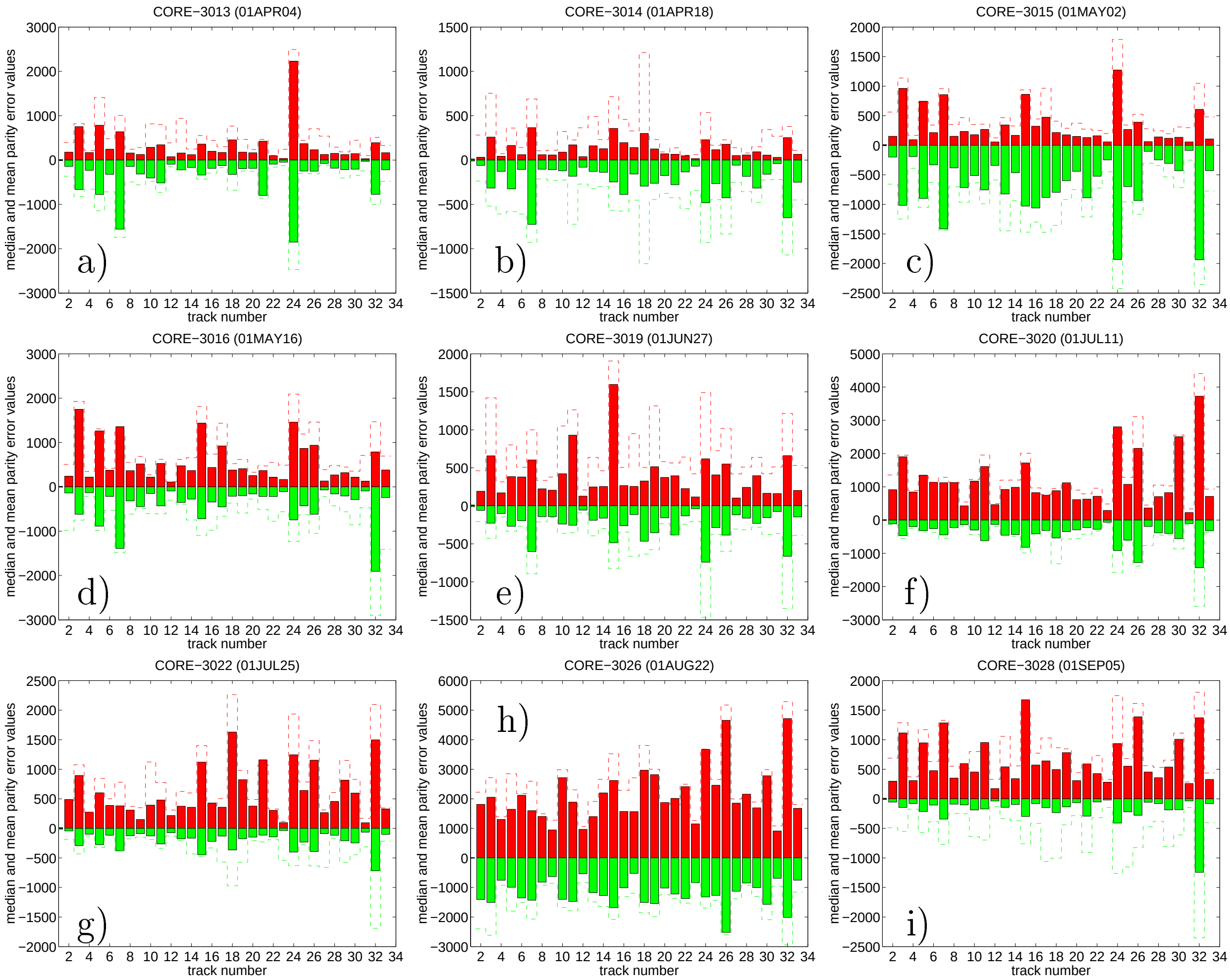

Figure 2. Median (full) and mean (dashed lines) parity errors per track during CORE-3013 (a), CORE-3014 (b), CORE-3015 (c), CORE-3016 (d), CORE-3010 (e), CORE-3020 (f), CORE-3022 (g), CORE-3026 (h), CORE-3028 (i). Forward parity errors are shown as positive values, reverse parity errors as negativ values.

During July 2001 the IVS network coordinator Ed Himwich visited the Onsala Space Observatory and inspected the VLBI system together with the local staff. Head calibration and write voltage were inspected and found to be correct, and the Onsala VLBI system did not show any obvious major defects. A 10 dB variation in the bandpass over 300 MHz and a small bump in the bandpass were detected which apparently is introduced in IF distribution. The IF distribution box was checked for poor connectors and reflecting signals but no obvious defect was detected.

During experiment CORE-3024 the recorder brakes blocked the tape movement due to a total wear-out of the brake-disc on one of the reel-motors. The tape was damaged and the experiment could not be continued but was lost. New brake assemblies were installed at both reel motors. The old ones had been operating for some 20 years without failures.

The installation of new idle rollers is planned for the near future.

The new formatter firmware was successfully installed in the spring of 2001. The Mark IV decoder was successfully installed in the autumn of 2001 and the Field System has been upgraded to version 9.5.2 during October 2001.

References

[1] Bergstrand, S., Haas, R., and Elgered, G., "Geodetic Very-Long-Baseline Interferometry at the Onsala Space Observatory 1999–2000", In: P. Tomasi, F. Mantovani, and M. Pérez-Torres: *Proceedings of the 14th Working Meeting on European VLBI for Geodesy and Astrometry*, Instituto di Radioastronomia, Bologna (Italy), 105–106, 2000.

[2] Haas, R., Elgered, G., Bergstrand, S., Gradinarsky, L., Stoew, B., and Johansson, K.-Å., "The IVS Network Station Onsala Space Observatory", In: N.R. Vandenberg and K.D. Baver (eds.): *International VLBI Service for Geodesy and Astrometry 2000 Annual Report*, **NASA/TP-2001-209979**, 113–116, 2001.

[3] Haas, R., Elgered, G., Stoew, B., and Pettersson, L., "The IVS Technology Development Center at the Onsala Space Observatory", In: N.R. Vandenberg and K.D. Baver (eds.): *International VLBI Service for Geodesy and Astrometry 2000 Annual Report*, **NASA/TP-2001-209979**, 283–286, 2001.

Robert M. Campbell: The EVN MkIV Data Processor at JIVE, Proceedings of the 15th Working Meeting on European VLBI for Geodesy and Astrometry, p.40–45
http://www.ieec.fcr.es/hosted/15wmevga/proceedings/campbell1

The EVN MkIV Data Processor at JIVE

Robert M. Campbell[1]

Joint Institute for VLBI in Europe
e-mail: campbell@jive.nl

Abstract

The inauguration of the EVN MkIV data processor at JIVE took place at the 4^{th} EVN/JIVE Symposium in October 1998. Since then, we have been increasing the capabilities, flexibility, and reliability of the correlator, and have now processed many test, pilot, and user experiments. Milestones include the first scientific publication resulting from data correlated at JIVE: detection of HI absorption within 20 light-years of the nucleus of NGC4261. We will discuss these developments and accomplishments at the JIVE correlator, with a few concluding thoughts on processing geodetic experiments.

1. Introduction

A key item in the MkIV upgrade of the EVN was the construction of the EVN MkIV data processor at the Joint Institute for VLBI in Europe (JIVE). JIVE is hosted by ASTRON in Dwingeloo, the Netherlands, and is funded by science councils of a number of European countries. Special projects have been funded directly by the EU. The EVN MkIV data processor [1] was constructed in the context of the International Advanced Correlator Consortium through which the other MkIV geodetic correlators were also built, with significant contributions, from European members, in hardware from CNR/IRA, control software from Jodrell Bank, and correlator software from ASTRON.

The first fringe on the EVN MkIV data processor was seen on 21 July 1997 [2], and its official inauguration took place on 22 October 1998. The "first science" resulting from data correlated on the EVN MkIV data processor detected HI absorption against the counterjet very close to the nucleus of NGC4261, providing the ability to see the transition from molecular to atomic gas in the disk, and hence to say something about its thermal structure [3].

Since then, we have made a great deal of improvements in the capability and operation of the JIVE correlator. This paper will concentrate on areas of interest to the user having data correlated at JIVE: tools for planning observations with regard to the data processor's capabilities, current operational and communication flow between JIVE and the PI, and what we at JIVE do to get your data to you in a usable form. More information about using the EVN and JIVE can be found at the JIVE website: www.jive.nl. A brief concluding section looks at some of the issues relating to future processing of geodetic experiments on the JIVE correlator.

2. Capabilities

Basic characteristics of the design of the EVN MkIV data processor include: correlation of up to 16 stations with 16 channels per station, 1 Gb/s recording (via 2 head-stacks $\times$ 32 heads $\times$ 16 Mb/s/track), and use of either MkIV and VLBA format recordings. Figure 1 shows the data playback units, the station units, the data distributor unit, and control computers. The correlator itself is housed in a separate room out of this view. Various infrastructural capabilities are, or are being, integrated into an automated experiment management system; figure 2 shows a newly-arrived tape being scanned for inclusion in the tape database.

[1]on behalf of the JIVE Data Processor Group.

Figure 1. A view of the data playback units, the station units, the data distributor unit, and control computers of the JIVE MkIV Data Processor.

Figure 2. A view of principal components of the automated tape management system.

The principal science drivers behind the development of the correlator include the ability to handle continuum dual-polarization observations, spectral line experiments (*i.e.,* providing lots of frequency points and narrow bandwidths), and phase-reference mapping.

Current capabilities include:

- 2-bit sampling.
- cross-polarization.
- up to 2048 frequency points for correlation of up to 8 stations on 1 subband/polarization (see the discussion following equation 1).
- fan-out modes, where 1 channel was written onto 2 or 4 tracks during recording, increasing bandwidth without using higher tape-speeds.
- processing of MkIV, VLBA, and MkIII type recordings.
- sustained 256 Mb/s recordings, a capability that is currently unique to the EVN (see, *e.g.,* [4]) — full 1 Gb/s awaits all stations being equipped with two heads and 320 ips recording.
- Oversampling at 2 or 4 times the Nyquist frequency in order to provide bandwidths down to 500 kHz. (*i.e.,* 2 MHz ÷ 4).

Capabilities whose development is still underway or not yet fully tested include:

⊙ Multi-pass correlation (*i.e.,* of observations with >16 stations simultaneously).

⊙ Pulsar gating.

⊙ Multiple field centers (correlation of >1 phase centers in one pass).

⊙ Playback at a tape speed different than that used in recording.

Capabilities that are yet to come include:

- Phase-cal extraction.
- Sub-netting.
- Reading observations with barrel-rolling.
- Recirculation — achieving >2048 frequency points via time-sharing the correlator.
- Space VLBI.

There are two equations that are useful when planning observations that will be correlated on the EVN MkIV data processor. The first relates to total correlator capacity:

$$N_{\mathrm{sta}}^2 \cdot N_{\mathrm{sb}} \cdot N_{\mathrm{pol}} \cdot N_{\mathrm{frq}} \leq 131072 \quad (= 2^{17}). \tag{1}$$

Here, N_{pol} is the number of polarization combinations wanted in the correlation (1, 2, or 4). N_{sb} represents the number of different frequency subbands, counting lower- and upper-sidebands from the same BBC as distinct subbands, but not multiple polarizations in the same sideband (these enter via N_{pol}). The value to use for N_{sta} is "granular" in multiples of 4: *e.g.,* if you have 5–8 stations, use "8". Independent of this equation, the maximum N_{sb} is 16 (a station-unit limitation), and the maximum N_{frq} is 4096 (a single baseline/subband/polarization must fit onto a single correlator board — the full correlator comprises 32 boards grouped in 4 crates). When recirculation is operational, the constant term 131072 will be multiplied by the recirculation factor used, with N_{frq} still subject to the maximum N_{frq} limit above. You should pick the various N parameters in designing your observation such that the equation holds, otherwise you will have to compromise on at least one of them when it's time to correlate. The spectral capabilities discussed

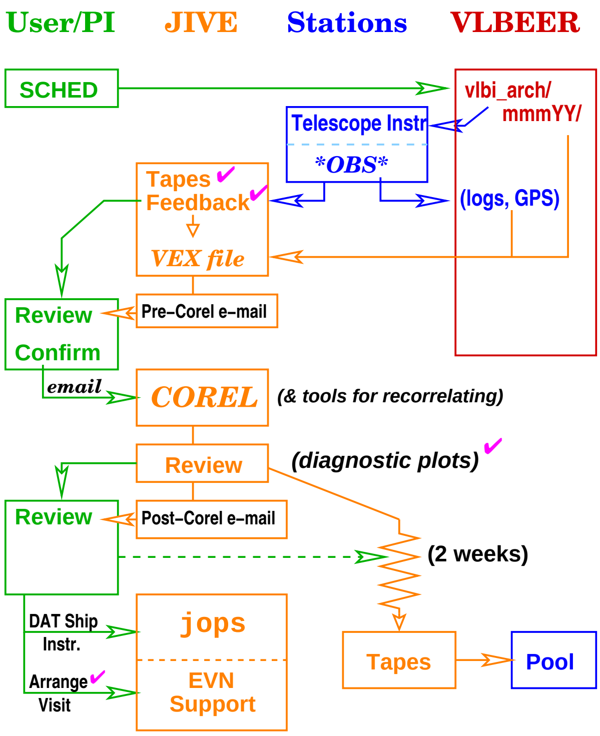

Figure 3. Operational flow for the observation and correlation of an experiment.

in this paragraph assume the of local validity, which avoids problems ensuing from the MkIV-format data-replacement headers correlating with each other in certain baseline-source geometries, but at the expense of a factor of two in $N_{\rm frq}$.

The second equation relates to output rate, $\mathcal{R}_{\rm out}$, capacity:

$$\left(\frac{N_{\rm sta}^2/2 \cdot N_{\rm sb} \cdot N_{\rm pol} \cdot 2N_{\rm frq}}{8192}\right) \cdot \frac{80}{t_{\rm int}} = \mathcal{R}_{\rm out} \quad [\mathrm{kB/s}]. \tag{2}$$

The left-hand factor above is the number of boards, $N_{\rm brd}$, required for the correlation. Our current peak output rate is ~350 kB/s, which puts a lower limit on integrations times: $t_{\rm int} \geq N_{\rm brd}/4$ s. We are working on gaining a factor of four by reading the crates out in parallel. In the future, with the Post-Correlator Integrator operational, the output rate may be as high as 160 MB/s.

3. Operational Concerns

Figure 3 summarizes operational and communication flow between the PI, JIVE, and the various EVN assets during an EVN astronomical experiment The user deposits `SCHED` output on `VLBEER`, from which individual stations draw their observing instructions. Help from JIVE may of course be requested during the scheduling process. Following the observations, the stations deposit logs and GPS data on `VLBEER`, send tapes to JIVE, and post comments to the JIVE website. We pull necessary information off `VLBEER`, prepare files that will drive the correlation, and send e-mail to the PI describing what we envision the correlation of the experiment to entail. The PI has the opportunity to review the parameters in our e-mail and all other available information (information about items with a check in figure 3 are available via the JIVE website or anonymous FTP server), and writes back to pass along any requests for changes (*e.g.*, improved source coordinates, *etc.*) and/or confirm that correlation can go ahead.

We operate the correlator 80 hours per week, from which time system testing and development

Figure 4. Activity in the JIVE visitor facility.

must also come. When correlation of the experiment is finished we review the output (as described in the following paragraph), make diagnostic plots available to the PI, send post-correlation e-mail to the PI summarizing the results of the correlation, and arrange for shipment of the resulting FITS-file DAT. Unless contacted by the PI to the contrary, we aim to release an experiment's tapes four weeks after the PI is notified of the diagnostic plots, in order to ensure the supply of tapes in the pool remains replenished. This scheme has worked well to date. Besides these review products mentioned above, the PI may also discuss the experiment/correlation with the responsible JIVE support scientist and/or arrange for visiting the EVN support group at JIVE for help in data reduction if desired. Figure 4 shows a view of visiting astronomers (representing three continents) taking advantage of some of the JIVE visitor-support facilities

Our internal data review process begins by transforming the lag-based correlator output into lag- and frequency-based AIPS++ Measurement Sets (MS). These MS contain a data-cube of the real & imaginary components of the correlation-function, spanning $N_{\rm pol}$, $N_{\rm int}$, and $N_{\{\rm lag|frq\}}$ for each subband for each baseline/autocorrelation. We can then investigate slices of the correlation functions in both time and lag/frequency, allowing us to detect and diagnose various problems with the recorded data or the correlation itself, and to determine any scans for which recorrelation would be profitable. There are also various plots more suited to providing feedback to the stations rather than to the PI (parity-error rates, sampler statistics, *etc.*). We usually flag subsets of the data for low weights and other known problems resulting in spurious correlation amplitudes and phases. The last step is converting the final MS into a FITS file, which can be read into AIPS directly using `FITLD`.

As of 1 October 2001, we have completed correlation of 57 user and 28 test experiments. A further 13 user and 4 test experiments were then under post-correlation review, in the process of running, or in the queue. Eight user experiments were on hold awaiting specific correlator features. A total of 44 different PIs from 15 different countries are represented among the user experiments.

4. Geodetic Considerations

As mentioned in the itemized list of current and future capabilities in § 2, we can not yet extract phase-cal tones. Without this capability, computation of multi-band delays required for geodetic processing would be slowed by necessitating the determination of manual phase-cal phases.

More importantly, output data format remains a major issue. For geodetic or astrometric experiments, the final desired product is a time-series of "totals" for multi-band delay, (phase) delay rate, and possibly phase delay for each baseline. Here, "total" denotes that the correlator model, which shifted and slowed down the fringes sufficiently to allow correlation over a reasonable integration time and number of lags, has been added back into the correlator (model-residual) output. These totals are then used as constraints in one the various estimation software packages (*e.g.,* `CALC/SOLV`, `OCCAM`, `MODEST`, `SPRINT`, `VLBI3`, *etc.*) to refine various subsets of the model parameters (Earth orientation, shape, and rotation; tropospheric propagation; for astrometry, source position). The correlator outputs lag-based correlation-function data in a JIVE-specific binary ("CDF") format. This format has no relation to the root/corel/fringe file and record structure inherited from the MkIII type 50/51/52 files, and which feed directly into HOPS for fringe-fitting (`fourfit`) and exporting totals (`fringex`). Of course, this variance of correlator-output binary formats is not an unprecedented occurrence: data processed on the VLBA correlator also do not have a direct way into HOPS — the resulting FITS files need to be processed through AIPS in order to obtain the desired totals data-files for final geodetic/astrometric analysis.

Our FITS files can follow the same path as those from the VLBA correlator. We both use a `CALC`-based fifth-order polynomial as the correlator model. However, for recovery of totals, we first need to gain the capacity to write the associated AIPS MC and IM tables, which in broad terms hold, respectively, the `CALC` output and the polynomial coefficients per station. We currently save the model polynomials used by the station units to use in automatically flagging data at times corresponding to specific *a priori* baseline/source geometries (*e.g.,* rates ∼0 allow phase-cal tones to correlate against each other), but they do not currently find their way into the Measurement Set (nor, hence, into the FITS data). `CALC` output was extracted separately during testing a few years ago, and could be reinstated. Even so, validation of the data path through FITS will require a substantial amount of verification, as was needed for the VLBA. EVN document #68 [5] discusses various aspects of data output formats and consequences on processing for other possible paths to totals, notably reproducing HOPS-compatible file structure.

References

[1] Casse, J. L., The European VLBI Network MkIV Data Processor, in *Proceedings of the* 4^{th} *EVN/JIVE Symposium*, eds. M.A. Garrett, R.M. Campbell, & L.I. Gurvits, *New Astron. Rev.*, **43**, 503–508, 1999.

[2] Phillips, C. J. & Van Langevelde, H. J., Fringes on the EVN MkIV Data Processor at JIVE, in *Proceedings of the* 4^{th} *EVN/JIVE Symposium*, eds. M.A. Garrett, R.M. Campbell, & L.I. Gurvits, *New Astron Rev.*, **43**, 609–612, 1999.

[3] Van Langevelde, H. J., Pihlström, Y. M., Conway, J. E., Jaffe, W., & Schilizzi, R. T., A Thin Hɪ Circumnuclear Disk in NGC4261, *Astron. & Ap.* **454**, L45–48, 2000.

[4] Garret, M. A., Muxlow, T. W. B., Garrington, S. T., *et al.*, "EVN Observations of the Hubble Deep Field", *Astron. & Ap.*, **366**, L5–8, 2001.

[5] Van Langevelde, H. J. & Noble, R., JIVE/EVN Correlator Output: Formats & Diagnostic Tools, *EVN Document #68*, 1996.

Walter Alef and Arno Müskens: Status of the MPIfR-BKG MK IV correlator, Proceedings of the 15th Working Meeting on European VLBI for Geodesy and Astrometry, p.46–49
http://www.ieec.fcr.es/hosted/15wmevga/proceedings/alef

Status of the MPIfR-BKG MK IV correlator

Walter Alef [1], *Arno Müskens* [2]

[1] *Max-Planck-Institut für Radioastronomie*
[2] *Geodätisches Institut der Universität Bonn*
Contact author: Walter Alef, e-mail: `walef@mpifr-bonn.mpg.de`

Abstract

A summary of the present status, capabilities and usage of the MK IV VLBI correlator in Bonn is given. MPIfR's plans for MK 5 data acquisition/playback units for Effelsberg, mm-VLBI and the correlator will be discussed.

1. Introduction

The MK IV correlator in Bonn is jointly operated by the MPIfR[1] and the BKG[2]. It is a major correlator for MPIfR's astronomical projects, the CMVA[3], and geodetic observations. After the installation in December 1999 production correlation was started a few months later. The initially incomplete correlator software has been upgraded since the installation by Haystack under contract with NASA, USNO, and BKG.

2. Improvements Since The 14th Meeting

A fairly detailed description of the MK IV correlator system is given in the report of the 14th Working Meeting on European VLBI for Geodesy and Astrometry[1]. Nearly all of the missing features of the correlator software which were known at that time have been implemented by the time of the 15th meeting.

The correlator software can now handle all 9 tape units in a correlator mode with 32 lags, auto-correlations and 1 s pre-averaging. Full polarization correlation is possible with 8 stations simultaneously. For spectral line resolution correlator modes with up to 4096 lags are available. This drives the correlator control computer (CCC) to its limits. To be able to process the data from 9 tape drives simultaneously a second HP workstation had to be acquired for correlation setup, data inspection, fringe-fitting, and data export. Also the amount of correlated data grew so much that the disk space had to be increased to a total of about 200 GBytes.

A big improvement in throughput was achieved by the introduction of parallel correlation streams. This means that up to 4 independent experiments or sub-nets can be processed simultaneously, provided a sufficient number of tape drives is available. Geodetic and mm VLBI observation with a lot of sub-netting can be correlated more efficiently. Also the introduction of better pass/track finding software, including a data base of pass positions for each tape, can be counted as a big improvement for the correlation, as well as numerous bug fixes.

In the middle of 2001 the correlation of mm VLBI observations became possible with the introduction of switchable equalizers for normal and double speed recordings in all tape units. The present version of the correlator software cannot handle speed-up factors other than 1 so that recordings can only played back at the speed at which they were recorded. With this improvement mixed correlation of 4 and 8 Mbit/s/track modes is possible. Another upgrade that was necessary

[1] Max-Planck-Institut für Radioastronomie, Bonn
[2] Bundesamt für Kartographie und Geodäsie, Frankfurt
[3] Coordinated mm VLBI Array

to reduce the backlog of mm VLBI correlation drastically was the fine tuning of the tape synchronisation: the time needed to synchronize the tapes was reduced to less than 10 s for all playback speeds. Another important milestone is the extraction of 510 kHz phase-cal tones, as are often used in mm VLBI. It is even possible now to extract any phase-cal frequency in steps of 10 kHz.

Better data inspection software written by members of the geodetic correlator group in Bonn, as well as software for automatic generation of re-correlation lists, further increased the throughput of geodetic correlation.

In the summer of this year finally data export became possible for astronomical observations by the introduction of the program MK4IN written at MPIfR and a new version of FOURFIT. In a first step a best data set without duplicates is selected using the HOPS software (Haystack). The data are fringe-fitted with FOURFIT in a special mode where the cross-spectrum of each accumulation period of each frequency channel is stored on disc. These cross-spectra are fully "sanitized" by applying all correlator flags, and all phase-corrections like phase-cal and lower-/upper-sideband corrections. The resulting data file is read by the AIPS[4] task MK4IN, and is stored as an AIPS disk file. AIPS allows fringe-fitting, calibration and mapping of the data. For sending data to other observatories the data can be written to tape (or disk) in FITS[5] format.

An up-to-date list of correlator capabilities can be found on the Internet under http://www.mpifr-bonn.mpg.de/EVN/MK4CORstatus.

3. Problems

3.1. Correlator

The 4 data input boards of the correlator show a fairly high failure rate of input channels. Each board has 16 input channels of which 9 are connected to the 9 tape units. In most cases an already obsolete chip is the reason for the failure. It is not clear whether the present supply of these chips will be sufficient in the future.

The correlator hardware is fairly stable; so far we had 2 correlator chips fail. When the correlator has been powered down it is often difficult to resynchronize the high speed data links between the correlator and the station units.

3.2. Station Unit

The station unit software (and hardware) is the most fragile part of the MK IV data processor. About every 10 to 20 scans the SUIM (station unit interface to the correlator) transmits faulty data, so that the scan being correlated has to be repeated. There are a few less frequent failures which can be identified on the operator screen during correlation. A very annoying problem is that under some conditions data bytes of some channels are labeled with a time which is off by 1 byte. This leads to a delay shift in this channel, which can only be seen in the fringe-fitting process, provided the fringes are of sufficient strength.

3.3. Computers

The Correlator Control Computer and the correlator crate computers are not fast enough to handle 9 stations with less than 1 or 2 s pre-averaging or more than 32 lags. This seems to be mostly a restriction in the data output rate of the correlator. While CCC could be replaced by a faster computer the crate computers cannot.

[4] Astronomial Image Processing System, NRAO

[5] Flexible Image Transport System, NRAO, see e.g. [2] and references therein

3.4. Software

The biggest worry in the software area is that the contract with Haystack for upgrading the software will end September 30, 2001. It is not clear how the remaining bugs can be removed, and how necessary improvements in the software can be made in the future. For example the operator interface sometimes hangs, and for pass finding too much manual interaction is needed; in addition there are various other problems that reduce the efficiency of the correlation process.

4. Correlation Statistics

The correlator is operated on average for 15 hours on 7 days per week. In 2001 data has been correlated during 50% of the total wall clock time. This efficiency is close to the maximum of about 60% which was reached with the MK III correlator. Up to the time of the meeting 19 astronomical and 36 geodetic observations were correlated. For the whole year it is expected that about 50 geodetic observations will be processed, which is 1/3 of the worldwide geodetic correlation. The ratio of correlation time is high time over observing time is very good; it is in the range between 1 to 2 for single pass correlation.

The present performance is achieved with 2 full time operators and 12 student operators, 10 of which are being paid by the geodesists. The geodetic observations are supervised by the equivalent of 2.75 people. The correlator hardware is maintained by 2 engineers and 1 technician, while the manpower which goes into software is more than 50% of the time of one of the operators and a small fraction of one scientist. The group is lead by one scientist. The 2 scientists are also responsible for supervising the correlation of astronomical projects.

5. Wish-list for Improvements

Further improvements in the correlator software are needed to bring the data processor closer to the original specifications. The implementation of speed-up factors other than 1 is being worked on at Haystack. The same is true for better pass finding software which will utilize the information written into the AUX-fields of the data on tape.

The correlator throughput could be increased if a continuous correlation mode was implemented. At present a scan-wise mode is used in which each observed scan is set up for correlation and is then correlated. In a continuous mode the scan boundaries are not "visible" to the correlator, the tapes are kept running, and the set-up time for each scan drops out. Only later the data is split again into scans. This mode is implemented at NRAO and JIVE.

Other missing features are:

- Pulsar gating.
- Extraction and application of a second phase-cal tone. A second phase-cal tone would remove the difference between single- and multi-band delays.
- Software for checking the correlator hardware in situ.

... and of course more bug fixes.

At MPIfR we are working on the next version of MK4IN which will have optional transfer of the FOURFIT solutions to a so called BS-table and of the correlator model to the CL-table.

6. MK V

After Haystacks' successful tests of a prototype disk-based VLBI system it became clear that when a few more logistical and technical problems have been solved, MK V VLBI systems will rapidly replace the difficult-to-maintain and expensive MK IV and VLBA systems.

MPIfR decided to financially support Haystack in the development of the MK V A and the MK V B systems. The major advantage of MK V for MPIfR's scientific projects is in the higher bit-rate of up to 1 Gbit/s per unit. With MK V B two units can be used in parallel to record a maximum of 1.8 Gbit/s with 14 BBCs, which is essential for future progress in mm-VLBI.

In 2002 we want to install at least two MK V units for test purposes. After a successful test phase, more units will be acquired, both for the correlator and for mm-VLBI.

References

[1] Alef, W., Graham, D.A., Zensus, J.A., Müskens, A., Schlüter, W., "The new MPIfR-BKG MK IV correlator", in Proceedings of the 14th Working Meeting on European VLBI for Geodesy and Astrometry, edited by P. Tomasi, F. Mantovani, M. Perez Torres, Consiglio Nazionale delle Ricerche - Istituto di Radioastronomia, 2000.

[2] Cotton, W. D., Tody, D. B., and Pence, W. D., Binary Table Extension to FITS, Astronomy and Astrophysics Supplement Series, 113, 159-166, 1995.

Arno Müskens: Improvements of the Geodesy MK IV Correlation during the Last Year, Proceedings of the 15th Working Meeting on European VLBI for Geodesy and Astrometry, p.50–54
http://www.ieec.fcr.es/hosted/15wmevga/proceedings/mueskens

Improvements of the Geodesy MK IV Correlation during the Last Year

Arno Müskens

Geodetic Institute of the University of Bonn
e-mail: mueskens@mpifr-bonn.mpg.de

Abstract

A short overview on the correlation status and the improvements of the MK IV correlator at the *Max–Planck–Institute for Radioastronomy (MPIfR)* in Bonn is given. We explain in which way and how they are essential for present and future MK IV correlation progress and throughput.

1. Introduction

The new MK IV correlator was installed at the *MPIfR* in December 1999. The correlator is used partly by the *MPIfR* for astronomical observations and partly by the *Bundesamt für Kartographie und Geodäsie (BKG)* in cooperation with the *Geodetic Institute of the University of Bonn (GIUB)* for geodetic applications. In the first months of operations different correlator sites reported about the teething problems of the new correlator, which of course had to be expected with an entirely new system of such high complexity. From July 2001 we had a nine station correlator capable of processing all 36 baselines with 16 tracks including phasecal.

2. Main improvements since the last year

At first let me explain two of the main software bugs which were fixed in the first months of MK IV operation. On our last 14th Working Meeting at Castel San Pietro near Bologna (Italy), we reported that we had found inconsistencies between the FOURFIT results of the same dataset processed with MK III and MK IV.

We detected in some scans with SNR lower than 20 divergences in some of the processed frequently channels. The reason was that the SNR, which was calculated from the fringe amplitude and the total number of AP's, was in cases of 'non detections' often too high and the quality code of '9' follows from the high SNR. In some cases FOURFIT can turn a non-detection into an apparent detection, or could influence the delay estimation. The new plots show us that the updated FOURFIT version now yields correct delay estimations as compared to the older MK3 FRNGE outputs (see Fig. 1).

2.1. Subnetted observations or 'streamlined processing'

Subnetting is a special observing mode which is frequently used in geodetic experiments. Due to different visibilities of different participating stations, we have to use as much as possible different sky directions on different stations.
In generating the schedule special considerations has to be given to a number of points:

- the most recent source flux models are used
- SNR goals are about 20 at X- and S-band for all baselines
- observations are weigthed by their expected SNR's

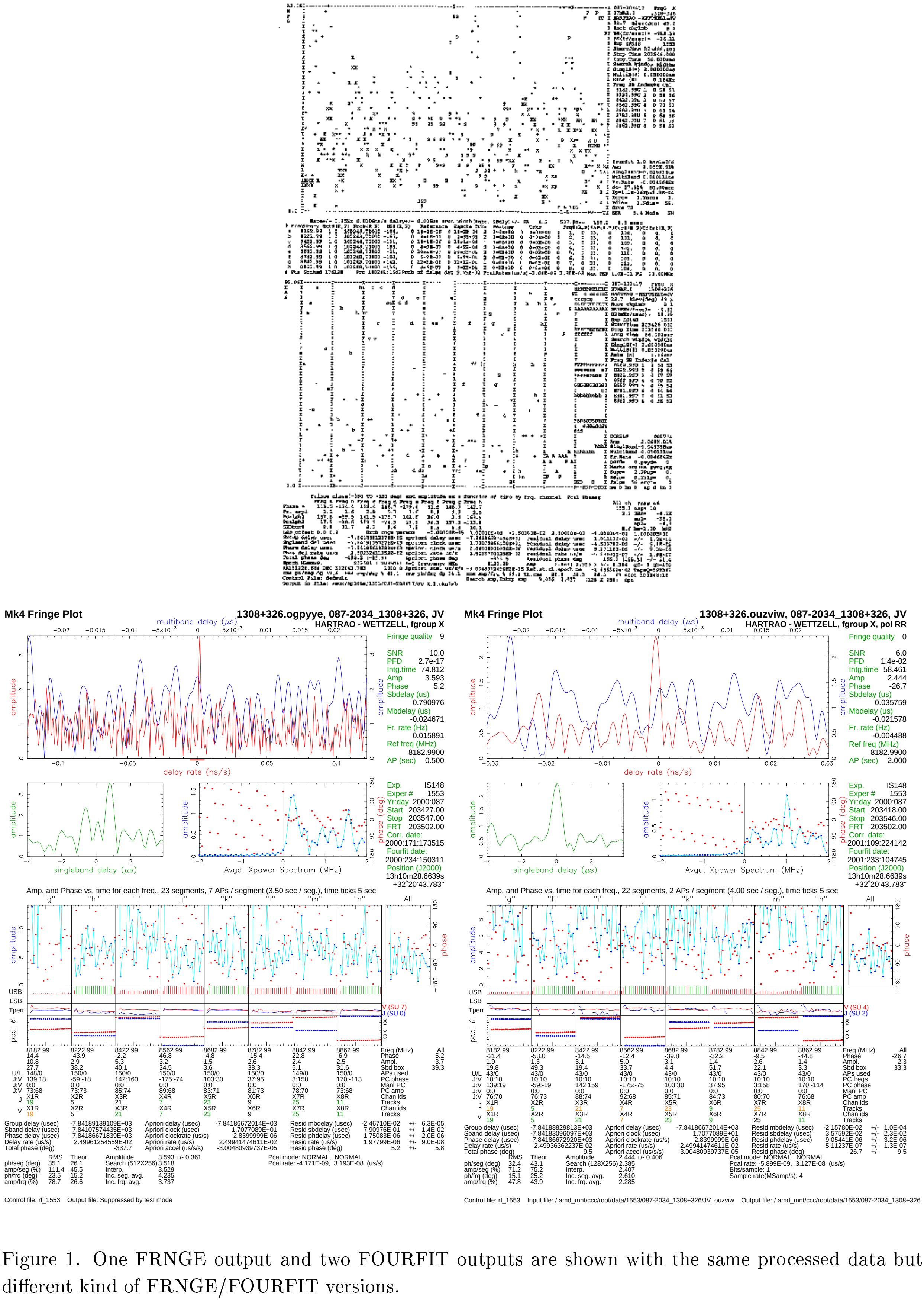

Figure 1. One FRNGE output and two FOURFIT outputs are shown with the same processed data but different kind of FRNGE/FOURFIT versions.

- maximum number of observations in a minimum of time (scan)
- optimal sky coverage
- using a large number of sources (50-70) improving the sky coverage

In order to achieve these goals a schedule with subnetted observations or subconfigurated networks has to be set up. Consequently we will have two or three observations with up to 2 to 3 station looking at different sources simultaneously, often with different recording durations. This typically results an observation schedule with a large number of subnetted observations and/or subconfigured 'mini' networks.
Since July this year, we have the possibility to correlate all these subnets and observations simultaneously in one pass with the MK4 processor (multiple pass processing).
Consequently the amount of required processing time could be significantly reduced.

2.2. Faster synchronisation

The exchange of the more than 15 year old MK III system to the newly developed MK IV hardware and software system allows faster synchronisation on up to 9 playback stations which was in some case similar to 4 playback MK III system. Therefore we are able to further reduce scan duration times to a minimum during scheduling which allows up to 10% more observations for an entire experiment.

3. Throughput reduction

All of the above mentioned improvements allows us to reduce the so called processing factor (PF) by 20% - 40% depending on the subnetting of the processed experiment. We can see that different experiments have different PF factors, depending on the amount of subnetting. The main contribution is achieved by the 'streamlined processing' :

- EUROPE has no more than 10 to 15 % PF reduction
- CORE-3 yields 15 to 20% PF reduction
- IRIS-S has around 35% PF reduction

4. SNR Comparison between MK III and MK IV

The following plot (Fig. 2) compares the SNR achieved with the MK III and MK IV system and displays the difference in SNR for all scans (S/X) excluding all FQC of '0'. We can see that in general MK IV has an increased SNR of about 3 % compared to the MK III system.
A better and faster synchronisation results in most processed scans in an increased number of AP's (Accumulation Periods) for all baselines and frequencies (S/X). This should be the reason that we can see a small but significantly higher SNR on all scans. Some scans may differ on a bigger scale depending on many different processing and reprocessing reasons. One example for different SNR's could be the observation of a strong source (60 sec. and 4C38.25) which can bring us a different in SNR by 20 or more. A few data points less or more due to better synchronisation could have a strong impact on the SNR result.

5. Processing goals and outlook

Due to the fact that we have a 50/50 percentage of usage time at the Bonn correlator, from the geodesy side we permanent try to reduce the processing time and work to an optimal level for

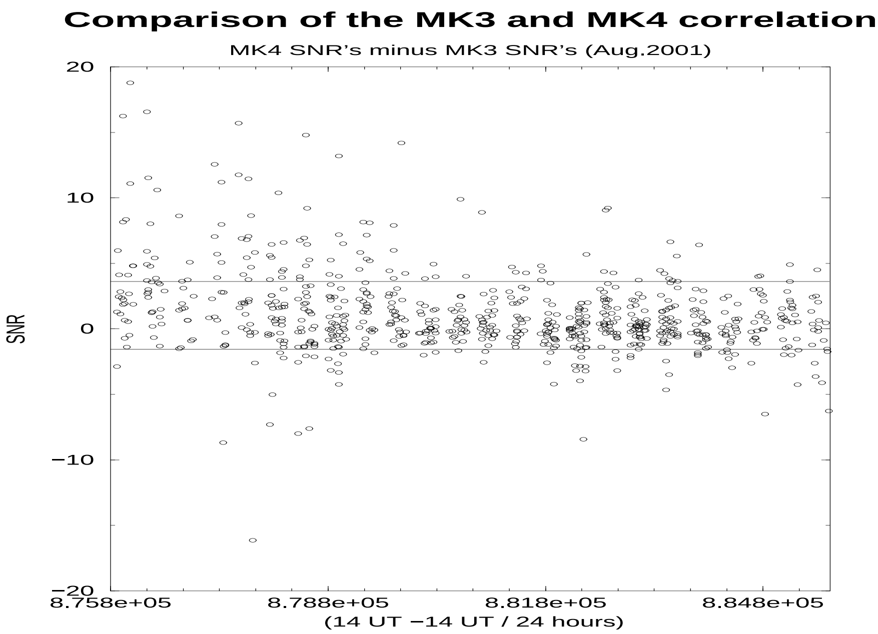

Figure 2. SNR comparison between MK III and MK IV correlation.

supervision, correlation analysis and as well as for the whole correlation process from logistics till the final creation of the database version 1.
Students are a valuable help for routine operations and night hours processing, but require more time and supervision compared to contracted and well trained operators. Station problems and observation faults are one of the most critical problems we have to deal with on the processor side, which cause a higher processing factor as desired.
In the next years, new technology improvements like the MK V system will allow even higher data rate recordings and will improve station and correlator reliability and efficiency by reducing a huge number of possible problems which is caused at present mainly by the tape recording and tape technology. MK V and e-VLBI will reduce the time delay between observation and the final IVS results.
The permanent verification and improvement of our correlator operations have to be adjusted to the future technology and develepments. In the future we expect a shift away from the experimental phase towards a service oriented routine operation.

References

[Alef W, Graham D A, Zensus J A, Müskens A, Schlüter W (2000)] The Bonn MK IV Correlator Project, Proceedings of the First IVS General Meeting, N.R.Vandenberg and K.Baver, Eds., NASA Center for AeroSpace Information, 7121 Standard Drive, Hanover, MD 21076–1320, Publ.No. NASA/CP-2000-209893.; p.210-214

[Kingham K A, Martin J O (2000)] Early Experiences with the Mark 4 Correlator, Proceedings of the First IVS General Meeting, NASA Center for AeroSpace Information, 7121 Standard Drive, Hanover, MD 21076–1320

[Müskens A, et al (2000)] Comparison of MK III and MK IV Correlation using a 4-station IRIS-S experiment, Proceedings of the 14th Working Meeting on European VLBI for Astronomy and Geodesy, Castel San Pietro Terme / Italy), Edit by : P.Tomasi, F. Mantovani, M. Perez Torres; p.125-136

[Nothnagel A (2000)] VLBI Data Analysis User's Guide, (unpublished)
[Nothnagel A (1997)] On the Effect of Missing Tracks, Proceedings of the 12th Working Meeting on the European VLBI for Geodesy and Astrometry, Edited by Bjorn R. Pettersen, Statens Kartverk Geodesidivisjonen, p.66-73

Zinovy Malkin: On Computation of Combined IVS EOP Series, Proceedings of the 15th Working Meeting on European VLBI for Geodesy and Astrometry, p.55–62
http://www.ieec.fcr.es/hosted/15wmevga/proceedings/malkin1

On Computation of Combined IVS EOP Series

Zinovy Malkin

Institute of Applied Astronomy of Russian Academy of Sciences (IAA)
e-mail: malkin@quasar.ipa.nw.ru

Abstract

Three topics related to computation of the combined IVS EOP series are discussed. The first one is the consistency of the VLBI EOP series with the IERS reference frames ITRF and ICRF. Not all IVS analysis centers use ITRF/ICRF as reference system for EOP solutions. Some of them realize global solution for simultaneous determination of CRF, TRF and EOP with no-net-rotation constrains w.r.t. ITRF/ICRF. Analysis shows that such a method can hardly provide consistency of computed EOP series with the IERS reference frames with sufficient accuracy. Direct use of ITRF and ICRF for computation of EOP series submitted to the IERS seems preferable. Second problem is the long-time stability of the IVS EOP series. Analysis of yearly biases w.r.t. C04 and NEOS is presented. A possible ways are proposed to save long time stability of the combined IVS EOP series. At last, various strategies of computation of weighted mean value are considered. It's shown that usual methods used for this purpose do not provide satisfactory result for the error of the mean. A new method is proposed.

1. Introduction

The IVS combined EOP series computed at the IVS Analysis Coordinator Office located at the Geodetic Institute of the University of Bonn is available beginning from the end of 2000. Analysis of this series routinely provided by the IERS EOP Product Center at the Paris Observatory shows that its accuracy is better than accuracy of individual solutions provided by the IVS Analysis Centers. However, some topics related to the quality of the IVS combined EOP series seems to be investigated more carefully. This paper is intended to consider the following points:

- Consistency of the VLBI EOP series with the IERS reference frames ITRF and ICRF.
- Systematic stability of the VLBI EOP series.
- Computation of weighted mean values.

2. Consistency of the IVS EOP series with the IERS reference systems

According to the IVS Terms of Reference, IVS serves as the VLBI Technique Center for IERS. In turn, the IERS Terms of Reference said that one of the IERS primary objectives is providing Earth orientation parameters (EOP) required to transform between ICRF and ITRF. It is supposed that after completion of new IERS structure the IERS EOP product will be computed combining several EOP series delivered by the IERS Technique Centers one of which is the IVS. So, the evident goal of the IVS is computation of the combined IVS EOP series providing the transformation parameters between ITRS and ICRS.

However, not all IVS analysis centers use ITRF/ICRF as reference system for EOP solutions. Some of them realize global solution for simultaneous determination of CRF, TRF and EOP. To tie a global solution to IERS reference frames no-net-rotation constrains w.r.t. ITRF and ICRF are usually applied. The question is can such a method provide the consistency of VLBI EOP series with ITRF/ICRF with required accuracy?

Usually global VLBI solution is made using all available sessions and application of no-net-rotation provides zero translation and rotation of full set of stations and radio sources w.r.t. ITRF and ICRF. However, commonly speaking, it is not the case for the subset of stations participating in a particular session. Therefore EOP estimate obtained from processing of a session observations may systematically differ from ITRF/ICRF.

Besides, number of observations for stations and sources differ very much. Table 1 shows statistics of observations for stations and sources for all sessions and for NEOS-A ones. One can see that in fact the NEOS-A EOP series used in the IVS combined solution is practically defined by subset of 8 stations and 66 radio sources.

Table 1. Statistics of observations (Nobs in thousands).

NEOS-A				All sessions			
Stations		Sources		Stations		Sources	
Nsta	Nobs	Nsou	Nobs	Nsta	Nobs	Nsou	Nobs
5	100–200	11	10–30	15	100-700	14	50–200
3	50–100	25	5–10	32	10–100	49	10–50
7	1–6	39	1–5	52	1–10	76	1–10
6	< 1	95	0.1–1	50	< 1	299	0.1–1
		177	< 0.1			341	< 0.1

Let us see how close is the tie between different subsets of station and source catalogs with ITRF/ICRF. We use results of the USNO9903 global solution as most fresh publicly available one. Tables 2 and 3 present transformation parameters between USNO solution and ITRF(ICRF) for all common stations (sources), for all stations (sources) participating in the NEOS-A program, and for most frequently observing stations (observed sources). These data show that the transformation parameters including ones defining EOP system are not equal to zero and differ for various subsets of stations and sources. This mean that EOP system is not correspond to ITRF/ICRF and differ for various observational programs.

Therefore, CRF and TRF realization obtained from a global VLBI solution can hardly provide consistency of computed EOP series with ITRF/ICRF with sufficient accuracy. Direct use of the ITRF and ICRF for computation of EOP series submitted to the IERS seems preferable.

This does not mean indeed that the IVS Analysis centers should not compute global solutions. The reasonable strategy may be using individual CRF and TRF realizations for improving the IERS reference frames, and further using ICRF and ITRF for regular EOP computation. This strategy provides consistency between VLBI EOP series and the IERS reference frames and makes individual VLBI EOP series more homogeneos that allows to simplify combination procedure and improve quality of the IVS combined product.

Now the IERS and main space geodesy services are in the process of moving from ITRF97 to ITRF2000. What systematic changes in the VLBI EOP series can we expect? Table 4 shows the results of comparison between ITRF97 and ITRF2000 for different subsets of VLBI stations.

We also compared the EOP series computed at the IAA with ITRF97 and ITRF2000. The result is shown in Table 4. The computation was made with three radio source catalogues ICRF-Ext.1, RSC(IAA)99R02 and RSC(IAA)01R02, and no meaningful systematic differences between EOP series computed with ITRF97 and ITRF2000 was found.

Although ITRF2000 was constructed in such a way that no rotation w.r.t. ITRF97 was introduced, substantial value of rotation angle R2 (which corresponds to Y pole coordinate) is found both in direct comparison of two coordinate systems and in the result of EOP computation.

In conclusion, it's important to mention that errors of inconsistency between EOP series and terrestrial and celestial reference frames are systematic ones and even their relatively small values can be substantial.

Table 2. Transformation parameters between the TRF realizations USNO9903 and ITRF97 at epoch 1997.0 for different number of stations.

N sta	85	20	8
T1, mm	–0.1	–0.9	–2.2
σ	0.8	1.6	1.9
T2, mm	–1.6	–1.4	–1.3
σ	0.8	1.7	2.0
T3, mm	–0.6	–0.4	–0.3
σ	0.8	1.6	1.8
D, ppb	1.7	1.5	0.8
σ	0.1	0.2	0.2
R1, mas	–0.06	–0.05	–0.03
σ	0.03	0.07	0.08
R2, mas	0.01	0.02	0.08
σ	0.03	0.05	0.06
R3, mas	0.00	0.03	0.00
σ	0.03	0.05	0.06

Table 3. Transformation parameters between the CRF realizations USNO9903 and ICRF-Ext.1 for different number of sources.

N sou	626	303	66
A_1, mas	0.029	0.022	0.013
σ	9	9	7
A_2, mas	0.027	0.018	0.013
σ	9	8	7
A_3, mas	–0.018	–0.016	–0.013
σ	9	9	12
D_α, mas	–0.001	–0.001	0
σ	0	0	0
D_δ, mas	0	0	–0.001
σ	0	0	0
B_δ, mas	0.054	0.042	0.086
σ	9	10	12

Table 4. Transformation parameters between ITRF97 and ITRF2000 at epoch 1997.0 for different number of VLBI stations (98, 20, 8), nominal transformation parameters defined by the IERS (P_0) and systematic differences between EOP series computed with ITRF97 and ITRF2000 with the OCCAM package.

N sta	98	20	8	P_0	OCCAM
T1, mm	6.9	7.8	7.8	6.7	
σ	0.5	0.9	1.4		
T2, mm	3.9	3.9	3.6	6.1	
σ	0.5	1.0	1.6		
T3, mm	–20.2	–20.1	–21.3	–18.5	
σ	0.5	0.9	1.4		
D, ppb	1.5	1.3	0.9	1.55	
σ	0.1	0.1	0.2		
R1, mas	–0.17	–0.19	–0.20	0.0	–0.15
σ	0.02	0.04	0.06		0.02
R2, mas	0.01	–0.01	–0.01	0.0	0.09
σ	0.02	0.03	0.05		0.02
R3, mas	–0.01	–0.03	–0.03	0.0	–0.07
σ	0.02	0.02	0.04		0.01
$\dot{R}3$, mas/y				–0.02	–0.03
σ					0.02

3. Long-time stability of the IVS EOP series

Obviously, one of the main goal of maintenance of the IVS combined products is to provide systematically stable IVS EOP series. It is especially important now because the new IERS organization envisages computation of the IERS combined EOP series practically of the three series VLBI, GPS and SLR, and importance of each of them is very large. Several factors make this task difficult and in the first place it is instability of individual series. The main reason for that are:

- Using individual periodically updated TRF and CRF realizations. As shown in the previous section these realization are not tied to the unique (IERS) reference frames with sufficient accuracy and, in fact, every VLBI session yields EOP estimates in its own system.
- Change in systematic errors of EOP series after modification of models, algorithms and software.
- Change of set of contributed VLBI Analysis Centers. Besides a difference in used reference systems, each EOP series has its own systematic peculiarities.
- Change of network configuration. This is well established fact, and it is not quite clear how to handle it properly. For instance, we can mention the problem of joining 9-year IRIS-A and 8-year NEOS-A programs to avoid EOP jump directly affected results of determination of 18.6-year nutation term.

For listed above and other reasons the VLBI EOP series show long-time instability. To investigated this effect we use five VLBI EOP series BKG00001, GSF2000A, IAAO9907, SPU00001, USN99003 over a 7-year interval from May 1993 till April 2000 (NEOS-A data only). The whole 7-year interval was split in 7 one-year ones and each series was compared with combined C04 and NEOS series at these one-year intervals. During computation six parameters of systematic differences between VLBI and combined series were estimated for every year. These are: bias, rate, amplitude of sine and cosine of annual term and semiannual terms. In such a way we obtained seven values for each of six parameters of model of systematic errors for each VLBI series. The final step of this analysis was the computation of RMS values from seven epochs. Such a approach to investigation of long-time stability is analogous to a method used at the Paris observatory during computation of the IERS combined products. Result of analysis of yearly biases is presented in Table 5.

Obviously, this analysis cannot be fully objective because it depends on details of combination procedure (systematic corrections, weights, etc.) used during computation of C04 and NEOS series. One can see that differences between the left and the right parts of Table 5 is sometimes quite large, especially for UT1-UTC. Maybe using IVS combined EOP series for such a analysis would be preferable when it will have sufficient time span.

The results of analysis presented here and in the previous section confirm well known fact that each EOP series has own systematic errors and these errors are not stable at the required level of accuracy. Therefore it seems very important to develop appropriate strategy for computation of the IVS combined product to provide make its systematic stability. We would like to propose for discussion a possible strategy to keep long-time systematic stability of the IVS EOP combined series. This strategy includes the following steps.

1. Computation of the "reference" EOP series EOP_0 as the mean of existing long-time NEOS-A series *fixed at epoch of computation* with weights depending on long-time stability. Input series should be transformed to uniform TRF/CRF (preferably the IERS ones) as accurate as possible.

Table 5. Long-time stability of IVS EOP series (NEOS-A): statistics of yearly bias relative to the IERS C04 and NEOS combined series (7 years 1993.3–2000.3): bias, rate - result of approximation of yearly bias series by linear trend, rms - rms of residuals after removing trend.

		C04					NEOS				
EOP		BKG	GSF	IAA	SPU	USN	BKG	GSF	IAA	SPU	USN
X	bias	0.064	−0.088	−0.126	−0.074	−0.096	0.080	−0.071	−0.111	−0.058	−0.081
mas	rate	0.011	0.015	−0.002	0.002	0.009	0.034	0.037	0.021	0.024	0.032
	rms	0.025	0.026	0.025	0.027	0.023	0.034	0.028	0.041	0.034	0.036
Y	bias	−0.249	0.015	−0.065	−0.030	−0.034	−0.269	−0.004	−0.078	−0.043	−0.048
mas	rate	0.064	−0.003	0.052	0.049	0.043	0.064	−0.002	0.056	0.052	0.046
	rms	0.040	0.031	0.049	0.043	0.044	0.052	0.041	0.054	0.050	0.051
UT1	bias	0.101	−0.020	−0.037	−0.232	−0.041	0.163	0.038	0.025	−0.170	0.024
0.1 ms	rate	0.018	−0.056	−0.014	0.018	−0.003	0.010	−0.062	−0.016	0.014	−0.008
	rms	0.026	0.020	0.022	0.018	0.019	0.044	0.048	0.055	0.062	0.050
dPsi	bias	−0.066	−0.049	−0.061	0.030	0.080	0.066	0.087	0.072	0.165	0.212
mas	rate	−0.028	−0.014	0.013	0.002	−0.025	−0.009	0.006	0.027	0.016	−0.009
	rms	0.087	0.083	0.031	0.054	0.060	0.056	0.040	0.049	0.055	0.031
dEps	bias	0.001	−0.008	0.047	−0.021	−0.043	0.037	0.027	0.085	0.021	−0.002
mas	rate	0.006	−0.005	0.007	−0.012	−0.009	0.013	0.002	0.015	−0.003	−0.001
	rms	0.020	0.009	0.031	0.031	0.016	0.027	0.016	0.039	0.042	0.022

2. Using systematic corrections to individual series

$$dEOP_i = EOP_0 - EOP_i$$

derived from comparison with the reference series in further computations.

3. When an AC_i updates EOP series new systematic correction can be computed as

$$(EOP_{i,old} - EOP_{i,new}) + dEOP_i \ .$$

4. When a new EOP series of a new AC is to be included in the IVS combination systematic correction to that series will be

$$dEOP_j = EOP_0 - EOP_j \ .$$

5. Periodical update of the reference series, *e.g.* when new ITRF or ICRF realization is accepted. Evidenly, in such a case appropriate care of careful tie between the new and the old reference series must be taken.

A separate problem is the transformation of EOP obtained on different networks to the reference series. However, hopefully improvement of ITRF and models of VLBI observations will eliminate this problem in the future.

4. Computation of weighted mean

Computation of the weighted mean of several estimates is usually the final step in each EOP (and all others) combining procedure. Let we have n values x_i with associated errors s_i, $i = 1 \ldots n$. Then we have a well known statistics [1, 2]

$$p_i = \frac{1}{s_i^2} \,, \qquad p = \sum_{i=1}^{n} p_i \,, \qquad x = \frac{\sum\limits_{i=1}^{n} p_i x_i}{p} \,,$$

$$H = \sum_{i=1}^{n} p_i (x_i - x)^2 \;=\; \sum_{i=1}^{n} \left[\frac{(x_i - x)}{s_i} \right]^2 , \quad \chi^2/dof = \frac{H}{n-1} \,,$$

where x is a estimate of the mean value. The question is how to estimate error σ of the mean? Two classical approaches are:

Maximum likelihood approach if σ_i are considered as absolute magnitudes of errors in x_i:

$$\sigma_1 = \frac{1}{\sqrt{p}} \,.$$

Least squares approach if σ_i are considered as relative values of errors in x_i and error of unit weight must be estimated from data itself:

$$\sigma_2 = \sqrt{\frac{\sum\limits_{i=1}^{n} p_i (x_i - x)^2}{p\,(n-1)}} \;=\; \sqrt{\frac{H}{p\,(n-1)}} \;=\; \sigma_1 \sqrt{\frac{H}{n-1}} \,.$$

It is easy to see that σ_1 depends only on a priori errors in averaged values x_i and σ_1 depends only on the scatter of x_i. Theoretically, solution of problem of choice between σ_1 and σ_2 depend on whether the scatter of x_i is a result of random errors or there are systematic differences between estimates x_i. Obviously, both effect are present in most of practical applications.

That is a known problem in data processing and no rigorous solution is proposed. However some practical ways to handle it were considered in literature. Evidently, the most statistically substantial approach was made in [1, 3]. According to this approach chi-square criteria is used to decide if the scatter of x_i is result of random errors, and error of the mean x is computed as

$$\sigma_3 = \begin{cases} \sigma_1, & \text{if } H \le \chi^2(Q, n-1) \,, \\ \sigma_2, & \text{if } H > \chi^2(Q, n-1) \,, \end{cases}$$

where Q is a fidication probability. Some other practical algorithms of choice between σ_1 and σ_2 were proposed too.

However, in practice values of σ_1 and σ_2 may differ by several times. It leads to instability of σ estimate. Table 6 shows some numerical examples of computation of weighted mean of two data points and its error (to compute σ_3 we use Q=99% which corresponds χ^2(0.99,1)=6.63). One can see that no one value of σ_1, σ_2, σ_3 provides a satisfactory estimate of σ. Moreover, value of σ_3 depends not only on data sample $\{x_i,\, s_i\}$ but also on subjective choice of Q.

After many experiments with test data we decided in favor of simple formula

$$\sigma_4 = \sqrt{\sigma_1^2 + \sigma_2^2} = \sqrt{\frac{1}{p}\left(1 + \frac{H}{n-1}\right)} \,,$$

which can be called "combined" approach. The last column of Table 6 shows that such a approach can provide stable and realistic estimate of error of the mean.

More detailed consideration of this topic is given in [4].

Table 6. Numerical examples of computation of weighted mean (see explanation in text).

No	x_1	x_2	$s_{1,2}$	x	H	σ_1	σ_2	σ_3	σ_4
1	1.0	1.0	0.5	1.0	0.00	0.354	0.000	0.354	0.354
2	1.0	2.0	0.1	1.5	50.00	0.071	0.500	0.500	0.505
3			0.2		12.50	0.141	0.500	0.500	0.520
4			0.3		5.56	0.212	0.500	0.212	0.543
5			0.5		2.00	0.354	0.500	0.354	0.612
6			1.0		0.50	0.707	0.500	0.707	0.866
7			2.0		0.12	1.414	0.500	1.414	1.500
8	10.0	20.0	0.1	15.0	5000.00	0.071	5.000	5.000	5.000
9			0.5		200.00	0.354	5.000	5.000	5.012
10			1.0		50.00	0.707	5.000	5.000	5.050
11			2.0		12.50	1.414	5.000	5.000	5.196
12			3.0		5.56	2.121	5.000	2.121	5.431
13			5.0		2.00	3.536	5.000	3.536	6.124
14			10.0		0.50	7.071	5.000	7.071	8.660
15			20.0		0.12	14.142	5.000	14.142	15.000
16	10.0	10.0	1.0	10.0	0.00	0.707	0.000	0.707	0.707
17	10.0	11.0		10.5	0.50	0.707	0.500	0.707	0.866
18	10.0	12.0		11.0	2.00	0.707	1.000	0.707	1.225
19	10.0	13.0		11.5	4.50	0.707	1.500	0.707	1.658
20	10.0	14.0		12.0	8.00	0.707	2.000	2.000	2.121
21	10.0	15.0		12.5	12.50	0.707	2.500	2.500	2.598
22	10.0	16.0		13.0	18.00	0.707	3.000	3.000	3.082
23	10.0	17.0		13.5	24.50	0.707	3.500	3.500	3.571

5. Conclusions

Results of this study allow to make the following conclusions:

- Procedure of computation of the IVS combined EOP series must be “absolute”, i.e. independent on any reference, e.g. IERS, series. Otherwise details of combination procedure used during computation of “external” reference series (systematic corrections, weights) will affect the results of analysis.
- It seems preferable to use ITRF and ICRF by the all IVS Analysis Centers for computation of VLBI EOP series submitted to the IVS and IERS. Using individual TRF/CRF lead to difficulties in interpretation of results. Usual procedure of determination of systematic differences between EOP series provides correction only for “global” orientation between TRF/CRF. But, as it was shown above transformation parameters between individual TRF (CRF) realizations depend on sub-set of stations (sources) used for comparison. This means that commonly speaking every session produce EOP in its own system, which makes it difficult to transform an individual EOP series to ITRF/ICRF with sufficient accuracy.
- A reference EOP series based on IVS combined solution for fixed set of individual solutions can be used to save the long-time stability. Also, it is important to develop appropriate

strategy to include new or updated solutions in the IVS combination, e.g. using strategy proposed in this paper.

- Weighting of individual series depending on their long-time stability seems useful for improvement of long-time stability of the IVS combined EOP series.
- Proposed method of computation of weighted mean EOP can be used to account for both formal error and scatter.

References

[1] Brandt S. Statistical and Computational Methods in Data Analysis. 1970.

[2] Bevington P. R. Data reduction and error analysis for the physical sciences. McGraw–Hill Book Company, USA, 1969.

[3] Rosenfeld A. H., Barbero-Galtieri A., Podolski W. J., Price L. R., Soding P., Wohl C. G. Data on Particles and Resonant States. Rev. Mod. Phys., 1967, **39**, No 1, 1–51.

[4] Malkin Z. M. On Computation of Weighted Mean. Comm. IAA, 2001, No 137. (in Russian)

Session 2

Data Analysis and New Developments

J. Campbell and B. Richter: Towards a stable European vertical velocity reference system using VLBI, GPS and absolute gravity measurements, Proceedings of the 15th Working Meeting on European VLBI for Geodesy and Astrometry, p.65–74
http://www.ieec.fcr.es/hosted/15wmevga/proceedings/campbell2

Towards a stable European vertical velocity reference system using VLBI, GPS and absolute gravity measurements

J. Campbell [1], *B. Richter* [2]

[1] *Geodetic Institute of the University of Bonn*
[2] *Federal Agency for Cartography and Geodesy*
Contact author: J. Campbell, e-mail: campbell@sn-geod-1.geod.uni-bonn.de

Abstract

The European VLBI-network has now been operational for a decade and is able to provide long term site motions in a stable inertial reference frame. More recently, GPS permanent stations in Europe have collected daily data and thus created time series of high density and quality that allow the determination of relative site motions. A comparison of vertical motions obtained independently from both techniques shows that there are common trends indicating the presence of 'real' motion in distinct areas. It is possible to define a reference site or a group of sites in central Europe with similar motion to form a vertical velocity platform which serves to describe the motion in other parts of the European continent. As an independent technique to verify vertical motion absolute gravity measurements can be employed. After the reduction of tidal and environmental mass effects (air pressure and groundwater) the long term trends in gravity time series from Wettzell, Germany and Medicina, Italy are used to derive first estimates of vertical motion at these sites.

1. Introduction

Referring to vertical land motion implies some sort of stable reference, against which this motion is measured. Traditionally Mean Sea Level is used, chiefly because classical terrestrial measurement techniques, such as spirit levelling are referred to this surface. However, if small motions on the order a few mm/yr are considered, the intrinsic temporal and spacial changes of the sea level have to be taken into account (Woodworth et al. 1999). Dynamic satellite methods as well as satellite altimetry have helped to determine and considerably improve our knowledge of the geoid, but the accuracy of absolute heights referred to a global geoid is still limited to the decimetre level (Rummel and Teunissen 1988, Ihde and Augath 2000).

A different situation arises if instead of absolute vertical motions only relative vertical motions are determined. The concept of relative vertical control has been in use for national height systems. One particular benchmark or a set of reliable benchmarks in a geologically stable area form the basis of the national height reference frame. A similar vertical motion frame can be realized by defining the secular vertical motion of the selected set of points to represent zero motion.

In the present paper, we propose to apply the relative approach to the entire European area and consider one site, or alternatively a selected set of sites, in central Europe to represent a stable platform of zero vertical motion. The selection will be carried out in several steps, starting with the fixing of one European site equipped with as many as possible of the available space and terrestrial techniques, located in a geologically stable area. The second step will include more sites in central Europe with reliable observational records of at least one space technique to form a suitably weighted mean.

2. Ongoing geodetic observing programs

The available terrestrial and space techniques to measure and record vertical changes are subject to systematic error sources which become critical when vertical rates at the level of a few millimetres per year or less are to be determined. In this situation it is imperative to use as many independent methods as possible. Then, the comparison of the individual results provides an estimate of the reliability of the final results.

In the European context there is a number of coordinated observing programs that are concerned with the improvement of vertical control and the time variant dimension of height.

To apply geodetic space techniques in geodynamic research, the WEGENER Group (Working group of European Geoscientists for the Establishment of Networks for Earth-Science Research) has been established as an interdisciplinary group to encourage and facilitate the interaction between members of the geodetic and geophysical communities (Wilson 1998, Plag et al. 1998).

For terrestrial techniques (precise levelling) the UELN (United European Levelling Network) has been designed to connect the national networks in Europe and to create a common vertical datum. Its primary task is to provide a time invariant the height system (its definition as a 'dynamic' system should not be mistaken: the realization is in potential differences instead of metric, which requires gravity measurements along the levelling lines). The latest realization UELN-95/98 has an accuracy of about 10 cm or better over distances $\leq$ 2000 km. The accuracy of the levelling networks approaches or is better than the accuracy of relative height determination by the space techniques at distances below $\sim$300 km. Therefore, in smaller areas the repeated levellings are of great value for the detection of vertical change on shorter ranges.

The creation of a combined vertical system that includes all available geodetic and other techniques was initiated in 1995 in the IAG Sub-Commission for Europe (EUREF) leading to the formation of a commission within EUREF responsible for the European Vertical Reference System (Ihde, Augath 2000). The EVRS is planned as a kinematic vertical network including the estimation of vertical rates from repeated levellings, GPS permanent observations and other relevant data. The existing networks and organisations listed below are encouraged to cooperate in this effort (Plag et al. 1998):

EUREF (EPN, EUREF Permanent GPS Network)
WEGENER-MEDLAS and related projects (SLR)
EUROPEAN VLBI (Working Group on European VLBI for Geodesy and Astrometry)
(geodetic VLBI)

In addition, tidal records on European coastlines are collected and analysed at many national oceanographic centres and at the Permanent Service of Mean Sea Level (PSMSL) of the Proudman Oceanographic Service (Woodworth et al. 1999). More recently, European tide gauge data have become an important component to establish the EUVN (Wöppelmann et al. 2000).

3. Geodetic constraints on vertical motion from regional campaigns

In contrast to horizontal crustal motions, vertical crustal motions are in most areas much smaller and rarely exceed the 1 mm/year level. In fact, even the vertical motions associated with the young alpine orogeny are not expected to rise above 2 mm/year. Repeated levellings in Switserland have shown the present-day vertical rates to remain within these bounds (Schneider et al. 2000, p. 320).

Vertical crustal motion is also found outside the orogenic belts, for example in the case of old massifs subject to recent plateau uplift. A good example is the Rhenish Massif which has experienced an average uplift of 200 meters in the past 800.000 years, amounting to an average annual vertical rate of +0.25 mm/y (Fuchs et al. 1983). Of course, this average rate cannot be seen as a true image of the uplifting process. The geological evidence rather points to a succession of relatively quiet phases interrupted by phases of accelerated motion. In active phases, the rate could have reached up to 1 mm/y (Ahorner 1975). The analysis of repeated levellings in the Rhenish Massif and adjacent areas seems to indicate that the present-day uplift of about 1 mm/y w.r.t. surrounding areas reflects an active phase (Fuchs et al. 1983). Recent GPS campaigns appear to confirm this trend (Campbell et al. 2001).

Another example has recently become available by the analysis of the repeated lowlands levellings in the Netherlands (Kooi et al. 1998). Here, a significant subsidence of the coastal areas can be seen at the level of -1 mm/yr. In geological terms this is clearly too high by an order of magnitude and can only be explained by fairly recent (man-induced?) developments on coastal areas.

Among the vertical motions seen in the present time, there is only one phenomenon that produces vertical change of more than 10 mm/y over wide areas of continental size, i.e. the well-known effect of postglacial rebound in areas once covered by important ice and snow masses. Present-day geodetic measurements of different type have established beyond doubt that the uplift is continuing at the expected rate. Recent results of intensified GPS measurements are used to discriminate between different geophysical models of the underlying process (Scherneck et al. 2000).

Without having to expand this rather cursory list of examples of vertical crustal motion, we may summarize that within the European region there are distinctly different regimes of vertical motion, that have been examined closely at the smaller and medium scales (Gueguen et al. this volume). Apart from the massive bulge of the Fennoscandian uplift, we may expect only minor vertical crustal deformation of up to 1 to 2 mm/y, except for more local effects of volcanic origin (e.g. at Pozzuoli near Naples, Italy (Plag et al. 1998)).

4. Observed vertical motions by VLBI and GPS

Although precise levelling has been the prime technique for the determination of vertical motions this method has its deficit on larger distances (Ihde and Augath 2000). Space techniques, on the other hand, have lacked the resolution in the millimetre range. It is only very recently that time series with dense data over long enough time spans have become available. These have shown that the lack of resolution can be overcome (at least partially) by the sheer volume of data. Another precondition is of course that the technique itself provides a stable large scale reference frame.

VLBI has the advantage of being directly connected to the inertial system and providing very strong geometric ties between the vertices of a spatial network. The entire network is free to be translated within in certain bounds, but it cannot be rotated because its orientation is given by the Earth Orientation Parameters (EOP), which are a product of the global space geodetic networks. The residual errors of the globally determined orientation may be estimated to remain below 0.3 mas (milliseconds of arc) for both short and long periods of time. This leads to maximum tilt errors of 3 mm at a distance of 2000 km from the central fixed point. In a 10 year time series, this amount shrinks to an average velocity error of merely 0.3 mm/y.

Vertical rates for most of the stations participating in the European VLBI campaigns are now available from data covering a time span of around ten years. Several solutions based on different strategies have been produced by the groups involved in the European VLBI project (Campbell and Nothnagel 2000), enabling to see the influence of different approaches on the final results. In short, there are differences in the amount of data used (only the EUROP-sessions, the EUROP-sessions plus those global VLBI sessions containing at least 3 European stations and finally all available observations except some sub-standard sessions), and in the way the solutions are designed (time series solutions or combined coordinate and site velocity vector solutions).

In table 1 the vertical velocities are listed for both the OSO 2000 and the CNR 2000 solutions to obviate the degree of agreement between independent VLBI solutions. Details of the analysis background can be found in Campbell and Nothnagel 2000 and Gueguen et al. 2001. Except for the stations with much less data than average (Effelsberg, Yebes and Crimea) the agreement is better than 1 mm/y.

Table 1. Comparison of vertical site velocities for the European VLBI stations and collocated permanent GPS. The two columns for GPS represent the JPL series translated to GPS zero velocity at Wettzell using a) combined rate for WETB and WTZR: −1.97 mm/y and b) rate for WTZR only: −1.03 mm/y.

Vertical velocities with respect to Wettzell fixed (mm/y)					
	VLBI (OSO)	VLBI (CNR)	GPS (JPL.a)	GPS (JPL.b)	Diff.
Ny Ålesund	+5.9±1.8	+6.4±0.3	+7.16±1.8	+6.22±1.8	+0.76
Onsala	+1.8±0.7	+2.9±0.3	+2.24±0.1	+1.30±0.1	−0.66
Effelsberg	+1.0±2.6	−0.8±0.8	–	–	–
Wettzell	+0.0	+0.0	+0.0	+0.0	+0.00
Madrid (DSN)	+2.0±0.8	+2.8±0.3	+2.75±0.3	+1.81±0.3	−0.05
Villafranca	–	–	−0.43±0.2	−1.37±0.2	–
Yebes	–	–	–	–	–
Medicina	−2.7±0.9	−1.2±0.3	−1.13±0.3	−2.07±0.3	+0.07
Matera	+0.2±0.6	+1.0±0.3	+0.40±0.3	−0.54±0.3	−0.60
Noto	−0.5±0.7	−1.2±0.3	−1.26±0.3	−2.20±0.3	−0.06
Crimea	−0.8±4.5	+4.3±1.1	–	–	–

GPS provides strong geometric ties between stations although its frame critically depends on the quality of GPS orbit determination. In recent years the number of permanent GPS stations around the world has increased in a way that the resulting realizations of the terrestrial reference frame have become almost as stable as the VLBI frame, converging to a level of ±0.3 mas (Rothacher 2000).

In this paper, we concentrate on the GPS solution provided by JPL in its 'sideshow', available in the web (http://sideshow.jpl.nasa.gov/mbh/). This solution has several features which are important in the comparison with VLBI:

- most of the data available globally have been used
- the longest data spans are used in the solutions (by comparison with other series)
- small rotations due to successive realizations of the ITRF have been taken care of

Some problems remain due to the lack (or misinterpretation) of station information. In order to avoid critical cases, we have only used those time series that could be checked with direct information from the sites, in particular those being collocated GPS sites of the VLBI stations.

In the quality assessment of GPS positional time series the local effects are dominant:

- changes in the antenna setup (antenna type used, mounting, with or without radome etc)
- multipath environment, changes in the near field of the antenna
- ground condition (humidity, snow coverage)
- variations in the groundwater table

The time series plots of the JPL sideshow are less well suited to examine the subtle periodic and quasi-periodic effects because of the reduced scale of the plots and the overlaid error bars. A much closer look at the course and shape of the time series is provided by the Central Bureau of the EUREF permanent GPS network (http://www.epncb.oma.be), which offers an enlarged scale without error bars. The EUREF time series show the weekly solutions starting in 1996, when the ITRF94 came into effect (ITRF96 is the reference used in the multi-year solutions). These

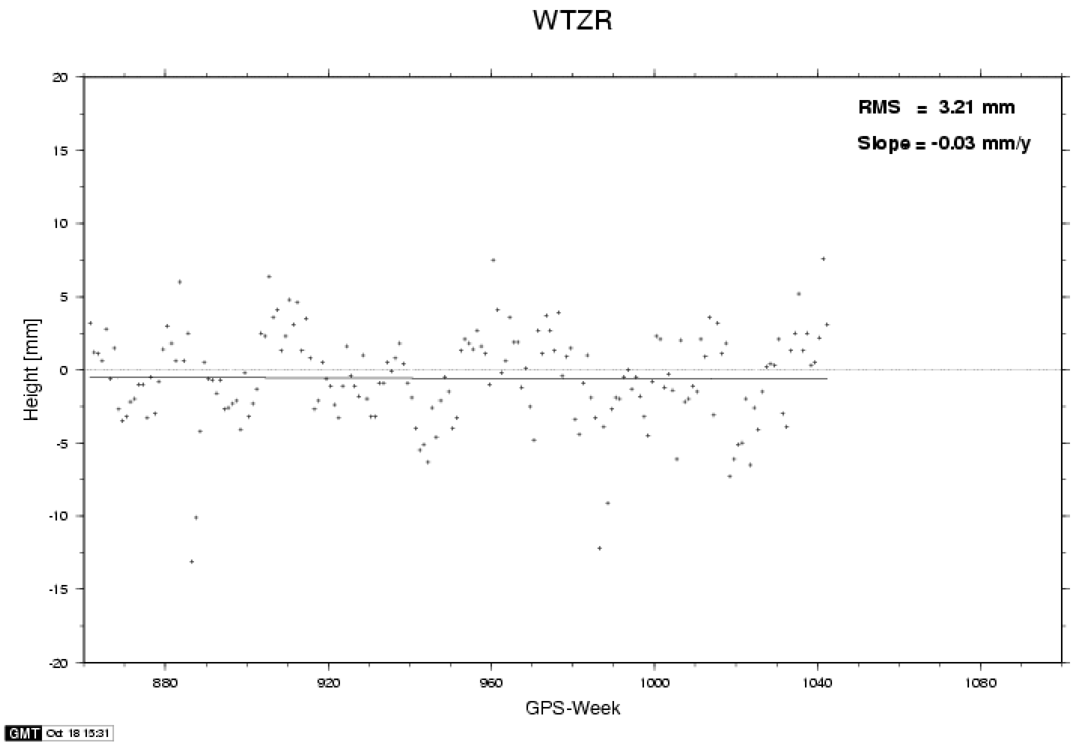

Figure 1. Weekly solutions for the vertical component of position of Wettzell (WTZR) from the BKG-CODE-contribution to EUREF (Becker et al. 2000).

solutions are constrained to a set of European stations with reliable performance (BOGO, GLSV, GRAZ, KOSG, MATE, ONSA, PENC, POTS, VILL, WARE, WTZR, ZECK and ZIMM).

An example for the vertical component of a GPS-time series is shown in Fig. 1. At Wettzell, the seasonal variations have an amplitide of about 4 mm (8 mm peak-to-peak). This has to be understood as a signal relative to the mean established by the set of constrained stations. The wrms scatter of ±3.2 mm is typical for weekly solutions, corresponding to a ±9 mm daily scatter (see Tab. 2). The negligible slope confirms that the vertical motion of WTZR is consistent with the average motion of the above set of reference stations (in the period 1996 to 2000).

From the EUREF time series velocities are being derived by different analysis centres. Definitive velocity solutions are imminent and will be used in the present work of defining a stable velocity reference in Europe. However, considering the large amount of annual and quasi-periodic signals in the time series it will be crucial to avail oneself with a long enough uninterrupted data span, preferably more than 5 years, before any firm conclusions on real tectonic vertical motions can be drawn. Therefore, in the comparison of table 1 only the JPL time series have been considered for the time being.

5. A central European velocity platform

Even before selecting a confined set of central European stations which could serve to form a platform of firmly established vertical velocity, it is useful to consider one particular site that comes close to the required specifications, such as:

- well defined antenna set up

- low multipath environment
- free horizon down to 10° elevation
- stable support structure
- solid tie to local bedrock
- well documented groundwater situation
- precise survey ties to ground markers and footprint network
- collocated site (with other space techniques)
- absolute and cryogenic gravity measurements

The fundamental station of Wettzell combines most of these requirements to a high degree of perfection and has no alternative in central Europe if a VLBI facility is to be included. The only problem at this station concerns a discontinuity in the GPS time series: the total time span from July 1991 to 2000 is disconnected by the fact that IGS observations have been transferred from the initial Rogue SNR-800 receiver with its choke ring antenna (WETT) to a new Rogue SNR-8000 with a new choke ring antenna (WTZR) on the same tower but on a different mount ($\Delta s \approx 3$ m). Hence, there are in fact two time series with slightly different multipath environment. A connection using individual antenna calibrations has not yet been attempted, so that both series have to be treated either independently (yielding two different slopes) or in conjunction with a vertical offset, yielding one mean slope.

In the JPL analysis (as of March 2001), the two series have been treated independently yielding a vertical rate of -2.91 mm/y in the first period of 5 years and -1.25 mm/y in the second period (Tab. 2.).

The rather large rate difference of 1.66 mm/y between the two data sets has to be attributed mainly to the change in the ITRF's due to the small number of stations available globally during the early phase of the IGS (Tregoning et al. 1998).

Table 2. Vertical rates from the JPL analysis of permanent GPS observations at Wettzell for two successive occupations: WETT (erroneously given as WETB in the JPL sideshow) from 1992.3 until 1997.1 and WTZR from 1995.1 until 2000.3.

Site	Vertical rate (mm/y)	Time span (yrs)	Repeatability (mm)
WETT	-2.91 ± 0.32	4.8	± 9.0
WTZR	-1.25 ± 0.29	5.2	± 9.1

A closer look at the time series of the other VLBI/GPS stations reveals discontinuities in most of the series. Due to the repair of the wheel-and-track bearing of the radiotelescopes at Medicina, Effelsberg and Madrid, vertical offsets arose that had to be determined by local geodetic measurements. Before the definitive results of the surveys are available offsets are introduced in the analysis of the VLBI data (Campbell and Nothnagel 2000). A similar procedure is used in the GPS analysis. Among the collocated GPS sites Madrid (8 jumps) and Matera (2 jumps) are affected. It is quite clear that the estimation of the rates deteriorates with the number and position of breaks that have to be introduced in the processing. Therefore, efforts to 'repair' the time series with reliable survey results should have a high priority.

The compilation in table 1 of results of vertical site velocities from VLBI (two different solutions) and GPS (JPL-solution referred to two different reference velocities at Wettzell) shows an unexpected degree of agreement between the two nearly independent techniques. The mean difference GPS-VLBI for case a) yields -0.54 mm/y. The differences are all below 1 mm/y (last column of Tab. 1), the rms difference being ± 0.21 mm/y. This result shows that there is a clear convergence of VLBI and GPS in the vertical velocities and raises hopes that a set of reliable reference stations for the definition of a European velocity platform can indeed be found.

6. Prospects for the use of gravity measurements

According to the well-known law of Newton, the gravitational force is a function of the mass and distance between the attracting bodies. Variations in the height change the geometrical relation between the test mass and the attracting bodies and therefore gravity. But also mass redistribution within the attracting bodies leads to equivalent effects. Therefore, both absolute (AG) and superconducting (cryogenic) (SG) gravity measurements have recently been considered to verify vertical crustal motions (Zerbini et al. 2001).

Absolute gravity measurements are based on the principle of free fall. The acceleration of a free falling body is calculated by measuring the travel time between the crossing of interferometer fringes in an evacuated tube. Because the quantities time and distance are derived in-situ from absolute standards one defines these classes of measurements as absolute ones. They are, by their inherent stability, well suited for the study of long term gravity changes. Superconducting gravity meters are also very sensitive to gravity changes although they lack the absolute standard. In turn, they provide a high temporal resolution and are perfectly suited to interpolate gravity between absolute gravity measurements (Plag et al. 2000, p. 184, 186). The two types of gravity observations complement each other. In fact, the combination of both makes use of the sub-μGal resolution of the SG and the long-term stability of the AG.

If we want to infer pure geometric height variations from the gravity data it is necessary to determine the gravity field of mass variations independently, e.g. by additional external information and modelling. The effects that have to be taken into account are:

1. solid Earth and ocean tides
2. attraction of ocean tides
3. attraction of atmospheric tides
4. polar motion and changes in LOD
5. changes in the local groundwater table
6. local soil moisture

In the routine reduction of absolute (and superconducting) gravity measurements the effects 1 to 4 are normally accounted for, while there is inadequate information available on item 5 and 6.

How important these effects are, can be shown by a recent analysis of absolute gravity measurements taken at Wettzell using information on the variations of the local groundwater table. The recordings at a well near the site of the gravity measurements cover a period from October 1998 to August 2000 and display variations of up to 3 meters (Fig. 2).

Applying empirical corrections based on a correlation analysis between the groundwater recordings and the gravimetric data reduces the wrms scatter about the mean value from ± 4 nms^{-2} to ± 8 nms^{-2} (Fig. 2). The 'corrected' time series produces a gravity change of -5 ± 10 nms^{-2}/yr, which, using the conversion factor of -3.06 nms^{-2}/mm, results in a height change of -1.5 mm/yr ± 3 mm/yr (Fig. 3).

As an additional example the gravity series in Medicina/Italy is displayed in Fig. 4. To interpret the gravity variation, the step between July 97 and October should be ignored because its origin is not yet understood. After October 97 gravity has increased by about 15 nms^{-2}/yr. This would correspond to a subsidence of the crust of approximately -5 mm/yr.

To correctly model the hydrological reduction, detailed information on the spatial and temporal distribution of the groundwater is required (Kümpel et al. 2001). Even if this level of modelling is still far ahead, the results do show that at good sites the monitoring of vertical change by gravity measurements will be possible within the 1 mm/y range if time spans of the measurements are extended to 5 years or more.

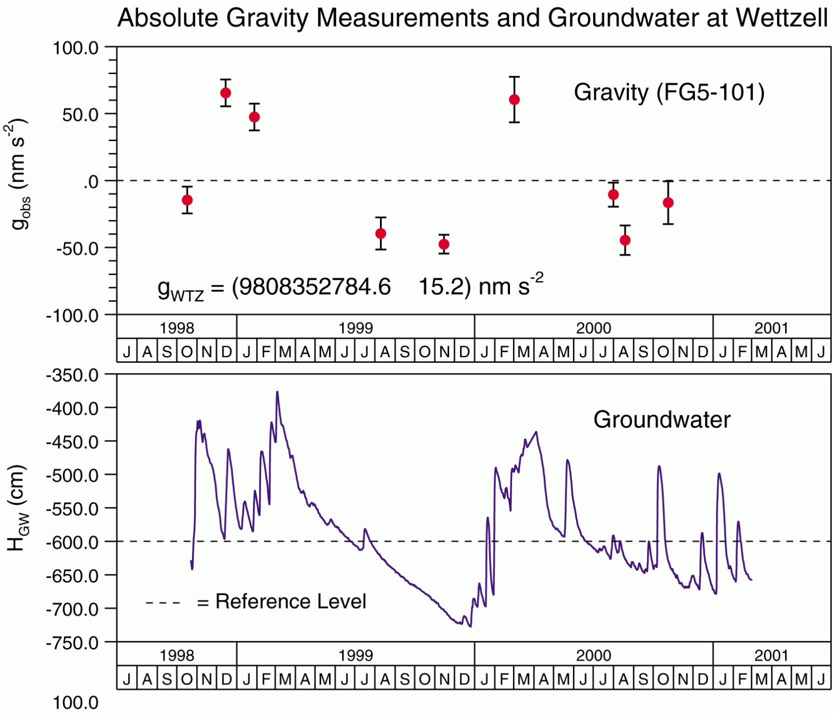

Figure 2. Absolute gravity variations observed at Wettzell and the changes in the groundwater table in the equivalent time frame.

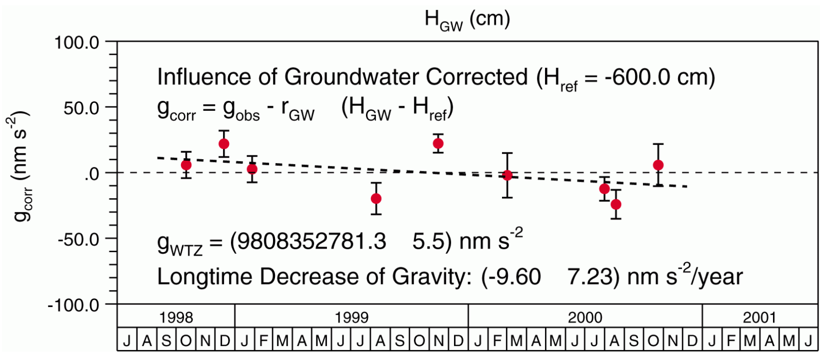

Figure 3. Gravity variation in Wettzell corrected for groundwater effects. A linear regression leads to a trend in gravity of about -5 ± 10 nms^{-2}/yr.

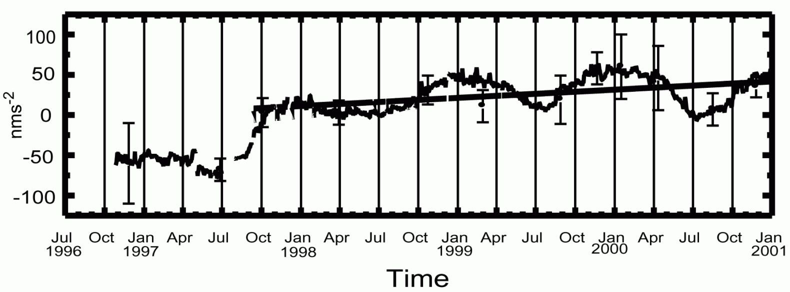

Figure 4. Gravity time series at Medicina registered by the superconducting gravimeter SG-023 together with sporadic absolute measurements performed with absolute gravimeters type FG-5.

7. Conclusions

The determination of vertical motions on larger scales by geodetic means is difficult because the motions are usually distinctly smaller than horizontal motions. Exceptions exist on local scales, where vertical motions can be sometimes even larger than horizontal motions. We realize that space techniques have proven superior to terrestrial techniques on large scales ($\geq$ 300 km), but the fact remains that observational errors have a stronger influence on vertical than horizontal position.

The present status of time series analysis for both VLBI and GPS is characterised by the following accuracies:

wrms of linear fit: ± 7 to ± 15 mm (24h-sessions)

rms of estimated slope: ± 0.3 to ± 2.5 mm/y (10 years down to 4 years time span)

Problems do persist, because most of the time series show periodic and quasi-periodic variations (mainly seasonal). Most of these seasonal effects can be explained by loading effects initiated by seasonal mass changes in the atmosphere, ocean and hydrosphere (Zerbini et al. 2001)

Time series of absolute gravity measurements, if successfully corrected for local groundwater and soil moisture effects can provide vertical motion on the 1 mm/yr level (time span $\geq$ 5 y).

The comparison between VLBI and GPS time series for the major collocated European stations has shown that a stable central European vertical velocity platform can be found. The fundamental station of Wettzell would be a god candidate considering most of the relevant site parameters.

Further work has to concentrate on the comparison of results with geophysical models, such as postglacial rebound, and comparisons with results from external data such as absolute gravity and tide gauge records. Areas of major concern persist and require full attention:

- local site parameters, such as
  - multipath environment
  - monument stability
  - local geology
  - local hydrological effects (i.e. groundwater flow)
- other seasonal effects.

References

[1] Ahorner, L.: Present-day stress field and seismotectonic block movements along major fault zones in Central Europe. Tectonophysics, Vol. 29, p. 233–249, 1975

[2] Becker, M., J. Campbell, A. Nothnagel, Ch. Steinforth: Comparison and Combination of Recent European VLBI- and GPS-Solutions. Proc. of the 14^{th} Working Meeting on European VLBI for Geodesy and Astrometry at Castel S. Pietro Terme, 8–9 Sept. 2000, Tomasi, Mantovani, Perez-Torres (eds.), p. 35–40, 2000

[3] Campbell, J., A. Nothnagel: Comparison of European VLBI solutions from different Analysis Centers. Proc. of the 14^{th} Working Meeting on European VLBI for Geodesy and Astrometry at Castel S. Pietro Terme, 8–9 Sept. 2000, Tomasi, Mantovani, Perez-Torres (eds.), p. 3–6, 2000

[4] Campbell, J., H.-J. Kümpel, M. Fabian, B. Görres, Ch. J. Keysers, D. Fischer, and K. Lehmann: Recent movement pattern of the Lower Rhine Basin from tilt, gravity and GPS data. Accepted for NJG (Netherlands Journal of Geosciences/Geologie en Mijnbouw), Vol. 80, 2001

[5] Fuchs, K., K. v. Gehlen, H. Mälzer, H. Murawski, and A. Semmel (eds.): Plateau uplift - The Rhenish Shield - A Case History, 411 p., Springer Verlag 1983

[6] Gueguen, E., P. Tomasi, H.-G. Scherneck, R. Haas and J. Campbell: Recent crustal movements: geological meaning of European geodetic VLBI network observations. Proc. of the 15^{th} Working Meeting on European VLBI for Geodesy and Astrometry at Barcelona, 7–8 Sept. 2001, this volume

[7] Ihde, J, Augath, W.: The Vertical Reference System for Europe. In: Veröff. Bayer. Komm. Int. Erdmessung, Heft 61, IAG-Subcommission for Europe (EUREF), Publication No. 9, EUREF-Symposium held at Tromsø, 22–24 June 2000, Eds. J.A. Torres, H. Hornik, p. 99-110, München 2000

[8] Kooi, H., P. Johnston, K. Lambeck, C. Smither, R. Molendijk: Geological causes of recent (~100 yr) vertical land movement in the Netherlands. Tectonophysics, Vol. 299, p. 297–316, 1998

[9] Kümpel, H.-J., K. Lehmann, M. Fabian, and Gy. Mentes: Point stability at shallow depths - experience from tilt measurements in the Lower Rhine Embayment, Germany, and implications for high resolution GPS and gravity recordings. Geophys. J. Int., Vol. 146, p. 630-644, 2001

[10] Plag, H.-P., B. Ambrosius, T.F. Baker, G. Beutler, G. Bianco, G. Blewitt, C. Boucher, J.L. Davis, J.J. Degnan, J.M. Johansson, H.-G. Kahle, I. Kumkova, I. Marson, S. Mueller, E.C. Pavlis, M.R. Pearlman, B. Richter, W. Spakman, S. K. Tatevian, P. Tomasi, P. Wilson, S. Zerbini: Scientific objectives of current and future WEGENER activities. Tectonophysics, Vol. 294, p. 177–223, 1998

[11] Rothacher, M.: Towards an Integrated Global Geodetic Observing System. IAG Symposium No. 120: Towards an Integrated Global Geodetic Observing System (IGGOS), Munich Oct. 5–9, 1998, Rummel, Drewes, Bosch, Hornik (Eds.), p. 41-52, Springer Verlag, 2000

[12] Rummel, R. and P. Teunissen: Height Datum Definition, Height Datum Connection and the Role of the Geodetic Boundary Value Problem. Bull. Géodesique, Vol. 62, p. 477-498, 1988

[13] Scherneck, H.-G., J.M. Johansson, R. Haas: BIFROST Project: Studies of Variations of Absolute Sea Level in Conjunction With the Postglacial Rebound of Fennoscandia. IAG Symposium No. 120: Towards an Integrated Global Geodetic Observing System (IGGOS), Munich Oct. 5–9, 1998, Rummel, Drewes, Bosch, Hornik (Eds.), p. 241-249, Springer Verlag, 2000

[14] Schneider, D., E. Brockmann, U. Marti, A. Schlatter, U. Wild: National Report of Switzerland. In: Veröff. Bayer. Komm. Int. Erdmessung, Heft 61, IAG-Subcommission for Europe (EUREF), Publication No. 9, EUREF-Symposium held at Tromsø, 22–24 June 2000, Eds. J.A. Torres, H. Hornik, p. 315- 322, München 2000

[15] Tregoning, P., K. Lambeck, A. Stolz, P. Morgan, S.C. McClusky, P. Van der Beek, H. McQueen, R. J. Jackson, R.P. Little, A. Laing, B. Murphy: Estimation of current plate motions in Papua New Guinea from Global Positioning System observations. J. Geophys. Res., Vol. 103, p. 12,181–12,203, 1998

[16] Wilson, P.: The Working Group of European Geoscientists for the Establishment of Networks for Earth-Science Research (WEGENER). Journal of Geodynamics, Vol. 25, p. 177-178, 1998

[17] Wöppelmann, G., J. Adam, W. Gurtner, B.G. Harsson, J. Ihde, M. Sacher, W. Schlüter: Status report on the sea-level data collection and analysis within the EUVN Project. In: Veröff. Bayer. Komm. Int. Erdmessung, Heft 61, IAG-Subcommission for Europe (EUREF), Publication No. 9, EUREF-Symposium held at Tromsø, 22–24 June 2000, Eds. J.A. Torres, H. Hornik, p. 146-153, München 2000

[18] Woodworth, P.L., M.N. Tsimplis, R.A. Flather and I. Shennan: A review of the trends observed in British Isles mean sea level data measured by tide gauges. Geophys. J. Int., Vol. 136, p. 651-670, 1999

[19] Zerbini, S., B. Richter, M. Negusini, C. Romagnoli, D. Simon, F. Domenichini, W. Schwahn: Height and gravity variations by continuous GPS, gravity and environmental parameter observations in the southern Po Plain, near Bologna, Italy. Earth and Planetary Science Letters 5949, p. 1-13, 2001

W. Schwegmann: Automatic VLBI Data Analysis using Calc/Solve and a Knowledge-Based System, Proceedings of the 15th Working Meeting on European VLBI for Geodesy and Astrometry, p.75–82
http://www.ieec.fcr.es/hosted/15wmevga/proceedings/schwegmann

Automatic VLBI Data Analysis using Calc/Solve and a Knowledge-Based System

W. Schwegmann

Geodetic Institute of the University of Bonn
e-mail: schwegma@chagall.geod.uni-bonn.de

Abstract

An important contribution to the acceleration of the VLBI procedure is a faster and semiautomatic data analysis, in particular in view of the increasing amount of geodetic observing sessions to be expected in the future. A system for automatic VLBI data analysis is being developed. Its main components are a Knowledge-Based System (KBS) and the Mark-4 VLBI Analysis Software CALC/SOLVE which are connected by an interface in order to be able to transfer data and information between the two systems. The knowledge needed for the VLBI data analysis is modelled within the KBS and can be applied to automate the data analysis within the existing analysis software and to support the analyst during the analysis. The concept of the KBS and the interface to the Mark-4 software is described and it is shown how the knowledge about the VLBI data analysis procedure can be modelled and applied to automate the data analysis.

1. Introduction

The VLBI data analysis is a very complex process and needs a lot of manual interactions. It is very time consuming and a partial automation would be very useful to accelerate the VLBI procedure, in particular with regard to the increasing number of geodetic observing sessions to be expected in the future. Most tasks of the geodetic VLBI data analysis require a comprehensive knowledge of the whole procedure of the data analysis and the analyst needs a lot of experience and knowledge for solving the complex problems within the data analysis.

Knowledge-Based Systems (KBS) can be used to administer, store and evaluate specific knowledge needed for the VLBI data analysis, to provide targeted informations for the user and to solve the complex tasks within the data analysis automatically. A KBS is less susceptible to errors, allows to conserve the knowledge of several analysts and to check the decisions of the analyst. Moreover, it can be used to guide and support the analyst during the data analysis, to evaluate situations, to solve problems and to analyse and check the data and the results. The KBS can be used as teaching system for less experienced analysts and to exonerate the analyst in his work.

Investigations of the Mark-4 data analysis system, a widely used VLBI software system (Ryan et al., 1980), have shown that almost all steps of the data analysis can be supported by a KBS (Schwegmann and Schuh, 1999). A KBS called IADA (**I**ntelligent **A**ssistent for VLBI **D**ata **A**nalysis) is being developed to automate to a high degree the VLBI data analysis procedure. It is an important component of a general concept for VLBI in near real-time (Schuh and Schwegmann, 2000). IADA can be used to support the analyst in his decisions, to guide him through the data analysis or to automate the data analysis. The KBS contains the knowledge about the VLBI data analysis procedure and can be applied for solving the complex problems within the data analysis automatically by processing this knowledge with respect to specific rules and instructions. An interface has been developed to manage the transfer of data and information between IADA and the Mark-4 software.

2. A Knowledge-Based System for the VLBI Data Analysis

2.1. Knowledge-Based Systems

Knowledge-Based Systems are software systems in which the knowledge about a problem domain is isolated and stored in a so-called Knowledge Base (KB) and is processed and evaluated by a domain-independent problem-solving component (Fig. 1; Sundermeyer, 1991). Modifications of the KB as well as its extensions do not influence the problem-solving component. Only the KB has to be modified to adapt the KBS to new situations or tasks.

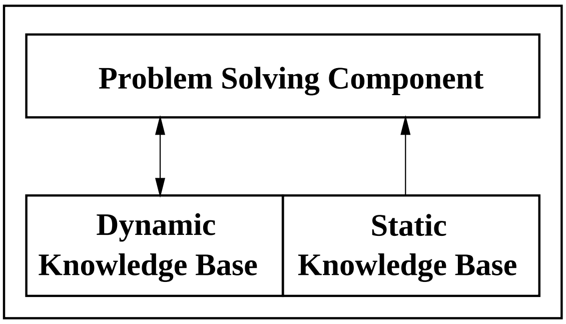

Figure 1. Basic architecture of a KBS.

The most important and even critical task when developing a KBS is to build the KB, the main component of a KBS, because its efficiency depends on the qualitiy of the KB, which should be modular, flexible and extensible. The KB consists of a static and a dynamic part. The first one contains general knowledge about the VLBI data analysis which does not depend on the current experiment, e.g. it does not change during the analysis of a VLBI experiment. The dynamic part stores knowledge depending on the current experiment and the status of the analysis. Additionally, it contains the results achieved by investigating the data by the problem-solving component of the KBS. Detailed information about KBS can be found in Schnupp et al. (1989).

2.2. Development of IADA

To build a KBS, the knowledge needed for the problem domain must be collected, structured and organized first (*Knowledge Acquisition*). Then, it has to be formally represented and stored in the Knowledge Base (*Knowledge Representation*). The main aspects of the knowledge acquisition and representation that have been taken into account during the generation of IADA are summarized in the following. A detailed explanation can be found in Schwegmann (2000).

Within the scope of the knowledge acquisition a so-called *concept* of the VLBI data analysis has been set up to collect the knowledge about its general procedure. The concept is divided into three main parts: the so-called *analysis steps*, *analysis substeps* and *substep descriptions*. The analysis steps define the global frame of the VLBI data analysis procedure. They are performed one by one in the standard data analysis and are subdivided into analysis substeps to describe the tasks of the data analysis in more detail (see Tab. 1). The KBS can be applied to automate the whole process of the data analysis or to perform single steps or substeps, in particular with respect to investigate specific problems. Each substep is characterized in the substep descriptions to define the parameterizations and calibrations that should be used during this stage of the data analysis. By comparing these specifications to the current settings within the analysis software the system is able to check all actions done by the analyst or to set up the correct parameter settings automatically. The specification of so-called *evaluation criteria* within the substep descriptions allow to evaluate the results of each substep. Additionally, *problem handling* methods can be designated to overcome problems, for example if the results do not meet the evaluation criteria. An example for a substep description of a specific step and substep is given in table 2.

Table 1. *Steps* and *substeps* of the *concept* of the VLBI data analysis.

ANALYSIS STEPS	ANALYSIS SUBSTEPS
Data Loading	-
Initial Solution	Apriori Clock
	Ambiguity Solution
	Evaluate Results
Intermediary Solution	Outlier Elimination
	Evaluate Results
Final Solution	Outlier Elimination
	Examine Solution
	Final Outlier Elimination
	Check Cable Cal
	Evaluate Results
Database Update	-

Table 2. A *substep description* for a specific *step* and *substep* of the VLBI data analysis procedure.

STEP: Intermediary Solution SUBSTEP: Evaluate Results	
Parameter	estimate station positions
	estimate baseline dependent clocks
	estimate atmosphere path delay
	estimate clock parameters
Evaluation Criteria	solution is good if total wrms is less than 100 psec and more than 80% of observations are in solution
	solution is poor if total wrms is between 100 and 250 psec and between 50% and 80% of observations are in solution
	solution is unsatisfactory if wrms is greater than 250 psec and/or less than 50% of observations are in solution
Problem Handling	solution=poor: check calibrations and check for outlier
	solution=bad: check ambiguity solution and check for clock breaks and strong outlier

WETTZELL

Instance of Frame: VLBIStationFrame

SLOT	VALUE
Name	Wettzell
Diameter	20 m
AxisType	AZEL
Nuvel-1	EURA
ClockBehavior	GOOD
. . .	. . .
ClockPara	ReferenceStation
CoordPara	0 0 0
CableCalData	available (not checked)
. . .	. . .

Static Knowledge   Dynamic Knowledge

Figure 2. Instance `WETTZELL` of frame `VLBIStationFrame`.

Table 3. A *rule-set* to evaluate preliminary results of the data analysis.

	STEP: Intermediary Solution SUBSTEP: Evaluate Results	
1	IF	total wrms < 100 psec AND ObsInSol > 80%
	THEN	solution = GOOD
2	IF	total wrms >= 100 psec AND <= 250 psec AND ObsInSol >= 50% AND <= 80%
	THEN	solution = POOR
3	IF	total wrms > 250 psec OR ObsInSol < 50%
	THEN	solution = BAD
4	IF	solution = POOR
	THEN	check calibrations check for outlier
5	IF	solution = BAD
	THEN	check ambiguity solution check for clock breaks check for strong outlier

The concept of the VLBI data analysis procedure has been transformed and stored in the Knowledge Base of IADA. Several knowledge representation techniques have been applied to formalize the knowledge. Among these, the most important formalisms are *Frames* and *Rules*.

Frames are used to represent knowledge about objects, for example a VLBI station. They consist of several *slots* to describe the attributes of an object. A so-called *instance* of such a general object description is generated by specifying values for the attributes of the object (Fig. 2). Frames can represent both dynamic knowledge, e.g. to describe the current parameterization, and static knowledge, such as the a-priori coordinates or the clock behavior at a VLBI station. While the static knowledge is a 'stable' part of the KB the dynamic knowledge depends on the current experiment and the status of the analysis. Thus, the dynamic knowledge has to be collected from the analysis software and to be transferred into the KB at the beginning of each step of the data analysis.

Rules are suited to model knowledge which depends on conditions. They are applied to check whether the current parameterization is correct (e.g. with respect to rank deficiencies), to examine the results of the analysis, etc. Rules are organized in so-called *rule-sets*. Each rule-set combines rules that are responsible for a specific task. When evaluating rules the problem-solving component has to verify the arguments within the condition part of a rule. These arguments are usually attribute values of a specific instance which can be accessed and read by the problem-solving component.

Depending on the step of the data analysis specific rule-sets will be applied. For example, rules for the evaluation of preliminary results of the data analysis are listed in table 3. The rules 1, 2, and 3 determine whether the results are satisfactory. The arguments within the condition parts are read from the instance `CurrentSolution` of the frame `SolutionFrame`, which contains several arguments to characterize the results of the data analysis. Depending on the value of the argument `solution` (`GOOD`, `POOR`, or `BAD`) rule 4 (`solution=POOR`) or rule 5 (`solution=BAD`) will be applied in order to investigate the reasons for an unsatisfactory solution by evaluating the functions within the action part of the respective rule.

The substep descriptions are an important part of the KB, because they contain the knowledge needed to perform the tasks within all substeps of the data analysis and to investigate its results. In fact, the rules in table 3 are generated with respect to the information within the fields evaluation criteria and problem handling in table 2. If the analyst changes the numerical values within these fields the above rules will be updated automatically. Thus, the knowledge within the substep descriptions is considered to be dynamic, because it depends on the respective step and substep of the data analysis and because the analyst is able to modify it. These information, that are used within the substep descriptions, are stored in external files and have to be loaded into the KB before the analysis within the KBS starts. The files can be modified easily without profound knowledge of the knowledge representation techniques. Hence, the KBS can be adapted to a specific analysis program without modifying the KB, because the general procedure of the VLBI data analysis is very similiar in all programs. It just has to be specified which analysis steps and substeps and which parameterizations and calibrations are supported by the specific software.

3. The Mark-4 Data Analysis System and the interface to IADA

3.1. The Mark-4 Data Analysis System

The Mark-4 data analysis system is being developed since the middle 70-s and is maintained by the NASA Goddard Space Flight Center. The Mark-4 software is one of the most powerful VLBI data analysis software packages and is widely used around the world. Although the developed KBS can be adopted to different VLBI software packages, it has been designed for an optimal cooperation with the Mark-4 data analysis system.

Most of the steps during the data analysis with the Mark-4 software have to be performed manually. Although almost all steps can be supported by a KBS, not all steps have to be supported by such a system, because some tasks can be automated easily by extensions to the existing software. Figure 3 shows the dataflow within the Mark-4 data analysis system and its most important programs. The programs surrounded by a dashed box have been developed to automate the data analysis procedure and will be described later. The Mark-4 data analysis system can be divided into two main parts. The programs shown in the left part in Fig. 3 are used to prepare a database for the parameter estimation within the SOLVE software package, which is displayed in the right part in Fig. 3. These programs are DBEDIT to generate a database or to add apriori information to a database, CALC to calculate theoretical delays, and partial derivatives, PWXCB to extract calibration data from the station log-files and DBCAL to put these data into the database. All programs require considerable manual interactions, which are time consuming, and their results have to be checked by the analyst.

The new programs GET_DB, XCALC and XLOG allow an automatic data analysis up to the

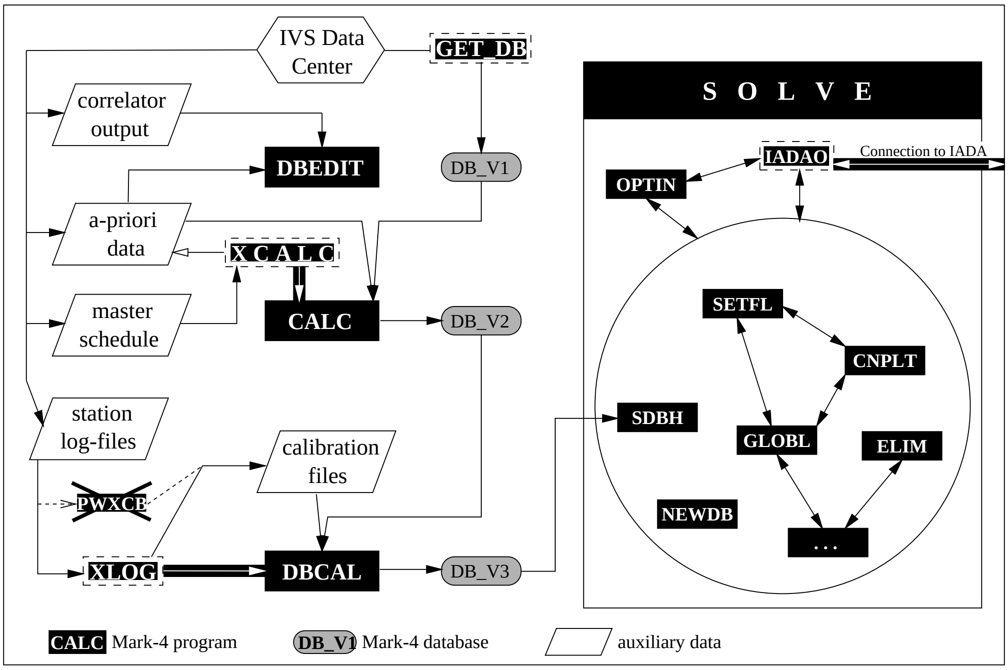

Figure 3. Dataflow within the Mark-4 data analysis system.

creation of a new version of a database using the program Dbcal. They perform the following tasks:

- Get_Db: automatic download of databases from an IVS data center; import of databases into the local catalogue.[1]
- Xcalc: build the control file for Calc; check all input data; start Calc; check results.
- Xlog: download all input files from an IVS data center; extract calibration data from log-files; check extracted data; save calibration files; start program Dbcal; check results. (Xlog substitutes the old program Pwxcb.)

The second group of programs within the Mark-4 data analysis system is formed by the Solve software package. It is used to get the estimates of targeted parameters, such as station positions and velocities, source coordinates, Earth orientation parameters, Love numbers and many others. Solve consists of several programs which can be accessed from the program Optin. Iada has been developed to automate the tasks performed by Solve, because the analysis procedure within Solve requires a lot of knowledge and experience. Thus, the program IadaO ('Iada Options Menu') has been developed in order to be able to call Iada by using an interface.

3.2. The Interface between Iada and Solve

To apply Iada during the VLBI data analysis an interface has been developed to manage the dataflow between Iada and the Mark-4 software package Solve. The interface is part of Solve and has to perfom the following tasks:

1. Extract data and information needed by Iada to control and automate the data analysis.
2. Transfer data and information to Iada and receive the results from Iada.
3. Process the results received from Iada.

The program IadaO is used to specify the information needed for the application of Iada, e.g. analysis step and substep, and to start Iada by calling the interface (Fig. 4). The functionality

[1]Dbedit has to be used instead of Get_Db if the analyst wants to create the first version of the database.

of the interface is shown in Fig. 5. When the analyst calls the KBS from within IADAO the interface extracts all data and information needed by IADA from so-called *scratch-files*[2] with respect to the current analysis step and substep and writes them into a *data-file*. This file is processed by IADA and the results of the KBS are written into a *result-file*, which is read by the interface in order to apply the results and to modify the scratch-files, if necessary. Then the analyst is able to proceed with the next step of the data analysis or to go back to program OPTIN.

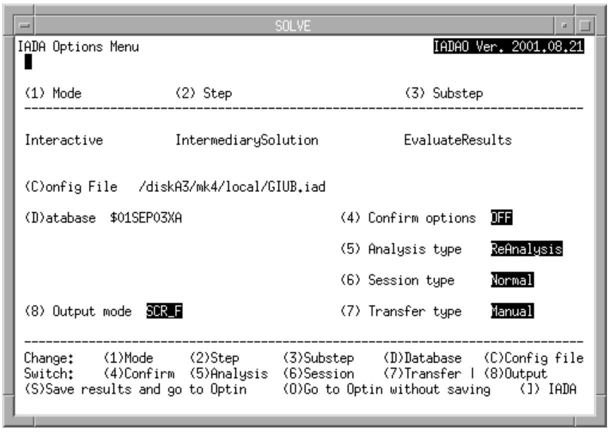

Figure 4. IADAO - Menu to specify options for the application of IADA.

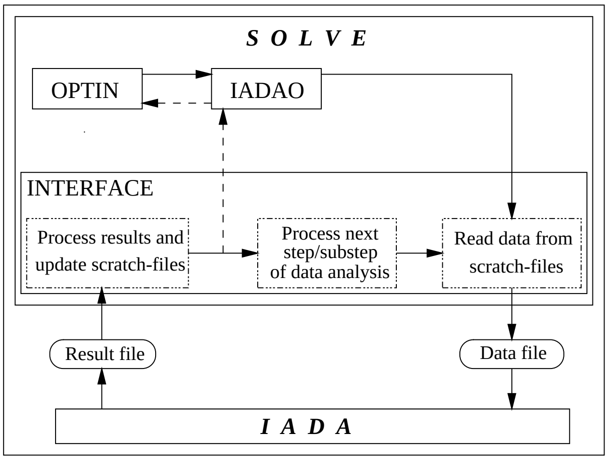

Figure 5. The interface between IADA and SOLVE.

4. Examples

Two examples for the application of IADA to automate the VLBI data analysis within the Mark-4 data analysis system are given. They describe the detection of clock breaks at a VLBI station and the detection of a wrong ambiguity solution at a baseline.

In general, the results of each analysis step are checked by IADA by applying the evaluation criteria, that are stored in the substep descriptions, with respect to the current status of the data analysis. This is carried out in two steps, starting with a check of the 'overall' results to determine whether they are satisfactory. If necessary, IADA tries to find in a second step the reasons for an unsatisfactory solution by using the methods specified in the problem handling part of the substep descriptions. The system investigates the distribution of the residuals at every baseline looking for patterns that are typical for a specific problem. Figure 6 shows such a typical residuals plot for a baseline containing a station with a clock break. The station that is affected by the clock break will show a similar pattern in all baselines containing that station. Such baselines can be detected by their considerable higher wrms compared to the other baselines. If a 'suspicious' station could be detected the localization of the clock break with respect to time will be done within SOLVE. The messages given by the interface during the course of this procedure are displayed in Fig. 7. The interface starts by running a least sqaures solution in order to update the results with respect to the current parameterization which has already been checked by IADA. All information needed by IADA are extracted from the scratch-files, the interface calls IADA and waits for the results. In this case, IADA proposes to look for a clock break at station ALGOPARK. Thus, the interface calls the proper subroutine to investigate this station for a clock break and the results are displayed and applied. Finally, the analyst is able to continue with the next step of the data analysis or to go back to program OPTIN.

[2]In SOLVE all information and data related to the current experiment is stored within a set of scratch-files.

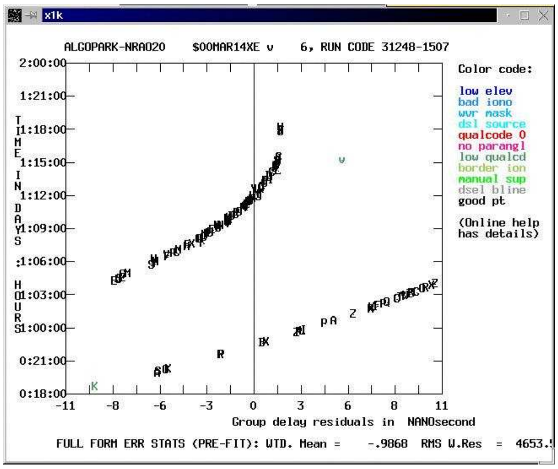

Figure 6. A characteristic residuals plot of a baseline with a clock break.

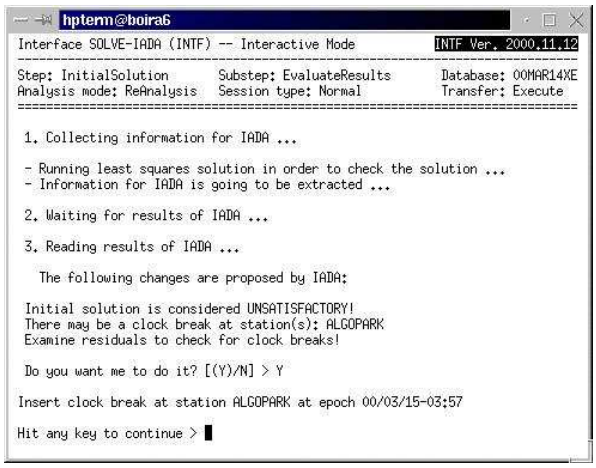

Figure 7. Messages of the interface when detecting the clock break shown in Fig. 6.

In the second example IADA detects an unsatisfactory solution by evaluating the ruleset shown in table 3. Further investigations lead to the presumption that there might be a wrong ambiguity solution at the baseline FORTLEZA-KOKEE. The system asks the user to check the specific baseline manually, because it does not have use of a method to verify this presumption. The messages given by the interface during the course of this procedure are displayed in Fig. 8.

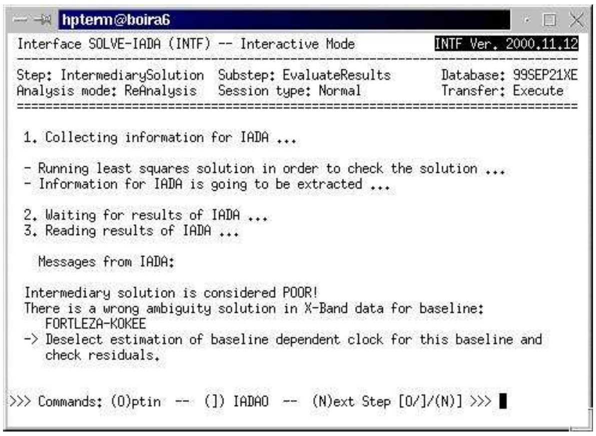

Figure 8. Messages of the interface when detecting a wrong ambiguity solution at a baseline.

5. Conclusions and Outlook

The application of knowledge-based techniques for the automation of the VLBI data analysis yields many benefits, because they allow an explicit modelling of the multifaceted knowledge needed for these tasks. Thus, the knowledge of several analysts can be conserved and applied by the KBS to solve the complex tasks within the data analysis automatically or to support the analyst during the data analysis and to check his decisions. Moreover, the system can be used to teach less experienced analysts. The very general concept of IADA allows to adapt the system to different VLBI software packages without modifying its Knowledge Base. The interface between the VLBI data analysis software package SOLVE and IADA allows to exchange data and information between these two systems to control and to automate by the KBS the regular analysis done in SOLVE. When applying IADA in cooperation with the described extensions to the Mark-4 data analysis system some VLBI experiments could already be analyzed automatically without requiring manual interaction. However, the Knowledge Base of IADA does only cover a small subset of problems that might appear during the course of the geodetic VLBI data analysis. Thus, it has to be extended in order to be able to use IADA in the routine data analysis.

Acknowledgements

IADA has been developed at DGFI, Munich, within a research project called 'Applications of Methods of AI for the VLBI Data Analysis'. This project was supported by the Deutsche Forschungsgemeinschaft (DFG), project Schu 1103/2-1. The development of the interface between IADA and SOLVE has been supported by the European Union within the TMR programme under contract FMRX-CT960071.

References

[1] Ryan, J.W., Ma, C., Vandenberg, N.R.: The Mark III VLBI Data Analysis System, NASA Goddard Space Flight Center, publication X-945-80-25, 1980.

[2] Schnupp, P., Huu, C.T.N., Bernhard, L.W.: Expert Systems Lab Course, Springer-Verlag, Berlin/Heidelberg, 1989.

[3] Schuh, H., Schwegmann, W.: A Vision Towards Automated Real-Time VLBI, Physics and Chemistry of the Earth, Vol. 25/12, p. 813-817, 2000.

[4] Schwegmann, W., Schuh, H.: On the Automation of the Mark III VLBI Data Analysis System, Proc. of the 13^{th} Working Meeting on European VLBI for Geodesy and Astrometry, Viechtach, February 1999, eds. W. Schlüter and H. Hase, p. 265-272, Bundesamt für Kartographie und Geodäsie, Wettzell, 1999.

[5] Schwegmann, W.: Using a Knowledge-Based System for the VLBI Data Analysis, Proc. of the 14^{th} Working Meeting on European VLBI for Geodesy and Astrometry, Castel San Pietro Terme, September 2000, eds. P. Tomasi, F. Mantovani and M. Perez Torres, Bologna, 2000.

[6] Sundermeyer, K.: Knowledge-Based Systems: terminology and references, BI-Wissenschaftsverlag, Mannheim/Wien/Zürich, 1991.

Volker Tesmer et al.: Reassessment of Highly Resolved EOP Determined with VLBI, Proceedings of the 15th Working Meeting on European VLBI for Geodesy and Astrometry, p.83–90
http://www.ieec.fcr.es/hosted/15wmevga/proceedings/tesmer

Reassessment of Highly Resolved EOP Determined with VLBI

Volker Tesmer [1], *Hansjörg Kutterer* [1], *Burghard Richter* [1], *Harald Schuh* [2]

[1] *Deutsches Geodaetisches Forschungsinstitut, DGFI*

[2] *Institute of Geodesy and Geophysics, Vienna University of Technology*

Contact author: Volker Tesmer, e-mail: tesmer@dgfi.badw.de

Abstract

VLBI is the only geodetic space technique which directly links the terrestrial and the celestial reference frame. Since nearly all observing networks are of global nature, VLBI is particularly suitable to deduce the Earth orientation parameters (EOP). In this paper, investigations are presented which were carried out to assess highly resolved EOP determined by means of VLBI. A theoretical consideration shows that an attempt to estimate simultaneously daily nutation parameters and subdaily pole coordinates would lead to high correlations between these parameters so that they are practically not separable. Furthermore, the relation between the observing geometry and highly resolved EOP was investigated using typical NEOS-A, CORE-A and IRIS-S sessions. Systematic correlation schemes were detected between highly resolved EOP and also very weakly determined EOP in single time intervals were found. Amplitudes of the eight diurnal and semidiurnal main tides in ΔUT1 were deduced from one-hourly estimates of 52 simultaneous NEOS-A and CORE-A sessions. The results were compared with results of other geodetic space techniques as well as the model for daily and subdaily ocean tidal variations in the Earth's rotation by Ray (IERS Conventions, 1996). The computations were done with the OCCAM 5.0 software using a least-squares approach in the Gauss-Markov model.

1. Theoretical separability of daily nutation parameters and subdaily EOP

The Earth's orientation in space can be described by the rotation matrix **R** transforming between a celestial reference frame (CRF), which is defined by the coordinates of radio sources, and a terrestrial reference frame (TRF), which is defined by the station coordinates of the observing network.

$$\mathbf{R} = \underbrace{\mathbf{W}^T \cdot \mathbf{S} \cdot \Delta\mathbf{N}}_{\mathbf{M}} \cdot \mathbf{N} \cdot \mathbf{P}$$

P - precession model
N - nutation model
ΔN - correction to nutation model ($\Delta\psi$, $\Delta\varepsilon$)
$\mathbf{W}^T$ - motion of CEP (2003: CIP) relative to TRF (X, Y)
S - daily rotation about CEP (θ)

Principally, a transformation between two reference frames can always be performed using three angles only, whereas the matrix **R** consists of five parameters. This is why dependences between some parameters in **R** are to be expected under certain circumstances.
Let the rotation matrix **R** or, after deduction of the precession matrix **P** and the nutation matrix **N**, the remaining matrix **M** be given from observations for a certain instant. Its elements can be used to estimate the orientation parameters. Most interesting is the question to what extent the nutation corrections $\Delta\psi$, $\Delta\varepsilon$ and the pole coordinates X, Y, which both describe the direction of the celestial ephemeris pole (CEP) in different reference systems, can independently be estimated. The fifth parameter θ (equivalent to ΔUT1) is independent from the others and is excluded by considering only four elements.

$$\mathbf{M} = \mathbf{W}^T \cdot \mathbf{S} \cdot \Delta\mathbf{N}$$

Coefficients of **M** specifying $\Delta\psi$, $\Delta\varepsilon$, X, Y:

$$M_{1,3} = -\cos\theta \cdot \sin\varepsilon \cdot \Delta\psi - \sin\theta \cdot \Delta\varepsilon + X$$
$$M_{2,3} = \sin\theta \cdot \sin\varepsilon \cdot \Delta\psi - \cos\theta \cdot \Delta\varepsilon - Y$$
$$M_{3,1} = \sin\varepsilon \cdot \Delta\psi - \cos\theta \cdot X - \sin\theta \cdot Y$$
$$M_{3,2} = \Delta\varepsilon - \sin\theta \cdot X + \cos\theta \cdot Y$$

These four equations (only two of which are linearly independent) define the functional model which leads to the Jacobian matrix presented in Figure 1 for one day of observation. The nutation corrections $\Delta\psi$, $\Delta\varepsilon$ are assumed as constant during the whole day while the pole coordinates X, Y are estimated for n time intervals over the day.

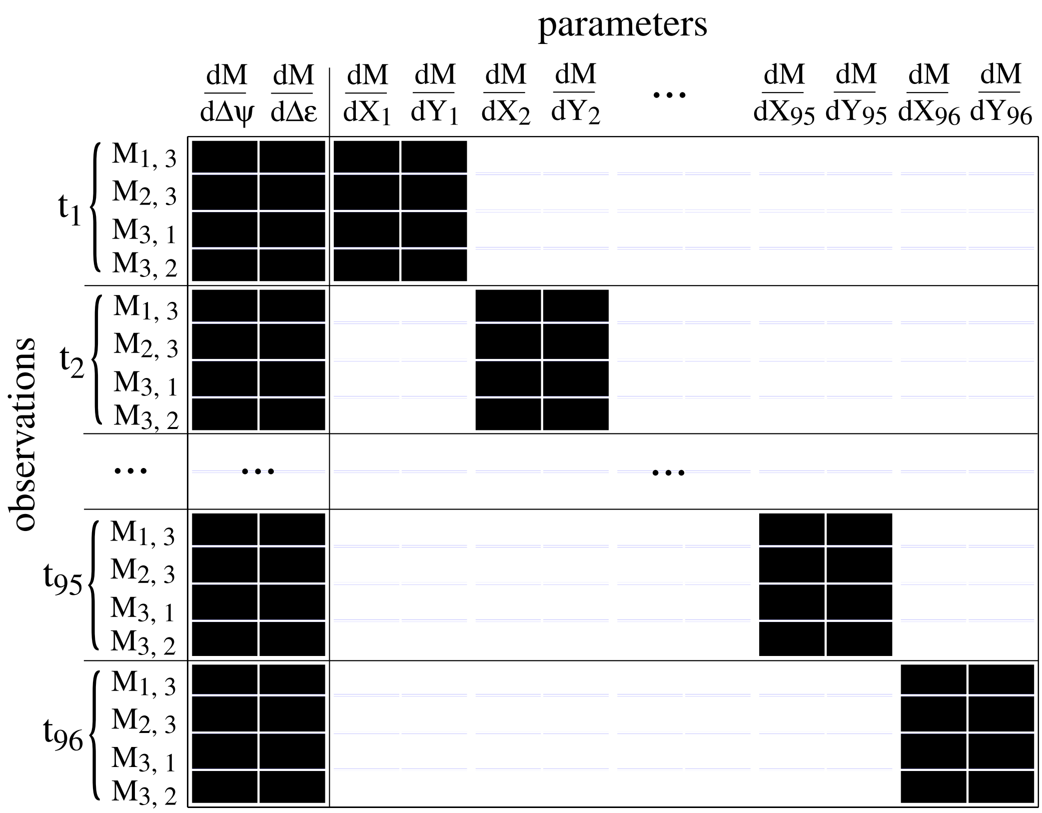

Figure 1. Jacobian matrix for estimating both nutation corrections and pole coordinates from elements of the rotation matrix **M**

The coefficients of the Jacobian matrix are the partial derivatives of the four elements $M_{1,3}$, $M_{2,3}$, $M_{3,1}$, $M_{3,2}$ of the matrix $\mathbf{M}$ with respect to the orientation parameters $\Delta\psi$, $\Delta\varepsilon$ and X_i, Y_i, where the subscript i denotes the respective time interval ($i = 1, 2, ..., n$).
The corrections to the nutation model $\Delta\psi$ and $\Delta\varepsilon$ and $2n$ pole coordinates X_i and Y_i are the unknown parameters, where n specifies the temporal resolution of the pole coordinates, e.g. $n = 1$ means a 24-hour interval, $n = 96$ a 15-minute interval. The correlation matrix of the estimated parameters can be derived based on the error propagation law.
In the following it is assumed that the coefficients $M_{1,3}$, $M_{2,3}$, $M_{3,1}$, $M_{3,2}$ are observed every 15 minutes. Thus there are altogether 384 observations in 24 hours, corresponding with the optimistic assumption that the orientation of the Earth in space can be fully determined every 15 minutes by means of VLBI.

Figure 2 shows six correlation scenarios derived from the coefficients of the rotation matrix **M**. The column on the left ('nutation estimated') represents an approach where pole coordinates were estimated in time intervals of 24 hours, 4 hours and 1 hour together with daily corrections to the nutation model. The matrices in the right column ('nutation fixed') are obtained without estimating corrections to the nutation model.
If both pole coordinates and corrections to the nutation angles are estimated together in a 24-hour interval, there are no correlations (Figure 2, upper row). Pole coordinates estimated in high temporal resolution are highly correlated with daily corrections to the nutation angles if estimated simultaneously (Figure 2, lower row). As a consequence, the nutation angles must be fixed to best known a-priori values of the model MBH proposed by the new IERS Conventions (2000).

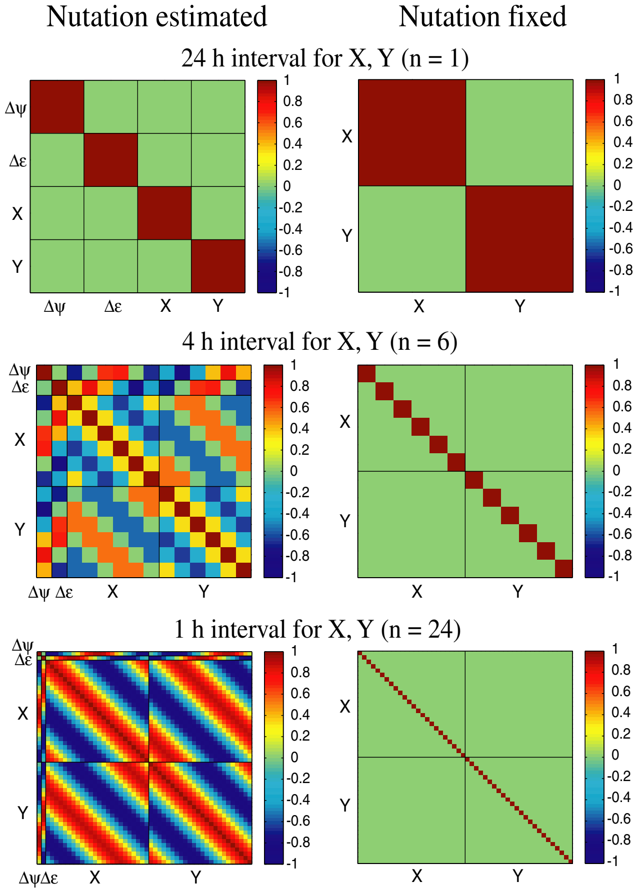

Figure 2. Correlations between $\Delta\psi$, $\Delta\varepsilon$, X, Y determined by a theoretical approach

2. Relation between the observing geometry and highly resolved EOP

In this section, real observation data from representative VLBI sessions are analysed using the OCCAM 5.0 software using a least-squares approach in the Gauss-Markov model (see [4] Titov et al., 2001). The stations were fixed to ITRF2000 coordinates and the observed radio sources to the ICRF-Extension 1. A usual parameterisation was carried out except for the EOP, which were solved in intervals of 1 hour (Sect. 2.1) and 15 minutes (Sect. 2.2), respectively. Nutation parameters were fixed to the values of the MBH model. Some evidences concerning the relation between the reference frames and highly resolved EOP are given and discussed.

2.1. Systematic correlations of EOP due to network configurations and scheduling

The upper row of Figure 3 displays the network configuration of three typical VLBI networks, NEOS-A, CORE-A and IRIS-S. All these 24h-sessions consist of 1200 to 1600 observations, involving 5 or 6 stations and 50 to 60 radio sources. The lower row illustrates the correlations between one-hour EOP estimates of these sessions. The X, Y and ΔUT1 parameters are almost independent, but there are two kinds of minor systematic correlations between highly resolved EOP due to network configurations and observation scheduling:

- **Systematic correlations between temporally consecutive parameters of one type**
  The one-hour X estimates of the IRIS-S session (see Figure 3, right) show a distinct band of correlation with a width of up to three hours. The values between temporally consecutive parameters are on average +0.6, and can reach +0.9 and more for contiguous time intervals. The one-hour X estimates of the NEOS-A session (see Figure 3, left) show less significantly the same. The reason for the relatively high correlations is a slowly varying observing geometry in consecutive intervals. A high number of well-distributed stations can reduce this effect. The CORE-A session in Figure 3 (center), e.g., containing six observing stations has the smallest correlations between the EOP. Besides this, a close look into the VLBI observation schedule has to be carried out because both the number and the geometric distribution of the observed sources also play important roles for the correlations between temporally consecutive parameters of one type.

- **Systematic correlations between different EOP within the same time interval**
  NEOS-A X and ΔUT1 estimates show a clear correlation structure for parameters within the same time interval. This is in agreement with a previous investigation: usual 24-hour EOP estimates of 52 NEOS-A sessions in 1999 showed highly correlated X and ΔUT1 estimates, too. Their average correlation of -0.67 has the same order of magnitude as the correlation of the NEOS-A one-hour EOP estimates shown in Figure 3 (between -0.4 and -0.8). The fact that these similar correlations appear between the 24-hour estimates as well as between one-hour estimates is a clear hint that the geometry of the observing network is decisive for systematic correlations of different EOP within the same time interval. The NEOS-A configurations usually cover only a quarter of the Earth, what is not sufficient for an optimal separability of the EOP. The highly resolved EOP estimates derived from the IRIS-S session which are presented in Figure 3 (between -0.3 and -0.5) show less distinctly the same.

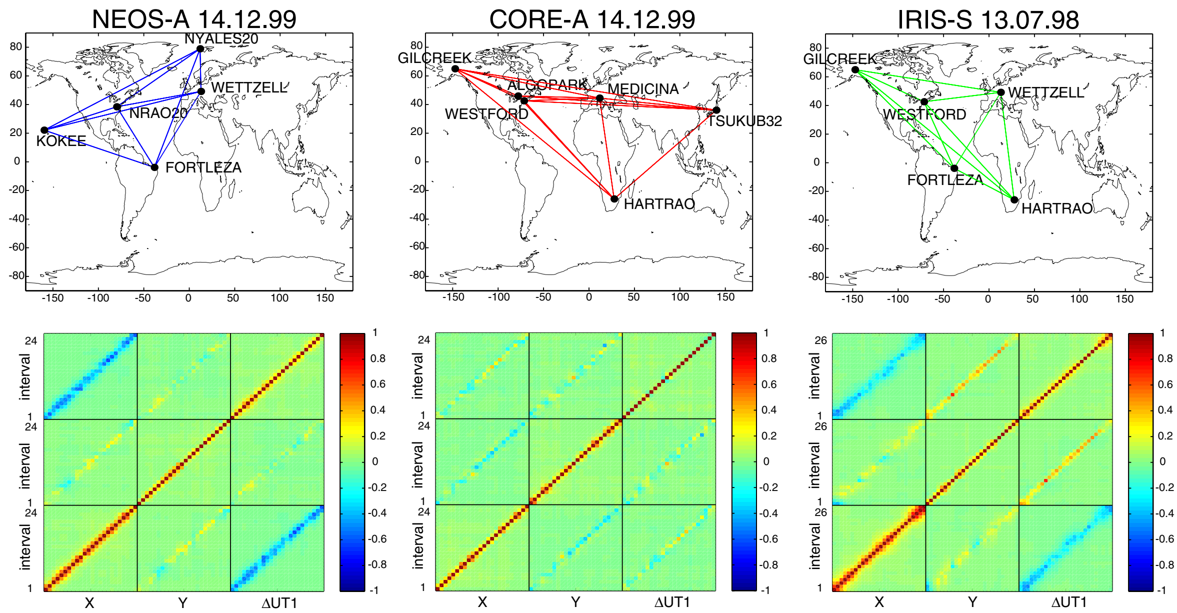

Figure 3. Network configurations and correlations between one-hour EOP estimates of typical VLBI sessions

2.2. Observing geometry in short intervals

Highly resolved EOP are of interest for geodesists, as corrections to their measurements, and for geophysicists who want to understand the characteristics of the Earth's body like its resonance frequencies which are expected to have periods of one hour or even less. Currently, the technical limit of time resolution of VLBI-determined EOP is supposed to be about 15 minutes. This is because each slewing of the telescope and each observation take several minutes and because usually several temporally subsequent observations are necessary to determine the EOP. The upper plots of Figure 4 show one-hour and 15-minute estimates of ΔUT1 and their formal errors from a typical CORE-A session of 24 hours. The ΔUT1 values were corrected for daily and subdaily ocean tidal variations by Ray (IERS Conventions (1996), [2] McCarthy, 1996). In the series of one-hour ΔUT1 estimates shown in the left upper plot, the formal errors are in the order of magnitude of $8\,\mu$s. There is one irregular value at 21 h which is distinctly different from the neighbouring values. Its formal error of $13\,\mu$s is much larger, too. Since the formal errors do not represent the inaccuracy situation completely, the variance-covariance matrix was further investigated. One eigenvalue is equal to $180\,\mu s^2$, all the others are below $110\,\mu s^2$. The coordinates of the normalized eigenvector which belongs to the maximum eigenvalue are shown in the lower left plot of Figure 4. All of them are approximately zero, except the coordinate at 21 h which is equal to -1. So the semi-major axis of the error hyperellipsoid has the direction corresponding to the ΔUT1 parameter at 21 h. That means that the large eigenvalue is exclusively assigned to this particular parameter which can therefore be regarded as independent of the others.

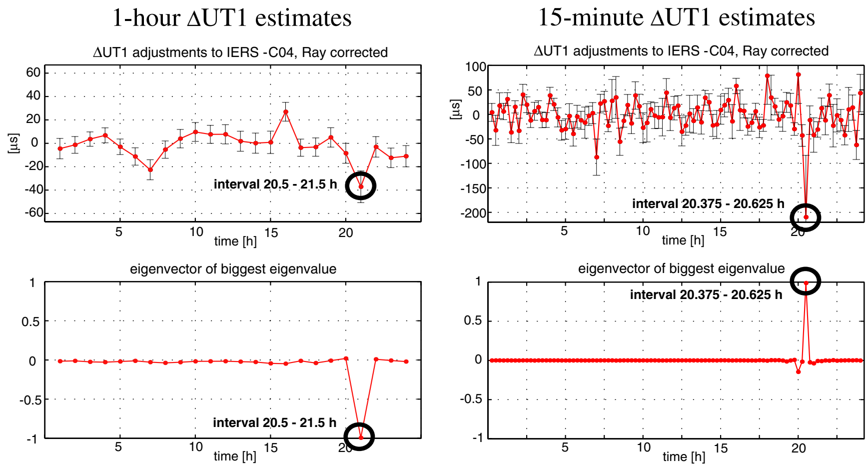

Figure 4. CORE-A 14.12.99 ΔUT1 estimates

The 15-minute estimates of ΔUT1 shown in the upper right plot are much more irregular than the one-hour estimates in the upper left plot. Also their formal errors, ranging from $20\,\mu s$ to $45\,\mu s$, are two to four times larger than those of the one-hour estimates. This is not surprising because the number of observations contributing to the estimation of one parameter is now smaller by a factor of four on avarage. In this high temporal resolution, the irregularity detected previously at the one-hour interval from 20.5 h until 21.5 h appears to be much more pointed: its temporal location is specified to the quarter hour from 20.375 h to 20.625 h, whereas the immediately neighbouring parameters are quite regular, and the deviations of both the estimated parameter and its formal error ($125\,\mu s$) are much larger than in the former case. This is also reflected in the eigenvalues of the variance-covariance matrix: all but one are smaller than $3500\,\mu s^2$; only one eigenvalue is equal to $16300\,\mu s^2$. Again, the coordinates of the normalized eigenvector belonging to the largest eigenvalue in the lower right plot of Figure 4 reveals that the large inaccuracy is solely attributed to the one parameter estimation at 20.5 h.

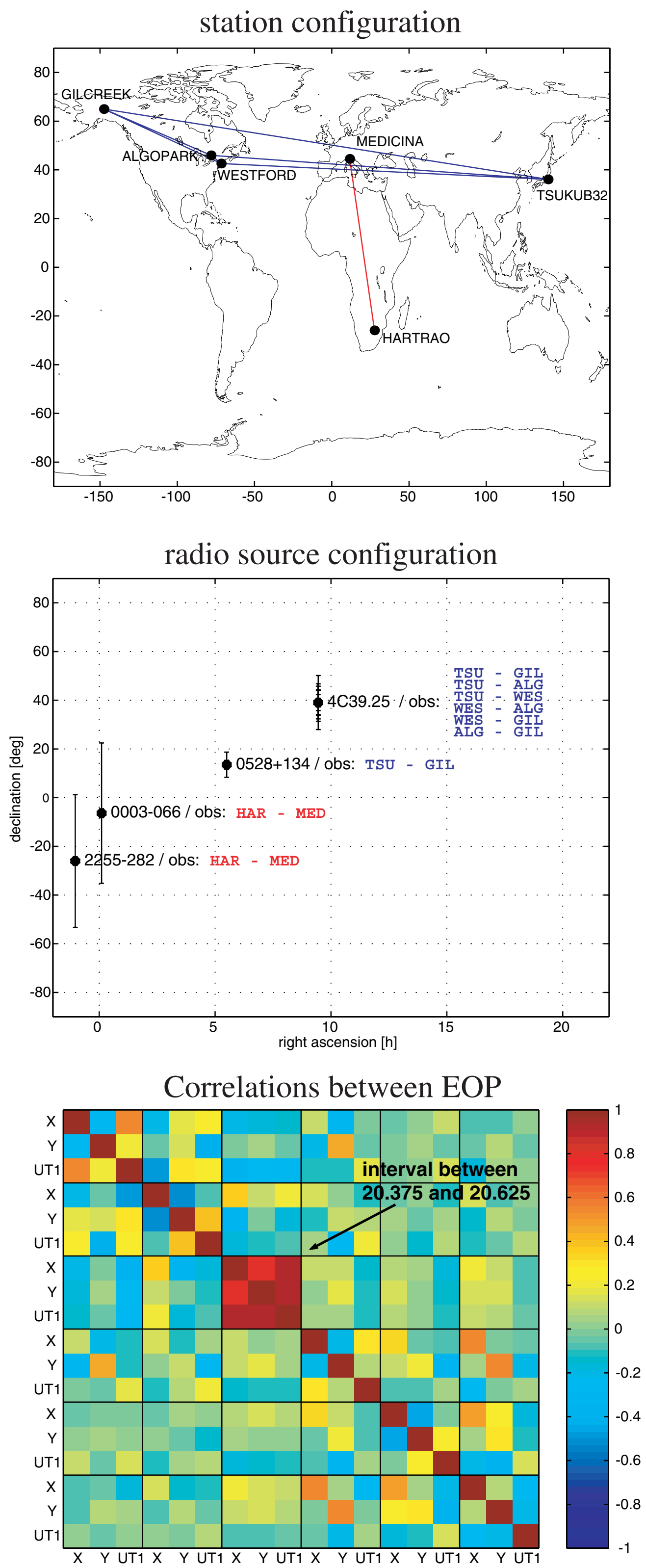

Figure 5. Particular 15 min interval between 20.375 and 20.625 h (CORE-A 14.12.1999)

Quite generally, one can state that the uncertainty superposing the EOP signal is the larger, the smaller the time intervals of EOP estimation are. This uncertainty is caused by inavoidable observation errors and imperfect models in connection with an unfavourable arrangement of observations. Especially the influence of (random) observation errors is reduced by extending the time intervals of EOP estimation because of the levelling effect of a larger number of observations contributing to the estimation of one parameter.

The poor ΔUT1 estimation in the 15-minute interval between 20.375 h and 20.625 h gave occasion to scrutinize the observing situation during this time interval. The upper picture of Figure 5 illustrates the station configuration in this interval. It shows a typical well-distributed station network.

But there were only four radio sources observed, which were not well distributed over the whole sky (middle picture of Figure 5). Only nine observations were performed during the 15-minute interval. Six of them were directed to one radio source, and the other three sources were observed from only one baseline each. Two of these observations, both from the baseline Medicina – HartRao, have very large formal errors as indicated by the error bars. This is definitely not a good arrangement of observations for determining the instantaneous orientation of the terrestrial reference frame with respect to the celestial one.

As illustrated in the lower picture of Figure 5, the poor observing geometry leads to very high correlations between the estimated EOP in this interval, what means that the rotation angles cannot well be separated from each other (see [1] Kutterer, 2001).

3. Preliminary results: validation of ocean tidal amplitudes in ΔUT1 derived using OCCAM

The capability of the upgraded VLBI software package OCCAM 5.0 LSM (least-squares method in the Gauss-Markov model) for subdiurnal EOP resolution was assessed keeping the results of the previous sections in mind. For this purpose the four diurnal and the four semidiurnal oceanic main tide responses in ΔUT1 were derived by means of a weighted least-squares adjustment from hourly estimated values of 52 representative simultaneous CORE-A and NEOS-A sessions between January 1997 and April 2000. As the observations of the parallel sessions are mostly independent, they are a good basis for an assessment of the software in use. External comparisons were carried out using most recent high-resolution results of other groups based on geodetic space techniques (VLBI, GPS) and the model for daily and subdaily ocean tidal variations in the Earth's rotation by Ray (IERS Conventions, 1996).
The signal amplitudes obtained using the OCCAM software (Figure 6, A, B, C) show a good agreement among each other. They are quite consistent with the values by Ray (D), which are based on a TOPEX-POSEIDON constrained ocean tide model. Small differences caused by other excitations are to be expected. In addition, the results fit quite well to values derived by other scientists which are based on VLBI data (E: C. Ma and M. Rothacher) and GPS data (F: M. Rothacher) ([3] Rothacher, 2001). The small differences may be due to the number and time span of the data taken into account and needs to be subject of further investigations.

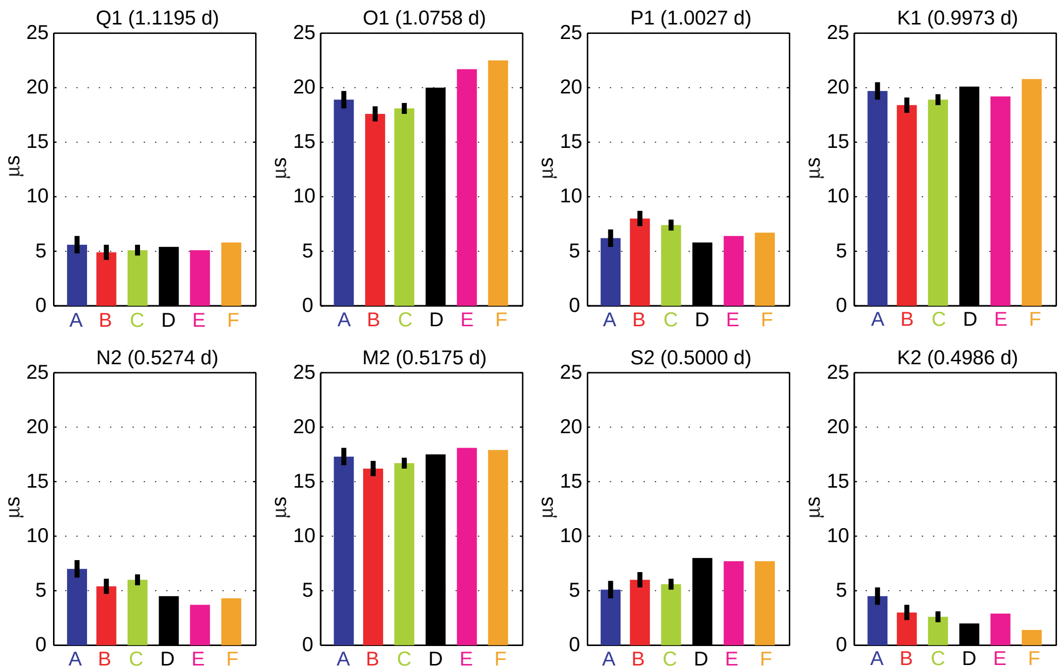

Figure 6. Amplitudes of the four diurnal and four semidiurnal main tides in ΔUT1

legend:

A: DGFI solution (OCCAM 5.0) with formal errors, from 52 NEOS-A Sessions
B: DGFI solution (OCCAM 5.0) with formal errors, from 52 CORE-A Sessions
C: DGFI solution (OCCAM 5.0) with formal errors, from simultaneous Sessions type A and B
D: Ray model (TOPEX/POSEIDON data), IERS Conventions (1996)
E: 20 years VLBI ΔUT1 time series provided by C. Ma, computed by M. Rothacher
F: 4 years GPS ΔUT1 time series, by M. Rothacher

4. General remarks and conclusions

Highly resolved EOP can be determined very well by means of VLBI using the OCCAM 5.0 software with its least-squares approach in the Gauss-Markov model. When increasing the EOP resolution to less than 24h, the nutation angles have to be fixed to best-known model values. Significant correlations between highly resolved EOP and clock as well as tropospheric parameters were not found. Today's observing schedules generally allow to obtain reliable EOP with a one-hour resolution. A higher resolution is possible if by dedicated observing schedules high correlations between EOP could be mitigated. But for technological reasons, currently the time intervals cannot be shorter than about 15 minutes.

There are mainly two kinds of systematic correlation between highly resolved EOP due to network configurations and scheduling of observations. Firstly, correlations between temporally consecutive parameters of the same type occur because the observing geometry varies too slowly. They are significant within a time span up to three hours and can take on positive values up to +0.8, depending on the length of the time intervals. Secondly, there are correlations between different EOP within the same time interval. They result from an anisotropy of the accuracy of the orientation of the Earth, which is due to the instantaneous observation geometry and to the orientation of the terrestrial reference axes of the parameters X, Y, ΔUT1 within the Earth. (The correlations would vanish if the axes of the terrestrial reference frame coincided with the principal axes of the error ellipsoid). Depending on the network, these correlations of the second kind from the investigated sessions are nearly zero or take on values between -0.4 and -0.8.

The observation geometry consists of three factors, namely the configuration of the terrestrial station network, the distribution of the observed radio sources on the celestial sphere, and the scheduling of observations connecting radio sources and stations. They all influence the accuracy of EOP estimation. Existing programs for generating observation schedules do not ensure a good observation geometry in each time interval with regard to a high resolution of EOP. A poor observation geometry during one time interval can lead to correlations between EOP estimates of 0.9 and more. Additionally, if there are very few observations only, both errors in the functional and stochastic models and the technical limitation of the observation accuracy can lead to unreliable estimates and huge formal errors. For further analysis and interpretation it is generally recommended to take the full variance-covariance matrix of the highly resolved EOP into account. In case of resolution shorter than one hour, neglecting the full variance-covariance matrix can cause substantial errors.

References

[1] Kutterer, H., Tesmer, V.: Subdiurnal Earth Orientation Parameters from VLBI – Determinability and Significance. Proceedings of the IAG Scientific Assembly, Budapest 2001, to be published.

[2] McCarthy, D.D. (ed.): IERS Conventions (1996), IERS Technical Note 21. Observatoire de Paris, 1996.

[3] Rothacher, M.: Private Communication, 2001.

[4] Titov, O., Tesmer, V., Boehm, J.: OCCAM 5.0 Users Guide. AUSLIG Technical Reports 7, AUSLIG, Canberra, 2001.

Yasuhiro Koyama et al.: Internet VLBI system and 1 Gbps VLBI System Based on the VSI, Proceedings of the 15th Working Meeting on European VLBI for Geodesy and Astrometry, p.91–98
http://www.ieec.fcr.es/hosted/15wmevga/proceedings/koyama

Internet VLBI system and 1 Gbps VLBI System Based on the VSI

Yasuhiro Koyama, Tetsuro Kondo, Junichi Nakajima, Mamoru Sekido, Moritaka Kimura

Communications Research Laboratory
Contact author: Yasuhiro Koyama, e-mail: koyama@crl.go.jp

Abstract

Recent technological developments at the Communications Research Laboratory are mainly aiming for improvements of the sensitivity by expanding the observation frequency bandwidth and establish real-time capabilities of the VLBI observations and data processing. For these purposes, Giga-bit VLBI system and the IP-based real-time VLBI system are currently under developments. Among of these research and developments, recent achievements and future plans will be reported.

1. Introduction

As the technology development center of the International VLBI Service for Geodesy and Astrometry, Communications Research Laboratory (CRL) has been developing and performing researches in various fields of VLBI, including technological developments of data acquisition and data processing systems. The recently established Key Stone Project (KSP) VLBI network is an integration of the researches and developments at CRL. For the KSP VLBI Network system, a lot of technological challenges were made and realized. Among of all, the real-time VLBI system was realized by using high speed data transmission system over the Asynchronous Transfer Mode network which connects the four observation sites at Kashima, Koganei, Miura, and Tateyama. The observation and data processing systems were also fully automated. As the results, frequent VLBI experiments became possible and the results of an experiment became available immediately after each observation session. The usefulness and the power of the automated real-time VLBI system was clearly demonstrated by the dense measurements during the dramatic crustal deformation event associated with volcanic activities of the Miyake-jima volcano started in June 2000. Figure 1 shows the horizontal site coordinates of the Tateyama site measured by the KSP VLBI network. As clearly seen in the figure, the north-eastward motion of the site starting the end of June 2000 was observed. The motion continued for a few months and the accumulated motion reached about 5cm. Similar large site motions were observed at other sites by VLBI and GPS techniques as shown in the Figure 2. These site motions can be explained with the theoretical model assuming a combination of a strike slip fault and a dyke as illustrated in the Figure 3. Such a irregular site motions were first studied by the VLBI technique and it was made possible by the real-time and automated features of the KSP VLBI Network.

This real-time VLBI technique is also used to connect a 64-m antenna at Usuda Deep Space Center of the Institute of Space and Astronautical Science (ISAS) and a 34-m antenna at Kashima Space Research Center of CRL to realize a real-time VLBI baseline of a length of 208 km under the collaboration of CRL, ISAS, National Astronomical Observatory (NAO), and Nippon Telegraph and Telephone Corporation (NTT). Test observations were successfully carried out in December 1998 at the data rate of 256 Mbps and this project was named GALAXY since then. The observation sessions of the GALAXY project have been performed once every several months. After developing Giga-bit VLBI systems and ATM network interfaces, test observations were carried out at the date rate of 1024 Mbps on June 23, 2001. The test observations were successful and the improved sensitivity of the observations with the extended bandwidth was demonstrated. Efforts

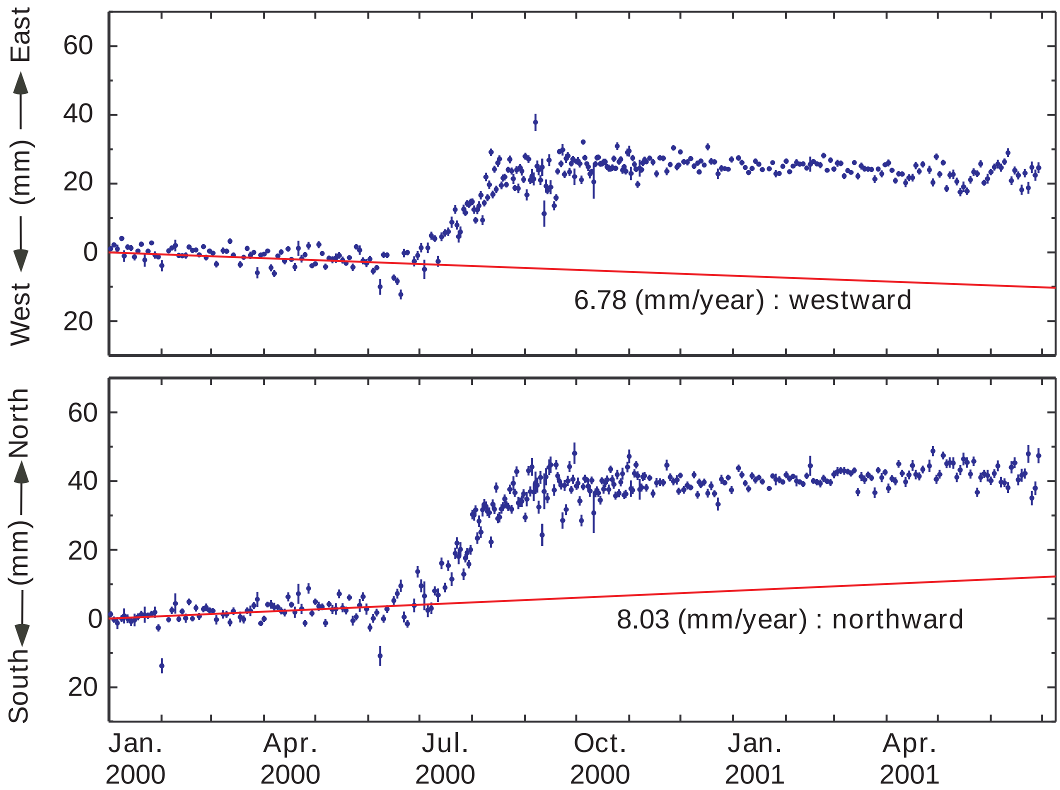

Figure 1. Horizontal site coordinates of Tateyama determined from KSP VLBI observations. Error bars are the estimated one-sigma formal error uncertainties of the coordinates. In each plot, a least square fit for the data before June 2000 is shown by a slanted line.

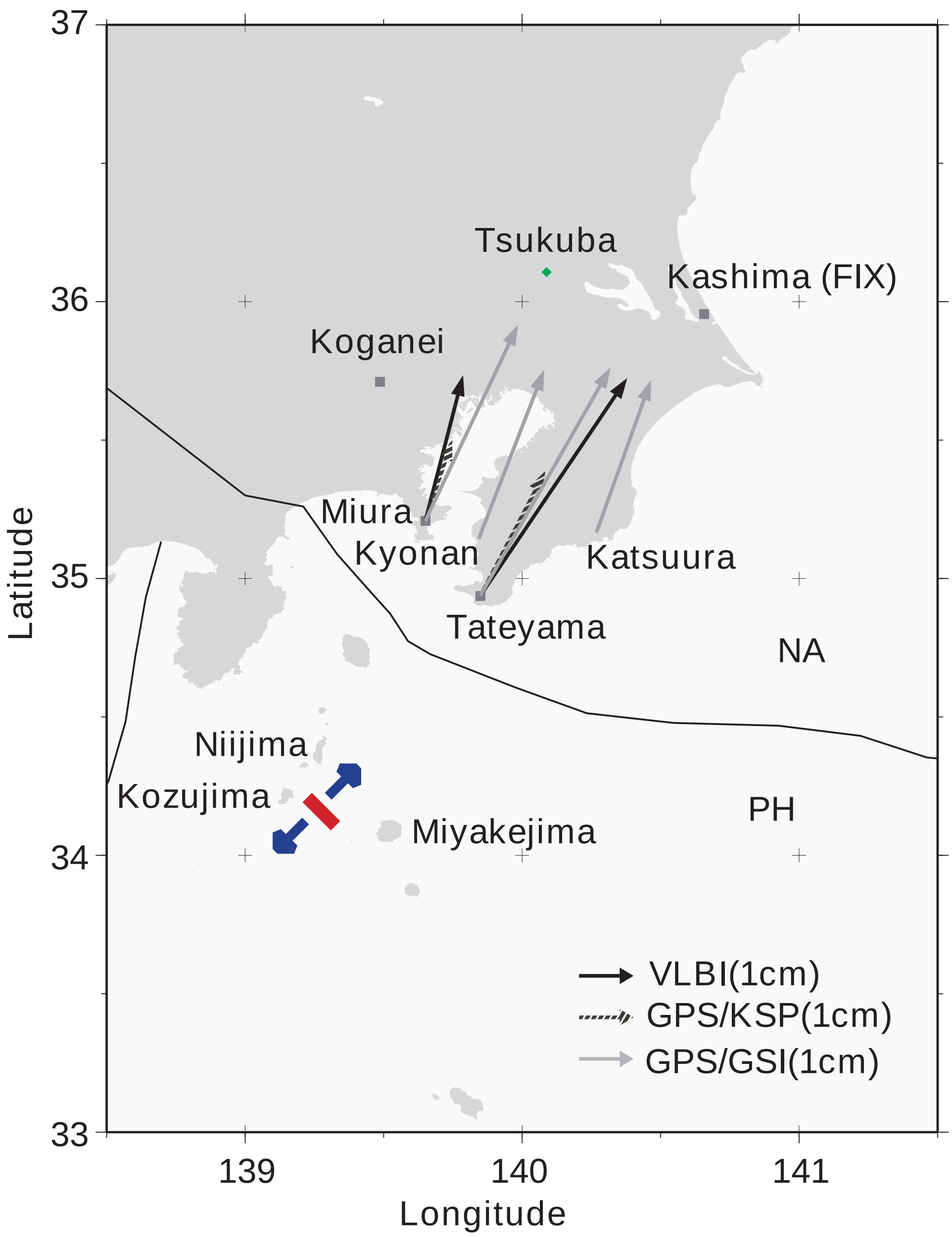

Figure 2. Horizontal site motions detected at south-Kanto area observed by VLBI and GPS techniques.

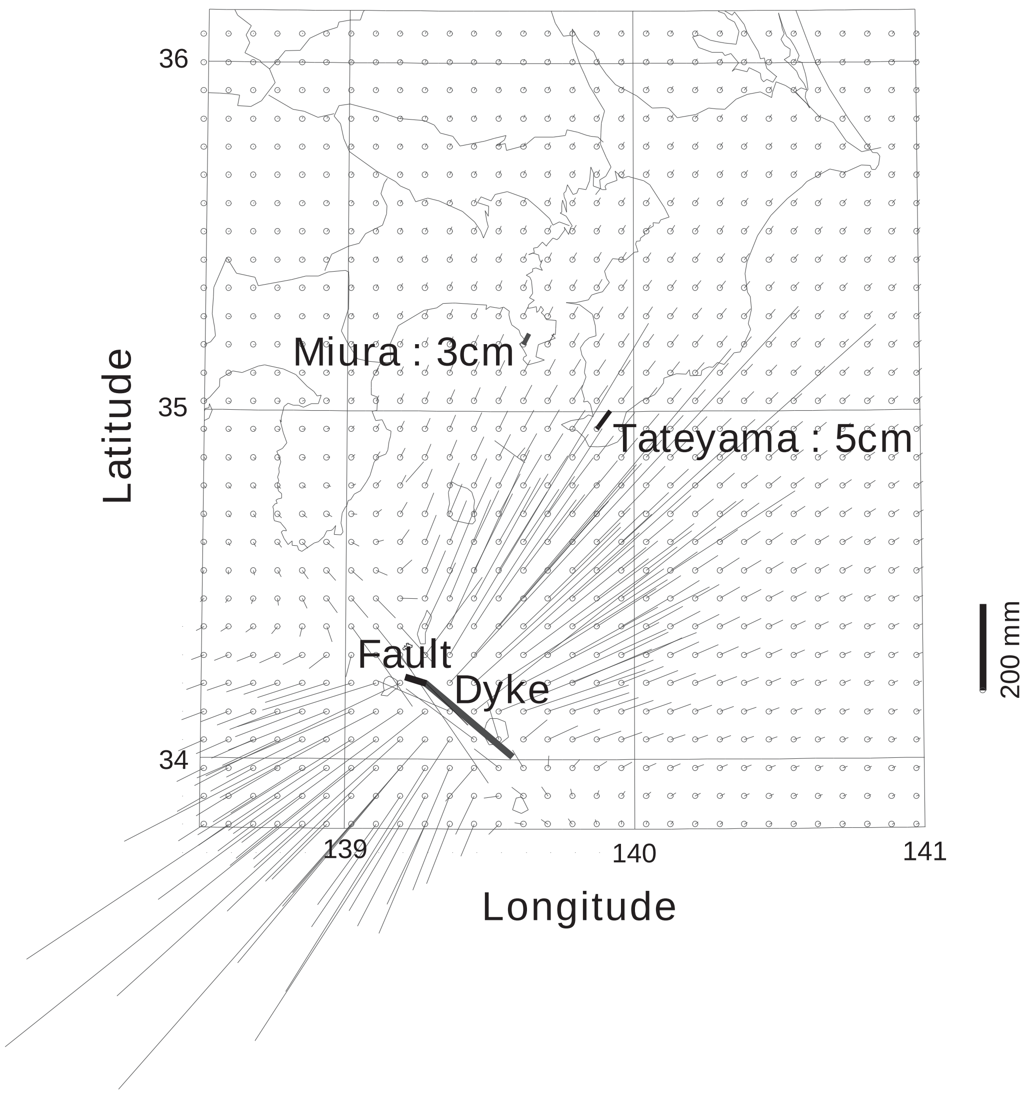

Figure 3. Proposed theoretical model which explains the crustal deformation observed in the south-Kanto area. A combination model with a strike slip fault and a dyke is assumed and the resulting horizontal deformation pattern by using the assumption is shown in the figure.

are continuing to make it possible to use most of the network speed of 2.4 Gbps by realizing 2048 Mbps real-time VLBI observations. We are expecting to perform test observations at the data rate of 2048 Mbps in early 2002.

After the realization of the KSP VLBI systems, CRL has been concentrating its efforts in two major directions. One of the directions is to realize real-time VLBI system over the Internet by using IP protocol. The other direction is to enhance the sensitivity of the VLBI system by increasing the data rate of the data acquisition system. The current status of these developments will be described in this report.

2. Giga-bit VLBI System

The developments of the giga-bit VLBI system began in 1996 and the first successful observations were performed on October 19, 1999. The system is consisted by a sampler system, a data recording system, and a data correlation system. The sampler system was initially developed by modifying a commercially available digital oscilloscope unit so that the observed data are sampled at the data rate of 1024 Msps and only one bit data stream out of 4 sampling bits is extracted. The data recording system was developed by modifying commercially available high definition broadcasting recorder system so that it can record at the data rate of 1024 Mbps. The correlator system was initially developed as the real-time correlator for the Nobeyama Millimeter Array of NAO. These systems constitute the initial version of the Giga-bit VLBI system and were used in a series of geodetic and astronomical VLBI sessions since the year 1999.

The developments of the second generation Giga-bit VLBI system have began to adapt the hardware specifications of the VLBI Standard Interface (VSI) of which the first version was agreed in August 2000. All the systems were re-designed to meet the specifications. The Figure 4 shows the new data recorder unit which is capable to record digital data stream at the data rate of 1024 Mbps. Multiple data recorder units can be synchronized so that multiple channels can be recorded simultaneously by using two or more units. The Figure 5 shows the new sampler unit which uses high speed digital sampling chip and it is capable to sample 1 channel data at 1024 Mbps 1 bit/sample.

Figure 4. The VSI based Giga-bit data recorder unit.

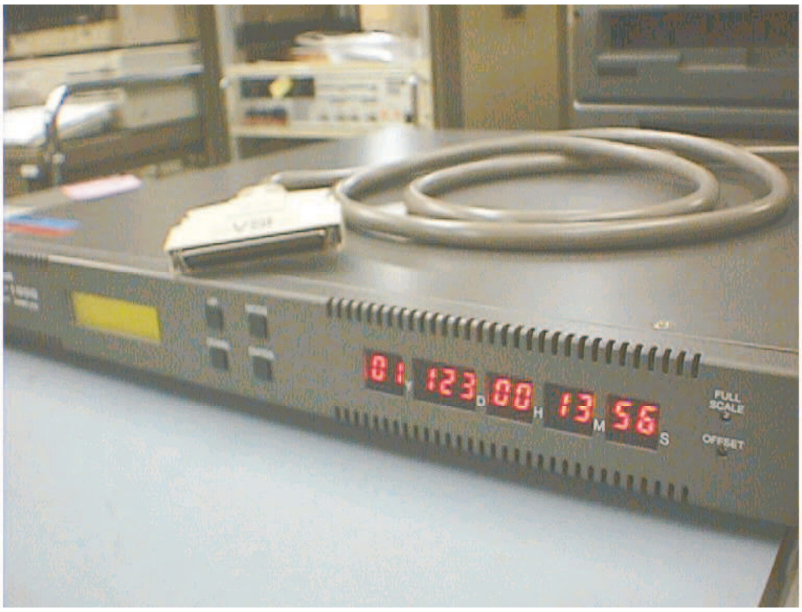

Figure 5. The VSI based Giga-bit data sampler unit.

The new data correlator unit is capable to correlate two data streams at the data rate of 1024 Mbps. The unit can be used to correlate two data channels for single baseline or one data channel for two baselines simultaneously by synchronizing the data recorder units. All these new systems are interfaced with each other based on the VSI specifications. Therefore, these systems can be connected with other VLBI systems as far as the other systems are also based on the VSI specifications.

3. Internet VLBI System

In the KSP real-time VLBI system, data are transmitted through the high-speed ATM network. However, the cost of the ATM network is still expensive and connection sites are extremely limited, and hence the ATM-VLBI is not yet well generalized. Therefore, We started developments of the new real-time VLBI system using IP (Internet protocol) technology expecting we can reduce the cost of the network and to expand connected sites for the real-time VLBI observations. We call this system Internet VLBI system, and started the development in late 1999. We have been developing the PC-based Internet VLBI system consisting of a PCI-bus sampler board (Figure 6) and softwares to make real-time data transmission and reception. We also intend to carry out the real-time correlation on a PC system. One sampler board can have four video signal inputs and is designed to be able to sample analog signal with a frequency of up to 16 MHz for one bit sampling level. The sampler board has been evaluated by using actual signals from radio sources. Real-time characteristics have been evaluated by using the Local Area Network at Kashima Space Research Center. So far, we confirmed the sufficient performance of coherent sampling up to 16 MHz sampling. Regarding the real-time correlation processing by using a PC system, we can process 4 MHz sampling data in real-time at present. Improvements on the software algorithm to make correlation processing faster are in progress.

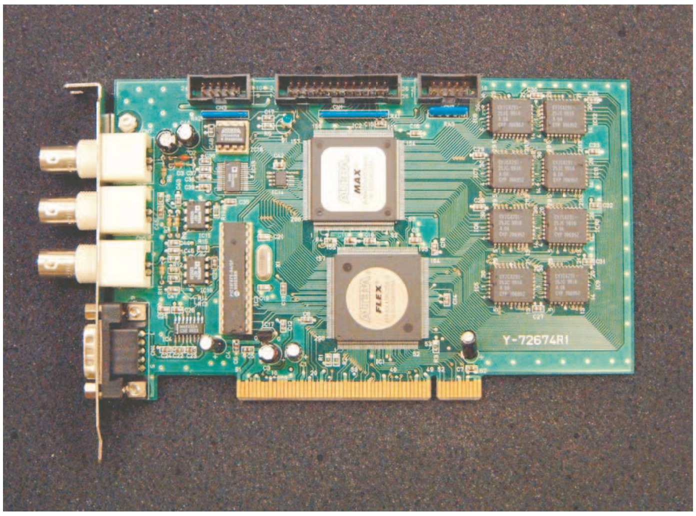

Figure 6. The sampler board for the Internet VLBI. The board has three BNC connectors to receive observed data, 10 MHz reference signal, and 1 PPS (pulse-per-second) signal. The board is expandable to sample four input data channels.

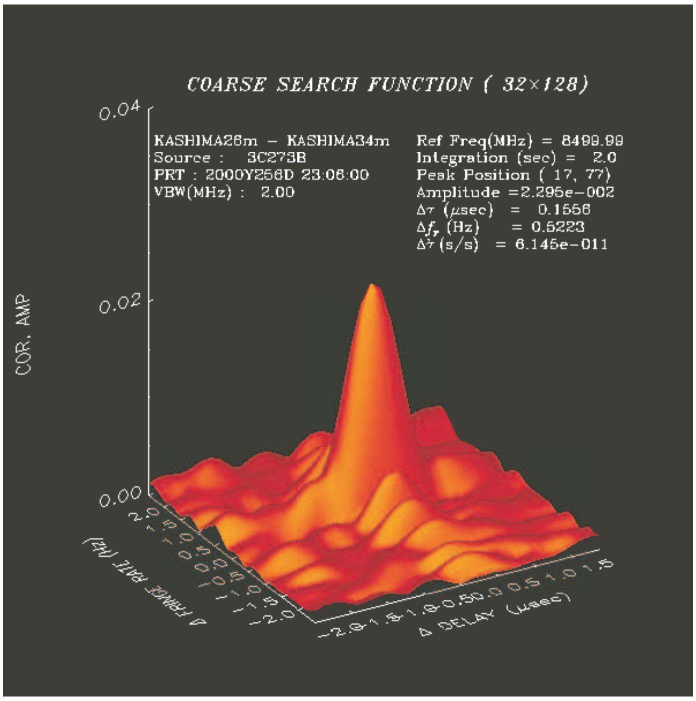

Figure 7. The coarse search function which indicate successful detection of a fringe for the baseline between 26-m antenna and 34-m antenna at Kashima Space Research Center. The correlation processing was performed on a PC system after the sampled data were locally stored on a disk and then transfered to a PC for correlation processing.

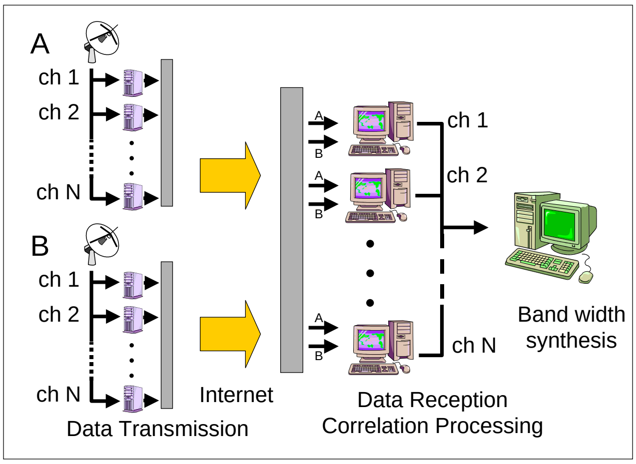

Figure 8. A concept of multiple channel observations and real-time correlation processing for geodetic VLBI observations.

4. Conclusions and Future Perspectives

The researches and developments of the Giga-bit VLBI system and Internet VLBI system were described. Both systems are in developments and we are expecting to complete these systems in 2002. The Giga-bit VLBI system will enable us to perform sensitive VLBI observations at 1024 Mbps, or much faster data rates if we use multiple data recording system. The Internet VLBI system, on the other hand, will enable us to perform real-time VLBI observations with more sites other than the currently connected sites. In the future, our vision is to establish variety of the VLBI data acquisition systems based on the VSI specifications so that users can select the system according to the necessity of the observations. Real-time VLBI observation capability between inter-continental baselines, we will be able to improve the timeliness of the VLBI observation results.

Erwan Gueguen et al.: Recent Crustal Movements: Geological Meaning of European Geodetic VLBI Network Observations, Proceedings of the 15th Working Meeting on European VLBI for Geodesy and Astrometry, p.99–107
http://www.ieec.fcr.es/hosted/15wmevga/proceedings/gueguen

Recent Crustal Movements: Geological Meaning of European Geodetic VLBI Network Observations

Erwan Gueguen [1], *Paolo Tomasi* [2], *Hans-Georg Scherneck* [3], *Rüdiger Haas* [3], *James Campbell* [4]

[1] *ITIS-CNR*
[2] *ITIS-CNR and IRA-CNR*
[3] *Onsala Space Observatory (OSO), Chalmers University of Technology*
[4] *Geodetic Institute of the University of Bonn (GIUB)*

Contact author: Erwan Gueguen, e-mail: gueguen@itis.mt.cnr.it

Abstract

The European geodetic VLBI network has been operating for 11 years and has demonstrated that space geodesy techniques now represent a powerful tool for understanding present-day geodynamics. In the last years research has been stressed on the improvement of accuracy and precision of VLBI observations and analysis in particular regarding the height component. In this paper we confront the results of both Italian CNR-2000 and Swedish OSO-2000 solutions with geological and geophysical data over Europe. In particular we focus on post-glacial rebound phenomena in northern Europe and on the present-day geodynamic evolution of the central Mediterranean domain. Whereas for horizontal motions there is a good agreement between the different methods and techniques, for vertical movements the space geodetic results show some discrepancies w.r.t. geological data and geophysical models.

1. Introduction

The European geodetic VLBI network has been operating for 11 years now and has demonstrated that space geodesy techniques represent a powerful tool for understanding present-day geodynamics (e.g. [38], [41]) even in area where the movements are slower than those observed in “fast” areas like the Pacific region. In the last years a special effort has been dedicated to the improvement of their accuracy in particular concerning the height component. Since 1996 this has been supported by EU fundings in the frame of the ‘Training and Mobility of Researchers’ programme. In this paper we confront the results of the Italian CNR-2000 and Swedish OSO-2000 solutions with geological and geophysical data. The European network is particularly interesting because it extends over different geodynamic situations and allows us to investigate both post-glacial rebound in the Scandinavian area and active orogenic processes in the Mediterranean region.

2. VLBI analysis

Both the CNR-2000 and the OSO-2000 solutions are based on the Euro-VLBI network observations and are using the CALC/SOLVE software package [24]. Nevertheless, there are some important differences in the analysis strategies that will enlighted in the following. The horizontal and vertical velocities shown later in the paper are relative to Wettzell, which is assumed to move according to the NUVEL-1A-NNR model [14].

The CNR-2000 solution is a global solution using not only Euro-VLBI sessions but all 24 hours VLBI databases that include at least 3 European VLBI stations plus all datbases including Ny-Ålesund, in total 198 databases. The analysis has been performed as so-called ‘vector-solution’ considering the position and the velocity of the European stations as global parameters. Solutions of this type determine the station velocities in one step from least-squares of a large number of

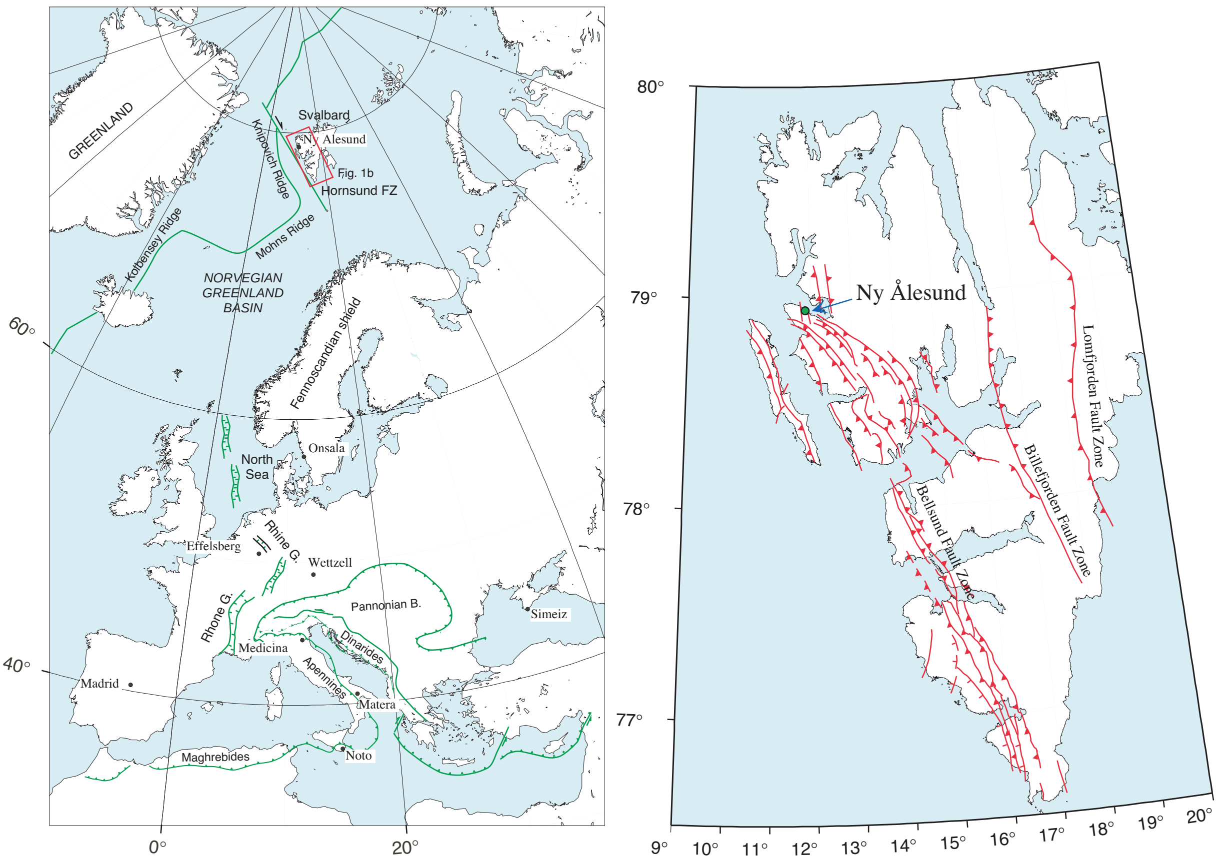

Figure 1. Left: Map of the European VLBI Network with the main geological structures in Europe. Right: Map and main geological structures of the most northern part of the European VLBI network, Svalbard.

observations. Thus the formal errors are quite small and have to be multiplied by a factor of at least 1.5 to represent realistic values [25].

In contrast to that, the OSO-2000 solution is a so-called 'baseline-solution'. From this type of solution in a first step time-series of station positions are determined and following that in a second step the station velocities are estimated from least-squares fits to the time-series. Because time-series of station positions are determined, this solution type gives a very good insight in the repeatability of the VLBI measurements. On the other hand, due to the two-step approach to estimate the station velocities, the formal errors are larger than in a 'vector-solution' and thus represent upper bounds. In the OSO-2000 solution a recent ocean loading model, corrections for atmospheric loading and a model for thermal expansion of the telescopes have been applied. For further details on the two different solutions the reader is referred to [20], [22].

3. Scandinavian uplift

The northern part of the Euro-VLBI network covers the Fennoscandian shield and the Svalbard archipelago, see Fig 1. This region is usually considered as stable from the plate tectonics standpoint. But if this is true for continental Scandinavia the situation of Svalbard is quite different. The western Svalbard fold-and-thrust belt has a complex tectonic history linked to the opening of the Northern Atlantic Ocean. This area is located close to the Hornsund Fault Zone, one of the major active fault zones during the separation of the NE Greenland and Svalbard-Barents shelves. The last recognised important tectonic event in this area is dated from the Tertiary [7]. But in recent time, high heat flow anomalies and a light seismic activity have been recorded offshore west-

Table 1. Horizontal and vertical motions with respect to Wettzell (Velocities in mm/yr).

	CNR-2000			OSO-2000		
Station	**East**	**North**	**Vertical**	**East**	**North**	**Vertical**
Madrid	$+0.6 \pm 0.1$	-0.2 ± 0.1	$+2.8 \pm 0.3$	$+0.6 \pm 0.2$	-0.0 ± 0.3	$+2.0 \pm 0.8$
Effelsberg	$+1.2 \pm 0.2$	-1.1 ± 0.2	-0.8 ± 0.9	$+0.3 \pm 0.3$	-1.1 ± 0.4	$+1.0 \pm 2.6$
Matera	$+1.5 \pm 0.1$	$+4.1 \pm 0.1$	$+1.0 \pm 0.4$	$+1.6 \pm 0.1$	$+4.1 \pm 0.2$	$+0.2 \pm 0.6$
Medicina	$+2.3 \pm 0.1$	$+1.4 \pm 0.1$	-1.2 ± 0.3	$+2.1 \pm 0.2$	$+1.7 \pm 0.3$	-2.7 ± 0.9
Noto	-0.4 ± 0.1	$+4.4 \pm 0.1$	-1.2 ± 0.4	-0.1 ± 0.2	$+4.5 \pm 0.2$	-0.5 ± 0.7
Onsala	-0.9 ± 0.1	-0.7 ± 0.1	$+2.9 \pm 0.3$	-1.1 ± 0.2	-0.8 ± 0.2	$+1.8 \pm 0.7$
Ny-Ålesund	-2.2 ± 0.1	-0.5 ± 0.1	$+6.4 \pm 0.3$	-2.1 ± 0.4	-0.6 ± 0.7	$+5.9 \pm 1.8$
Crimea	$+0.5 \pm 0.3$	$+1.6 \pm 0.3$	$+4.4 \pm 1.1$	$+1.4 \pm 1.1$	$+1.4 \pm 1.1$	-0.8 ± 4.5

ern Svalbard, which is located only 150 km from the Knipovich oceanic ridge (Fig. 1), showing that the area is still tectonically active. During Pleistocene time this area was covered by a thick ice sheet. The entire region is now affected by a post-glacial rebound due to isostatic response to the melting of the ice shield about 10,000 years ago. This phenomenon induces an obvious vertical motion but also a tangential deformation with horizontal displacement in particular at the transition between the central dome and the fore-bulge area.
The horizontal motions of Ny-Ålesund and Onsala (Table 1; Fig. 2a) relative to Wettzell are in quite good agreement with the predicted horizontal motion due to post-glacial rebound of 1.0 mm/yr with azimuth 271.5° for Ny-Ålesund and 0.9 mm/yr with azimuth 193.9° for Onsala with respect to Wettzell. These post-glacial rebound predictions were calculated using the ice model ICE-3G by Tushingham and Peltier [36] and applying the formalism by Mitrovica et al. [26] with a lithospheric thickness of 120 km, elasticity and desinity following the PREM model [16], and viscosities of $2.0 \cdot 10^{21}$ Pas and $1.0 \cdot 10^{21}$ Pas for the lower mantle and the upper mantle, respectively. The sea-level equations have been solved according to the suggestions by Mitrovica and Peltier [27], however using mobile coastlines, which were iterated at each time step (1Kyr) by constraining the available oceanic water.

In the northernmost part of the network there is a discrepancy between geodetic results (Fig. 2) for Ny-Ålesund with an uplift ranging from 6.4 ± 0.4 mm/yr (CNR-2000) to 5.9 ± 1.8 mm/yr (OSO-2000) and the predicted values from glacial isostatic adjustment models that range from $+1.3$ mm/yr according to the post-glacial rebound model as described before, to $+1.8$ mm/yr according to the ICE-4G model [34]. This difference might be explained by the tectonic activity due to the vicinity of Knipovich Ridge. The influence of other local geological processes like high erosion rates during and after the glaciation events might also take part to this high uplift rate, even if to a lesser degree. Onsala also shows a large vertical movement of $+2.9 \pm 0.3$ mm/yr (CNR-2000) to $+1.8 \pm 0.7$ mm/yr (OSO-2000) with repect to Wettzell. For this station, these two observed values are a little larger than the $+0.98$ mm/yr uplift predicted by a post-glacial rebound model as described above.

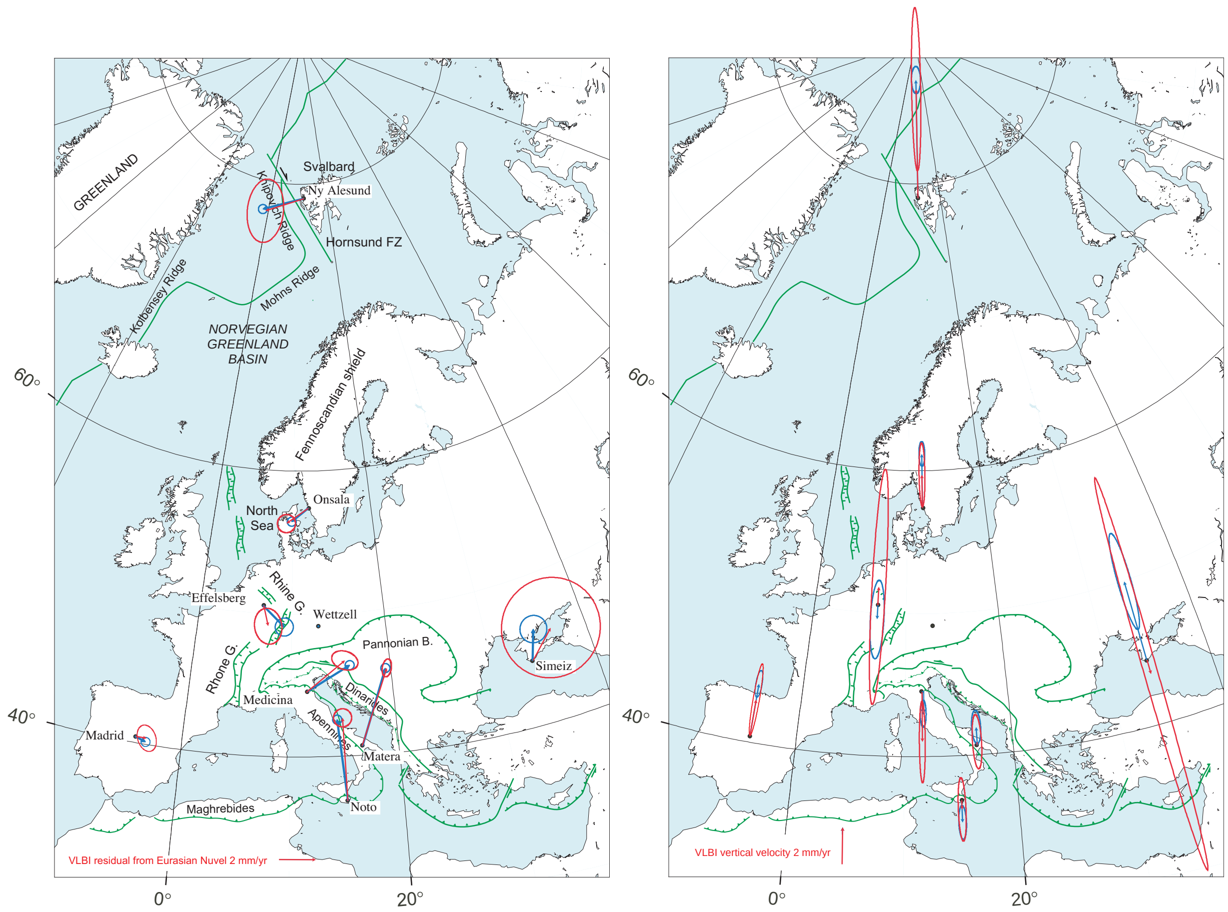

Figure 2. Left: Horizontal velocities w.r.t. Wettzell. Right: Vertical velocities w.r.t. Wettzell. Shown are the results from the two solutions CNR-2000 (blue) and OSO-2000 (red) together with their formal errors.

4. Cenozoic rift zone in central Europe

Central Europe is usually considered as stable even if it is affected by some important structures (i.e. Rhine Graben and Rhone Graben). But the movements are so small that they are within the error of the Space Geodesy measurements. This poses the problem of the detection of intraplate deformations. The Effelsberg station is the only Euro-VLBI station available in this area as the Wettzell station is used as reference in the Euro-VLBI analysis. However as the telescope of Effelsberg is mainly used for radio-astronomy, the number of Euro geodetic experiments including this station is rather small and the results are not so reliable. Nevertheless the motion of Effelsberg with respect to Wettzell (Table 1) may be related to the light active tectonics in the Rhine Graben, evidenced by recent eartquakes [37], [9].

5. Central and western Mediterranean

5.1. Geological setting

The Mediterranean region (Fig. 1a, Fig. 3) is mainly affected by horizontal tectonics. The Neogene and Quaternary evolution of the western Mediterranean geodynamics was apparently dominated by the 'eastward' migration of the Apenninic arc and extension propagated eastward in the hangingwall of the retreating West dipping subduction zone [29], [19]. Even if this point is still under debate (i.e. slab break-off, [40]) the evidences for the Apenninic subduction have

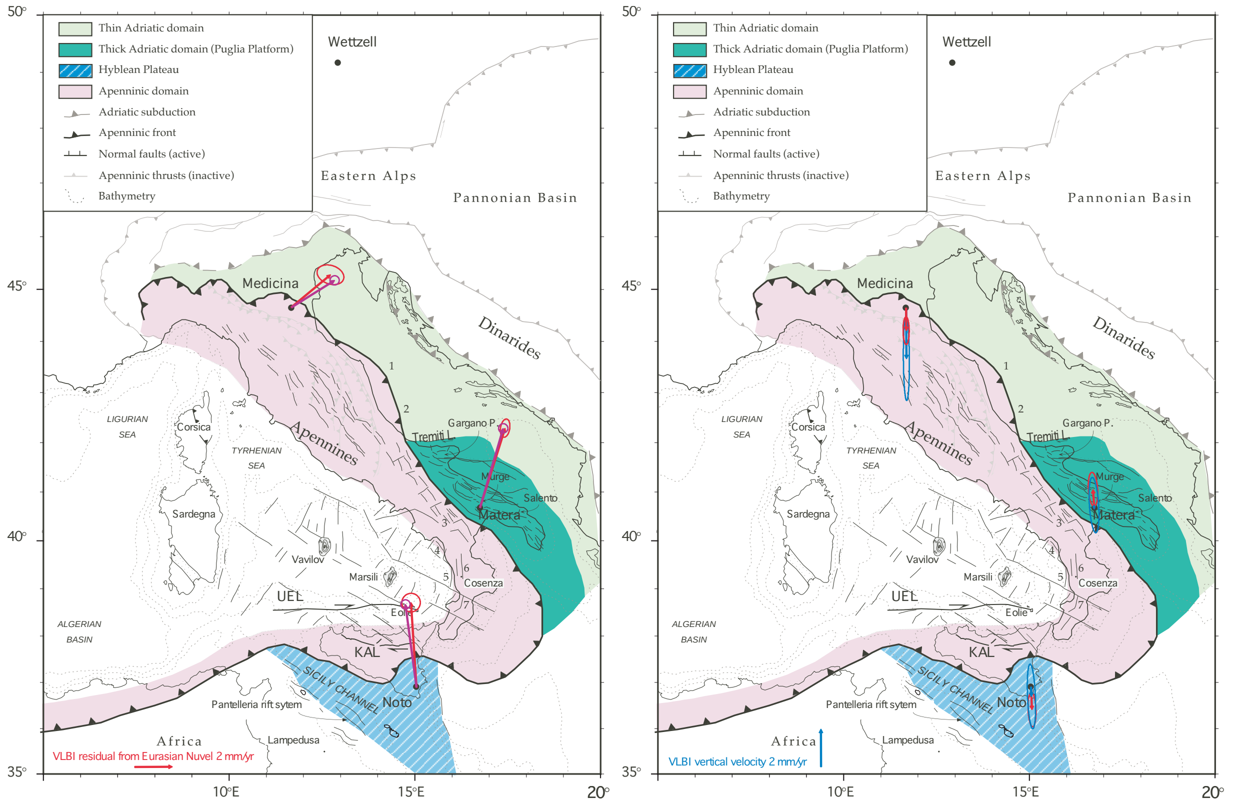

Figure 3. Geological map of central Mediterranean area. Left: with Horizontal velocities w.r.t. Wettzell. Right: with Vertical velocities w.r.t. Wettzell. Shown are the results from the two solutions CNR-2000 (blue) and OSO-2000 (red) together with their formal errors.

been deeply reinforced in the last decade by geophysical and volcanological data that indicate W-directed subduction of the Adriatic plate underneath Italy, see e.g. [28], [39], [2], [32], [3], [2]. The differences in seismicity and tomography between northern and southern Apennines can be explained by the different migration rate of the slab [18] and by the different nature of the subducting lithosphere, i.e. continental below the central-northern Apennines and oceanic below the southern Apennines and Calabria. However during in the last 5 Ma, the interference of the subduction zone with the thicker continental crust of the Puglia platform slightly modified the geodynamics settings of the Apenninic system. Due to the presence of the Ionian oceanic crust the Calabrian arc continued to rollback quickly, whereas in the Southern Apennines segment the migration of the hinge slowed down by a factor of 6 in 10 Ma [18]. Coevally Africa slowly moving towards Eurasia deforms the southernmost segment of the subduction zone [1], [18].
As a consequence of this evolution, we can divide the Mediterranean Region in three main domains characterised by their tectonic regime:
The first one corresponds to the back-arc basins of the Apenninic subduction (see Fig. 3) and this entire domain is under a tensional stress field [6]. It is important to note that the ages of the basin are younger eastward. Nowadays only the basins close to the Italian coast are active.
The second domain corresponds to the Apennines chain itself, see Fig. 3. It represents a Neogene roughly E-verging thrust system, which is now affected by a Plio-Quaternary extensional tectonics. All the major compressive features are dislocated by normal faults. For these faults, the seismological data suggests a high angle geometry up to 10–12 km. The compressive tectonics is now located along a very narrow band along the Apenninic front. The active thrusts are usually visible only on seismic profiles (e.g. CROP3 profile [5]) and are blind-thrusts. This is also confirmed by

seismological data [31]. The major part of the Apennines is now under an extensional regime. During Lower-Middle Pleistocene the extensional tectonics began to be very active leading to the formation of lacustrine basins.
The third domain is the Adriatic plate (Fig. 3). The lithospheric thickness of Italy [8] shows that this domain has to be divided in two sub-plates, separated by the so-called Tremiti Line which is a roughly E-W trending active shear, lying offshore northward of the Gargano Promontory. On the basis of seismicity and geophysical data this structure is interpreted as a lithospheric boundary between two Adriatic subplates, allowing a major rollback of the subduction hinge of the northern Adriatic block characterised by a thinner lithosphere (70 km). Puglia represents the foreland of both the Apenninic and Dinaric orogens. This foreland is weakly deformed and consists of an emerged domain in southern Italy and of a submerged area in the Adriatic and Ionian seas. It is formed by a thick continental lithosphere (100 km). Like in the Apenninic domain the Quaternary tectonics activity is characterised by tensional and transtensional faults associated with a horst-and-graben system. But the origin of this tectonics is completely different. In fact it is due to the buckling of the thick Adriatic lithosphere. The northern boundary of the Adriatic plate is formed by the foredeep of the Southern Alps, which are the backthrust belt of the Alps. It slowly migrates southwards between Late Cretaceous and Pliocene. It is now nearly stopped and according to sediment thickness the subsidence rate is very low (0.3 mm/yr).

5.2. Geodetic results (see Table 1 and Fig. 3a,b)

Madrid: The small horizontal vector of Madrid confirms that the Iberian Peninsula is quite stable with respect to the main European block. Regarding the vertical motion, Madrid seems to uplift at a rate of 2.8 ± 0.3 mm/yr (CNR-2000) to $+2.0 \pm 0.8$ mm/yr (OSO-2000), but so far there is no tectonic explanation for such an uplift in the central part of the Iberian peninsula, so it might be due to local phenomena.

Medicina: The Medicina station is located in the Adriatic foredeep basin at the footwall of the Apennines in a complex geological setting characterised by the buried active thrusts of the Apenninic front as shown on the Neotectonic map of Italy [12]. Its NE-ward horizontal motion is in good agreement with the direction of transport of these buried thrusts. This area underwent strong subsidence during the last 5 Ma and record up to 1.6 mm/yr subsidence rate [15]. This situation is also complicated by the effects of subsidence due to anthropic activities in this area, mainly ground water pumping [35] even if these effects have been reduced in the recent years [42]. The observed vertical velocity of Medicina in the range of -1.2 ± 0.4 mm/yr (CNR-2000) to -2.7 ± 0.9 mm/yr (OSO-2000) is thus in good agreement with the local geological context and can be explained by tectonic process combined with anthropic activity.

Matera: The Matera station towards NNE is representative for the displacement of the Adriatic microplate. Both Euro-VLBI solutions show a horizontal motion of Matera towards NNE by about 4.5 mm/yr. This result is in good agreement with the tectonic structures along the boundaries of the Adriatic plate (Fig. 3) and with the earthquake data showing that the Adria is surrounded by earthquakes along all the Balkan coasts, the southern Alps, and the Apennines [4], [33]. The uplift rate in the range of $+1.0 \pm 0.3$ mm/yr (CNR-2000) to $+0.2 \pm 0.6$ mm/yr (OSO-2000) is in good agreement with geological data as testified by the presence of numerous uplifted paleo-shorelines and marine terraced deposits, overlying the older units [11]. According to late Pleistocene geochronological and stratigraphic data, long-term uplift rates are in the order of $0.2 - 0.5$ mm/yr [13], [10].

Noto: Noto moves roughly northward with a light westward component with respect to Wettzell. This is in good agreement with the recent evolution of the Southern Tyrrhenian basin, see [23], [30], [19], and with the motion of the African plate with respect to the European plate [14], even if the Sicily Channel and the Pelagian shelf are affected by active extensional tectonics (e.g. Pantelleria rift system) and thus the Hyblean block cannot be simply considered as rigidly linked to Africa. The difference in the direction of Matera and Noto vectors confirms that the domain in between is still undergoing extensional tectonics. These data are in good agreement with the geological data in Calabria, where there is some evidence of active extensional tectonics, e.g the Lower Crati, Catanzaro and Siderno basins [17].

Crimea: Crimea is still affected by low measurement accuracy and thus it is difficult to interpret its motion. The two VLBI solutions give contradictory results and very large error bars for Crimea, reflecting the poor quality of the observed data. The results are not to be considered as significant yet.

6. Conclusions

It appears that, after 11 years of observations the geodetic data analysis applying different analysis strategies are converging both for the horizontal and the vertical components and are now in quite good agreement with the geological models. The difference between the predicted and the observed value of the vertical motion of Ny-Ålesund can be explained by a combination of post-glacial rebound, tectonics and erosion unloading. In some places where the local geological structure is complex (i.e. Medicina), further geological studies are necessary to better understand the tectonic processes that obviously are leading the observed results.

Acknowledgments

Erwan Gueguen and Rüdiger Haas are supported by the EU under contract FMRX-CT960071.

References

[1] Albarello, D., Mantovani, E., Babbucci, D., and Tamburelli, C., "Africa-Eurasia kinematics: main constraints and uncertainties" , *Tectonophysics*, **243**, 25–36, 1995.

[2] Amato, A., Alessandrini, B., Cimini, G., Frepoli, A., and Selvaggi, G., "Active and remnant subducted slabs beneath Italy: evidence from seismic tomography and seismicity", *Annali di Geofisica*, **36(2)**, 201–214, 1993.

[3] Amato, A., and 15 others, "Quadro geodinamico dell'Appennino settentrionale da dati di sismologia passiva", *Soc. Geol. It., Crop 03 Proceedings Meeting*, Rome, 1–2, 1996.

[4] Anderson, H., and Jackson, J., "Active tectonics of the Adriatic region", *Geophys. J. R. Astr. Soc.*, **91**, 937–983, 1997.

[5] Barchi, M., Minelli, G., and Pialli, G., "The Crop 03 profile: a synthesis of results on deep structures of the Northern Apennines", *Mem. Soc. Geol. It.*, **52**, 383-405, 1998.

[6] Bassi, G., Sabadini, R., and Rebaï S., "Modern tectonic regime in the Tyrrhenian area: observations and models", *Geophys. J. Int.*, **129**, 330–346, 1997.

[7] Blythe, A. E. and Kleinspehn, K. L. "Tectonically versus climatically driven Cenozoic exhumation of the Eurasian plate margin, Svalbard: Fission track analyses", *Tectonics*, **17(4)**, 621–639, 1998.

[8] Calcagnile, G., and Panza, G. F., "The main characteristics of the lithosphere-asthenosphere system in Italy and surrounding regions", *Pure and Applied Geophysics*, **119**, 865–879, 1981.

[9] Camelbeeck T., and Meghraoui, M., "Large Earthquakes in Northern Europe More Likely Than Once Thought", *EOS*, **77**, 42, 1996.

[10] Ciaranfi, N., Pieri, P., and Ricchetti, G., "Linee di costa e terrazzi marini pleistocenici nelle Murge e nel Salento: implicazioni neotettoniche ed eustatiche", *Riass. 77 Congr. Soc. Geol. It.*, Bari, 170–172, 1994.

[11] Ciaranfi N., Pieri, P., and Ricchetti, G., "Note alla carta geologica delle Murge e del Salento (Puglia centro-meridionale)", *Mem. Soc. Geol. It.*, **4**, 449–460, 1988.

[12] Consiglio Nazionale delle Ricerche, AA.VV., "Neotectonic Map of Italy", 1983.

[13] Dai Pra, G., and Hearty, P. J., "I livelli marini pleistocenici nel Golfo di Taranto. Sintesi geocronostratigrafica e tettonica", *Mem. Soc. Geol. It.*, **41**, 637–644, 1988.

[14] De Mets, C., Gordon, R. G., Argus, D. F., and Stein, S., "Effect of recent revision to the geomagnetic reversal time scale on estimates of current plate motions", *Geophys. Res. Lett.*, **21(20)**, 2191–2194, 1988.

[15] Doglioni, C., "Foredeeps versus subduction zones", *Geology*, **22**, 271–274, 1994.

[16] Dziewonski, A., and Anderson, D. L., "Preliminary Reference Earth Model (PREM)", *Phys. Earth Planet. Int.*, **25**, 297–356, 1981.

[17] Ghisetti, F., and Vezzani, L., "Contribution of structural analysis to understandig the geodynamic evolution of the Calabria Arc (Southern Italy)", *Journ. Struct. Geol.*, **3**, 371–381, 1981.

[18] Gueguen, E., Doglioni, C., and Fernandez, M., "On the post-25 Ma geodynamic evolution of the Western", *Tectonophysics*, **298**, 259–269, 1998.

[19] Gueguen, E., Renda, P., Tavarnelli, E., and Tramutoli, M., "Neogene evolution of the central Madonie Mountains (northern Sicily, Italy). Implication on the Central Mediteranean geodynamics", In: *Evoluzione geologica e geodinamica dell'Appennino., Mem. Soc. Geol. It.*, (in press), 2001.

[20] Gueguen, E., Haas, R., Nothnagel, A., Tomasi, P., and Campbell, J., "Vertical crustal motion in Europe by means of VLBI. Comparison with geological and geophysical data", *Wegener 2000 Meeting*, San Fernando, Spain, Sept 2000.

[21] Haas, R., Gueguen E., Scherneck H.-G., Nothnagel A. and Campbell J. "Results for crustal motion derived from observations in the European geodetic VLBI network", *Earth Planets Space*, **52**, 759–764, 2001.

[22] Haas, R., Nothnagel, A., Campbell, J., and Gueguen, E., "Recent crustal movements observed with the European geodetic VLBI network: 1) geodetic analysis and results", *IAG SRCM'01*, Helsinki, August 2001.

[23] Lavecchia, G., "The Tyrrhenian-Appenines system: structural setting and seismotectogenesis", *Tectonophysics*, **147**, 236–296, 1988.

[24] Ma, C., Sauber, J. M., Bell, L. J., Clark, T. A., Gordon, D., and Himwich, W. E., "Measurement of horizontal motions in Alaska using very long baseline interferometry", *J. Geophys. Res.*, **95**, 21991–22011, 1990.

[25] Macmillan, D. S., and Ma, C., "Using meterological data assimilation models in computing tropospheric delays at microwave frequencies", *Phys. Chem. Earth*, **23(1)**, 97–102, 1998.

[26] Mitrovica J. X., Davis J. L., Shapiro I. I., "A spectral formalism for computing three-dimensional deformations due to surface loads, 2. Present-day glacial isostatic adjustment", *J. Geophys. Res.*, **99**, 7075–7101, 1994.

[27] Mitrovica J. X., and Peltier, W. R., "On post-glacial geoid relaxation over the equatorial oceans", *J. Geophys. Res.*, **96**, 20053–20071, 1991.

[28] Mongelli, F., Loddo, M., and Calcagnile, G., "Some observations on the Apennines gravity field", *Earth and Planetary Science Letters*, **24**, 385–393, 1975.

[29] Réhault, J. P., Mascle, J., and Boillot, G., "Evolution géodynamique de la Méditerranée depuis l'Oligocene", *Mem. Soc. Geol. It.*, **27**, 85–96, 1984.

[30] Renda P., Tavarnelli, E., and Tramutoli, M., "La distensione tetidea ed il suo controllo sulle strutture compressive del sistema Appenninico-Maghrebide: l'esempio dei Monti delle Madonie, Sicilia centro-settentrionale", *Boll. Soc. Geol. It.*, **118**, 179–190, 1999.

[31] Selvaggi, G., and Amato, A., "Subcrustal Earthquakes in the Northern Apennines (Italy) : Evidence for a still active subduction ?", *Geophys. Res. Lett.*, **19(21)**, 2127–2130, 1992.

[32] Selvaggi, G., and Chiarabba, C. "Seismicity and P-wave velocity image of the Southern Tyrrhenian subduction zone", *Geophys. J. Intern.*, **121**, 818–826, 1995.

[33] Slejko, D., Camassi, R., Cecic, I., Herak, D., Herak, M., Kociu, S., Kouskouna, V., Lapajne, J., Makropoulos, K., Meletti, C., Muco, B., Papaioannou, C., Peruzza, L., Rebez, A., Scandone, P., Sulstarova, E., Voulgaris, N., Zivcic, M., and Zupancic, P., "GSHAP seismic hazard assesment for Adria region", In: *GSHAP special volume, Annali di Geofisica*, http://seismo.ethz.ch/gshap/adria/report.html, 1999.

[34] Soudarin, L., Crétaux, J.F., Cazenave, A., "Vertical crustal motions from the DORIS space-geodesy system", *Geophys. Res. Lett.*, **26(9)**, 1999.

[35] Tomasi, P., Mantovani, F., Negusini, M., Orfei, A., and Sarti P., "Activities and recent results in Geodynamics", In: *Proc. of the 12th Working Meeting on European VLBI for Geodesy and Astronomy*, 102–110, Hønefoss, Norway, 1997.

[36] Tushingham A. M. and Peltier W. R. "Ice-3G: a new global model of Late Pleistocene deglaciation based upon geophysical predictions of post-glacial relative sea level change", *J. Geophys. Res.*, **96**, 4497–4523, 1991.

[37] Vanneste, K., Meghraoui, M., and Camelbeeck, T., "Late Quaternary earthquake-related soft-sediments deformation along the Belgian portion of the Feldbiss Fault, Lower Rhine Graben system", *Tectonophysics*, **309**, 1999.

[38] Ward, S. N., "Constraints on the seismotectonics of the central Mediterranean from Very Long Baseline Interferometry", *Geophys. J. Int.* **117**, 441–452, 1994.

[39] Wilson, M. and Bianchini, G., "Tertiary-Quaternary magmatism within the Mediterranean and surrounding regions", In: Durand, B.,Jolivet, L., Horvath F. and Séranne M. (Eds), The Mediterranean Basins: Tertiary Extension within the Alpine Orogen, *Geol. Soc. Spec. Pub.*, **156**, 141–168, 1999.

[40] Wortel, M.J.R., and Spackman W., "Structure and dynamic of subducted lithosphere in the Mediterranean", *Proc. K. Ned. Akad. Wel.*, **95**, 25–347, 1992.

[41] Zarraoa, N., Rius, A., Sardon, E., and Ryan, J.W., "Relative motions in Europe studied with a geodetic VLBI network", *Geophys. J. Int.*, **117**, 763–768, 1994.

[42] Zerbini, S., Negusini, M., Romagnoli, C., Domenichini, F., Richter, B., and Simon, D., "Height and gravity variations by continuous GPS and gravity measurements in the southern Po Plain", *IAG SRCM'01*, Helsinki, August 2001.

Machiel Simon Bos and Rüdiger Haas: Observing Long-period Tides in Gravity and VLBI Observations at Ny-Ålesund (Svalbard) – A Progress Report, Proceedings of the 15th Working Meeting on European VLBI for Geodesy and Astrometry, p.108–115
http://www.ieec.fcr.es/hosted/15wmevga/proceedings/bos

Observing Long-period Tides in Gravity and VLBI Observations at Ny-Ålesund (Svalbard) – A Progress Report

Machiel Simon Bos [1,2], *Rüdiger Haas* [1]

[1] *Onsala Space Observatory (OSO), Chalmers University of Technology*

[2] *now at: Delft Institute for Earth-Oriented Space Research (DEOS), Delft University of Technology*

e-mail: `m.s.bos@citg.tudelft.nl` and `haas@oso.chalmers.se`

Abstract

The M_f body tide is studied from gravity and space geodesy observations performed at Ny-Ålesund (Svalbard). Observations with a superconducting gravimeter are analysed and gravimetric factors for 13 tidal harmonics are determined. The observed gravimetric factor of the M_f tide deviates from theoretical values within two times the formal error. Global Very Long Baseline Interferometry data including Ny-Ålesund are analysed in two ways, with and without modelling of the M_f tide in the apriori body tide model. The M_f tide is clearly visible in the spectrum of the time series of topocentric up-component when the tide is not included in the apriori modelling of the VLBI analysis.

1. Introduction

The motivation for this study is to investigate the Earth's elastic properties by observing the amplitude and phase lag of the solid body tide. For a completely rigid Earth this amplitude is zero and any non-zero value can directly be related to the elasticity, any phase lag to inelasticity. Several theoretical body tide models have been published in the past, differing in assuming some or no inelasticity of the Earth. So far the observation accuracy of gravimetric methods has been too low to discriminate between the different body tide models [2].

In this report we focus on the tidal harmonic M_f because at this period (13.66 days) the effect due to inelasticity is supposed to be relatively large. The inelasticity effect is even larger for longer periods but then the larger disturbing influence of the atmosphere complicates an accurate observation of the body tide with gravimetric techniques. Next, this tidal harmonic lies between the periods of the Chandler wobble and the semi-diurnal tides. At both these periods estimates of the inelasticity have been made using Earth rotation and satellite tracking observations, see e.g. [15], [12]. Studying M_f can add important information on how inelasticity changes with frequency.

We will measure the solid Earth tide effects observed with a superconducting gravimeter (SG) and Very Long Baseline Interferometry (VLBI). In recent years superconducting gravimetry has become more and more advanced to study geophysical effects and space geodesy techniques have been more and more successful in studying tidal effects, for recent reviews see e.g. [10], [4]. Thus, a combined approach of investigation using both, superconducting gravimetry and space geodetic techniques promises to give more insight into tidal phenomena and the Earth's elastic properties.

2. Gravimetric factors, Love and Shida numbers

The body tide is generated by the gravitational attraction of the solar system bodies, primarily by the Moon and the Sun. This attraction can conveniently be described by a tidal potential which is related to the tidal forces observed with gravimeters via the so-called tidal gravimetric factor δ. Equation 1 shows the relation in a simplified form for a non-rotating, spherical and elastic Earth. In this relation $\vec{a}_{tides}$ describes the tidal forces observed by a gravimeter, $W_{nm}(tide)$ is the contribution of a tide of degree n and order m to the tide generating potential, r depicts the radial direction and $\delta_{nm}(tide)$ is the gravimetric factor of a tide of degree n and order m.

$$\vec{a}_{tides} = \sum_{n=1}^{n_{max}} \sum_{m=0}^{n} \sum_{tides} \delta_{nm}(tide) \frac{\partial W_{nm}(tide)}{\partial r} \tag{1}$$

The three dimensional site displacements due to Earth tides which can be observed with space geodetic techniques like VLBI are related to the tide generating potential via the so-called Love and Shida numbers h and l. Equations 2 to 4 show the relations, again in a simplified form for a non-rotating, spherical and elastic Earth. Here, ΔU, ΔE and ΔN are the topocentric displacements in up, east and north direction, λ and β are the site's longitude and latitude, respectively, g_0 is the gravity at the equator and $h_{nm}(tide)$ and $l_{nm}(tide)$ are the Love and Shida numbers of a tide of degree n and order m.

$$\Delta U = \sum_{n=1}^{n_{max}} \sum_{m=0}^{n} \sum_{tides} h_{nm}(tide) \frac{W_{nm}(tide)}{g_0} \tag{2}$$

$$\Delta E = \sum_{n=1}^{n_{max}} \sum_{m=0}^{n} \sum_{tides} l_{nm}(tide) \frac{\partial W_{nm}(tide)/\partial \lambda}{g_0 \cos(\beta)} \tag{3}$$

$$\Delta N = \sum_{n=1}^{n_{max}} \sum_{m=0}^{n} \sum_{tides} l_{nm}(tide) \frac{\partial W_{nm}(tide)/\partial \beta}{g_0} \tag{4}$$

For the simplified case of a non-rotating, spherical and elastic Earth the gravimetric factors, Love and Shida numbers do not vary for different tidal harmonics. The relations shown in equations 1 to 4 become more complicated for a more realistic Earth. The Earth's ellipticity and rotation introduce a coupling between spheroidal displacements of degree n and toroidal displacements of degree $n-1$ and $n+1$ and spheroidal displacements of degree $n-2$ and $n+2$. The existence of a fluid Earth core results in a free core nutation (FCN) and causes the gravimetric factors and Love and Shida numbers of the second degree diurnal tides to be very frequency dependent. Inelasticity of the Earth's mantle causes dissipation. The amount of dissipation is indicated by the fraction $1/Q$ where Q is the quality factor. When the value of Q is low the dissipation is high. An associated effect is a phase lag between the tidal potential excitation and the Earth deformation. Its mathematical description requires complex Love and Shida numbers, see e.g. [18]. In this report we will only talk about the modulus or length of these complex numbers. It is custom to model the quality factor Q with a frequency power α model [1]. The result is an increase of inelasticity with increasing tidal period. More details on the calculation of body tide models can be found for example in [17], [7], [8] and [3].

The influence of inelasticity on the Love and Shida numbers and gravimetric factors are listed in Table 1, based on results given in [3]. The changes in percentage for the Love and Shida numbers and gravimetric factors increase by a factor of more than two comparing the semi-diurnal tide M_2 and the long-period tide S_{sa}. M_2 is a second degree sectorial tide reaching maximal effects at the equator, while M_f and S_{sa} are second degree zonal tides that reach maximal effects in polar regions. Thus, the long-period tides with maximal effects in polar regions are the most interesting to study inelasticity.

Nevertheless, the accuracy requirements are very high even in the long-period tidal band since the analysis of the observations has to give results with standard deviations that are several times smaller than the changes due to inelasticity. Though the internal precision of superconducting gravimeters is well below these requirements, the calibration accuracy is the critical point. Extra complications arise due to the masking effects of ocean tide and atmospheric loading that have to be removed. Thus, this study is a challenging investigation.

Table 1. Changes in percentage for Love and Shida numbers and gravimetric factors when assuming an elastic or an inelastic Earth model, based on [11].

tidal band	tide type	tide	Δh [%]	Δl [%]	$\Delta\delta$ [%]
semi-diurnal	sectorial	M_2	1.4	2.5	0.1
diurnal	tesseral	O_1	1.5	2.9	0.1
long-period	zonal	M_f	2.4	4.2	0.2
long-period	zonal	S_{sa}	3.5	5.9	0.3

3. Observations at the Ny-Ålesund Geodetic Observatory

The Ny-Ålesund Geodetic Observatory is equipped with several collocated geodetic techniques, among those VLBI and a superconducting gravimeter (SG) (see Fig. 1). Geodetic VLBI is performed with the 20 m telescope at Ny-Ålesund since 1994. In autumn 1999 the Japanese superconducting gravimeter group installed the SG instrument #CT039 at Ny-Ålesund [13]. Both techniques are collocated within ca 100 m distance at the observatory. Due to the location at 78.9 degrees northern latitude, geodetic observations taken at Ny-Ålesund present an excellent opportunity to investigate whether the required observational accuracy can be achieved with gravimetry and space geodesy in order to study long-period tides and the Earth's inelasticity.

Figure 1. Collocated geodetic techniques at Ny-Ålesund: Left: The 20 m radio telescope used for geodetic VLBI. Right: The Japanese superconducting gravimeter #CT039.

4. Analysis of the SG observations

Prof. Tadahiro Sato from the National Astronomical Observatory (NAO), Mizusawa, Japan, kindly provided the tidal gravity observations performed with the Japanese superconducting gravimeter. The SG instrument is described in [13] and appears to have a very low drift rate which should help to observe long-period signals. The calibration accuracy of this instrument is 0.5% [13]. Fortunately, a new calibration has recently been performed (Sato, personal communication 2001). The results of this calibration are at this moment of writing still unknown but there is hope that the calibration accuracy will be increased.

The original 1 second data were already sampled to 1 hour and cover the time span of September

20, 1999 to November 30, 2000. The data processing was performed using the ETERNA software package [19]. The atmospheric pressure correction was done using the local air pressure recorded at Ny-Ålesund and the necessary instumental calibrations were applied.

Different signal processing strategies were performed to obtain the spectrum of the SG data: Fast Fourier Transform (FFT), Maximum Entropy Method (MEM) and Lomb periodogram (LP). The latter allows for unevenly sampled input data. For the spectrum computed with the FFT the data was broken up into segments to reduce the variance and a Welch window function was applied. Figure 2 shows the spectra obtained with the three different methods. All three methods clearly identify the long-period, diurnal and semi-diurnal tidal effects measured with the SG and indicate that a good estimation of the M_f body tide amplitude should be possible.

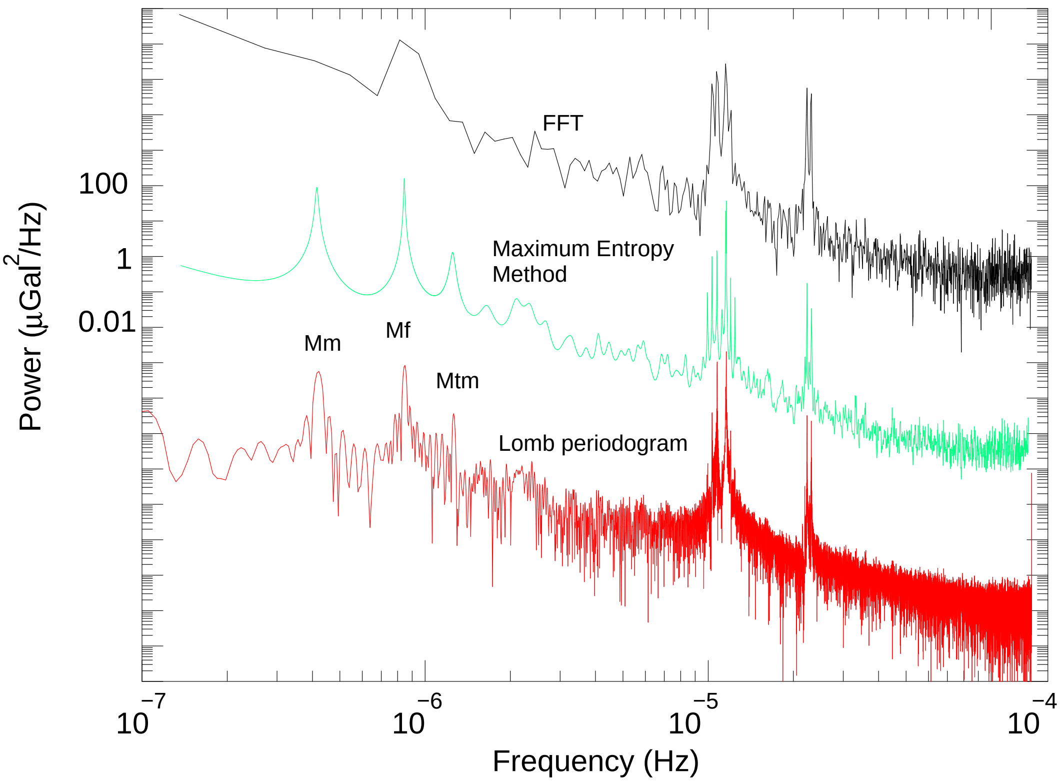

Figure 2. Spectra of the SG data derived with three different signal analysis techniques: Top: Fast Fourier Transform (FFT), Middle: Maximum Entropy Method (MEM), Bottom: Lomb periodogram (LP).

In the next step the results for 13 tides from the analysis of the SG data with ETERNA were analysed together with the ocean tide loading contributions. Scaling coefficients for the gravimeter observations and the ocean loading contributions were determined from a least-squares approach in order to obtain a best fit to the theoretical body tides as calculated using theoretical values given in [3]. For all tides except one the ocean tide loading effects were modelled using the FES99 ocean tide model, a data assimilation update of the the FES98 model [5]. For the tide M_{tm} the NAO99b ocean tide model [9] was used. Figure 3 shows the results for the gravimetric factors of the 13 tides with their formal errors together with the model values for an elastic and an inelastic Earth model according to [3].

It becomes clear that the gravimetric factor for the M_f tide does not coincide with the predicted value from either Earth model but shows some deviation. Nevertheless, the deviation from the predicted values is still within two times the formal error. To reach the aim of our investigations a reduction of the formal error by a factor of 20 is required. It is hoped that this can be achieved by better filtering methods and longer time series of SG data. Sato [13] discovered that the heat

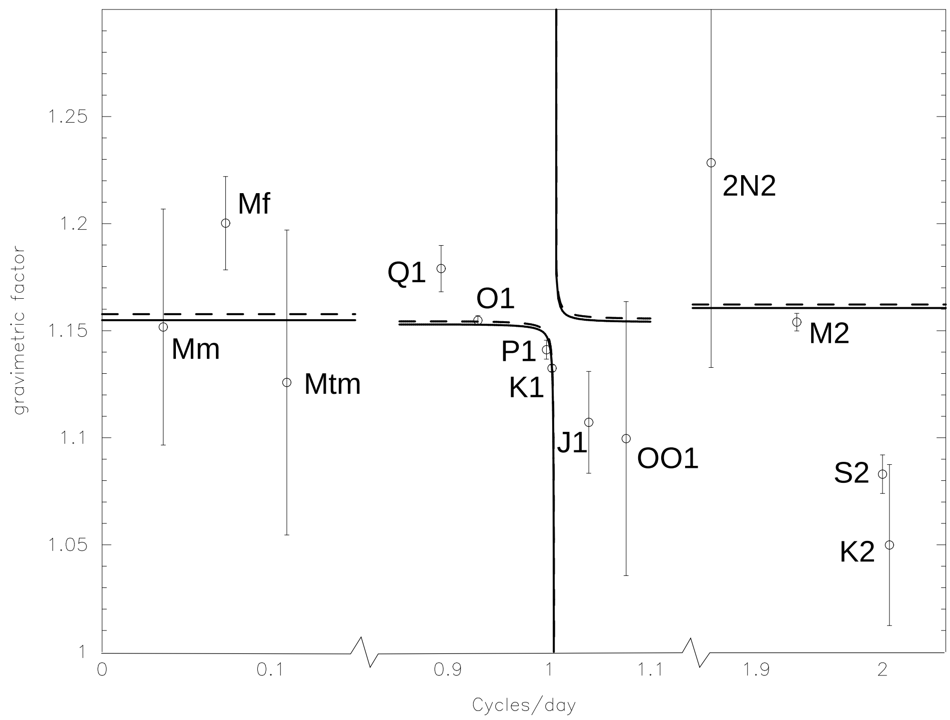

Figure 3. Gravimetric factors for the SG at Ny-Ålesund. The results are corrected for ocean tide loading and are shown with their 1-σ formal errors together with predicted values for an elastic Earth model (solid lines) and an inelastic Earth model (dashed lines) according to [11].

produced by the electrical chiller for the SG influenced the observations. Therefore this chiller has been moved to another building on May 26, 2000. Thus, there is hope that observations performed after this date will produce a lower formal error.

The two semi-diurnal tidals S_2 and K_2 give gravimetric factors that do not agree with the model predictions. These deviations are probably due to unmodelled effects of atmospheric and thermal origin. Further investigations have to be performed to explain these discrepancies.

5. Analysis of VLBI observations

A data set of more than 200 VLBI data bases involving Ny-Ålesund, covering the time span October 1994 to December 2000, was analysed in a so-called 'arc-solution' approach, i.e. determining station coordinates for all stations in a VLBI session except a reference station. From this type of solution result time series of station coordinates. Earth rotation parameters were kept fixed on apriori values from a global VLBI solution, precession was modelled according to the IAU 1976 model [6], and nutation offsets were estimated with respect to the IAU 1980 nutation model [14]. Radio source positions were kept fixed on their apriori values. A no-net-translation constraint was used to stabilise the network of observing sites. Atmospheric zenith wet path delays, horizontal gradients and clock-parameters were estimated as piece-wise linear functions. The Niell mapping functions [11] were used and the elevation cutoff was set to 5 degrees.

In a first solution the solid Earth tides were modelled complex, frequency and latitude dependent using the harmonic expansion of the tide generating potential by Tamura [16], including 1214 partial tides. Figure 4 shows the corresponding LP spectra from the de-trended time series of topocentric station components of Ny-Ålesund.

In a second solution, the apriori solid Earth tide modelling was modified slightly and the apriori contribution of the M_f tide was set to zero. The rest of the modelling was identical to the first solution. Figure 5 shows the corresponding LP spectra of the de-trended time series of topocentric station components of Ny-Ålesund obtained from solution two.

As to be expected, there are no significant peaks to be detected for the tide M_f in the spectra for the vertical station positions (Fig. 4a) and for the horizontal station positions (Fig. 4b) from the first type of VLBI solution. On the other hand, there is a significant peak for the M_f tide in the spectrum for the up-component of the second VLBI solution (Fig. 5a). But even here the spectra of the horizontal components do not show peaks for the M_f tide (Fig. 5b).

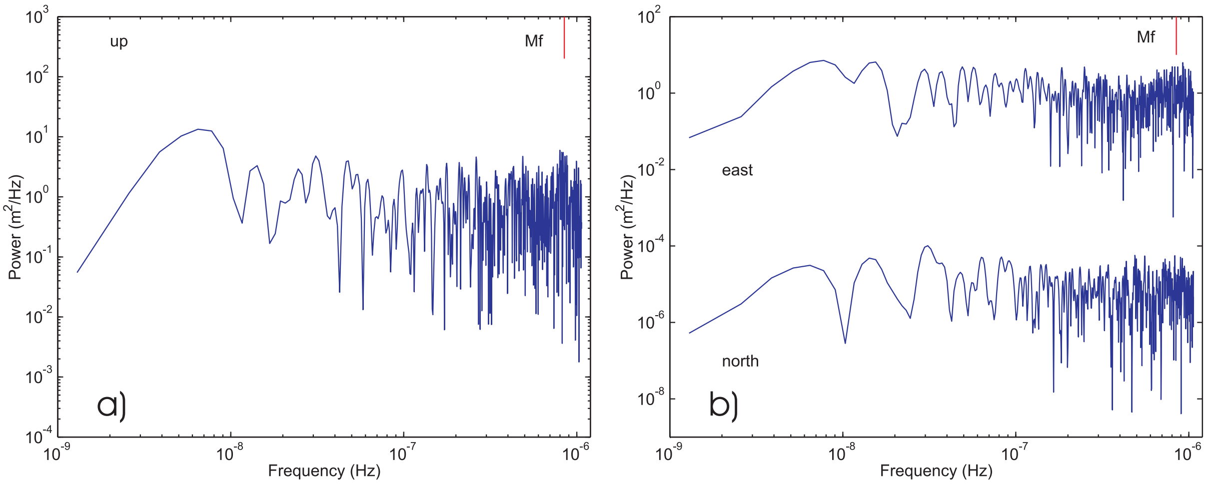

Figure 4. Lomb periodogram spectra of the de-trended time series of a) vertical and b) horizontal station components of Ny-Ålesund from VLBI analysis with a complete apriori modelling of the solid Earth tides, i.e. including the M_f tide. The spectrum of the north-components is offset for visibility reasons. The frequency of the M_f tide is marked on the top frame.

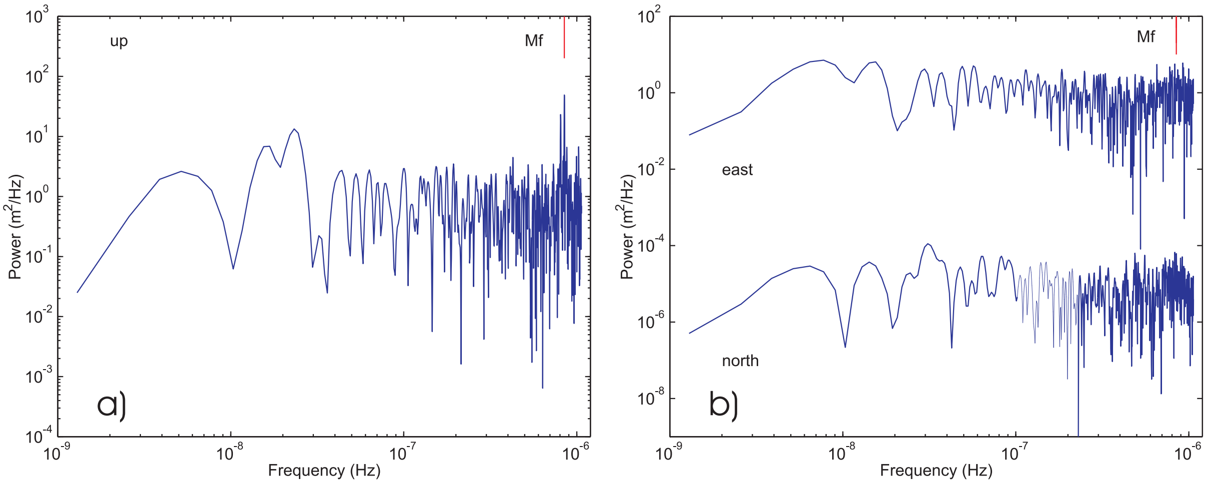

Figure 5. Lomb periodogram spectra of the de-trended time series of a) vertical and b) horizontal station components of Ny-Ålesund from VLBI analysis when omitting the M_f tide in the apriori modelling of the solid Earth tides. The spectrum of the north-components is offset for visibility reasons. The frequency of the M_f tide is marked on the top frame.

This proves that using this time series approach the VLBI observations sense the tidal deformation at tide M_f in particular for the up-component. On the other hand, with this time series approach the M_f tidal deformation effect is not sensed significantly for the horizontal station components. This is not too much surprising since the tidal deformation effect for the horizontal station components is smaller than the one for the up-component by a factor of ca 7.5. Thus, the detection of the M_f signal in the measurement noise of the horizontal components is more difficult.

6. Discussion and outlook

The analysis of 15 months of SG observations at Ny-Ålesund shows that the observed gravimetric factor for the M_f tide deviates from the theoretical values for an elastic and an inelastic Earth model. Nevertheless, the discrepancy is within two times the formal error and therefore the accuracy of the SG results is not yet high enough to distinguish between the theoretical models. Since long-period noise due to a chiller problem at the SG site is reduced since spring 2000, a longer time series of SG data will reduce the formal errors of the analysis and allow increased measurement accuracy. There is also hope that the recently performed calibration will result in an increased accuracy. Thus, we are looking forward to analyse a longer time series of SG data from Ny-Ålesund in order to investigate M_f and eventually other long-period tides, e.g. S_{sa}.

The analysis of the VLBI data so far concentrated on to study whether the M_f tide can be directly detected from time series of VLBI station positions. This study was successful and we could identify M_f in the spectra of the topocentric up-component for Ny-Ålesund when this tide was not modelled in the apriori solid Earth tide model of the VLBI data analysis software. The tide could clearly be detected, although the sampling of VLBI data at Ny-Ålesund, often with 14 days, is not ideal to study a tide with a period 13.66 solar days. We could not identify a peak in the spectrum for the horizontal station components from our time series approach. As the next step we plan to directly determine the corresponding Love and Shida numbers for Ny-Ålesund from a different type of VLBI analysis without involving time series of station positions.

Acknowledgements

Rüdiger Haas is supported by the European Union under contract FMRX-CT960071. Machiel Bos stayed at the Onsala Space Observatory during February to August 2001 holding a scholarship by the the European Union under contract FMRX-CT960071. We thank Prof. Tadahiro Sato for providing the data observed with the Japanese superconducting gravimeter at Ny-Ålesund. We thank the VLBI data and analysis center at the Bundesamt für Kartographie und Geodäsie (BKG) Leipzig for access to the BKG's computer facilities.

References

[1] Anderson, D.L. and Minster, J.B., "The frequency dependence of Q in the Earth and implications for mantle rheology and Chandler wobble", *Geophy. J. R. Astron. Soc.*, **58**, 431–440, 1979.

[2] Baker, T.F., Curtis, D.J. and Dodson, A.H., "A new test of Earth tide models in central Europe", *Geophys. Res. Lett.*, **23(24)** 3559-3562, 1996.

[3] Dehant, V., Defraigne, P., and J.M. Wahr, "Tides for a convective Earth", *J. Geophys. Res.*, **104(B1)**, 1035–1058, 1999.

[4] Haas, R., "Tidal Effects and Space Geodetic Techniques", *J. Geod. Soc. Japan*, **47(1)**, 161–168, 2001.

[5] Lefèvre, F., Lyard, F.H., and Le Provost, C., "FES98: A new global tide finite element solution independent of altimetry", *Geophys. Res. Lett.*, **27(17)** 2717–2720, 2000.

[6] Lieske, J.H., T. Lederle, W. Fricke, and B. Morando, "Expressions for the Precession Quantities Based upon the IAU (976) System of Astronomical Constants", *Astron. Astrophys.*, **58**, 1–16, 1977.

[7] Mathews, P.M., Buffet, B.A., and Shapiro, I.I., "Love numbers for a rotating spheroidal Earth: New definitions and numerical values", *Geophys. Res. Lett.*, **22(5)**, 579–582, 1995.

[8] Mathews, P.M., Dehant, V., and Gipson, J.M., "Tidal station displacements", *J. Geophys. Res.*, **102(B9)**, 20469–20477, 1997.

[9] Matsumoto, K., Takanezawa, T. and Ooe, M., "Ocean Tide Models Developed by Assimilating TOPEX/POSEIDON Altimeter Data into Hydrodynamical Model: A Global Model and a Regional Model Around Japan", *J. Oceanog.*, **56**, 567–581, 2000.

[10] Meurers, B., "Superconducting Gravimetry in Geophysical Research Today", *J. Geod. Soc. Japan*, **47(1)**, 300-3078, 2001.

[11] Niell, A.E., "Global mapping functions for the atmosphere delay at radio wavelength", *J. Geophys. Res.*, **101**, 3227–3246, 1996.

[12] Ray, D.R., Eanes, R.J. and Lemoine, F.G., "Constraint on energy dissipation in the Earth's body tide from satellite tracking and altimetry", *Geophys. J. Int.*, **144**, 471–480, 2001.

[13] Sato, T., Asari, K., Plag, H.-P., Digre, H., Fukuda, Y., Hinderer, J., Kaminuma, K., and Hamano, Y., "Continous Gravity Observations at Ny-Ålesund, Svalbard, Norway, with a Superconducting Gravimeter CT#039", *J. Geod. Soc. Japan*, **47(1)**, 341–346, 2001.

[14] Seidelmann, P.K., "1980 IAU Nutation: The Final report of the IAU Working Group on Nutation", *Celestial Mech.*, **27**, 79–106, 1982.

[15] Smith, M.L., Dahlen, F.A., "The period and Q of the Chandler-Wobble", *Geophys. J. R. Astron. Soc.*, **64(1)**, 223–281, 1981.

[16] Tamura, Y., "A harmonic development of the tide-generating potential", *Bull. d'Inf. Marées Terr.*, **99**, 6813–6855, 1987.

[17] Wahr, J.M., "Body tides on an elliptical, rotating, elastic and oceanless Earth", *Geophys. J. R. Astron. Soc.*, **64**, 677-703, 1981.

[18] Wahr, J.M., and Bergen, Z., "The effects of mantle inelasticity on nutations, Earth tides, and tidal variations of rotation rate", *Geophys. J. R. Astron. Soc.*, **87**, 633–668, 1986.

[19] Wenzel, H.G., "The Nanogal Software: Data Processing Package ETERNA 3.3", *Bull. d'Inf. Marées Terr.*, **124**, 9425–9439, 1996.

Zinovy Malkin et al.: Length Variations of European Baselines Derived from VLBI and GPS Observations, Proceedings of the 15th Working Meeting on European VLBI for Geodesy and Astrometry, p.116–123
http://www.ieec.fcr.es/hosted/15wmevga/proceedings/malkin2

Length Variations of European Baselines Derived from VLBI and GPS Observations

Zinovy Malkin, Natalia Panafidina, Elena Skurikhina

Institute of Applied Astronomy of Russian Academy of Sciences (IAA)
Contact author: Zinovy Malkin, e-mail: malkin@quasar.ipa.nw.ru

Abstract

Results of VLBI and GPS observations were analyzed with goal to investigate differences in observed baseline length derived from both techniques. VLBI coordinates for european stations were obtained from processing of all available observations collected on european and global VLBI network. Advanced model for antenna thermal deformation was applied to account for change of horizontal component of baseline length. GPS data were obtained from re-processing of the weekly EPN (European Permanent GPS Network) solutions. Systematic differences between results obtained with two techniques including linear drift and seasonal effects are determined.

1. Introduction

European region is one of the most intensively studied areas of the Earth from the point of view of regional geodynamics. There are more than 100 permanently operating GPS receivers, about 10 permanent VLBI stations and more than 10 permanent SLR stations. Lately much attention has been devoted to comparison and combination of results obtained using different space geodesy techniques. This work is devoted to comparison of baselength variations derived from GPS and VLBI observations, continuing the cycle of works on this problem, see e.g. [1–5, 7, 11, 13]. It should be mentioned here that observed changes of the baselength on the one hand are resulted by insufficient corrections for observational effects such as thermal deformations of VLBI antennas, for example, or errors in modeling of tropospheric refraction, but on the other hand they are subjected to a number of insufficiently studied or not taken into account properly geophysical effects that can result in the real changes of the baselength, these effects may be atmospheric and snow loading, tides, postglacial rebound, and so on. It is important that the majority of these effects has both seasonal and secular components.

In this study we have analyzed VLBI and GPS observations at 6 european stations carrying out both VLBI and GPS regular observations and having long enough observational history.

2. Data used

2.1. VLBI observations

VLBI baselengths were computed with the OCCAM package using all available 24h sessions for the period of 1983.9–2001.5. Details of the method used can be found in [9].

Linear trend in the baselengths was computed for the whole period of observations and, for more accurate comparison with GPS data, for the period of 1996.0-2001.0. Only later results are presented in this study. In [5] we compared linear trend in variations of baselength derived from the observations over the period 1996.0–2001.0 with ones computed using all available VLBI sessions over a period 1990.0–2001.4. Differences of estimated rates are inside one sigma interval for all baselines analyzed here.

For more strict account for variation in baselengths due to thermal antenna deformations we used advanced model of this effect [10] which allow to correct observed station position not only for vertical but also for horizontal displacement. At this stage of the research we used zero time delay between change of air and telescope construction temperature, because of lack of such a data for most of antennas. However, this mismodelling will effect only intra-day displacement of the telesope reference point, but not seasonal variations.

It should be mentioned here that account for horizontal displacement is especially important for processing regional networks, whereas vertical displacement due to thermal deformations prevails in variations of global baselines length. In particular, errors in modelling of this effect may be a possible reason of seasonal baselength variations found e.g. in [12].

Variation of baseline lengths obtained from VLBI data are shown in Figure 1. Unfortunately, stations Crimea and Yebes are not equipped with GPS receiver.

2.2. GPS observations

For computation of baseline lengths between european GPS stations we used weekly EPN solutions distributed in SINEX files. However, this solutions are not suitable for immediate use in geodynamical analysis because they cannot provide homogeneous long-time coordinate time series due to periodic changes in reference coordinate system and set of fiducial stations. For this reason, direct use of the EUREF solutions shows jumps in baselength variations [4]. Besides, method of computation of station coordinates used in EPN is based on using tight constrains to fiducial stations which cause a distortion of the network, i.e. fictive variations in baselengths (see e.g. [6]).

So, variations of baseline lengths from GPS data were obtained from analysis of coordinate time series for EPN stations computed by the method described in [8]. This computation is based on de-constraining of the official EPN solutions with further transformation to ITRF2000. For this study we used 6-parameter Helmert transformation to avoid loss of seasonal geophysical signal in baselength. Using our independent coordinate time series allows us to obtain realistic station displacement practically free of network distortion for all EPN stations over the period 1996.0–2001.0.

Variation of baseline lengths obtained from GPS data are shown in Figure 2. Unfortunately, MADR coordinate time series is too short (less than two years) that does not allow to get reliable results. It should be mentioned that errors in GPS baselength significantly decrease during a period under investigation. E.g., one can see abnormal trend in MATE displacement in 1996. However, that does not influence result very much due to relatively small weight of these data.

2.3. Atmospheric loading

One of the most important factor affecting variations of station coordinates derived from space geodesy observations is atmospheric loading. We investigated influence of this effect using 3-dimensional atmospheric loading time series provided by H.-G. Scherneck [14]. The data were averaged over a week interval corresponding to every GPS week and variations of baselengths were computed from these weekly values. Variation of baseline lengths obtained from analysis of atmospheric data are shown in Figure 3.

It is interesting that baselength variations contain not only seasonal but also secular component, even for short baselines, especially for continental-coastal ones, in particular baselines including Wettzell stations which are often used in studies on european geodynamics, e.g. [2–4, 13]. The reason of that may be long-periodic or progressive weather and climate changes, but period of our investigation is too short to separate them.

Since variations in height component of station displacement due to atmospheric loading prevail, this effect is especially significant for global baselines. For regional networks horizontal displacements yield main contribution to variation of baselengths.

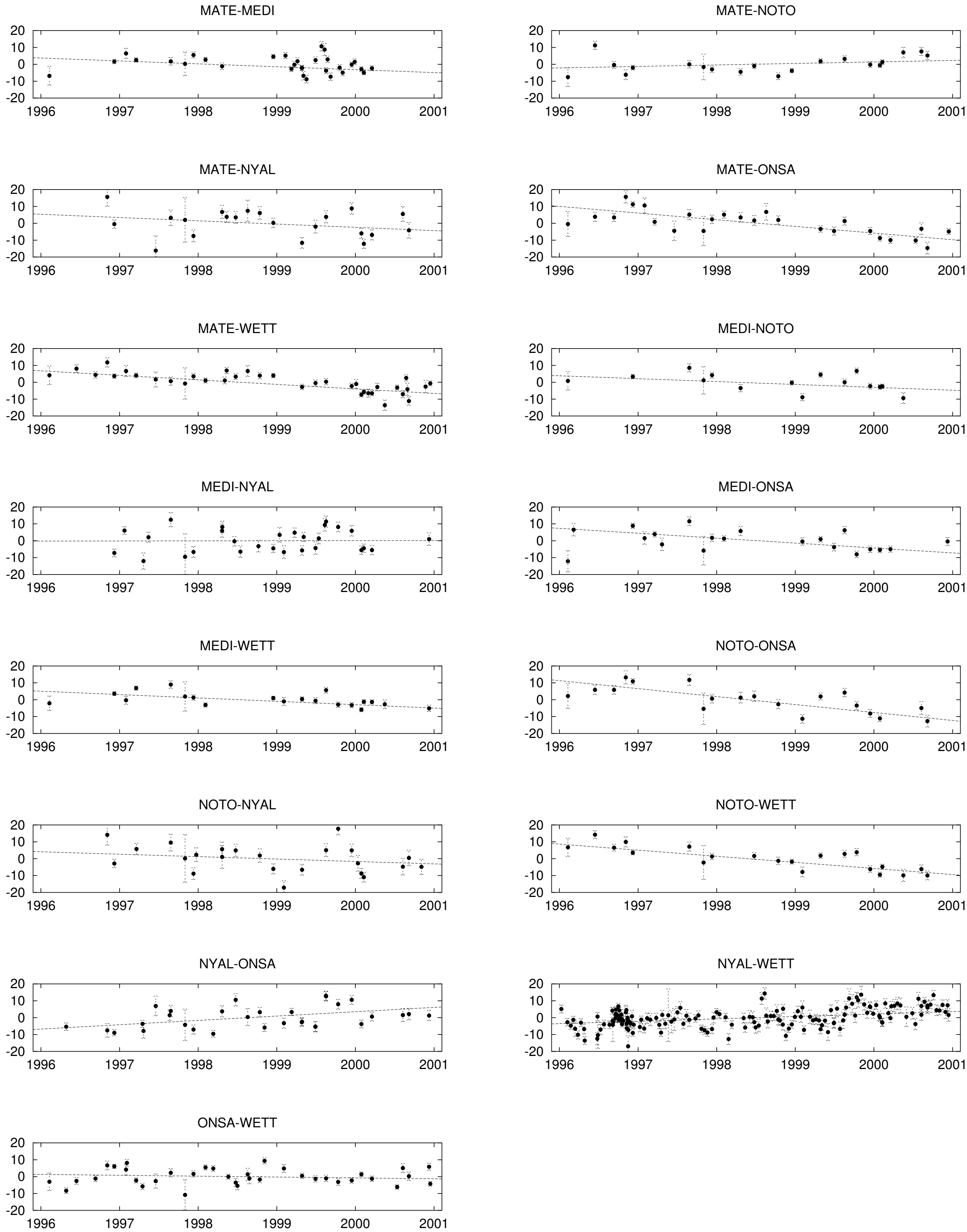

Figure 1. Variation of VLBI baselengths, mm.

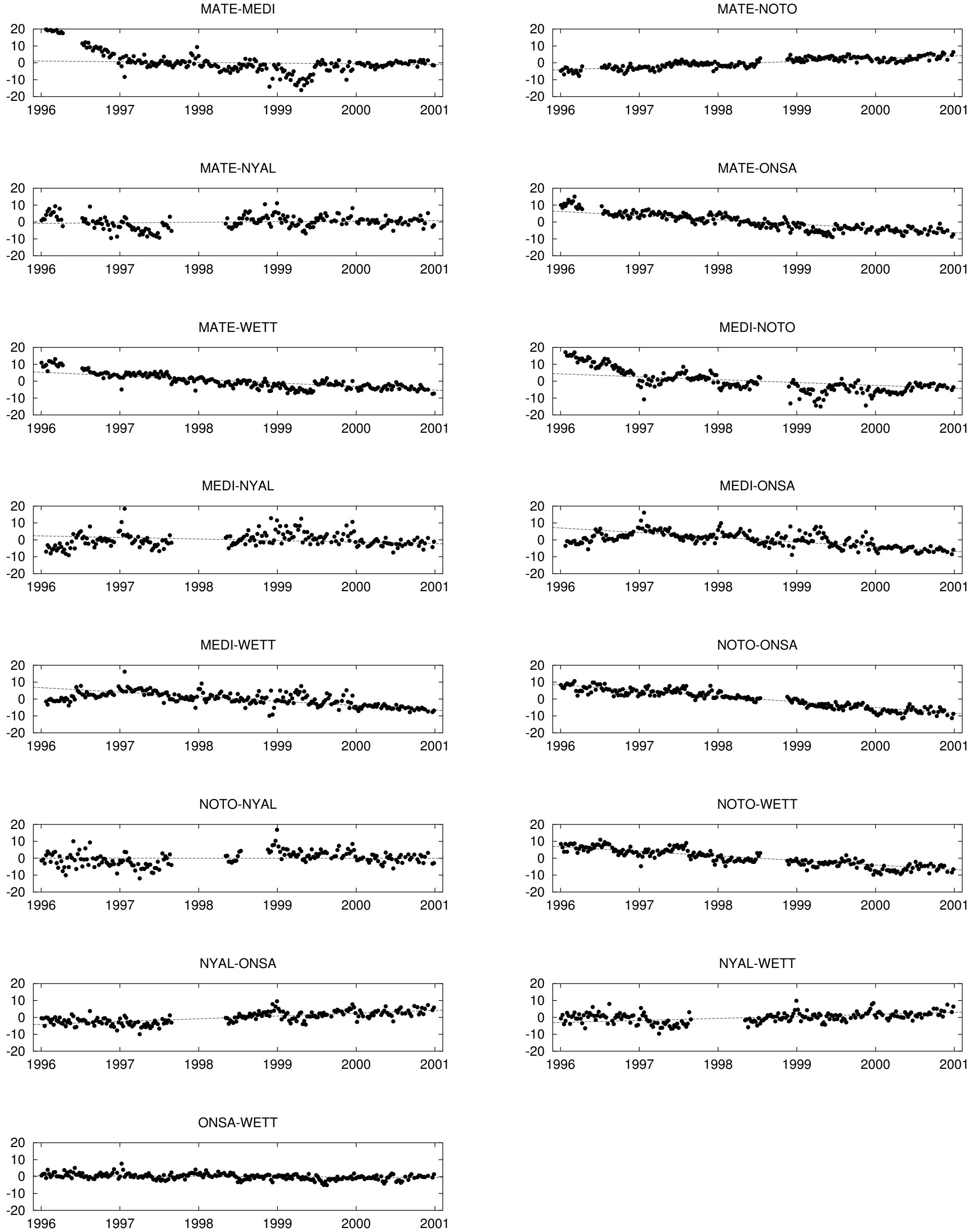

Figure 2. Variation of GPS baselengths, mm.

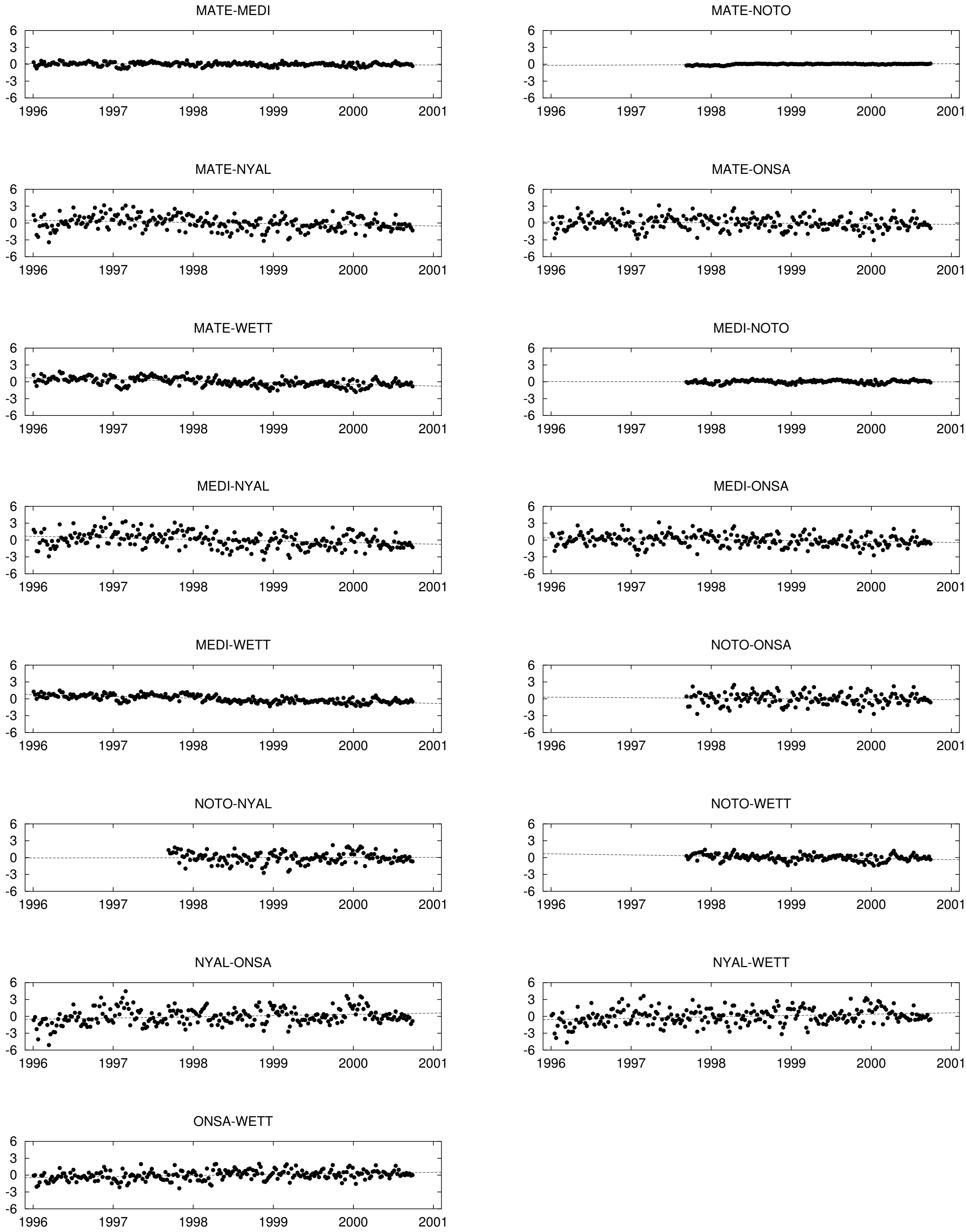

Figure 3. Variation of baselengths due to atmospheric loading, mm.

3. Results and conclusions

Results of computation of variations in baseline lengths are presented in Table 1. One can see that values of rates obtained from VLBI and GPS observations are in good agreement for most baselines. Unfortunately, it is not the case for seasonal variations. Obviously, interval of investigation is too short and number of used VLBI observations is too small for many baselines.

Indeed, it would be important to verify our results using data obtained from other space geodesy techniques, but only MATE and WETT stations are equipped with SLR units, and only NYAL station is equipped with DORIS beacon (which is explained by difficulties in collocation of DORIS beacon and VLBI antenna due to radio frequency interference).

It is also remarkable that influence of atmospheric loading on baseline length rate is significant for many baselines. Evidently, this effect must be investigated more carefully and properly accounted during geodynamical analysis.

Figure 4 shows dependence of error in baselength rate on length of baseline. It is interesting that for GPS data error is practically the same for all baselines unlike VLBI data.

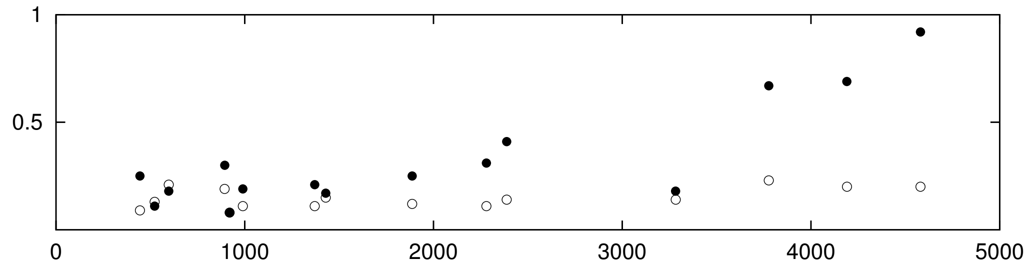

Figure 4. Dependence of error in rate (mm) on baselength (km) for VLBI (filled circles) and GPS (light circles) data.

Further steps of our work will include new re-computation of EPN coordinate time series based on new combination of individual EPN Analysis Center solutions, reprocessing of VLBI data with new version of software, and more complete analysis of various factors effected variations of baselengths. Analysis of variations in vertical component of station displacement is also planned.

Acknowledgements

This research was partially supported by a grant of the St. Petersburg Scientific Center of the Russian Academy of Sciences.

Table 1. Results of analysis of variation of baselengths: baseline length (L), km, number of epochs (N) processed and found in the IVS data base, linear trend (Rate), mm, amplitude of annual term (As), mm, amplitude of semiannual term (Asa), mm.

Base	L	VLBI				GPS				Atmospheric loading		
		N	Rate	Aa	Asa	N	Rate	Aa	Asa	Rate	Aa	Asa
MATE	597	31	–1.78	0.37	2.23	224	–0.97	3.42	1.26	–0.05	0.16	0.05
MEDI		35	±0.63	±0.99	±1.12		±0.21	±0.43	±0.36	±0.01	±0.03	±0.03
MATE	444	20	+0.62	3.21	2.17	212	+1.57	0.51	0.35	+0.06	0.06	0.02
NOTO		23	±0.71	±1.16	±1.29		±0.10	±0.19	±0.16	±0.01	±0.01	±0.01
MATE	4190	21	+0.27	6.57	3.35	192	+0.16	0.70	0.53	–0.20	0.27	0.15
NYAL		24	±1.74	±2.28	±2.49		±0.21	±0.37	±0.30	±0.05	±0.11	±0.11
MATE	1886	26	–3.86	2.64	1.19	229	–2.69	0.89	0.74	–0.09	0.32	0.17
ONSA		29	±0.51	±1.13	±1.04		±0.13	±0.25	±0.20	±0.05	±0.10	±0.10
MATE	990	36	–2.51	1.83	1.46	229	–2.25	1.47	0.46	–0.29	0.25	0.10
WETT		42	±0.40	±0.82	±0.71		±0.10	±0.19	±0.17	±0.03	±0.05	±0.05
MEDI	893	15	–1.22	3.39	4.14	221	–2.37	3.90	1.33	–0.01	0.23	0.03
NOTO		19	±0.94	±1.62	±2.40		±0.17	±0.33	±0.28	±0.02	±0.03	±0.02
MEDI	3776	28	–0.55	3.13	3.31	201	–0.73	1.61	1.15	–0.28	0.41	0.08
NYAL		34	±1.13	±1.87	±1.92		±0.23	±0.38	±0.34	±0.06	±0.11	±0.11
MEDI	1429	20	–3.13	2.76	1.15	238	–2.48	1.87	1.43	–0.16	0.17	0.19
ONSA		25	±0.76	±1.75	±1.68		±0.13	±0.26	±0.22	±0.05	±0.09	±0.09
MEDI	522	20	–2.14	2.56	1.25	238	–2.41	1.55	0.88	–0.31	0.06	0.10
WETT		22	±0.49	±1.15	±1.11		±0.13	±0.26	±0.22	±0.02	±0.04	±0.04
NOTO	4580	23	–1.62	6.02	3.73	189	–0.05	0.39	0.44	+0.02	0.36	0.24
NYAL		27	±1.30	±2.34	±2.32		±0.22	±0.31	±0.32	±0.09	±0.11	±0.10
NOTO	2280	19	–4.10	3.61	2.26	226	–3.52	1.11	0.81	–0.09	0.26	0.10
ONSA		24	±0.91	±1.85	±1.73		±0.11	±0.20	±0.18	±0.10	±0.12	±0.11
NOTO	1371	21	–3.39	2.51	1.66	226	–2.98	1.81	0.92	–0.21	0.21	0.12
WETT		22	±0.61	±1.14	±1.20		±0.11	±0.22	±0.19	±0.05	±0.06	±0.06
NYAL	2387	31	+2.17	4.03	1.56	206	+1.44	1.28	0.50	+0.22	0.63	0.25
ONSA		31	±0.86	±1.47	±1.52		±0.15	±0.25	±0.22	±0.06	±0.12	±0.12
NYAL	3283	162	+1.67	2.49	2.06	206	+1.03	1.41	0.24	+0.24	0.42	0.10
WETT		174	±0.25	±0.49	±0.52		±0.14	±0.22	±0.21	±0.06	±0.12	±0.12
ONSA	919	36	–0.75	3.42	1.15	243	–0.23	0.57	0.46	+0.19	0.13	0.14
WETT		37	±0.49	±0.93	±0.96		±0.08	±0.13	±0.13	±0.04	±0.07	±0.07

References

[1] Campbell J. The European Geodetic VLBI Project — An Overview. In: P. Tomasi, F. Mantovani, M. Pérez-Torres (eds.) Proc. 14th Working Meeting on European VLBI for Geodesy and Astrometry, Castel San Pietro Terme, 8–9 Sep 2000.

[2] Campbell J., A. Nothnagel. European VLBI for crustal dynamics. J. of Geodynamics, 2000, **30**, 321–326.

[3] Haas R., E. Gueguen, H.-G. Scherneck, A. Nothnagel, J. Campbell. Crustal motion results derived from observations in the European geodetic VLBI network. Earth Planets Space, 2000, **52**, 759–764.

[4] Lanotte R., C. Ferraro, A. Nardi, C. Sciarretta, F. Vespe. The CGS VLBI EUR98 Geodetic Solution and comparison with the CGS GPS results. In: W. Schlueter, H. Hase (eds.) Proc. 13th Working Meeting on European VLBI for Geodesy and Astrometry, Viechtach/Wettzell, Feb 12–13, 1999, 101–107.

[5] Malkin Z. M., N. A. Panafidina, E. A. Skurikhina. Comparison of baselengths derived from GPS and VLBI observations on European Network. Presented at the All-Russian Astronomy Conference, St.Petersburg, Russia, 6–12 Aug 2001.

[6] Malkin Z. M., Voinov A. V. Preliminary Results of Processing EUREF Network Observations Using a Non-Fiducial Strategy. Phys. Chem. Earth (A), 2001, **26**, No 6–8, 579–583.

[7] NASA GSFC VLBI terrestrial reference frame solution number 1130 v. 1, Jan 2000, `ftp://gemini.gsfc.nasa.gov/pub/solutions/`.

[8] Panafidina N., Malkin Z. On Computation of An Homogeneous EUREF Coordinate Time Series. In: Abstracts "Vistas for Geodesy in the New Millennium". Presented at the IAG 2001 Scientific Assembly, Budapest, Hungary, 2–7 September 2001.

[9] Skurikhina E. EOP and station positions determined with OCCAM Package. In: N. R. Vandenberg, K. D. Baver (eds.), IVS 2000 General Meeting Proc., Koetzting, Germany, Feb 21-24, 2000, 350–354.

[10] Skurikhina E. A. On Computation of Antenna Thermal Deformation in VLBI Data Processing. This issue.

[11] Titov O. Tectonic Motion of European VLBI Sites. In: W. Schlueter, H. Hase (eds.) Proc. 13th Working Meeting on European VLBI for Geodesy and Astrometry, Viechtach/Wettzell, Feb 12–13, 1999, 186–191.

[12] Titov O. A., Yakovleva H. G. Seasonal variations in radial components of VLBI stations. Astron. Astropys. Trans., 2000, **18**, No 4, 591–603.

[13] Tornatore V., F. Sacerdote, M. Crespi. Comparison of deformation resulting from GPS and VLBI data: problems and preliminary results. In: W. Schlueter, H. Hase (eds.) Proc. 13th Working Meeting on European VLBI for Geodesy and Astrometry, Viechtach/Wettzell, Feb 12–13, 1999, 206–216.

[14] `http://www.oso.chalmers.se/~hgs/apload.html`

Elena Skurikhina: On Computation of Antenna Thermal Deformation in VLBI Data Processing, Proceedings of the 15th Working Meeting on European VLBI for Geodesy and Astrometry, p.124–130
http://www.ieec.fcr.es/hosted/15wmevga/proceedings/skurikhina

On Computation of Antenna Thermal Deformation in VLBI Data Processing

Elena Skurikhina

Institute of Applied Astronomy of Russian Academy of Sciences (IAA)
e-mail: sea@quasar.ipa.nw.ru

Abstract

For more accurate VLBI delay modeling, thermal deformations of the VLBI anntennas are to be accounted for. The size of these effects is about several millimeters. The model is supplemented for all types of antenna mounts. Influence the new model of thermal deformation account to the baseline length is under consideration.

1. Introduction

Due to the large VLBI antenna dimensions changing line sizes ones can reach several millimeters what is several picoseconds in delay value. Account of this effect is more important for the biggest antennas and for considerable temperature variations (diurnal and seasonal). IERS Conventions 2000 (as in the Explanatory Supplement to the IERS Conventions (1996) Chapters 6 and 7 (Schuh, 1999)) note that most VLBI telescopes are of Cassegrain type with alt-azimuth or polar mount and secondary focus and contain formulas for thermal deformations account for these antenna types only. Changes in antenna height and axis offset due to temperature changes can be present by simple way as a line dependence with constant coefficient. If V is the antenna height and A is the axis offset changes due to temperature will be given by the next:

$$dV = k \cdot V \cdot (T - T_0)\,, dA = k' \cdot A \cdot (T - T_0)\,,$$

where dV, dA are changes line sizes due to temperature, k and k' are coefficients of thermal expansion (are estimated for every material, typically they are of the order of 10^{-5} 1/°C). Thermal expansion coefficients

for steel (insulated or no insulated) equal $1.2 \cdot 10^{-5}$ 1/°C,

for aluminium $2.31 \cdot 10^{-5}$ 1/°C,

for concrete $1.0 \cdot 10^{-5}$ 1/°C;

T_0 is the reference temperature e.g. 20°C (which is the usual reference temperature used when designing and constructing buildings), T is the temperature of antenna.

Different types of antennas require relevant models. A time lag between external environment and the corresponding expansion of antennas can be taken into account. It depends on material of antenna structure.

The total effect on measured delay on the baseline between two telescopes (with signal from radio source arriving first at site 1) is:

$$\Delta\tau_{baseline} = \Delta\tau_1 - \Delta\tau_2 \tag{1}$$

2. Model for thermal deformation of VLBI antennas

2.1. Alt-azimuthal and polar mount

IERS Conventions 2000 includes formulas for the most often used alt-azimuthal mount without axis offset (see Figure 1) and polar types of mount (see Figure 2).

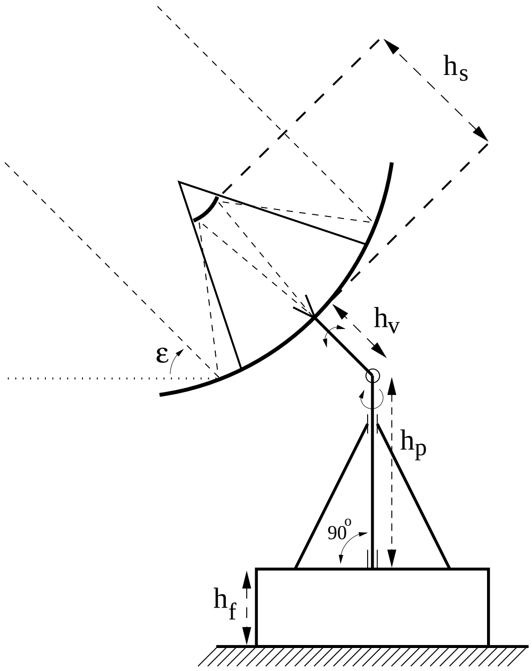

Figure 1. Alt-azimuthal telescope mount.

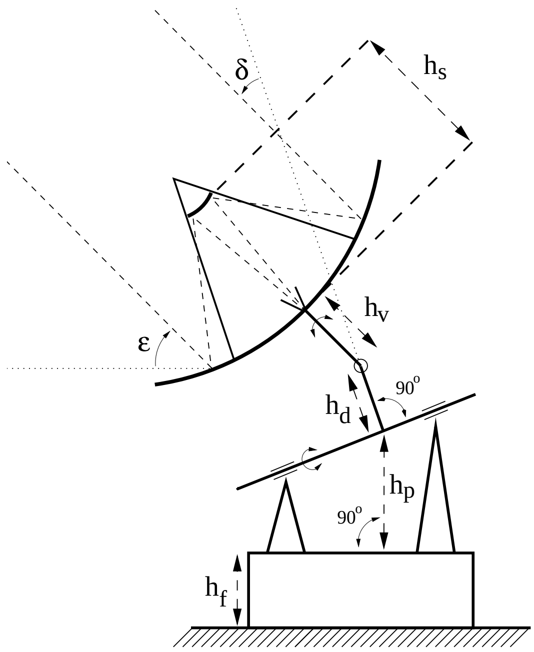

Figure 2. Polar telescope mount.

For alt-azimuth mounts:

$$\Delta\tau = \frac{1}{c}\cdot\left[\gamma_f\cdot(T(t-\Delta t_f)-T_0)\cdot(h_f\cdot\sin(\varepsilon))+\gamma_a\cdot(T(t-\Delta t_a)-T_0)\cdot(h_p\cdot\sin(\varepsilon)+h_v-F\cdot h_s)\right] \tag{2}$$

For polar mounts:

$$\Delta\tau = \frac{1}{c}\cdot\left[\gamma_f\cdot(T(t-\Delta t_f)-T_0)\cdot(h_f\cdot\sin(\varepsilon))+\gamma_a\cdot(T(t-\Delta t_a)-T_0)\cdot(h_p\cdot\sin(\varepsilon)+h_v-F\cdot h_s+h_d\cdot\cos(\delta))\right] \tag{3}$$

where c in m/sec is the speed of light;

γ_f and γ_a in $1/°C$ are the expansion coefficents for the foundation and for the antenna, respectively, values for any materials see above;

lets design the factor 0.9 for prime focus antennas and the factor 1.8 for secondary focus antennas in (IERS Conventions 2000 (27), (28)) as F;

T is the temperature of the telescope structure, If the actual temperature of the telescope structure is not available, which might be the case at most VLBI sites, the surrounding air temperature can be taken instead;

T_0 is a reference temperature, *e.g.* 20°C;

Δt_f is the time delay between the change in the surrounding air temperature and the expansion of the telescope structure for the foundation part;

Δt_a - for the antenna part and depend strongly on the material of the telescope. Measurements yielded values of Δt_a=2 hours for a steel telescope structure (Nothnagel *et al.*, 1995) and of Δt_f=6 hours for a concrete telescope structure (Elgered and Carlsson, 1995); but lets put this values as zero in later;

ε is the elevation of the observed radio source,

δ is the declination of the observed radio source;

and h_f, h_p, h_v, h_s and h_d are the dimensions of the telescopes in m:

h_f is the height of foundation above Earth's surface;

h_p is the height of pillar, either from track to elevation axis in the case of polar mounts from ground to VLBI reference point;

h_v is the height of vertex above declination or elevation axis;

h_d is the height of declination axis above hour angle axis (the declination shaft) only applicable for polar mounts, otherwise 0.0;

h_s is the height of subreflector above vertex of paraboloid.

Dimensions and expansion coefficients of frequently used geodetic VLBI telescopes can be found at http://miro.geod.uni-bonn.de/vlbi/IVS-AC/antenna dimensions for thermal expansion studies.

Table 1 contains the thermal variation $\Delta\tau$ of the VLBI delay observable based on equations (1), (2). Temperature variation $(T - T_0)$ of 10°C and radio source elevations between 5° and 90° were entered, time lags Δt_f and Δt_a were assumed to be zero.

2.2. Thermal deformation account for the other mount types

Usually antennas with other mount types take part in VLBI observations rather often too and some antennas with alt-azimuth mounth have an axis offset. The above formulas can be generalized for the other antena types so they differ the only item which is describing axis offset (axis shift in proection to the radio source direction corrected for refraction and aberration). We can assign the common part in both formulas and design it as $\Delta\tau_0$ (it is $\Delta\tau$ in (2)). Lets write

$$\Delta\tau = \Delta\tau_0 + \frac{1}{c} \cdot \gamma_a \cdot (T(t - \Delta t_a) - T_0) \cdot AX\_OFF \qquad (4)$$

Table 1. Thermal variations $\Delta\tau$ in *psec* of the VLBI delay observable for frequently used geodetic VLBI telescopes with alt-azimuth mount for a temperature variation of 10°C and different radio source elevations.

Telescope	$(T-T_0)$=10°C			
	Elevation ε			
	5°	30°	60°	90°
	$\Delta\tau$	$\Delta\tau$	$\Delta\tau$	$\Delta\tau$
	psec	*psec*	*psec*	*psec*
ALGOPARK	−3.4	0.0	3.0	4.1
CRIMEA	−3.1	−0.6	1.7	2.5
DSS15	−6.0	−2.8	0.0	1.0
DSS45	−6.0	−2.8	0.0	1.0
DSS65	−6.0	−2.8	0.0	1.0
EFLSBERG	−15.0	−6.8	0.6	3.2
FORTLEZA	−0.7	0.6	1.7	2.1
GGAO7108	0.1	0.8	1.5	1.7
HAYSTACK	−7.3	−3.7	−0.5	0.6
KASHIM11	−1.6	−0.4	0.7	1.1
KASHIM34	−5.8	−3.0	−0.6	0.3
KASHIMA	0.6	3.5	6.1	7.0
KOGANEI	−1.5	0.5	2.3	2.9
KWAJAL26	0.5	2.6	4.5	5.2
MATERA	−2.1	0.0	1.9	2.6
MIURA	−1.6	−0.4	0.7	1.1
MOJ 7288	−4.0	−1.7	0.4	1.2
OHIGGINS	0.2	1.4	2.4	2.8
ONSALA60	−2.2	−0.1	1.7	2.3
SESHAN25	−5.7	−1.2	2.8	4.3
TATEYAMA	−1.6	−0.4	0.7	1.1
TSUKUB32	−5.4	−2.3	0.5	1.5
URUMQI	−6.3	−2.2	1.5	2.8
WETTZELL	−3.8	−2.1	−0.5	0.1
YEBES	0.2	1.8	3.1	3.6

Term AX_OFF corresponds to mount types. Lets design axis offset as OFFS1.

its proection to the south position direction is $\pm OFFS1 \cdot \sqrt{1-(\vec{S}\cdot\vec{l}})$

$\vec{S}$ - source position direction, $\vec{l}$ - second axis rotation (fixed relative to the Earth) direction.

For alt-azimuthal mounts without axis offset: OFFS1 = 0

For alt-azimuthal mounts with axis offset: AX_OFF = $\pm OFFS1 \cdot \cos(\varepsilon)$,

For polar mounts (OFFS1 = h_d): AX_OFF = $\pm OFFS1 \cdot \cos(\delta)$,

For horizontal X_YN mount: AX_OFF = $\pm OFFS1 \cdot \sqrt{1-(\cos(\varepsilon)\cdot\cos(Az)^2}$,

For horizontal X_YE mount: AX_OFF = $\pm OFFS1 \cdot \sqrt{1-(\cos(\varepsilon)\cdot\sin(Az))^2}$

For Richmond mount AX_OFF $= -(OFFS1 \cdot SQRT(1D0 - (\sin(\varepsilon) \cdot \sin(0.6817256D0) + \cos(\varepsilon) \cdot \cos(0.6817256D0) \cdot (\cos(Az) \cdot \cos(0.0020944D0) - \sin(Az) \cdot \sin(0.0020944D0)))^2))$

All values are corrected for refraction.

Table 2 contains the thermal variation $\Delta\tau$ of the VLBI delay observable based on equations (3). For every station first line give the common part ($\Delta\tau_0$) and the second line give complete correction for thermal deformation $\Delta\tau$. Two last column are the mount type and axis offset. Temperature variation $(T - T_0)$ of 10°C and radio source elevations between 5° and 90° were entered, time lags Δt_f and Δt_a were assumed to be zero.

Table 2: Thermal variations $\Delta\tau$ in *psec* of the VLBI delay observable for frequently used geodetic VLBI telescopes temperature variation of 10°C and different radio source elevations.

Telescope	$(T-T_0)$=10°C					
	Elevation ε					
	5°	30°	60°	90°	MOUNT	OFFS1
	$\Delta\tau$	$\Delta\tau$	$\Delta\tau$	$\Delta\tau$		
	psec	*psec*	*psec*	*psec*		*m*
BR-VLBA	−4.9	−2.4	0.0	1.2	$AZEL$	2.135
BR-VLBA	−4.0	−1.7	0.4	1.2	$AZEL$	2.135
FD-VLBA	−4.9	−2.4	0.0	1.2	$AZEL$	2.135
FD-VLBA	−4.0	−1.7	0.4	1.2	$AZEL$	2.135
GILCREEK	−5.6	−3.5	−1.7	−1.0	$X-YN$	7.285
GILCREEK	−3.1	−0.9	1.1	1.9	$X-YN$	7.285
HARTRAO	−7.7	−5.7	−4.0	−3.4	$EQUA$	6.695
HARTRAO	−5.4	−3.3	−1.4	−0.8	$EQUA$	6.695
HATCREEK	−2.4	0.3	2.7	3.6	$EQUA$	0.000
HATCREEK	−2.4	0.3	2.7	3.6	$EQUA$	0.000
HN-VLBA	−4.9	−2.4	0.0	1.2	$AZEL$	2.135
HN-VLBA	−4.0	−1.7	0.4	1.2	$AZEL$	2.135
HOBART26	−11.2	−8.9	−7.1	−6.5	$X-YE$	8.190
HOBART26	−9.6	−6.7	−4.2	−3.2	$X-YE$	8.190
HRAS 085	−7.9	−6.4	−5.2	−4.8	$EQUA$	6.707
HRAS 085	−5.5	−4.0	−2.6	−2.1	$EQUA$	6.707
KAUAI	−2.0	−0.7	0.3	0.7	$X-YN$	2.438
KAUAI	−1.1	0.1	1.3	1.7	$X-YN$	2.438
KOKEE	−1.8	0.5	2.5	3.4	$AZEL$	0.508
KOKEE	−1.6	0.6	2.7	3.4	$AZEL$	0.508
KP-VLBA	−4.9	−2.4	0.0	1.2	$AZEL$	2.135
KP-VLBA	−4.0	−1.7	0.4	1.2	$AZEL$	2.135
LA-VLBA	−4.9	−2.4	0.0	1.2	$AZEL$	2.135
LA-VLBA	−4.0	−1.7	0.4	1.2	$AZEL$	2.135
MEDICINA	−1.5	1.5	4.3	5.6	$AZEL$	1.830
MEDICINA	−0.8	2.1	4.7	5.6	$AZEL$	1.830
MK-VLBA	−4.9	−2.4	0.0	1.2	$AZEL$	2.135
MK-VLBA	−4.0	−1.7	0.4	1.2	$AZEL$	2.135
MOJAVE12	2.2	3.3	4.2	4.6	$X-YN$	0.000
MOJAVE12	2.2	3.3	4.2	4.6	$X-YN$	0.000

NL-VLBA	−4.9	−2.4	0.0	1.2	$AZEL$	2.135
NL-VLBA	−4.0	−1.7	0.4	1.2	$AZEL$	2.135
NOTO	−2.0	1.0	3.8	5.1	$AZEL$	1.830
NOTO	−1.3	1.6	4.2	5.1	$AZEL$	1.830
NRAO85 3	−4.9	−2.8	−1.0	−0.3	$EQUA$	6.703
NRAO85 3	−2.6	−0.4	1.6	2.4	$EQUA$	6.703
NRAO85 1	−4.9	−2.8	−1.0	−0.3	$EQUA$	6.703
NRAO85 1	−2.6	−0.4	1.6	2.4	$EQUA$	6.703
NRAO20	−1.8	0.5	2.5	3.4	$AZEL$	0.508
NRAO20	−1.6	0.6	2.7	3.4	$AZEL$	0.508
NRAO 140	−18.5	−9.7	−2.3	0.3	$EQUA1$	4.928
NRAO 140	−8.6	0.6	8.8	11.8	$EQUA1$	4.928
NYALES20	−1.9	−0.1	1.6	2.2	$AZEL$	0.508
NYALES20	−1.7	0.1	1.7	2.2	$AZEL$	0.508
OV-VLBA	−4.9	−2.4	0.0	1.2	$AZEL$	2.135
OV-VLBA	−4.0	−1.7	0.4	1.2	$AZEL$	2.135
PIETOWN	−4.9	−2.4	0.0	1.2	$AZEL$	2.135
PIETOWN	−4.0	−1.7	0.4	1.2	$AZEL$	2.135
RICHMOND	−7.3	−4.9	−2.8	−2.4	$RICH$	5.179
RICHMOND	−5.4	−3.3	−1.4	−0.8	$RICH$	5.179
SANTIA12	2.2	3.2	4.1	4.4	$X-YN$	0.000
SANTIA12	2.2	3.2	4.1	4.4	$X-YN$	0.000
SC-VLBA	−4.9	−2.4	0.0	1.2	$AZEL$	2.135
SC-VLBA	−4.0	−1.7	0.4	1.2	$AZEL$	2.135
WESTFORD	−1.0	1.7	4.1	5.0	$AZEL$	0.318
WESTFORD	−0.8	1.8	4.2	5.0	$AZEL$	0.318

As we can see from Table 2 differences between the models are bigger for antennas with large axis offset. And differences in results will be more clear for baselines with these stations.

3. Comparison new and old model application

For example lets see in what way new model appears in baseline lengths. It is clear that differences can be on baselengths with the stations with axis offsets and the mounts not included in IERS Conventions 2000 model only. The baseline lengths were computed with the old and the new model for the thermal deformations. As one can see from Figure 3, differences between baseline lengths have a seasonal component with an amplitude of the order of 1.5 mm for the bases with Gilcreek station. Differences in the baseline HartRAO-Hobart do not have a clear seasonal component so both station located in the southern hemisphere with no big differences of seasonal temperatures. Baseline Gilcreek-NRAO85 differences do not have periodical component probably so these stations are located not very far from each other and their environment is not very different.

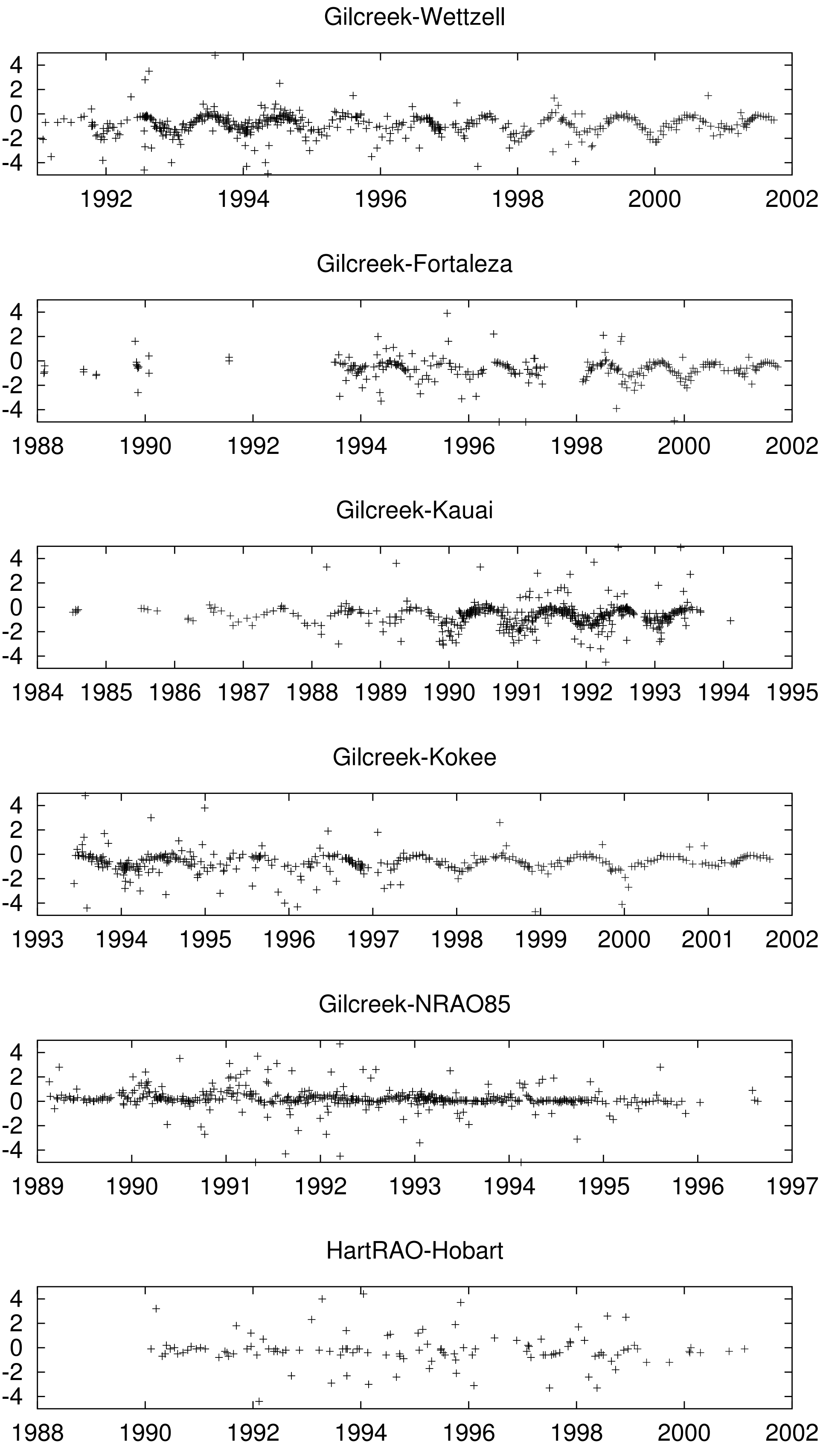

Figure 3. Differences in baseline length.

Session 3

Atmospheric Modelling

Arthur E. Niell: An a priori Hydrostatic Gradient Model for Atmospheric Delay, Proceedings of the 15th Working Meeting on European VLBI for Geodesy and Astrometry, p.133–136
http://www.ieec.fcr.es/hosted/15wmevga/proceedings/niell

An a priori Hydrostatic Gradient Model for Atmospheric Delay

Arthur E. Niell

MIT Haystack Observatory
e-mail: aniell@haystack.mit.edu

Abstract

The different mean heights of the hydrostatic and wet components of the atmosphere result in significantly different mapping functions for the azimuthally symmetric distributions. Similarly, the azimuthally asymmetric distributions, approximated as simple gradients over the field of view of a VLBI or GPS antenna, require different functional dependences if the highest accuracy is to be obtained in geodetic applications. A method has been developed to determine the a priori hydrostatic gradient function from the output of a numerical weather model. A more accurate model for the wet gradient can then be used for estimating the remaining gradient component.

1. Introduction

The importance to geodetic VLBI analysis of using separate mapping functions for the azimuthally symmetric distribution of the hydrostatic and wet components of the atmosphere delay has been amply demonstrated (for example, see [5]). The difference is due to the larger mean height of the hydrostatic component, resulting in a smaller increase in delay with decreasing elevation than for the wet component. Separation of the two in the data analysis is possible because the hydrostatic zenith delay can be accurately calculated from the surface pressure and the line of sight delay removed from the observable. The wet zenith delay can then be estimated from the observed delays, along with other geodetic parameters, by using the wet mapping function as the partial derivative.

Similarly, the importance of estimating a gradient in the atmosphere delay has been recognized for almost a decade ([3]). The functional form for a simple gradient model was derived by Chen and Herring ([1]), and they obtained average parameters for the hydrostatic and wet gradients by using three dimensional raytracing of a Numerical Weather Model. However, in contrast to the azimuthally symmetric hydrostatic delay, there is no simple measurement or meteorological parameter that can be determined at the surface to provide an accurate input for the calculation of the hydrostatic gradient delay, which is the product of the gradient mapping function and the zenith gradient delay. As a consequence a single gradient mapping function has been used up to now and only a combined gradient component estimated. Chen and Herring [1] used the hydrostatic mapping function in their evaluation. Other analysts ([4]; [6]) have used an even simpler mode! l obtained by Gardner [2] that has no parameters to allow for differences in vertical distributions of the refracting material.

Use of the wet gradient mapping function of [1] instead the hydrostatic amounts to about 30 mm of additional delay at 5° elevation for a typical gradient delay of 1 mm. The consequence of this in the estimation procedure is a difference of about 4 mm in the horizontal component of site position.

By analogy with the azimuthally symmetric mapping functions, a more accurate use of separate gradient mapping functions would be to apply an apriori hydrostatic correction and use a better wet function to estimate the remainder. This is practical because the hydrostatic atmosphere has a much larger scale length and a much longer temporal scale, both of which can be reasonably sampled by numerical weather models.

Several advantages are achieved by separating the hydrostatic and wet gradients:

- removal of an accurate apriori model provides more accurate observables to be used for the estimation
- a more accurate mapping function for the remaining pre-fit residuals gives a better partial derivative for the estimation
- the estimated excess wet delay can be compared directly and more accurately with other measurements of water vapor distribution, for example that of a water vapor radiometer.

As proposed for use with the Isobaric Mapping Function (IMF, [7]) a Numerical Weather Model provides information on the neutral atmosphere on a regularly spaced grid at many pressure levels (heights above the surface) several times per day. For IMF, the geopotential height of the 200 hPa level (approximately 10 km) was found to serve as a proxy for the hydrostatic mapping function. As an extension I propose to use the 'tilt' of the 200 hPa level over a site to describe the gradient of the hydrostatic atmosphere. However, rather than determine a separate hydrostatic gradient mapping function, I propose to directly adjust the apparent zenith direction to be the direction normal to the 200 hPa isobar above the site. The implications are described below.

2. Hydrostatic gradient mapping function

The tilt of the hydrostatic atmosphere is obtained as the direction of the normal to the surface defined by the geopotential heights of the 200 hPa surface at the four nearest grid points. The testing has been done using the Re-analysis of the Data Assimilation Office of the Goddard Space Flight Center ([9]). The horizontal grid spacing is 2.5° in longitude and 2.0° in latitude, and the values are given every six hours beginning at 00 UT.

I compared the variation of the excess delay with elevation with that of the hydrostatic form (c = 0.0032) of ([1], hereafter CHh). For a given tilt, obtained from the NWP, there is a value of the delay gradient that gives the same excess delay to within 1 mm down to 4° elevation. On the other hand, for the functional form used by [4], if the excess delay is matched at an elevation of 5°, the difference is up to 6 mm at 7° and changes sign to give a difference of 14 mm at 4°. It is difficult to determine the effect of these differences since a single function is used for the combined effect of the hydrostatic and wet, but a comparison will be made as part of the evaluation of the proposed gradient mapping function (not reported here).

The form of the hydrostatic gradient mapping function (GMFh) is:

$$\mathrm{GMFh}\,(\varepsilon_s, \alpha_g, z_g) = \mathrm{MFh}\,(\varepsilon_s - z_g \cdot \cos(\alpha_g)) \tag{1}$$

where

GMFh	=	hydrostatic gradient mapping function
MFh	=	azimuthally symmetric hydrostatic mapping function
ε_s	=	elevation of observation
α_g	=	gradient azimuth from North to East
z_g	=	gradient zenith angle

Any symmetric mapping function can be used. The apriori total line of sight hydrostatic delay is the product of the zenith hydrostatic delay (preferably calculated from surface pressure using the relation by [8]) and GMFh.

The best determined wet gradient mapping function is that of [1] with their value of c = 0.0010 (hereafter referred to as CHw) derived from similar data as used for IMF.

A difference from previous usage is that the apriori hydrostatic line of sight delay is not largest at the zenith. However for observed hydrostatic gradients obtained from the 200 hPa data, the difference between the calculated hydrostatic line of sight delay in the zenith direction and the

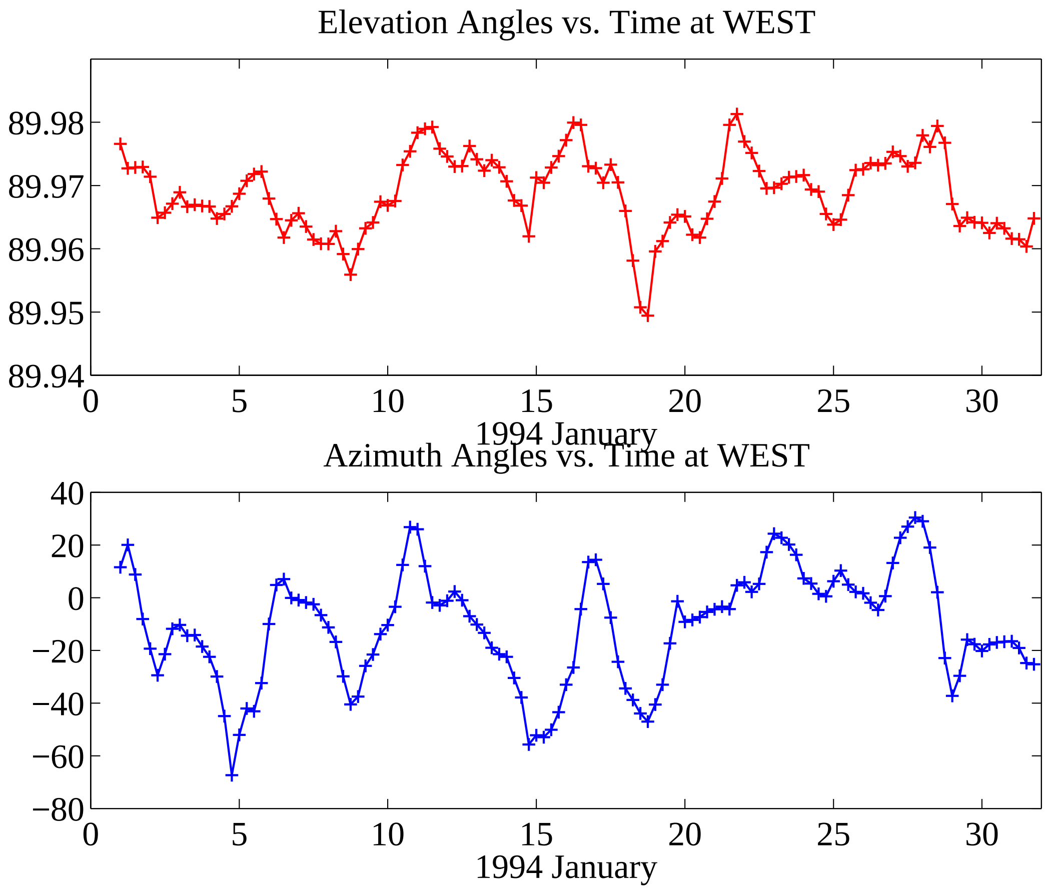

Figure 1. Elevation and azimuth of hydrostatic gradient tilt at Westford for 1994 January from geopotential heights of 200 hPa isobars.

apriori zenith hydrostatic delay is less than 0.5 mm. The CH wet mapping function has the traditional symmetry.

As an example, the azimuth and elevation angles of the hydrostatic gradient mapping function derived as described above are shown in Figure 1 for the Westford site (Massachusetts, USA) for 1994 January. Although the average tilt in the northern hemisphere is expected to be to the north, the azimuths shown in Figure 1 agree well with those calculated by [1] for the same site and time period.

3. Uncertainties

Uncertainties in estimated atmosphere parameters and in geodetic results arise from several sources, such as: accuracy of gradient mapping function as a description of the non-azimuthally symmetric distribution, accuracy of the isotropic mapping function, distribution of the observations on the sky, and characterization of time variability of both azimuthally symmetric and non-symmetric distributions, e.g. linear vs. stochastic, and if stochastic, the value of the variance per time.

The uncertainty in the calculated value of the tilt due to the uncertainties in the geopotential heights is negligible. There might also be a better pressure level to represent the gradient value, but for IMF, the 200 hPa level was found to be the best. Additional error in the estimation will be introduced by using the wet mapping function to estimate any hydrostatic component not properly removed as apriori, and by any error in the wet mapping function.

4. Implementation

NWP files have been obtained from DAO ([9]) for the years 1984 through 1996. Next the mapping function parameters must be extracted from these files on the same grid. (These files provide global information and could be made available as a service, similar to EOP and AAM.) For each experiment the parameters are then interpolated to the time of observation at the location of each site. The mapping function could then be either calculated ahead of time and stored or calculated at the time of estimation.

NWP data are yet to be obtained for 1997 through the present, and a service must be established to update the information daily.

5. Status

The global accuracy of using the tilt as a representation of the hydrostatic gradient is yet to be assessed. This will be done by comparing with 3-D raytracing, as done by [1]. Improvement of the wet gradient mapping function will be attempted using NWP data on a finer grid.

Acknowledgments

I thank M. Karki for data, and J. Tang for help with analysis.

References

[1] Chen, G., and Herring, T. A., "Effects of atmospheric azimuthal asymmetry on the analysis of space geodetic data", J. Geophys. Res., 99(B1), 637-651, 1994.

[2] Gardner, C. S.,"Effects of horizontal refractivity gradients on the accuracy of laser ranging to satellites", Rad. Sci., 11, 1037-1044, 1976.

[3] Herring, T. A., "Modelling atmospheric delays in the analysis of space geodetic data", in Symposium on Refraction of Transatmospheric Signals in Geodesy, J. C. DeMunk and T. A. Spoelstra, eds., Netherlands Geodetic Commission Series No. 36, 157-164, 1992.

[4] MacMillan, D. S., "Atmospheric gradients from very long baseline interferometry observations", Geophys. Res. Lett., 22, 1041-1044, 1995.

[5] MacMillan, D. S., and C. Ma, "Evaluation of very long baseline interferometry atmospheric modeling improvements", J. Geophys. Res., 99, 637-651, 1994.

[6] MacMillan, D. S., and C. Ma, "Atmospheric gradients and the VLBI terrestrial and celestial reference frames ", Geophys. Res. Lett., 24, 453-456, 1997.

[7] Niell, A. E., "Improved atmospheric mapping functions for VLBI and GPS", Earth Planets Space, 52, 699-702, 2000.

[8] Saastamoinen, J., "Atmospheric correction for the troposphere and stratosphere in radio ranging of satellites", in The Use of Artificial Satellites for Geodesy, Geophys. Monogr. Ser., vol. 15, edited by S. W. Henriksen, A. Mancini, and B. H. Chovitz, pp. 247-251, AGU, Washington, D.C., 1972.

[9] Schubert, S. D., J. Pjaendtner, and R. Rood, "An assimilated data set for Earth science applications", B. A. M. S., 74, 2331-2342, 1993.

Axel Nothnagel: On the Effects of Solution Types on Clock and Atmosphere Parameters, Proceedings of the 15th Working Meeting on European VLBI for Geodesy and Astrometry, p.137–142
http://www.ieec.fcr.es/hosted/15wmevga/proceedings/nothnagel1

On the Effects of Solution Types on Clock and Atmosphere Parameters

Axel Nothnagel

Geodetic Institute of the University of Bonn

e-mail: nothnagel@uni-bonn.de

Abstract

When comparing VLBI derived earth orientation parameters (EOP) with those of the IERS C04 series, significant differences are discernible in the period between 1984 and 1989. In an attempt to unravel the reasons of the apparently systematic behaviour of the EOP, we investigate possible differences in atmosphere and clock parameters estimated in a so-called TRF solution and in a solution where station coordinates are adjusted in each session independently. The differences between the two solutions clearly show an increased scatter in both the clock and the atmosphere parameters before the late 1980's deminishing abruptly at about August 1989. Further investigations of possible causes for these differences have so far not produced any results.

An analysis of data from 1990 onwards averaged over the individual months of year does not produce any conclusive evidence for seasonal dependencies.

1. Motivation

One of the tasks of the Analysis Coordinator of the International VLBI Service for Geodesy and Astrometry (IVS) is the monitoring of the earth orientation parameter (EOP) submissions of the individual IVS Analysis Centers to the IVS Data Centers and to the International Earth Rotation Service (IERS). In the process of intercomparisons between the individual EOP series submitted in early 2001 and the IERS C04 series (IERS 2001) significant deviations have been detected.

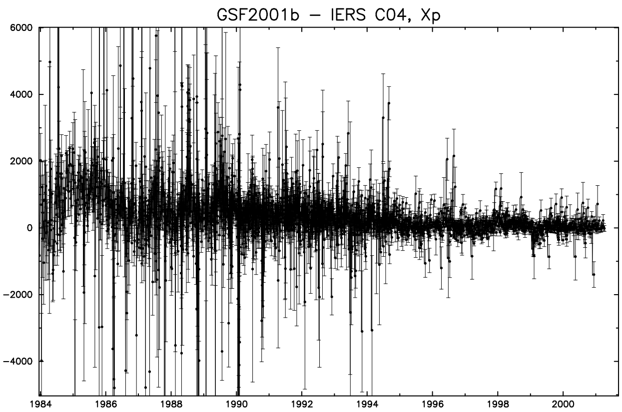

Figure 1. Differences in X pole component between GSFC solution 2001b and the IERS C04 series in microarcseconds.

As an example Fig. 1 depicts the differences between the X pole component of the GSFC 2001b (Goddard Space Flight Center) solution and the IERS C04 series. It is clearly discernible that a bump-like deviation is present in the period between early 1984 and late 1986 with a similar bump in the Y pole component. Comparisons show that the same behaviour is present in submissions of other IVS Analysis Centers using different analysis software packages clearly indicating that this is not a software related problem.

2. Data analysis

In an attempt to find out possible reasons for these deviations we have investigated the behaviour of the clock and atmosphere parameters in the least squares adjustment for the determination of the EOP. In general, two types of VLBI solutions of long VLBI observing series are often applied: a) the so-called "TRF" (terrestrial reference frame) solutions and b) the solutions in which station coordinates are estimated for each session independently. In the "TRF" solutions most of the stations are parametrized with X,Y,Z coordinates at a reference epoch plus three time derivatives dx/dt, dy/dt, dz/dt which represent the 3D station velocities or drift rates. This basic parametrization is often used for estimating global station parameters and EOP for each session.

A second type of solution assumes that EOP are well known and can be introduced externally. In this case in each session the coordinates of all stations except of a reference station can be estimated independently. Analogous to the solution of a single satellite arc these solutions may also be called "arc" solutions. It should be mentioned that in this type of solution the number of degrees of freedom is significantly smaller than in "TRF" solutions if the parametrization of the other parameters, e.g. clock and atmosphere parameters including gradients, is kept identical in the two solutions. Intercomparisons of identical parameters estimated in these two types of solutions should provide some insight into possible systematic differences and their origins.

The basis for the following intercomparisons is a data set with almost all VLBI sessions observed between January 1984 and December 2000 except of data of mobile VLBI antennas. Two solutions, an "arc" and a "TRF" solution, were computed with identical setups except for the parametrization of the station coordinates and EOP as described above.

In a first step the weighted root mean squared (WRMS) residual delay of the two solutions was intercompared. The WRMS residual delay is the best indicator of the quality of the fit of each session. The number of degrees of freedom of the "TRF" solution is significantly higher and it may be expected that possible systematic effects re-distribute in the larger number of parameters in the "arc" solution reducing the WRMS residual delay. However, both solutions show almost identical scatter in the residuals differing only at the level of 1 – 2 ps (picoseconds).

For the intercomparisons of estimated parameters some preparational work has to be carried out. In the absence of clock jumps, normally the least squares adjustment of VLBI sessions is based on second order polynomials plus a number of continuous piece-wise linear segments of certain lengths, e.g. 60 minutes, (called piece-wise linear functions) for the clock parameters. Piece-wise linear functions alone are similarly used to parametrize the atmospheric zenith path delays. While clock offset parameters of identical epochs from the two solutions can be compared directly, the atmosphere parameters have to be averaged over a 24-hour session in order to produce a representative value for each session. After these preparatory steps differences are computed for each session and stored for each station independently.

3. Results

The results of the intercomparisons come somewhat as a surprise. Figures 2 and 3 display the differences of the estimated atmospheric zenith path delays between the "arc" and the "TRF" solutions for each session for stations Wettzell and Westford. It is clearly discernible that the scatter is much larger prior to 1990 than after 1990. Wettzell and Westford are selected here because they have a long and rather continuous observing history. However, the differences of other stations show an almost identical behaviour independent of their observing history clearly emphasizing a change in the level of scatter at the same epoch. A similar effect is also obvious for the clock offsets (Fig. 4 and 5) and for the atmosphere gradients although less significant (not shown here).

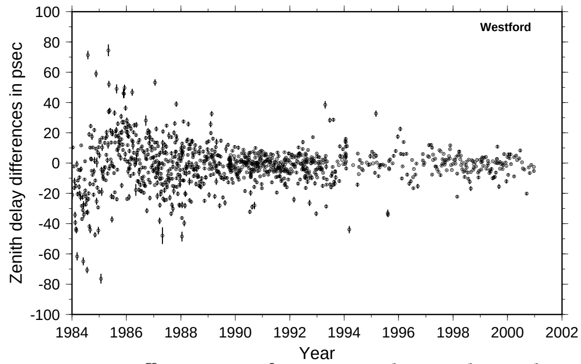

Figure 2. Differences of estimated zenith path delays (TRF - arc solution) for station **Westford**

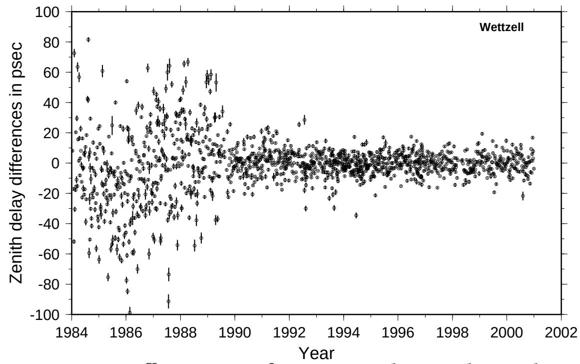

Figure 3. Differences of estimated zenith path delays (TRF - arc solution) for station **Wettzell**

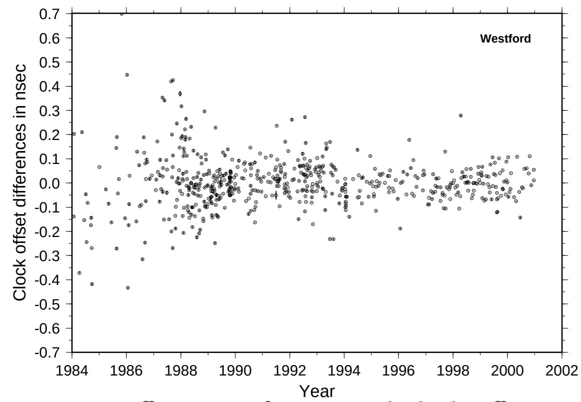

Figure 4. Differences of estimated clock offsets (TRF - arc solution) for station **Westford**

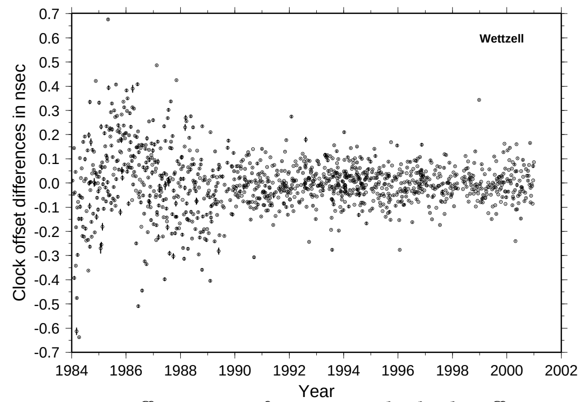

Figure 5. Differences of estimated clock offsets (TRF - arc solution) for station **Wettzell**

Ideally, the time series of differences should only show some noise-like behaviour which is of the same level during the whole observing period. However, this is not the case comparing these two types of solutions. Only the time series after 1990.0 seems to behave according to our expectations.

If we consider a single session analysed in an "arc" solution we can assume that the least squares adjustment distributes any possible errors in the observations into the parameters as best as possible without any external constraints. This means that all estimated station coordinates may freely adjust themselves to positions which best match the observations. In the "TRF" solution, however, each session is constrained by other sessions in that the station coordinates have to fit into the overall position and rate parameters estimated by the entire set of sessions. It is, thus, much more constrained than the individual "arc" solutions and deficits either in the observations or in the general setup may increase the scatter of the residuals or dissipate into the other parameters like clock and atmosphere unknowns. As was stated already above the scatter is not affected by the different types of solutions. Therefore, the reason for the discrepancies has to be looked for in the sessions themselves or in the general setup of the "TRF" solution.

4. Investigations

From the plots above an exact epoch of where the scatter diminishes is not discernable. Therefore, monthly averages were computed for most of the parameters and stored again independently for each station. In figures 6 to 9 the same data for Westford and Wettzell as above is displayed as monthly averages.

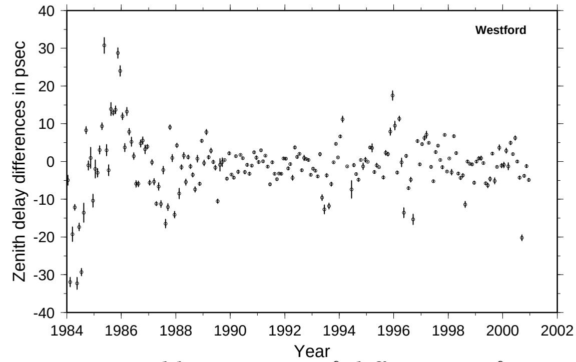

Figure 6. Monthly averages of differences of estimated zenith path delays (TRF - arc solution) for station **Westford**

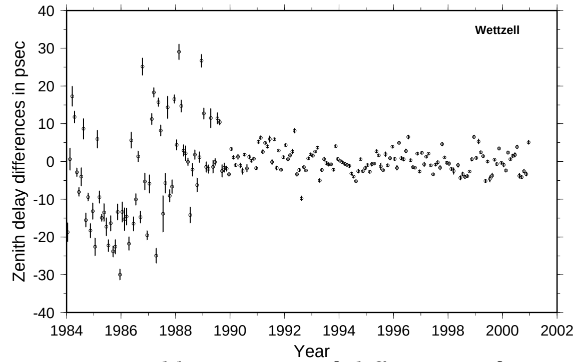

Figure 7. Monthly averages of differences of estimated zenith path delays (TRF - arc solution) for station **Wettzell**

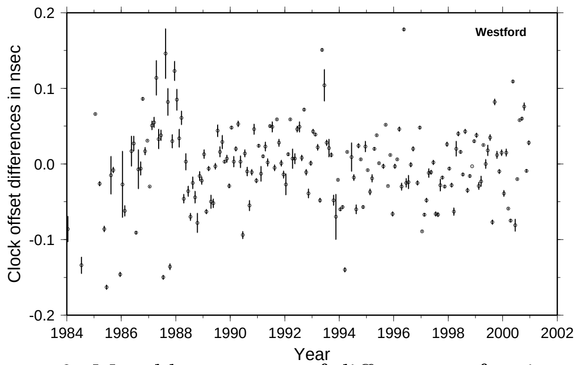

Figure 8. Monthly averages of differences of estimated clock offsets (TRF - arc solution) for station **Westford**

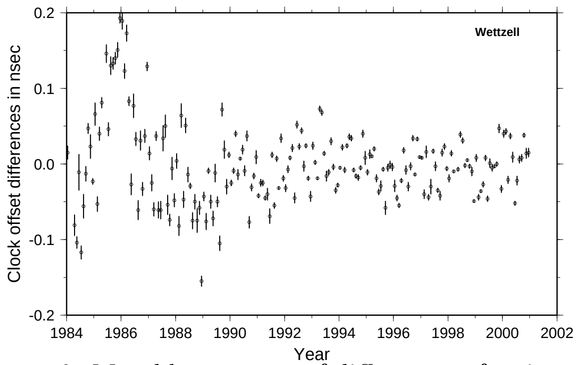

Figure 9. Monthly averages of differences of estimated clock offsets (TRF - arc solution) for station **Wettzell**

Here, the picture becomes much clearer and the epoch of the transition can be identified to be the month of August in 1989. It has to be emphasized that the same epoch has been found in the difference series of other stations as well.

In order to figure out possible causes for the abrupt change in behaviour of the differences, we looked at the history of stations and their first and last session in which they participated. Fig. 10 depicts the participation history of the major stations over the course of the last 17 years.

We found that around this time stations Maryland Point and Fort Davis (HRAS085) terminated their participation (last sessions August 24, 1989 and October 29, 1989, respectively) while Hobart started its operation (first session September 26, 1989). Several test computations excluding these stations were, therefore, carried out in order to figure out what influence the participation of these stations may have on the solutions. The preliminary result is that no conclusive evidence was found which permits to attribute the abrupt transition to a specific station.

5. Analysis of data after 1990.0

Another interesting aspect of the differences in the atmospheric zenith path delay parameters are possible systematic effects with an annual signature. In order to eliminate any unwanted effects by the earlier sessions, only data after 1990.0 was used in the following investigation. Here,

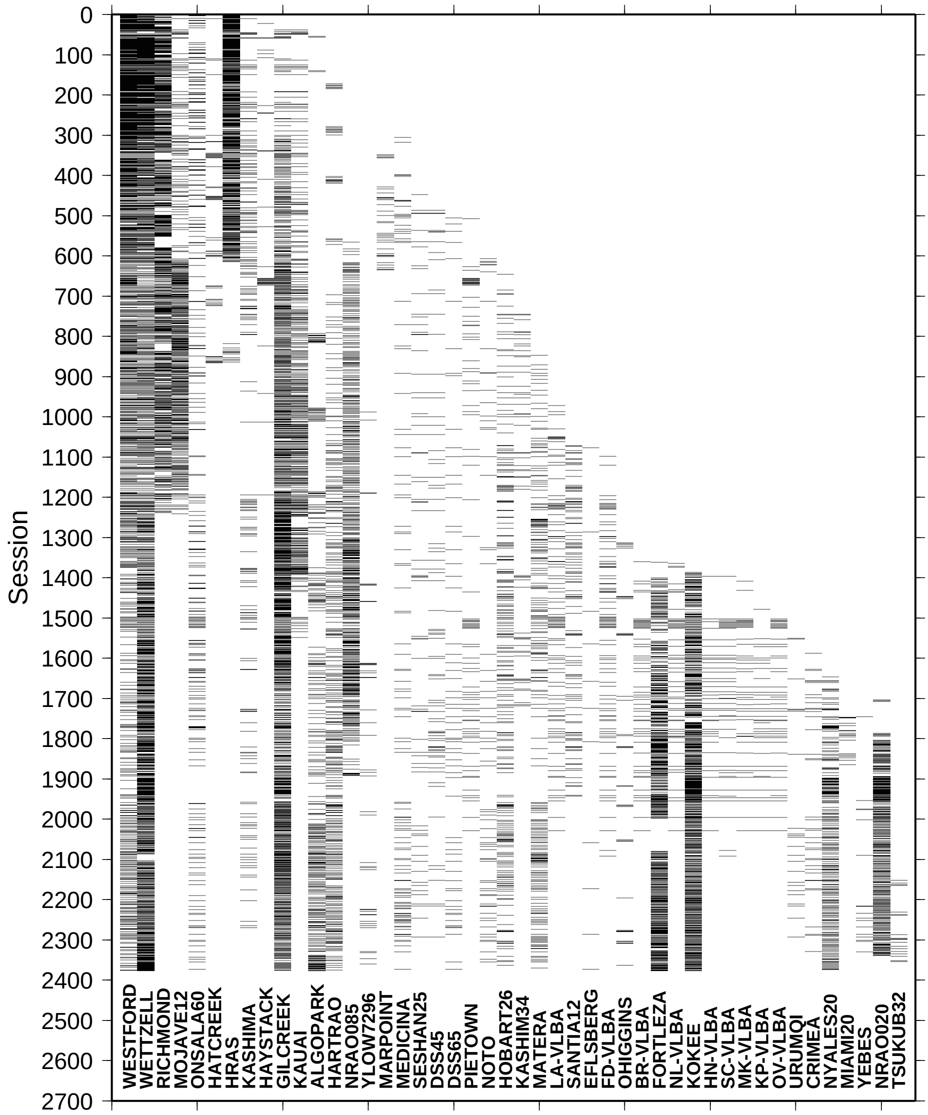

Figure 10. Participation history of major stations between Jan. 1984 (Session 1) and Dec. 2001 (Session 2380).

averages of the differences were computed with respect to the months of year, e.g. averages over all sessions observed in the months of January between 1990 and 2001. Figures 11 and 12 depict the average differences for a few selected sites separated by hemispheres.

Looking at figure 11 one may find systematic negative values for the months of July to September (7 – 9) as compared to the other months. Something similar but with an inverse signature may be supposed in figure 12 for the southern hemisphere. Computing further averages over all stations of the northern and the southern hemispheres separately did not shed more light onto this issue especially since other stations do not have such a long and dense time series. Although the results in the northern hemisphere are less noisy the scatter still dominates. In addition, the effect has a magnitude of only up to 1 or 2 picoseconds, which is equivalent to 0.3 to 0.6 mm, and is,

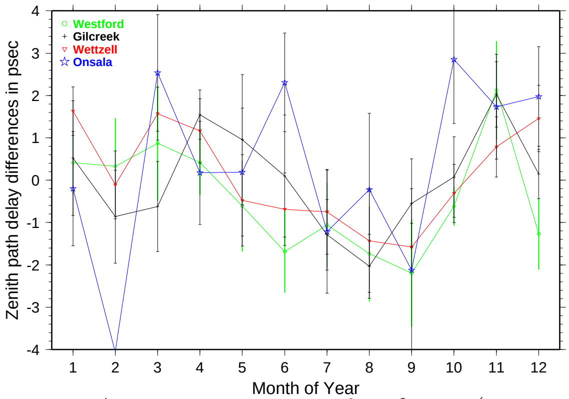

Figure 11. Averages w.r.t. months of year (1 = January, ... 12 = December) for selected stations in the northern hemisphere

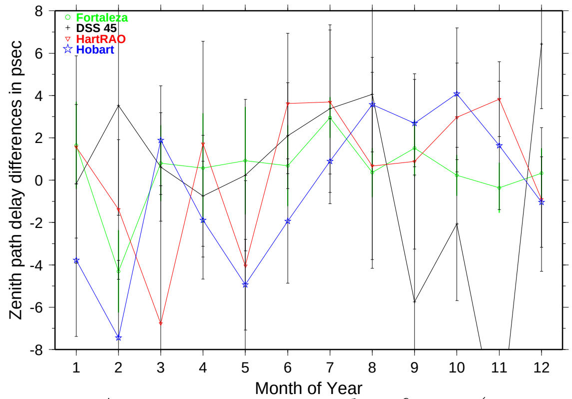

Figure 12. Averages w.r.t. months of year (1 = January, ... 12 = December) for selected stations in the southern hemisphere

thus, much too small to have any meaning in this context.

6. Conclusions

The parameters estimated in the least squares adjustment of a large number of VLBI observing sessions like zenith path delays and clock offsets are heavily affected by the type of solution prior to August 1989. So far, the causes for this cannot be traced back to a single observing site. Further investigations are underway studying possible secondary parameters like elevation cut-off in the scheduling of the sessions. With respect to possible annual variations in the differences it can be stated that no immediate conclusions can be drawn from the results reported above.

Acknowledgements

We are particularly thankful to Gerald Engelhard and Volkmar Thorandt, Bundesamt für Kartographie und Geodäsie, Leipzig, who carried out all the global solutions used in this investigation.

References

IERS (2001) *IERS 2000 Annual Report*, in press, Frankfurt a.M.

Johannes Böhm and Harald Schuh: Spherical Harmonics as a Supplement to Global Tropospheric Mapping Functions and Horizontal Gradients, Proceedings of the 15th Working Meeting on European VLBI for Geodesy and Astrometry, p.143–148
http://www.ieec.fcr.es/hosted/15wmevga/proceedings/boehm

Spherical Harmonics as a Supplement to Global Tropospheric Mapping Functions and Horizontal Gradients

Johannes Böhm, Harald Schuh

Institute of Geodesy and Geophysics, University of Technology, Vienna
Contact author: Johannes Böhm, e-mail: `jboehm@luna.tuwien.ac.at`

Abstract

Global mapping functions are used to map the tropospheric zenith path delays down to the path delays at certain elevations. Recently, horizontal tropospheric gradients have also been applied to account for azimuthal asymmetries of the path delays. Anyway, there are still deficiencies when combining the elevation-dependent mapping functions and horizontal gradients to model the tropospheric path delays. Spherical Harmonics to describe those deficiencies are tested by solving for the respective coefficients. Tests show that some combinations of Spherical Harmonics yield slightly better results than applying the standard approach of global mapping function plus gradient.

1. Introduction

1.1. Spherical Harmonics

As Spherical Harmonics are solutions of the Laplace equation in spherical coordinates (radius r, polar distance θ and longitude λ)

$$\Delta V(r, \theta, \lambda) = 0 \tag{1}$$

they are widely used for modeling the gravity field of the Earth (Ref. [2], Heiskanen, W.A. and Moritz H.,1967). Additionally, many other applications in geodesy have been found for these special functions, e.g. they are used for mapping the ionosphere or for describing GPS phase center variations. Setting the radius r to unity, the Spherical Harmonics SH_{nm} of degree n and order m on the surface are:

$$SH_{nm}(\theta, \lambda) = P_{nm}(cos(\theta)) \cdot [a_{nm}cos(m\lambda) + b_{nm}sin(m\lambda)] \tag{2}$$

The $P_{nm}(cos(\theta))$ are the so-called Legendre functions of degree n and order m with the polar distance θ being defined from 0 to π. The longitude λ is defined from 0 to 2π and the a_{nm} and b_{nm} are the coefficients of the Spherical Harmonics.

1.2. Tropospheric modeling

In VLBI and GPS global mapping functions are used to map the tropospheric zenith path delays down to the path delays at certain elevations. In principle, all mapping functions $mf(\epsilon)$ are based on continued fraction forms in terms of $1/sin(\epsilon)$ with the elevation angle ϵ:

$$mf(\epsilon) = \frac{1}{sin(\epsilon) + \frac{a}{sin(\epsilon) + \frac{b}{\cdots}}} \tag{3}$$

Additionally, horizontal tropospheric gradients are also applied in standard data analyses to account for azimuthal asymmetries of the tropospheric path delays (Ref. [1], Davis, J.L., Elgered, G., Niell, A.E. and Kuehn, 1993). Therefore combining global mapping functions and horizontal gradients yields eq. (4), which is the standard approach to model tropospheric path delays for observations at elevation ϵ and azimuth α.

$$\Delta L(\epsilon,\alpha) = mf(\epsilon)\cdot L^z + mf(\epsilon)\cdot cot(\epsilon)\cdot[\Sigma_n cos(\alpha) + \Sigma_e sin(\alpha)] \tag{4}$$

The product of the zenith path delay L^z and the mapping function $mf(\epsilon)$ corresponds to the path delay, that is due to the spherically symmetric part of refractivity. The second term of the right hand side of eq. (4) is the so-called gradient term. The $cot(\epsilon)$ factor accounts for the increase in horizontal change of refractivity along the signal path when the elevation decreases. Σ_n and Σ_e are the north and east gradients, respectively, with the units $[mm]$. A gradient of 1 mm corresponds to a path delay of 3 cm at an elevation of 10°.

2. Application of Spherical Harmonics

To be able to model additional deviations from the standard approach that is described in eq. (4), Spherical Harmonics are introduced:

$$\Delta L(\epsilon,\alpha) = mf(\epsilon)\cdot L^z + mf(\epsilon)\cdot cot(\epsilon)\cdot SH_{nm}(z,\alpha) \tag{5}$$

The zenith distance z corresponds to the polar distance θ of eq. (2) and the azimuth α to the longitude λ. Only observations at elevations above the horizon can be used to determine the coefficients of the Spherical Harmonics. The application of the double zenith distance would cover nearly all of the definition area of Spherical Harmonics, e.g. values would range from 0° to 166° when using a 7° cutoff elevation angle.

The cases m = 0,1,2 are dealt with in particular to illustrate the possibilities of the new approach.

2.1. Zonal Legendre functions m = 0

Using zonal (order m = 0) Legendre functions yields the following expression for the tropospheric path delays:

$$\Delta L(\epsilon) = mf(\epsilon)\cdot L^z + mf(\epsilon)\cdot cot(\epsilon)\cdot P_n(z)\cdot a_n \tag{6}$$

There is no azimuthal variation of the path delays with this approach. Solving for the a_n coefficients corresponds to estimation of a supplement to the global mapping functions. In principle, this is similar to estimating a combination of the a, b .. coefficients in eq. (3), in addition to the applied mapping function:

$$\Delta L(\epsilon) = L^z\cdot[mf(\epsilon) + \frac{mf(\epsilon)\cdot cot(\epsilon)\cdot P_{nm}(z,\alpha)\cdot a_n}{L^z}] \tag{7}$$

The term in brackets corresponds to the new local mapping function, because the coefficients are estimated for each station.

2.2. Legendre functions m = 1

Similarly to the standard model for GPS and VLBI (global mapping function plus gradient term), one azimuthal maximum for the tropospheric path delays is estimated, and the north and east gradients in eq. (4) are closely related to a_{n1} and b_{n1}. The only difference to the standard model is that the gradient term is multiplied by Legendre functions of the order m = 1.

$$\Delta L(\epsilon,\alpha) = mf(\epsilon)\cdot L^z + mf(\epsilon)\cdot cot(\epsilon)\cdot P_{n1}(z)\cdot[a_{n1}cos(\alpha) + b_{n1}sin(\alpha)] \tag{8}$$

Figure 1 shows the path delays for the application of different Legendre functions of the order m = 1. To be able to compare them properly, all path delays are fixed at 3 cm path delay for 10° elevation ($z = 80°$), what corresponds to a horizontal gradient of 1 mm. It is shown that some Legendre functions of the order m = 1 are able to absorb longer path delays at higher elevations (P_{21}) whereas other Legendre functions correspond to longer delays at low elevations (P_{31}).

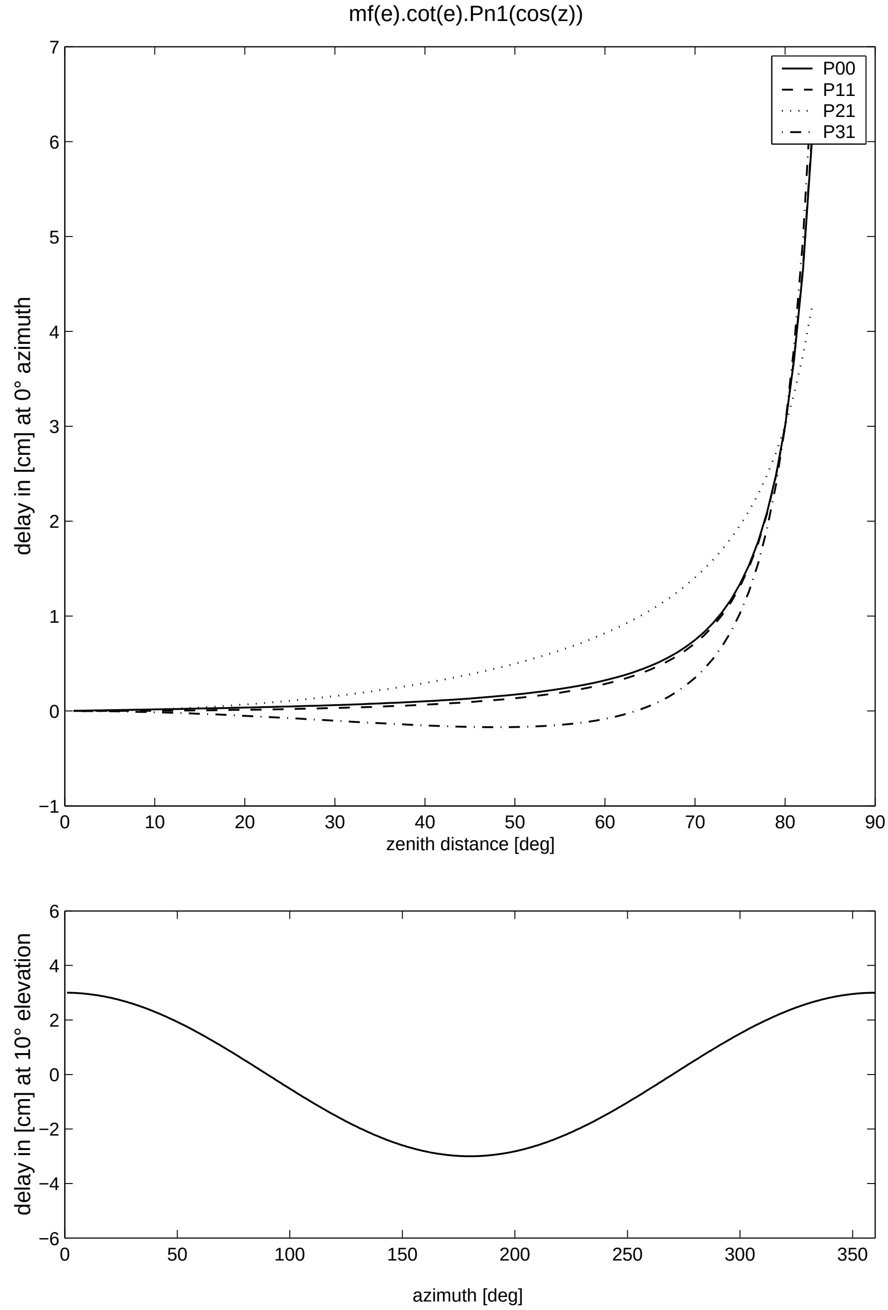

Figure 1. Path delays for Legendre functions of the order m = 1. All path delays are fixed at 3 cm for 10° elevation, what corresponds to a gradient of 1 mm (agrees with P_{00}). The lower plot shows the azimuthal variation for $\Sigma_n = 1mm$ and $\Sigma_e = 0mm$ or $a_n = 1mm$ and $b_e = 0mm$, respectively.

Thus, Legendre functions of the order m = 1 are not only capable of modeling azimuthal asymmetries with one maximum, but they are also able to account for particular deficiencies in the global mapping function.

2.3. Legendre functions m = 2

These functions correspond to two azimuthal maxima of the tropospheric path delays. Additionally, they are able to account for particular deficiences of the mapping functions.

$$\Delta L(\epsilon, \alpha) = mf(\epsilon) \cdot L^z + mf(\epsilon) \cdot cot(\epsilon) \cdot P_{n2}(z) \cdot [a_{n2}cos(2\alpha) + b_{n1}sin(2\alpha)] \quad (9)$$

3. Test of the new approach

So far, only the repeatabilities of VLBI station heights, derived from all NEOS-A experiments in 1999 and 2000, were determined to test the new models. A modified version of the OCCAM 5.0 software package (Ref. [4], Titov, O., Tesmer V. and Boehm J., 2001) was applied for the VLBI analyses. As far as the standard tropospheric modeling was concerned, the Niell mapping functions (Ref. [3], Niell, A.E., 1996) were used, and piecewise linear functions were estimated for the wet zenith path delays (2 hours time intervals, 15 mm/sqrt(hour) constraints).
In addition to the Spherical Harmonics themselves, the following properties of gradients and Spherical Harmonics were varied to check their impact on station height repeatabilities:

- time interval: 12 and 6 hours
- elevation cutoff angles: 7° and 5°
- constraints: 0.1, 0.3, 0.5, and 0.7 mm

As far as the Spherical Harmonics were concerned, 13 different combinations were tested (table 1). Legendre functions of the order m = 2 were discarded in advance, because preliminary tests showed that they did not yield better results in terms of VLBI station height repeatabilites.

Table 1. Repeatabilities of station heights in [cm] from NEOS-A (1999-2000) for different solutions

(1) station (no. of sessions)	(2) no gradients no SH	(3) best gradient solution (cutoff/time/constr.)	(4) best SH solution (cutoff/time/constr.)	(5) improvement from (3) to (4) in %
Fortaleza (97)	2.006	1.892 (7/06/0.3)	1.890 SH[00+11] @ (7/06/0.3)	0.1
Kokee Park (102)	1.546	1.362 (7/06/0.7)	1.303 SH[00+31] @ (7/06/0.5)	4.5
Wettzell (101)	1.236	1.190 (5/12/0.5)	1.155 SH[00+11] @ (5/12/0.3)	3.0
Gilcreek (50)	0.997	0.827 (7/06/0.5)	0.795 SH[00+31] @ (7/06/0.7)	4.0
Algopark (41)	1.421	1.294 (7/06/0.1)	1.212 SH[00+10] @ (7/06/0.7)	6.8
Ny-Alesund (49)	1.749	1.408 (7/12/0.1)	1.399 SH[31] @ (7/12/0.1)	0.6

At first, station height repeatabilities were determined for all stations that were taking part in at least 40 NEOS-A sessions in 1999 and 2000. Neither gradients nor Spherical Harmonics were applied. These values are shown in the second column of table 1.
The third column shows the best repeatabilities that could be achieved by applying gradients and varying the parameters described above. For most stations the best results were obtained using a 7° cutoff elevation angle and a 12 hours time interval for the piecewise linear functions for the wet zenith path delay. The station height repeatabilities improved on the average by about 2 mm when applying gradients.

The fourth column shows the best repeatabilities for the solutions with Spherical Harmonics. Similarly to the gradient approach, the best result were achieved with a 7° cutoff elevation angle and a 12 hours time interval. Out of the 13 combinations of Spherical Harmonics, the estimation of coefficients for the Spherical Harmonics [P_{00} plus P_{11}] or [P_{00} plus P_{31}] yielded the best repeatabilities. These solutions correspond to estimating a supplement to the global mapping function and an azimuthal asymmetry with one maximum. Only for the station Algopark, the best results were achieved by using the zonal Legendre functions [P_{00} plus P_{10}]. There, the repeatability was improved by almost 1 mm. In the fifth column the improvement from the best gradient solution to the best SH solution is given in %. It can be seen that for the stations treated in the tests the SH solutions yielded slightly better results in terms of height repeatability.

Additional investigations showed that there were no significant shifts of the mean of the station heights when applying the Spherical Harmonic models.

Table 2 shows the differences of the repeatabilities derived by the Spherical Harmonic models from the standard model (horizontal gradients, second column in table 1). The first column specifies the combination of Spherical Harmonics and the last column simply shows the mean value of each row. If this value is positive, the respective SH combination generally yielded better results than the gradient approach (as far as station height repeatability is concerned). [P_{00} + P_{11}], [P_{00} + P_{21}] and [P_{00} + P_{31}] are those combinations that yielded better repeatabilities. As mentioned before, additional tests showed that the application of Spherical Harmonic models as mapping functions did not cause shifts of the mean station heights.

Table 2. Differences of station height repeatabilities the SH solutions and the best gradient solution in [mm]; positive values correspond to improved results

	Fortaleza	Kokee Park	Wettzell	Gilcreek	Algopark	Ny-Alesund	mean per row
SH 00	-0,88	-0,77	0,12	-0,45	0,74	-0,14	-0,23
SH 10	-1,10	-1,75	-0,34	-1,69	0,41	-0,11	-0,76
SH 11	-0,13	0,00	-0,07	0,03	-0,03	-0,03	-0,04
SH 20	-0,81	-0,77	0,05	-0,61	0,46	-0,14	-0,30
SH 21	-0,51	-0,85	-0,29	-0,25	0,08	-0,10	-0,32
SH 30	-1,13	-1,60	-0,34	-1,69	0,42	-0,07	-0,74
SH 31	-0,66	0,21	-0,08	0,04	0,04	0,09	-0,06
SH 00 11	0,02	0,51	0,35	0,32	0,23	-0,09	0,22
SH 00 21	-0,23	-0,08	0,23	0,26	0,37	-0,14	0,07
SH 00 31	-0,42	0,59	0,00	0,32	0,09	0,05	0,10
SH 00 10	-0,85	-0,75	0,13	-0,42	0,82	-0,14	-0,20
SH 00 10 20	-0,90	-0,73	0,14	-0,55	0,69	-0,16	-0,25
SH 00 10 20 30	-0,86	-0,73	0,14	-0,53	0,73	-0,15	-0,24

4. Conclusion and outlook

In the tests done so far, there was only a very small improvement of the station height repeatabilities when using Spherical Harmonics to model the tropospheric path delays. Anyway, considering these first results, it seems reasonable to apply station-dependent combinations of Spherical Harmoncis to account for site-specific variations of the path delays.

Future work should deal with the determination of coefficients of the Spherical Harmonics from numerical weather models in order to obtain a model that is based on real tropospheric properties. Otherwise the Spherical Harmonics are likely to absorb other effects that are not related to tropospheric path delays.

References

[1] Davis, J.L., Elgered, G., Niell, A.E. and Kuehn, C.E., Ground-based measurements of gradients in the "wet" radio refractivity of air, Radio Science, 28 (6), pp. 1003-1018, 1993.

[2] Heiskanen, W.A. and Moritz H., Physical Geodesy, W.H. Freeman and Company San Francisco, 1967.

[3] Niell, A.E., Global Mapping Functions for the Atmospheric Delay at Radio Wavelengths, J. Geophys. Res., 101 (B2), pp. 3227-3246, 1996.

[4] Titov, O., Tesmer V. and Boehm J., OCCAM Version 5.0 software. User Guide, AUSLIG Technical Reports 7, AUSLIG, Canberra, 2001.

María J. Rioja et al.: External tropospheric calibration for VLBI observations, Proceedings of the 15th Working Meeting on European VLBI for Geodesy and Astrometry, p.149–153
http://www.ieec.fcr.es/hosted/15wmevga/proceedings/rioja

External tropospheric calibration for VLBI observations

María J. Rioja [1], *Paolo Tomasi* [2]

[1] *Observatorio Astronómico Nacional*

[2] *Istituto di Radioastronomia*

Contact author: María J. Rioja, e-mail: `rioja@oan.es`

Abstract

We are investigating the potential of new routes of analysis, in particular combining products from different geodetic techniques, to improve the accuracy of VLBI geodetic estimates. We present comparative results from the standard route of analysis of VLBI data and a novel route which implements external GPS tropospheric estimates, with the CALC/SOLVE software package. We have performed repeatability tests on the estimates of both routes of analysis with very interesting results. A satisfactory interpretation of the observed improvement of the performance of the network with the novel route in terms of precision or accuracy is at present a main concern.

1. Introduction

The geodetic VLBI observations with a network of antennas at the Earth are affected by the propagation medium, mainly the ionosphere and the troposphere. The ionospheric contribution is exactly calibrated with simultaneous observations at 8.4 and 2.3 GHz. However, given the close functional dependence of the tropospheric and geometric contributions in the mathematical formulation of the group delay, unknown variations in the distribution of the water vapor content in the troposphere (usually called "wet component") corrupt the least squares adjustment of the vertical component of the site position. Nowadays, uncertainties in the tropospheric modelling are one of the main error sources in the geodetic measurements with VLBI.

The observational strategy implemented in VLBI observations to sample the atmosphere consists of a rapid switching of the antennas to cover the whole sky, including radio sources at low elevation angles. Instead, a GPS antenna collects the radio signals from simultaneous observations of a number of satellites at different directions, a favourable configuration to estimate unknown spatial and temporal irregularities of the wet component in the troposphere. For sites with both GPS and VLBI techniques, one could use the GPS tropospheric estimates in the analysis of VLBI observations. Previous attempts to combine products of this two different geodetic techniques have been carried out by other authors too with no conclusive results (Ref. [1]).

2. Analysis of the data and results

A detailed description of the data analysis path and tools used for comparison of results from different analysis strategies can be found elsewhere (Ref. [1]; Ref. [2]). Briefly, our working database consists of:

- The six 24-hours long Europe campaigns of VLBI observations in 1998, separated by about 2 months.
- Simultaneous GPS tropospheric estimates from the analysis of IGS data from Berna University (Markus Rothacher, priv. comm.), for stations with VLBI and GPS techniques, whenever available.

Table 1 lists the participating antennas, indicating the availability of GPS tropospheric estimates, for each epoch of VLBI observations.

Name/Date	Ny–Ålesund	Onsala	Wettzell	Tigo	Medicina	Crimea	Madrid	Matera	Noto
EUROP41 (Feb'98)	NO	YES	YES	YES	NO	NO	NO	YES	YES
EUROP42 (Apr'98)	YES	YES			NO	NO		YES	YES
EUROP43 (Jun'98)	YES	YES	YES	YES		NO		YES	YES
EUROP44 (Aug'98)	YES	YES	YES	YES	NO	NO		YES	
EUROP45 (Oct'98)	YES	YES	YES		NO	NO	NO	YES	NO
EUROP46 (Dec'98)	YES		YES	YES	NO	NO	NO	YES	YES

Table 1: Description of our working database: Epoch of observations, participating antennas and availability of GPS tropospheric estimates for each of the six Europe campaigns of VLBI observations in 1998. At each epoch, the entries YES or NO refer to the availability of GPS tropospheric data for the station. A blank entry in the table indicates that this station did not participate in the VLBI observations at that epoch.

The VLBI observations were processed with the least squares estimation program SOLVE, and using two different approaches to calibrate the wet zenith path delay contribution to the observables: 1) in the so called *standard route* (SR) the wet zenith path delays at all sites were estimated from the data themselves, using continuous piecewise linear functions in segments of 60 minutes; 2) in the novel route, *hybrid route* (HR) from now on, we fed external GPS tropospheric estimates from simultaneous observations, wherever available, into the VLBI analysis without any further adjustment.

We have computed the baseline length repeatabilities from the analysis of the 6 epochs of observations in 1998 and used them to quantify the errors in the baseline length estimates, for both the *standard route* and the *hybrid route*. Figure 1 displays the baseline length *wrms* (i.e. baseline length repeatabilities) as a function of baseline length, along with the best fit of a straight line. The comparison of the slopes of the best linear fits in Figure 1, corresponding to the *standard* and the *hybrid* routes (0.58ppb and 0.34ppb, respectively) indicates an improvement in the overall performance of the VLBI solution using the *hybrid* route.

Figure 2 displays the difference between the baseline length repeatability values in Figure 1, computed for the *hybrid* and *standard* routes, as a function of baseline length. This offers an equivalent tool to compare the results from the two routes of analysis. In each plot the solid line is the best linear fit, whose slope is proportional to the relative impact of elevation dependent errors in both routes of analysis. The upper plot in Figure 2 displays only the values for baselines with GPS tropospheric entries in both ends; instead, the lower plot includes all the baselines.

The agreement between the tropospheric estimates from VLBI and GPS is good, however there is a mean bias of the order of some millimeters which is always present. This bias is site/epoch dependent, i.e. varies from one station to another and from epoch to epoch. Such a difference propagates into changes in the estimated values for the station coordinates in the HR and SR analysis; the U,N, and E components of the individual station coordinates are affected in decreasing order. This is likely to be related to the dominant distribution of the network along the North-South direction.

Figure 3 displays differences between geometric estimates (ΔU, ΔE, ΔN) in the HR and SR analysis versus mean bias between GPS and VLBI tropospheric estimates (Δz), for 4 stations and at multiple epochs. The stations selected for this representation are: Ny–Ålesund, Onsala, Matera and Noto, with symbols "a", "x", "b" and "t", respectively, in the plots in Figure 3.

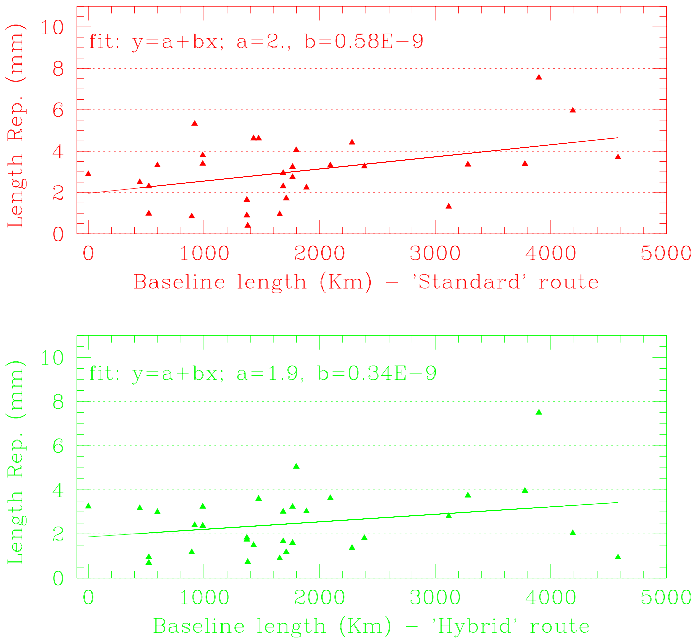

Figure 1. Baseline Length repeatabilities vs. baseline length, corresponding to estimates from *standard* (*Upper plot*) and *hybrid* (*Lower plot*) routes of analysis (see text). In each plot, the solid line is the best linear fit; the slope is proportional to the magnitude of elevation dependent errors present in the analysis.

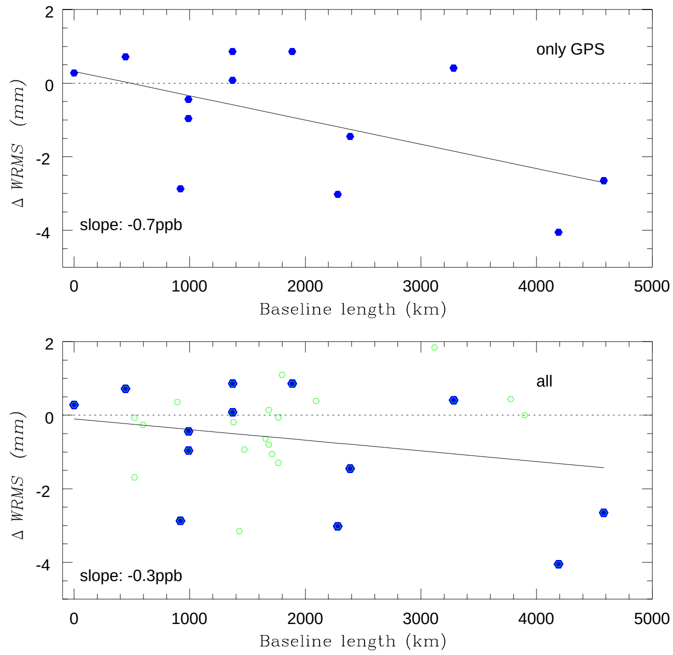

Figure 2. Differenced Baseline Length repeatabilities vs. baseline length, corresponding to estimates from *hybrid* minus *standard* routes of analysis (see text), for baselines with GPS entries on both ends (*Upper plot*) and for all baselines (*Lower plot*). The solid line is the best linear fit; the slope is proportional to the relative magnitude of elevation dependent errors present in the analysis.

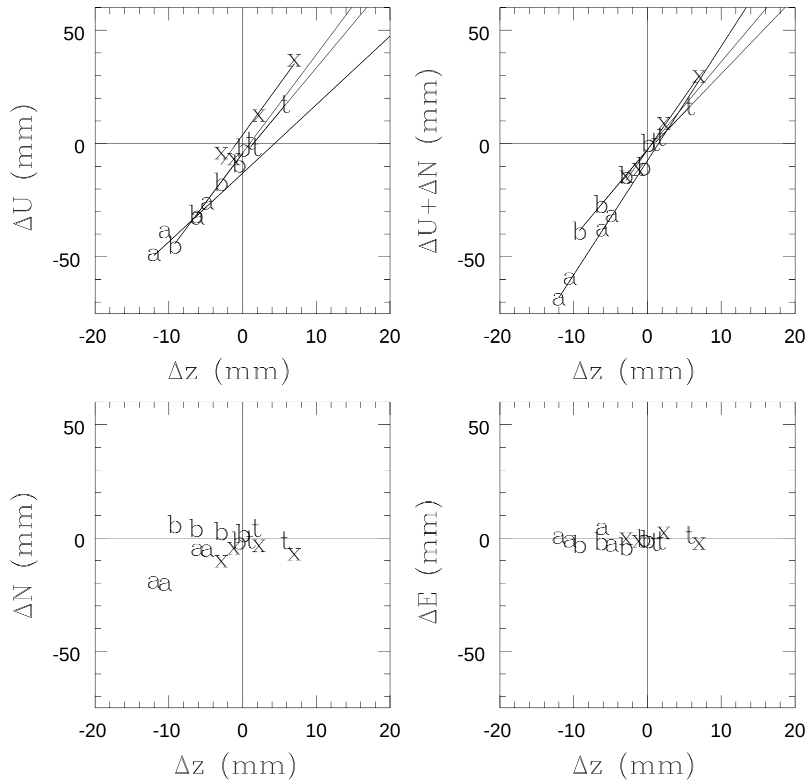

Figure 3. Representation of differences between estimates of U, N and E components of 4 stations in the HR and SR analysis versus the mean bias between GPS and VLBI tropospheric estimates for each station, at multiple epochs. The stations are Ny Alesund ("a"), Onsala ("x"), Matera ("b") and Noto ("t"). The solid lines in the plots correspond to best linear fits; the best correlation corresponds to the plot with the sum of changes in the N and U components, versus mean bias of GPS and VLBI tropospheric estimates.

For the 4 stations, the differences are largest for the U components, and follow a close linear dependence with the mean bias between GPS and VLBI tropospheric estimates at each epoch and at each station. The differences between the N components are smaller, only noticeable for far away stations. There is no significant difference between the estimates for E components for any of the 4 stations in the HR and SR analysis. The solid lines in the plots in Figure 3 correspond to best linear fits; in all 4 stations, the best correlation corresponds to the representation of the sum of changes in the N and U components ($\Delta U + \Delta N$) versus the mean bias between GPS and VLBI tropospheric estimates, at each epoch.

3. Conclusions

The working report presented in this contribution corresponds to the analysis of 6 epochs of VLBI observations spanned over 1-year with the CALC/SOLVE software package. We have performed parallel identical analysis, except for the implementation of the tropospheric calibration. The so-called *standard* route (SR) uses an auto-calibration algorithm and derives the tropospheric contribution to the VLBI observables from the data themselves; instead, the *hybrid* route (HR) feeds external simultaneous GPS tropospheric estimates in the VLBI analysis, whenever available, without further adjustment. The number of participating stations at each of the six epochs in our working database is in the range from 6 to 9, and in all cases at least half of them had external GPS tropospheric calibration in the HR analysis. We have calculated the baseline length repeatability values from the individual analysis of each epoch of observations, for both routes of analysis. A representation of the baseline length repeatabilities versus the baseline length has been used for a comparative study of the presence of elevation dependent errors in the HR and SR analysis. According to that, the results from our analysis are very encouraging for the potential of this new route of analysis, and support a better performance of the VLBI network in the HR. An interpretation of the results is still in progress: the issue of whether the observed improvement in the baseline length repeatabilities in the HR corresponds to a real improvement of the accuracy of the geometric estimates with VLBI is an open question.

References

[1] Carlsson, T.R., Elgered, G. & Johansson, J.M. 1995 Proc. 10th Working Meeting on European VLBI for Geodesy and Astrometry, p. 148

[2] Rioja, M.J., Tomasi, P., Sarti, P. & Pérez-Torres, M.A. 2000 Proc. 14th Working Meeting on European VLBI for Geodesy and Astrometry, p. 23

Alexander A. Stotskii and Irina M. Stotskaya: Structure Analysis of Wet Path Delays in IRIS-S Experiments,
Proceedings of the 15th Working Meeting on European VLBI for Geodesy and Astrometry, p.154–158
http://www.ieec.fcr.es/hosted/15wmevga/proceedings/stotskii

Structure Analysis of Wet Path Delays in IRIS-S Experiments

Alexander A. Stotskii, Irina M. Stotskaya

Institute of Applied Astronomy, Russian Academy of Sciences
Contact author: Alexander A. Stotskii, e-mail: stotskii@ipa.rssi.ru

Abstract

The stochastic properties of wet path delay values obtained at once in processing the data of VLBI observations in IRIS-S experiments were analyzed.

On the base of the Bonn VLBI group solutions for these observations the temporal structure functions of wet path delay were constructed. They appeared close to power functions with the slopes substantially different from the slopes of the structure functions following from direct measurements of path delays with WVR, radiosonds and interferometers and from the theory ("power law of 2/3").

The most probable cause of noted difference is using in processing the algorithm (LSQ with linear spline of the troposphere delays) that corresponds the stochastic model not adequate the real troposphere fluctuations. Therefore the found values of the path delay for every station in each particular time moment to a high degree represent the property of this model but not real values of the path delay.

For improving the accuracy of calculation the troposphere corrections it should be used not formal approximations and mathematics models but the adequate model of fluctuations corresponding the physical properties of the atmosphere.

1. Introduction

Path delay fluctuations in the Earth atmosphere, particularly troposphere wet delay fluctuations, are the principal natural source of errors that limits the accuracy of VLBI measurements.

There are three ways to determine the wet troposphere delay.

The first way is calculation based on the ground level meteorological data during the observations. For the wet delays this method is not enough accurate.

The second way is to measure wet delay using any independent from VLBI special method such as the Water Vapor Radiometry (WVR) or another one and to use the obtained data for correction the data of VLBI observations.

The third one is to obtain troposphere delay values at once in processing the data of VLBI observations and to get the solution with accounting of troposphere correction.

The last method seems very convenient and is usually used, as it does not require any additional equipment and measurements. The problem is that the value of troposphere delay is the random process. So for get the solution it is necessary to use the additional information or a stochastic model of troposphere path delay fluctuations.

In this paper we compare the statistical characteristics of wet troposphere path delay obtained at once in processing IRIS-S VLBI experiment and the characteristics of wet delays obtained in independent measurements and from the theory.

2. Database

We analyzed the wet path delays obtained by the Bonn VLBI group in solutions of IRIS-S experiments performed in 1999-2000 years (IRIS-S 135-146) [1]. There are twelve 24-hourly sessions carried out at different months. So the data was distributed equally in daytime and seasons.

Table 1. Stations participated in IRIS-S 135-146 experiments

Station	Location	Sessions
Fortleza	South America	135-146
Gilcreek	Alaska	135-146
HartRAO	South Africa	135-146
Westford	North America	135-146
Wettzell	Europe	135-146
Hobart	Australia	144
O'Higgins	Antarctic	144

Table 2. Parameters of structure functions in IRIS-S solutions and the Turbulent Model

Station	Power low slope μ	Structure coefficient C (cm.hr$^{-\mu/2}$)
Fortleza	0.95	0.91
Gilcreek	1.05	0.60
HartRAO	1.06	0.78
Westford	1.4	1.17
Wettzell	1.1	0.74
Average for all stations	1.2	0.86
Turbulent Model	0.67	1.23

The observations were made at 5 stations located in different climate zones. In the IRIS-S 144 session two more stations were added (Table 1).

Thus the database represents the path delays for different weather and climate conditions.

As a result of solutions the Bonn VLBI group gave values of zenith wet path delays for the each station with 1-hour interval. The set of these values is the source data for our analysis.

3. Structure Functions

As a statistical characteristic of path delays we used the temporal structure function.

$$D(\tau) = < [l(t+\tau) - l(t)]^2 >$$

where l is the path delay, t is the time, τ is the time interval and $<>$ denotes the expectancy value.

Based on path delay data the structure functions for every session for all stations were constructed (Fig. 1). One can see that there is no any regular dependence on season or station location.

The structure functions for five stations averaging on all sessions during a year are shown in Fig. 2. These structure functions close to power functions

$$D(\tau) = C^2 \tau^{\mu}$$

Parameters of these functions, slopes μ and structure coefficients C (defined from the small interval region of the functions where statistic is more reach), are presented in Table 2.

The average structure function for all stations was also calculated. It has a power law slope of 1.2. This value as well as the slope values for separate stations is substantially more than slope values obtained in direct measurements of troposphere path delay. The numerous observations with WVR, radiosondes and interferometers [2-6 and others] give the values of power law slope for this time interval close to 2/3 that follows from the theory of turbulence [7-9]. The average structure function of the IRIS-S solutions and the Turbulent Model of path delay [8] together with the examples of structure functions constructed on the data of WVR [3] and radiosondes [5] observations are shown in Fig. 3.

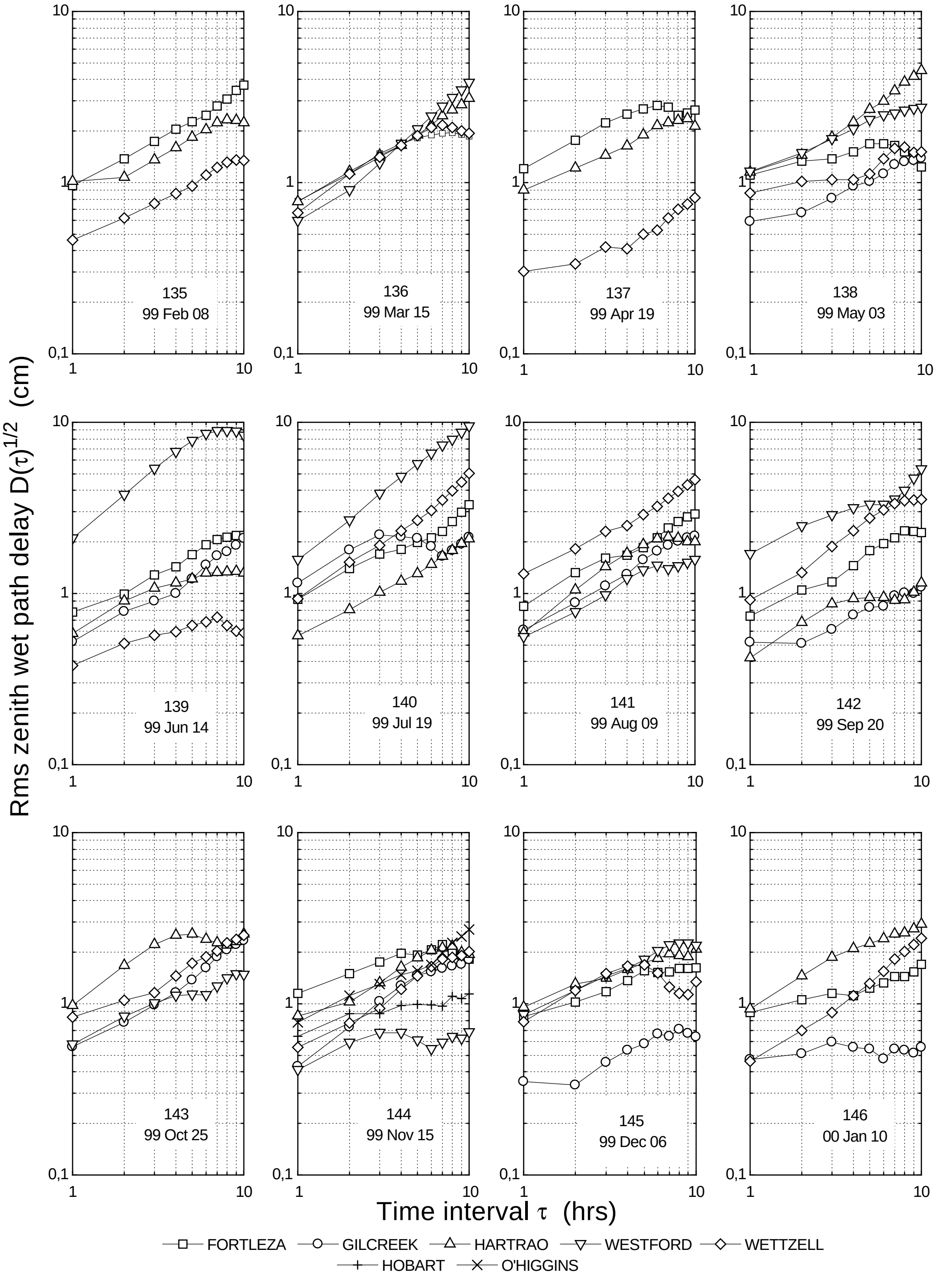

Figure 1. Zenith wet path delay structure functions from IRIS-S experiments

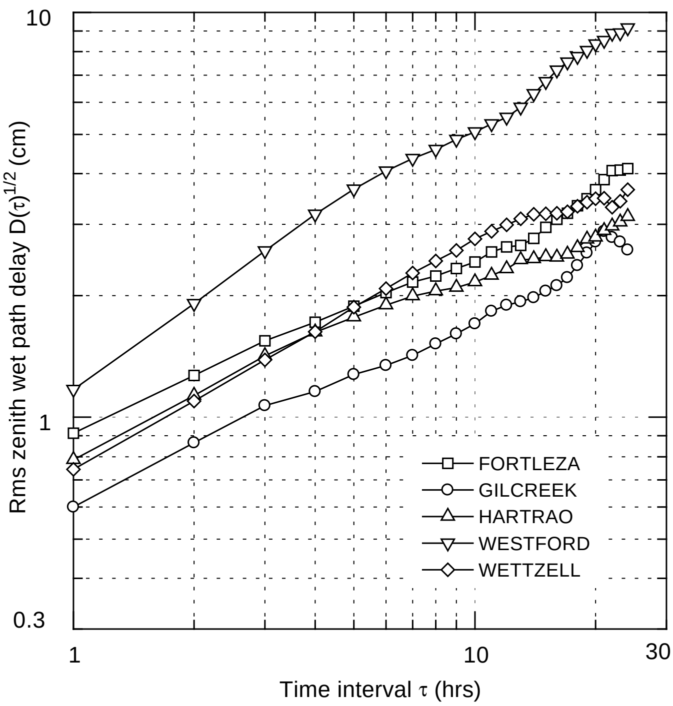

Figure 2. Average zenith wet path delay structure functions for five stations in IRIS-S experiments

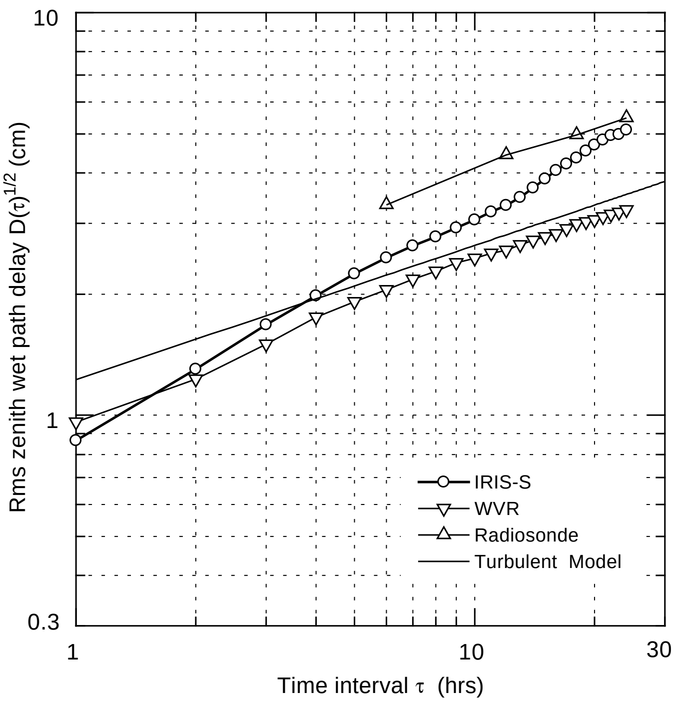

Figure 3. Temporal structute functions of zenith wet path delay obtained in different experiments and the Turbulent Model

4. Discussion and Conclusions

The found difference in the power law slope for the structure functions obtained in IRIS-S solutions and for special measurements of wet path delay may be explained by the character of the used processing algorithm.

The IRIS-S processing based on a least square analysis with modeling the atmosphere path delays by a linear spline with some constrains. In this algorithm the troposphere properties are represented by the stochastic model not adequate the real stochastic structure of troposphere path delay fluctuations. Therefore the found values of the path delay for every station in each particular time moment to a high degree present the property of this model but not real values of path delays.

The results of carried out comparison show that when processing the VLBI experiments it is necessary to use not formal mathematics methods for exclude the troposphere errors but the methods based on more adequate stochastic model that represents the real physical properties of the troposphere. This can allow to achive improving the accuracy of defining the corrections for the troposphere.

References

[1] Geodetic VLBI experiment IRIS-S: http//giub.geod.uni-bonn.de/vlbi/experiments/experiments html.

[2] Hogg D.C., F.O.Guiraud, and W.B.Sweezy. The Short-Term Temporal Spectrum of Precipitable Water Vapor. Science, **213**, 1112-113, 1981.

[3] G.Elgered et al. Data of WVR measurements in OSO, Onsala, April 1994.

[4] Stotskii A.A., K.G. Elgered, and I.M. Stotskaya. Structere Analysis of Path Delay Variations in the Neutral Atmosphere. Astr. and Astroph. Trans., **17**, 59-68, 1998.

[5] Stotskii A.A. and I.M. Stotskaya. Search of Correlation between Wet and Dry Components of Path Delay in the Troposphere. Commun. Inst. of Appl. Astron., 56, St.Petersburg, 1993.

[6] Sramec R.A. Atmospheric Phase Stabiliity at the VLA. In: J.E.Baldwin and Wang Shougan (Eds.): Proc. of URSI/IAU Symp. on Radio Astronomical Seeing, Beijing 15-19 May, 21-30, 1989.

[7] Stotskii A.A. On Fluctuation Characteristics of the Earth Troposphere. Izvestia VUZ (Radiofizika), **16**, 5, 806-809, 1973.

[8] Stotskii A.A. Path Length Fluctuations through the Earth Troposphere: Turbulent Model and Data of Observations. In: J.C. De Munk and T.H.Th. Spoelstra (Eds.): Proc. of the Symp. on Refraction of Transatmospheric Signals in Geodesy. The Hague, The Netherlands, 19-22 May, 179-182, 1992.

[9] Treuhaft R.N., and G.E. Lannyi. The Effect of the Dynamic Wet Troposphere in Radio Interferometric Measurements. Radio Science, **22**, 2, 251-265, 1987.

Session 4

Local Surveys

Luca Vittuari et al.: 2001 GPS and Classical Survey at Medicina Observatory: Local Tie and VLBI Antenna's Reference Point Determination, Proceedings of the 15th Working Meeting on European VLBI for Geodesy and Astrometry, p.161–167
http://www.ieec.fcr.es/hosted/15wmevga/proceedings/vittuari

2001 GPS and Classical Survey at Medicina Observatory: Local Tie and VLBI Antenna's Reference Point Determination

Luca Vittuari [1], *Pierguido Sarti* [2], *Paolo Tomasi* [3]

[1] *University of Bologna DISTART - Topografia e Geodesia*
[2] *Consiglio Nazionale delle Ricerche, Istituto di Tecnologia Informatica Spaziale*
[3] *Consiglio Nazionale delle Ricerche, Istituto di Radioastronomia*

Contact author: Pierguido Sarti, e-mail: `pierguido.sarti@itis.mt.cnr.it`

Abstract

During a 6 days campaign in June 2001, we have performed a local survey at Medicina Observatory using classical geodesy and GPS techniques in order to determine the effects of an undergone track repair. We have determined the position of the reference point **P** within a local and ITRF2000 (epoch 1997.0) reference frames using trilateration and triangulation:

$$\mathbf{P}clas^{2001}_{loc} = (21.580 \pm 0.001, 45.536 \pm 0.001, 17.699 \pm 0.001)$$

$$\mathbf{P}clas^{1997.0}_{ITRF2000} = (4461369.982 \pm 0.001, 919596.818 \pm 0.001, 4449559.207 \pm 0.001)$$

Kinematic GPS has also given interesting results:

$$\mathbf{P}GPS^{2001}_{loc} = (21.575 \pm 0.005, 45.536 \pm 0.003, 17.713 \pm 0.012)$$

$$\mathbf{P}GPS^{1997.0}_{ITRF2000} = (4461369.988 \pm 0.005, 919596.819 \pm 0.003, 4449559.220 \pm 0.013)$$

In order to roto-translate the estimated coordinates from the local frame to ITRF2000, thus having the possibility to compare results of both measurement approaches, we have computed a 4+1 parametres transformation (see section 5) using a triangol surveyed with both methods. Comparing results given above with the values obtained making use of the position and velocities given by IERS for Medicina in ITRF2000 the agreement is striking especially for the classical technique.

A complete tie between the 3-D forced centered local ground control network (materialised in May 2000) and the widely used older network (which is now experiencing some problems due to the disgregation of the concrete where bolts are situated) has also been realised. This will allow inter-comparison of results obtained by the different campaigns that have been carried out in the last decade. Finally, the position of the ASI-GPS permanent station has been estimated within the local ground control network. Thus, using classical methodology, a precise determination of the VLBI-GPS ex-centre vector has been possible.

1. Introduction

Monitoring the stability of the VLBI antenna reference point within a local ground control network is, nowadays, an important task that must be regularly scheduled. Major intervention (e.g.: track substitution, concrete repair) force observatories to organise *ad hoc* campaigns for detecting movements that might be originated by these maintainance operations. In July 2000 the track of the VLBI antenna has been removed in order to rebuild the concrete underneath its slots. The position of the VLBI reference point has been monitored before (Ref. [4]) and after the intervention using two different approaches: the first and more precise is based on a classical geodesy survey while the second on Kinematic GPS.

2. GPS survey

2.1. KGPS measurements

On 20 June 2001, a KGPS survey has been performed using a total of six GPS antennae and receivers: three Trimble 4000SSE on pillars P1, P3 and G7 (see figure 1) of the ground control

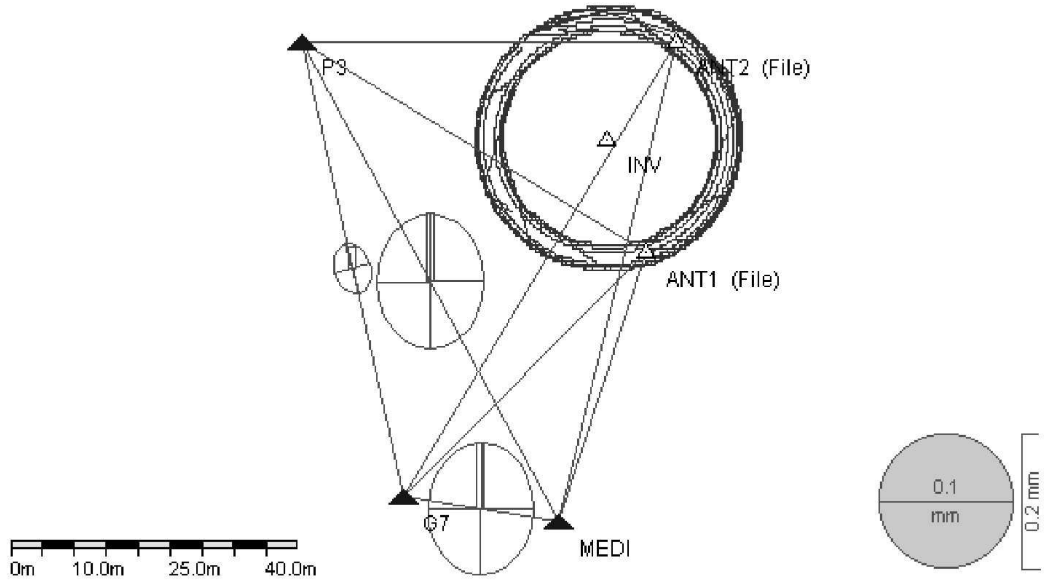

Figure 1. GPS ground control network and roving antennae.

network, two roving Trimble 4000SSI on the VLBI antenna and the ASI-GPS permanent station (MEDI).

Receiver on pillar P1 has experienced a major hardware failure that has caused a complete loss of data, thus reducing to three the control points of the ground network. Roving GPS antennae have been placed on the VLBI dish using a L-shaped device (see figure 2) that keeps the GPS antenna horizontal and the phase centre fixed with respect to the structure of the dish itself while VLBI antenna moves. On the base of the experience done in May 2000 (Ref. [4]), when a first KGPS survey of the antenna has been performed, we have optimised the surveying methodology writing a schedule that has controlled VLBI antenna movements during KGPS acquisition.

Starting from 5 deg elevation and 275 deg azimuth in ccw sector, the antenna has moved in azimuth describing circles of 530 deg at eight fixed elevations in steps of 15 deg. In a similar manner, each GPS antenna has moved in elevation describing arcs of circle of 110 deg at 17 different azimuth positions of the VLBI antenna. Data have been acquired every second for more then three hours.

2.2. GPS data analysis

Positions of ground control pillars have been determined using a static approach and processing with *GeoGenius 2000* a three hours dataset of observations with 1 second sampling rate. Table 1 shows positions and formal errors obtained for pillars G7, P3 and MED using L1 frequency and precise IGS ephemerides. KGPS survey resulted in a huge amount of data that have been analyzed using different software and different methodologies. Each fixed antenna on the ground pillars could determine roving antennae's positions thus producing a large set of results that have been post-processed with the approach described in section 4. In particular, we have used *GeoGenius 2000* and *Geotracer V.2.29* software packages using L1 and L1&L2, precise and broadcast ephemerides and fixing ambiguites OTF in order to validate the results by cross-checking positions obtained from different reference antennae and with different processing approaches. For a few azimuth circles, coordinates transformed (using parameters shown in table 3) into the local reference frame

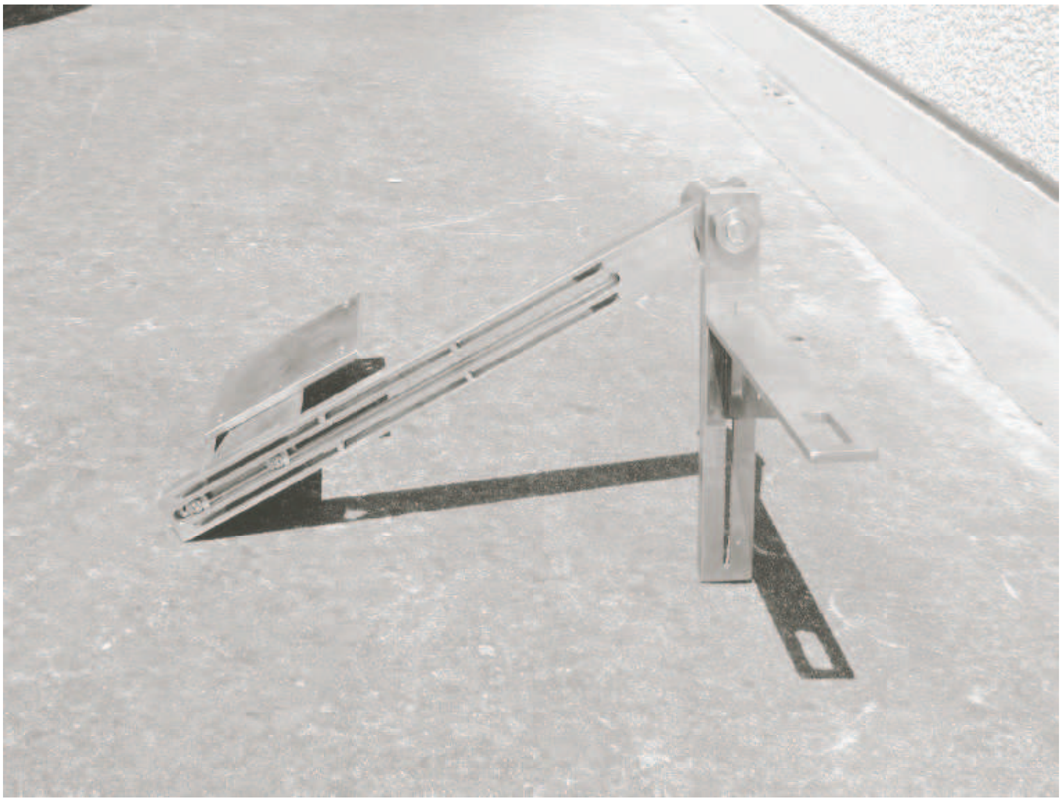

Figure 2. Device used for roving GPS antennae mounting on VLBI antenna dish.

have shown evidently wrong values of the height component. This is most probably related with a failure of the OTF procedure in fixing the ambiguites and thus resulting in precise but not accurate estimates of the roving antenna positions. Those circles showing remarkable height differences from the expected value have therefore been eliminated and their positions have not been used for the 3-D least squares approach estimate of the VLBI reference point (see section 4).

Point ID	X (m)	Y (m)	Z (m)
G7	4461402.1354 ± 0.0005	919568.8217 ± 0.0002	4449507.6618 ± 0.0005
MED	4461400.8110	919593.5120	4449504.7200
P3	4461356.9649 ± 0.0005	919545.7506 ± 0.0002	4449560.2637 ± 0.0005

Table 1. Positions of the pillars of the ground control network. Results expressed in ITRF2000, epoch 20 June 2001. MEDI (ASI-GPS) has been fixed to the values obtained applying the ITRF2000 velocities to the corresponding coordinates at reference epoch.

Roving antennae positions have also been selected using a more stringent criteria, often used in aerial photogrammetry. The mean reciprocal distance of the two different roving antenna (see figure 3) has been used as filter for rejecting those couples of positions (calculated from different reference pillars at the same epoch) that determined distances showing absolute differences from the mean value higher then 5 cm.

This has considerably decreased the number of points available for the post-processing, thus creating a smaller dataset that has also been analysed but has given less satisfactory results. Results presented in section 4 are based on the complete set of positions determined with KGPS except for those that have been wrongly estimated because of OTF failures.

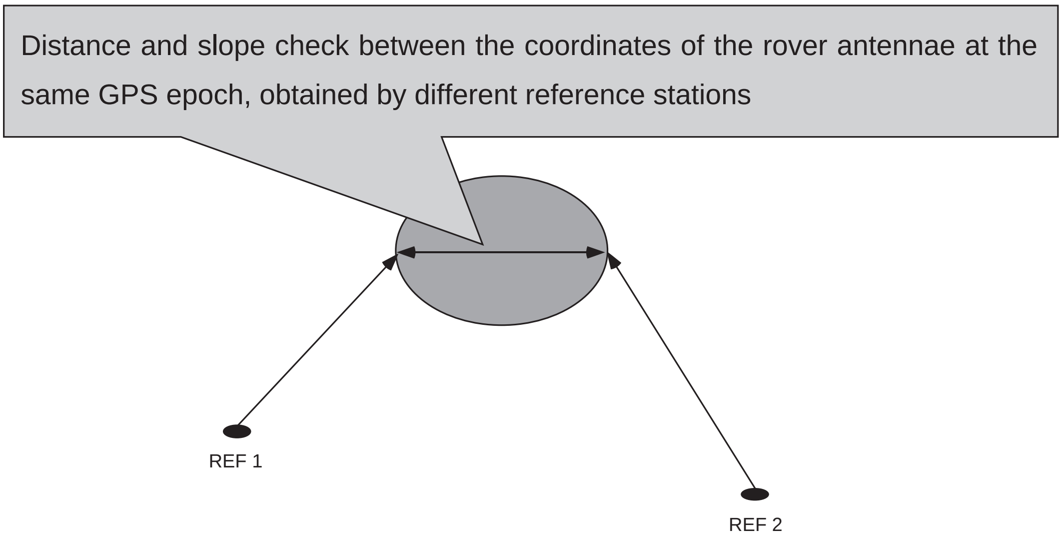

Figure 3. Outlier rejection procedure on roving antenna positions.

3. Classical survey

3.1. Terrestrial measurements

Classical geodesy data have been acquired during a 4 days campaign using two Leica total stations (a TC2003 and a TDA5005) and high precision tribrachs for standing on the new 3-D forced centre markers of the ground pillars. The old markers on the pillars have also been surveyed. A complete tie between the old, widely used ground network (Ref. [1], [2], [3]) and the new 3-D ground control network has been realized within the same adjustment procedure.
Eight points on the VLBI antenna have been materialized using retro-reflecting prisms and the network has been extended in the north and east directions using daily positioned tripods. VLBI antenna has been moved in 6 different azimuth positions at fixed elevation and 7 stepwise rotations of 15 deg at a fixed azimuth position. For each position all visible prisms on the antenna have been measured from the ground network (see figure 4). MEDI (GPS-ASI antenna point) is not shown in figure 4 because it has been surveyed and estimated separately within a smaller network.

More then 2000 collimations have been performed for completing the 3 strata planned for measuring the network.

3.2. Terrestrial data analysis

We have used triangulation and trilateration ending up with 838 indipendent observations of angles and distances that have been used in STAR*NET Starplus software Inc. least squares adjustment programme for solving the network. Height origin has been fixed in G7, a forced centering GPS benchmark placed on the laser pad, the planimetric origin in P3 and a fixed bearing from pillar P3 to P1. Adjustment has produced station coordinates error ellipses with axes equal or less then 1 mm on the 95% confidence level.

4. Post-Processing

Post-processing procedure is based on two f77 programmes that use a 3-D analitical geometry least squares approach for determining the best fit surfaces that, intersecting, uniquely define the reference point. This approach developes and refines the post-processing procedure that has already been successfully used in similar surveys (Ref. [5]).

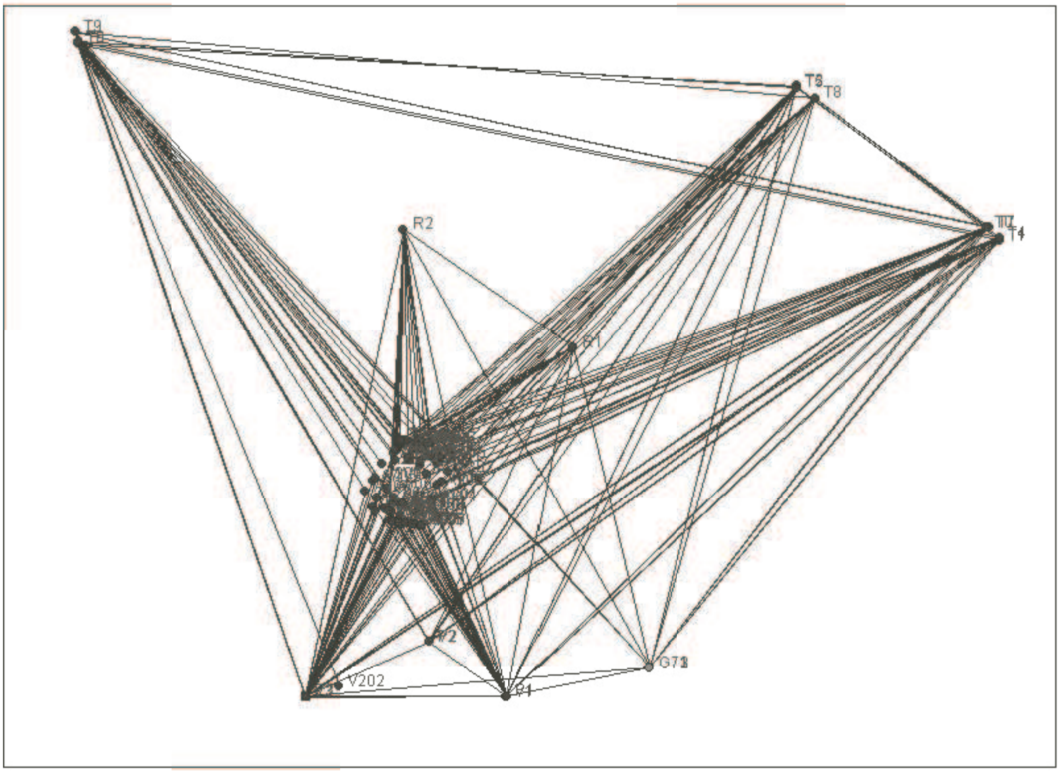

Figure 4. Classical control network and collimations lines.

VLBI reference point has been determined independently with KGPS and with terrestrial geodesy. For both survey procedures, VLBI antenna movements in azimuth (at fixed elevations) determine prisms or GPS antenna positions that ideally belong to a circle centered on the azimuth axis. In a similar manner, circles' centers described by movements in elevation at fixed azimuth positions, belong to the elevation axis. Developing this basic concept it is possible to determine the reference point on a purely analitical computation. The huge population defined by KGPS observations balances the lower accuracy and the greater scatter that is associated with the positions used in the least squares procedure. Nevertheless, as we expected, reference point estimate is less precise then using classical methodology. The latter determines a reference point that is statistically consistent with the one obtained with KGPS but its precision is much higher.

5. Results

Classical survey methodology has been used for surveying the markers that identify the old and the new permanent ground control network. In table 2 the estimated coordinates expressed in the local reference frame are listed for the new and the old markers.

A comparison between the different sets of positions obtained with the two survey techniques has been possible performing transformation from the local to the ITRF2000 reference frames (and backwards). Table 3 contains the Gaussian-Local transformation parameters estimated using the ground triangle MEDI-P3-G7 (the first transformation ITRF2000-Gauss is straightforward once the reference ellipsoid is given).

VLBI reference coordinates obtained using KGPS and transforming the ITRF2000 coordinates (epoch 20 June 2001) into the local frame are:

$$\mathbf{P}GPS_{loc}^{2001} = (21.575 \pm 0.005, 45.536 \pm 0.003, 17.713 \pm 0.012) \qquad (1)$$

Point ID	X (m)	Y (m)	Z (m)
P1	42.6586 ± 0.0002	0.0000	2.0772 ± 0.0003
P2	26.2885 ± 0.0008	11.6391 ± 0.0009	2.076 ± 0.001
P3	0.0000	0.0000	2.0195 ± 0.0003
V1	42.800 ± 0.001	-0.033 ± 0.001	2.103 ± 0.001
V2	26.2989 ± 0.0003	11.5167 ± 0.0002	2.1132 ± 0.0005
V3	0.0682 ± 0.0006	-0.1008 ± 0.0005	2.0267 ± 0.0007

Table 2. Positions of the pillars of the ground control network. Results expressed in the local reference frame. Pillars V represent the markers of the old network.

Scale	$0.999834107 \pm 0.000045620$
Rotation	(82.321244 ± 0.002614) deg
Tras. N	$(-1362865.1578 \pm 227.3679)$ m
Tras. E	$(4793167.4943 \pm 227.3679)$ m
Shift in H	(-49.4638 ± 0.0005) m

Table 3. Transformation parameters estimated using the ground triangol MEDI-G7-P3 between the local and the Gaussian coordinate systems.

while those obtained using triangulation and trilateration are:

$$\mathbf{P}clas_{loc}^{2001} = (21.580 \pm 0.001, 45.536 \pm 0.001, 17.699 \pm 0.001) \quad (2)$$

The same coordinates expressed in ITRF2000 but on epoch 1997.0 are:

$$\mathbf{P}GPS_{ITRF2000}^{1997.0} = (4461369.988 \pm 0.005, 919596.819 \pm 0.003, 4449559.220 \pm 0.013) \quad (3)$$

$$\mathbf{P}clas_{ITRF2000}^{1997.0} = (4461369.982 \pm 0.001, 919596.818 \pm 0.001, 4449559.207 \pm 0.001) \quad (4)$$

Comparing (1) and (2) with those obtained using triangulation and trilateration in May 2000 (Ref. [4]) before the intervention on the concrete:

$$\mathbf{P}clas_{loc}^{2000} = (21.581 \pm 0.001, 45.534 \pm 0.001, 17.699 \pm 0.001) \quad (5)$$

differences are statistically not significant on the 1σ level.
A striking agreement exists when considering Medicina VLBI ITRF2000 (1997.0) coordinates given by IERS (e.g.: http://lareg.ensg.ign.fr/ITRF/ITRF2000/results/ITRF2000_VLBI.SSC):

$$\mathbf{P}\,VLBI_{ITRF2000}^{1997.0} = (4461369.985 \pm 0.002, 919596.819 \pm 0.001, 4449559.208 \pm 0.002) \quad (6)$$

and comparing these coordinates with (4).

6. Conclusions

A comparison between the reference point coordinates estimated in May 2000 and in June 2001 does not point out any significant motion within the local ground control network.
It is worth remark that coordinates (4) represent ITRF2000 VLBI reference point (epoch 1997.0) that have been estimated using trilateration and triangulation only (i.e. terrestrial technique). In detail, coordinates (4) have been obtained applying the parameters of table 3 to the coordinates (2) and bringing backwards their values using the VLBI velocities estimated by IERS. On the other

hand, the coordinates (6) are obtained using uniquely space geodesy techniques (i.e. a completely different survey methodology). The agreement that can be observed comparing coordinates (4) and (6) is striking and points out the reliabilty of the Medicina velocities computed by IERS. It also confirms the high accuracy and precision obtainable in surveying small networks using classical geodesy, for which, data analysis procedures are well standardized.
At last, KGPS estimates of roving antennae positions are far too optimistic. Their precisions do not reflect the uncertainties related to the estimation process, especially concerning the biases introduced by OTF procedure's failure. The post-processing least squares approach, as we expected, takes great advantage from the large number of positions that constitute the populations used for computing the VLBI reference point. Nevertheless, we consider the final accuracy of the coordinates estimated with KGPS quite good but not satisfactory for this applications. Further optimization of the analitical least squares approach (introducing a best fit to a thorus) and use of high quality scientific KGPS analysis software (e.g.: GIPSY-OASIS II) might increase the final accuracy of the VLBI reference point estimate.
A final remark regards the static GPS network survey: it is strictly necessary to allow the computation of the transformation parameters from local to ITRF systems.

References

[1] Cenci, A., Vicomanni, G., Bianco, G., "Determination of the invariant point and of the axes offset for the VLBI antenna at Medicina", Telespazio, Roma, 1988

[2] Del Rosso, D., and Ambrico, F., "Survey of the Medicina site - September 1995", Nuova Telespazio, Roma, 1995

[3] Nothnagel, A. and Binnenbruck, B., "Determination of the 1996 displacement of the Medicina radio telescope by local surveys", in *Proc. of the XIV Working Meeting on European VLBI for Geodesy and Astrometry*, 61–66, Castel S. Pietro Terme (BO), Italy, 2000

[4] Sarti, P., Vittuari, L., Tomasi, P., "GPS and Classical Survey of the VLBI Antenna in Medicina: Invariant Point Determination", in *Proc. of the XIV Working Meeting on European VLBI for Geodesy and Astrometry*, 67–72, Castel S. Pietro Terme (BO), Italy, 2000

[5] Tomasi, P., Sarti, P., Rioja, M.J., "The determination of the invariant point of the VLBI antenna in Ny Aalesund", in *Memoirs of National Institute of Polar Research, Special Issue, No. 54*, 319–330, Tokyo, Japan, 2001

Axel Nothnagel et al.: Results of the 2000 Ny-Ålesund Local Survey, Proceedings of the 15th Working Meeting on European VLBI for Geodesy and Astrometry, p.168–176
http://www.ieec.fcr.es/hosted/15wmevga/proceedings/nothnagel2

Results of the 2000 Ny-Ålesund Local Survey

Axel Nothnagel [1], *Christoph Steinforth* [1], *Bernd Binnenbruck* [1], *Lars Bockmann* [2], *Leif Grimstveit* [2]

[1] *Geodetic Institute of the University of Bonn*
[2] *Norwegian Mapping Authority*
Contact author: Axel Nothnagel, e-mail: nothnagel@uni-bonn.de

Abstract

In August 2000 a local survey campaign was carried out for the determination of the tie between the VLBI and the GPS reference points at the Ny-Ålesund Geodetic Observatory. By determining the coordinates of the IGS GPS antennas NYAL and NYA1 relative to a local control network and measuring the VLBI reference point in the frame of the same network the tie between the reference points was computed. The results of the geocentric vectors between the GPS and the VLBI reference points as determined in this survey campaign very closely matches the vectors computed from ITRF2000 coordinate differences which are based on space geodetic measurements alone.

1. Introduction

In geodetic VLBI all parameters estimated in the data adjustments are referred to the so-called VLBI reference point. In the case of an azimuth-elevation mount the reference point is either the point where both axis intersect or, if they do not intersect as in the case of the Ny-Ålesund telescope (Fig. 1), it is the point of the azimuth axis where the distance to the elevation axis is minimal (e.g. Ma 1978; Nothnagel et al. 1995). This point should be invariant to any antenna movements necessary for the observations.

Figure 1. Ny-Ålesund 20 m VLBI Telescope.

The long term stability of radio telescope reference points is one of the great advantages which geodetic VLBI has upon other space geodetic techniques. Unlike GPS antennas, the phase center of a VLBI antenna always has a well determined geometric position relative to the reference or invariant point. Unfortunately, the long term stability of the VLBI reference point generally does not last indefinitely and various reasons may cause a local displacement of the invariant point on a decadal time scale.

For example man-made changes in the 3-dimensional position of the reference point or local movements of the underground may cause discontinuities in the time series measured with geodetic VLBI. Therefore, these displacements have to be determined within a local control network in order to permit a correction of the VLBI time series.

Another reason for local control networks and related surveys is the necessity for direct links between sensors of different space geodetic techniques collocated at observing sites. At Ny-Ålesund two permanent GPS units (NYAL and NYA1) which are part of the IGS (International GPS Service) network are located near the VLBI telescope. Both techniques contribute important information to the International Terrestrial Reference Frame (ITRF). Therefore, the excentricity vectors in a geocentric X,Y,Z system (e.g. the International Terrestrial Reference System ITRS) are important parameters for global investigations.

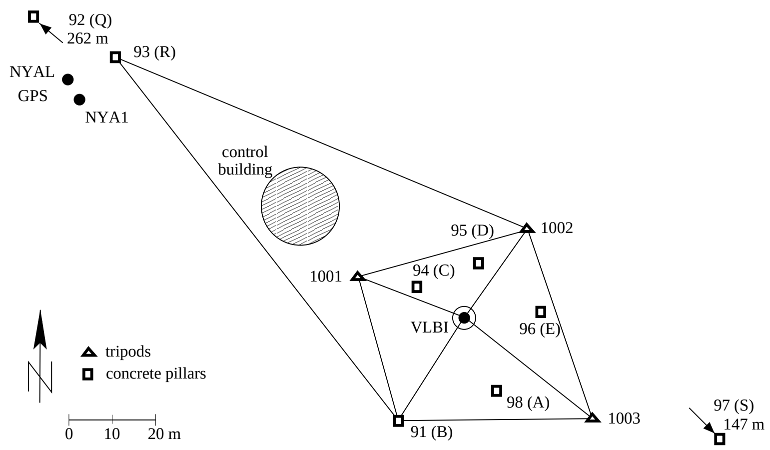

Figure 2. Layout of Ny-Ålesund control network.

In order to establish a high accuracy first epoch definition of the VLBI reference point relative to a number of survey pillars (Fig. 2) and to determine the vectors between the VLBI and the GPS reference points, a local survey has been carried out in August 2000. The survey campaign consisted of three different parts:

1. GPS survey of selected points
2. conventional survey of GPS antennas relative to ground points
3. conventional survey of VLBI reference point relative to ground points

2. Survey Setups

2.1. Survey of GPS Antennas

The survey network at the Ny-Ålesund geodetic observatory consists of eight concrete surveying pillars with Wild 5/8" screws and brass height reference bolts erected along the ridge on which the telescope is situated (Fig. 3).

A 5-day GPS campaign was carried out occupying two of the pillars of the control network (points #92 and #97) with Ashtech Z-Surveyor GPS receivers. Together with the data of the two permanently recording GPS systems of the IGS stations NYAL and NYA1 (TurboRogue and Trimble 4000SSE), all employing choke-ring antennas, a four-station GPS network was realized.

Figure 3. Surveying pillar at Ny-Ålesund.

The analysis of the GPS data carried out in the precise point positioning mode (Zumberge et al. 1997) produced geocentric X,Y,Z coordinates for the 4 points in the ITRF97 reference frame.

In a conventional survey with a Wild T2 theodolite, a Kern Mekometer ME5000 and a Zeiss DiNi12 levelling instrument directions, distances and heights were determined for computing the coordinates of the remaining pillars in a geocentric X,Y,Z system (ITRF97). In the least squares adjustment of the observations, the coordinates determined in the GPS campaign were introduced as observations.

Table 1. Geocentric Coordinates of Pillars and GPS Antennas

Point #	X [m]	Sigma [m]	Y [m]	Sigma [m]	Z [m]	Sigma [m]
91	1202487.289	0.002	252723.785	±0.002	6237751.305	±0.002
92	1202340.673	0.002	252387.081	±0.002	6237790.209	±0.002
93	1202420.581	0.002	252636.129	±0.002	6237768.862	±0.002
94	1202455.474	0.002	252722.383	±0.002	6237758.028	±0.002
95	1202448.114	0.002	252734.284	±0.002	6237758.040	±0.002
96	1202454.517	0.002	252752.691	±0.002	6237755.763	±0.002
97	1202503.039	0.002	252890.632	±0.002	6237738.901	±0.002
98	1202474.916	0.002	252746.733	±0.002	6237752.830	±0.002
NYAL	1202430.594	0.002	252626.676	±0.002	6237767.539	±0.002
NYA1	1202433.912	0.002	252632.261	±0.002	6237772.530	±0.002

2.2. Survey of VLBI Reference Point

Due to the fact that VLBI reference point cannot be materialized directly a more complicated survey setup had to be chosen in order to determine its coordinates in the frame of the surrounding pillars. For an alt-azimuth antenna the VLBI reference point is the intersection of azimuth and elevation axis. When rotating in azimuth each end point of the elevation axis ideally describes a circle about the VLBI reference point. The average height of the two end points represents the height of the VLBI reference point. In order to determine the reference point at Ny-Ålesund, the end points of the elevation axis were materialized by small pop rivets which were placed in the centric bores of the elevation bearings (Fig. 4). Determining the 3D positions of these markers at different positions subsequently permits the computation of the VLBI reference point as the center of the circles.

Figure 4. Target at end point of elevation axis.

In order to provide sufficient redundancy it was planned to rotate the antenna in azimuth angle increments of about 20° measuring each position by forward intersects, For full visibility coverage of the targets at the antenna end points three auxiliary temporary survey points on tripods, #1001, #1002 and #1003, were established augmenting the existing survey monuments (Fig. 2).

The whole network of existing pillars and auxiliary tripods was then observed with Wild T2 theodolites in all possible combinations using forced centering. Only very few of the lines were not observed since the control building or the base of the telescope blocked the view. The scale and the heights of the network were taken over from the measurements reported in 2.1.

The analysis of the observations was carried out with the least squares adjustment program PANDA (GeoTec 1998). The UTM coordinates of point #96 and one component of point #93 were fixed in the least squares adjustment resulting in topocentric coordinates for all points used (Tab. 2).

Table 2. Topocentric Coordinates of pillars

Point #	East [m]	Sigma [m]	North [m]	Sigma [m]	Up [m]	Sigma [m]
91	432911.0120	—	8763837.3288	±0.0002	77.0250	±0.0005
93	432843.6420	—	8763926.2180	—	78.2580	±0.0005
95	432931.2995	±0.0001	8763873.0857	±0.0002	76.6890	±0.0005
96	432947.4168	±0.0001	8763861.8989	±0.0002	76.3830	±0.0005
98	432936.3844	±0.0002	8763843.5153	±0.0002	77.1030	±0.0005
1001	432901.8911	±0.0002	8763870.6188	±0.0002	78.0078	±0.0006
1002	432942.8141	±0.0001	8763883.8476	±0.0003	72.1718	±0.0006
1003	432959.7062	±0.0002	8763837.0868	±0.0003	76.6655	±0.0006

For the determination of the VLBI reference point relative to the control network the method of choice was a conventional three dimensional triangulation of the end points of the elevation axis in different azimuth positions of the telescope. There are two advantages of this method as compared to a trilateration:

- In order to have decent visibility of the targets the network around the antenna has to be very small and distance measurement uncertainties would produce adverse error propagation.
- By rotating the telescope by 360° about its azimuth axis the least squares adjustment of the observations produces a solution with almost no correlations between the target parameters

which, in this case, are the radii and the center points of the circles described by the end points of the axis.

- The height of the antenna reference point is defined by multiple trigonometric height determinations of the elevation axis providing an ideal and simple way of redundancy.

On the ground, pillars #91 together with the temporary points #1001, #1002 and #1003 were then occupied pairwise with two Wild T2 theodolites for trigonometric intersection and trigonometric levelling. For the determination of the end points of the elevation axis at different azimuth positions of the telescope, the antenna was driven in azimuth into positions where the pairs of instruments could aim at the markers. Often the markers were obstructed by metal beams and the telescope had to be moved in incremental steps until the markers became visible. In all positions, horizontal directions and zenith distances were observed with both theodolites together with reference directions relative to one or two points in the network depending on the distance from the current instrument position. All measurements were carried out in double-sighting in order to eliminate collimation errors and errors of the transverse axes of the theodolites. Over a period of two days 18 azimuth positions of the telescope were observed for each marker at the ends of the elevation axis.

In the analysis the trigonometric intersects provided horizontal coordinates in the frame of the local coordinate system. The accuracy of the points were computed with the error propagation law resulting in errors in the horizontal coordinate components of the axis end points of < 1 mm RMS (Fig. 5). The height was transferred to the tripods by trigonometric levelling with ~ 1 mm (RMS) accuracy.

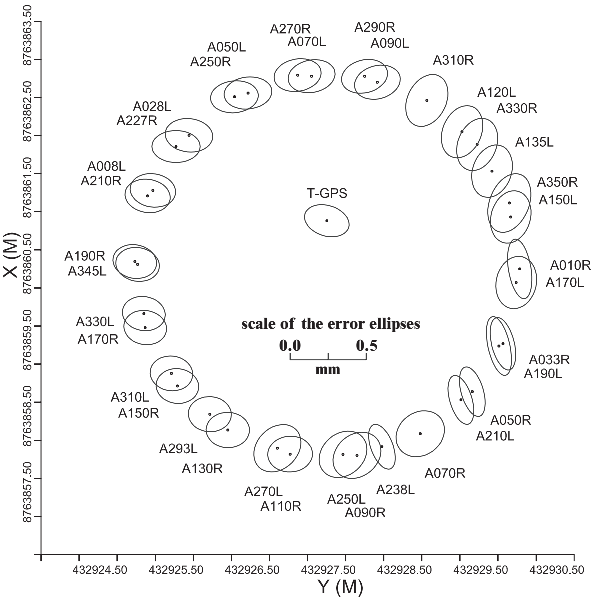

Figure 5. Error ellipses of targets in different positions.

Under the assumption that the telescope rotates around a central azimuth axis, the end points of the elevation axis should describe circles around this axis. The radii of these circles need not necessarily be identical since they depend on the location where the target markers were mounted. Taking the coordinates of the end points at different azimuth positions as inputs, two least squares adjustments can be performed solving for the coordinates of the centers and the radii of the circles. Table 3 lists the coordinates and radii of the targets at the left (TL) and at the right end of the elevation axis (TR). The weighted averages of the two materializations are taken as the final coordinates of the VLBI reference point in the local system. In addition, for each of the horizontal positions the trigonometric levelling yielded height values. Averages of these were formed to determine the average heights of the target marks. The heights of target TL and target TR may differ slightly due to inaccuracies of the construction of the telescope but are still at the sub-millimeter level.

The good quality of the measurements is confirmed by the behaviour of the residuals (Fig. 6 and 7).

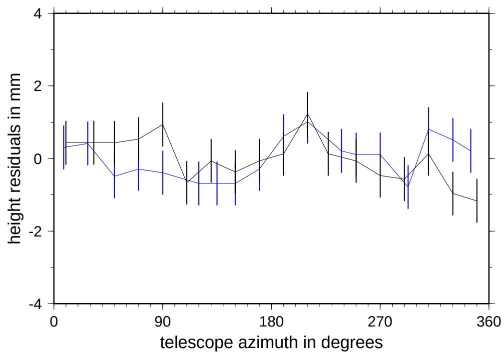

Figure 6. Residuals of height components

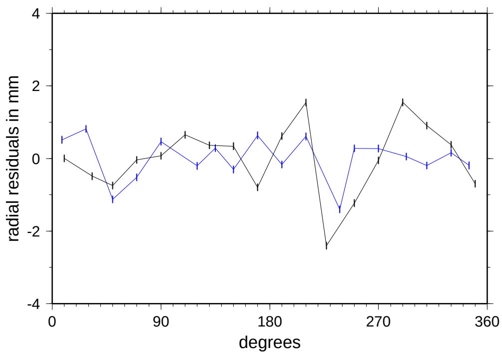

Figure 7. Residuals of radii

Table 3. Parameters of the circles fitted to the series of positions with their formal errors and the final coordinates in the local system

Target	East [m]	Sigma [m]	North [m]	Sigma [m]	Radius [m]	Sigma [m]	Height [m]	Sigma [m]
TL	432927.7704	±0.0002	8763860.7527	±0.0002	2.4915	±0.0001	87.2936	±0.0006
TR	432927.7704	±0.0003	8763860.7525	±0.0003	2.5277	±0.0002	87.2930	±0.0006
W. Avg.	432927.7704	±0.0002	8763860.7526	±0.0002			87.2933	±0.0004

Looking at the standard deviations of the individual points at different azimuth angles it can be stated that the measurements were carried out with extreme precision. In addition, the least squares fits of the circles on the one hand and of the average of the individual height determinations on the other hand also provide external quality checks. Owing to the minimal scatter and the 18 individual positions contributing to the final results the errors of the resulting parameters (center coordinates in 3D and radii) become even smaller. Since the coordinates of each antenna position are often determined from different pairs of ground positions the resulting formal errors are also a good indicator of the absolute accuracy of the network.

One of the environmental factors which has to be considered in addition to the purely geometrical circumstances is thermal expansion. The metal structure up to the elevation axis is 10.87 m high. During the measurements the ambient temperature varied only between 2.5° C in the morning to 3.5° C in the afternoon. Assuming a time lag of 2 hours which are needed for the ambient temperature to migrate into the metal and actually causing the expansion (NOTHNAGEL et al. 1995) the average temperature for the time of the measurements was 3.0° C. With an expansion coefficient for steel of 1.2×10^{-5} a one degree C increase causes a height increase of 0.12 mm. At the reference temperature of 0° C the height of the telescope had to be corrected by -0.39 mm resulting in a final height of 87.2929 m.

Table 4. Topocentric Coordinates of VLBI reference point at epoch 2000.08.30

East [m]	Sigma [m]	North [m]	Sigma [m]	Height [m]	Sigma [m]
432927.7704	±0.0002	8763860.7526	±0.0002	87.2929	±0.0004

3. VLBI Antenna Axis Offset

The coordinates of the end points of the elevation axis when the telecope is turned in different directions offered the opportunity for a computation of the VLBI antenna axis offset. This offset is the distance between the azimuth and the elevation axis and is a major calibrating value in geodetic VLBI data analysis. Provided that both ends of the elevation axis are determined when the antenna points at an identical azimuth, the VLBI reference point and the target marks establish a triangle where the distance of the VLBI reference point from the vector connecting the target marks, i.e. the elevation axis represents the axis offset (Fig. 8).

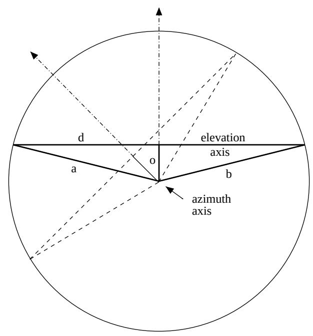

Figure 8. Axis geometry, o = axis offset, d = length of elevation axis.

With the coordinates of the three points known, the axis offset can be computed from

$$o = \sqrt{b^2 - \left(\frac{d^2 - a^2 + b^2}{2d}\right)^2} \tag{1}$$

Using this formula, different distances of the two target marks from the azimuth axis are not of any concern as long as the targets are mounted in the elongation of the elevation axis.

The measurements produced eleven pairs of coordinates of the target marks producing redundant elements and permitting a proper error estimate. The resulting axis offset and its formal error are

$$0.5245 \pm 0.0003 \text{ m}$$

which is about 16 mm larger than the value of 0.5080 m given by the manufacturer. One of the reasons for such a big discrepancy may be the fact that the VLBI reference point cannot be materialized and that the manufacturer determined this value just by trying to measure it with the help of a CAD program.

4. Excentricities between Space Geodetic Reference Points

Vectors between different observing techniques to be used as excentricities in the computations of the ITRF are normally given in geocentric X,Y,Z coordinate differences. Having the coordinates of the survey pillars in both systems, i.e. in X,Y,Z and in topocentric coordinates, it is now possible to transform one system into another by a simple 7-parameter transformation. This yields the

VLBI reference point in X,Y,Z coordinates (Tab. 5) and, as an independent check, the GPS points in topocentric coordinates.

Table 5. Geocentric Coordinates of VLBI reference point from transformation

X [m]	Sigma [m]	Y [m]	Sigma [m]	Z [m]	Sigma [m]
1202462.7053	±0.0003	252734.4285	±0.0003	6237766.0468	±0.0004

The differences between the geocentric coordinates of the VLBI and the GPS reference points yield the excentricities needed in the computation of the ITRF realizations (Tab. 6). In parenthesis are the coordinate differences listed which result from a differencing of the ITRF2000 coordinates (Altamimi 2001). The latter are purely determined within the ITRF computations since excentricies have not been determined locally so far.

Table 6. Geocentric Coordinate Differences relative to NYA1 determined in this measurement campaign and, in parenthesis, from differencing ITRF2000 coordinates.

to point	Δ X [m]	Sigma [m]	Δ Y [m]	Sigma [m]	Δ Z [m]	Sigma [m]	Distance [m]	Sigma [m]
NYAL	-3.319	±0.0020	-5.590	±0.0020	-4.990	±0.0020	8.195	±0.0030
	(-3.317)	(±0.0014)	(-5.583)	(±0.0014)	(-4.980)	(±0.0050)	(8.184)	(±0.0050)
VLBI	28.794	±0.0020	102.162	±0.0020	-6.470	±0.0020	106.339	±0.0030
	(28.794)	(±0.0014)	(102.166)	(±0.0014)	(-6.475)	(±0.0050)	(106.343)	(±0.0050)

5. Conclusions

The local surveys carried out at Ny-Ålesund in summer 2000 have produced a first epoch tie for the GPS and the VLBI reference points relative to a local control network of concrete pillars. Future measurements of this type will help to monitor the stability of the space geodetic sensors and to separate local sensor movements from tectonic effects.

The local determination of geocentric coordinate differences between space geodetic sensors was carried out in a two step method using a local GPS campaign for the determination of geocentric X,Y,Z coordinates of some points of the control network. By this method a direct transformation of the local topocentric coordinates into geocentric ones can be performed without the use of additional measurements like astronomical azimuth determinations and plumb line deflection which may introduce additional uncertainties. For this reason the procedure reported on here may serve as a good example for local surveys to be carried out at other space geodetic observatories.

Acknowledgements

The research carried out at Ny-Ålesund Geodetic Observatory was funded by the European Community (EC) - Access to Research Infrastructure - Improving Human Potential Programme and the Large Scale Facility Programme (LSF) under grant NMA-22/2000. We are particularly thankful to Helge Digre and Tom Pettersen of the Norwegian Mapping Authority and to the staff of Kings Bay AS who supported us in every aspect creating the basis for the success of this project.

References

Altamimi Z. (2001) *ITRF2000*, Available electronically via http://lareg.ensg.ign.fr/ITRF/ITRF2000

Geotec (1998) *Panda für Windows, Version 2.12*, Systemhandbuch, GeoTec GmbH, Laatzen

Ma C. (1978): *Very Long Baseline Interferometry Applied to Polar Motion, Relativity and Geodesy*, NASA Technical Memorandum 79582, Greenbelt MD

Nothnagel A., M. Pilhatsch, R. Haas (1995) *Investigations of thermal height changes of geodetic VLBI telescopes*, Proc. of the 10th Working Meeting on European VLBI for Geodesy and Astrometry, R. Lanotte and G. Bianco (eds.), Matera, 121–133

Zumberge et al. (1997) *Precise Point Positioning for the efficient and robust analysis of GPS data from large networks*, JGR, Vol. 102, 5005–5017

Rüdiger Haas and Michael Kirchner: Local survey activities at the Onsala Space Observatory 1999–2001, Proceedings of the 15th Working Meeting on European VLBI for Geodesy and Astrometry, p.177–184
http://www.ieec.fcr.es/hosted/15wmevga/proceedings/haas2

Local survey activities at the Onsala Space Observatory 1999–2001

Rüdiger Haas [1], *Michael Kirchner* [1, 2]

[1] *Onsala Space Observatory (OSO), Chalmers University of Technology*
[2] *now back at: Dresden University of Technology (DUT)*
Contact author: Rüdiger Haas, e-mail: haas@oso.chalmers.se

Abstract

We describe the local survey activities at the Onsala Space Observatory during 1999–2001. In the summer of 1999 we installed one GPS antenna behind the sub-reflector of the 20 m VLBI telescope and a second one close to the vertex of the paraboloid. They are denoted APEX and VTEX, respectively. Since then we perform campaign type tie-measurements between the reference monuments for the International VLBI Service for Geodesy and Astrometry (IVS) and the International GPS Service (IGS), using these two GPS antennas on the VLBI telescope. So far, the repeatabilities of the determined topocentric up, east and north components are 2.3, 0.8 and 1.0 millimetres for APEX, and 2.8, 0.4 and 1.9 millimetres for VTEX. In spring 2001 we performed a combined local and regional GPS campaign at the observatory and the surrounding region. The campaign lasted for 38 days and included in total 12 stations. Repeatabilities of 1–2 millimetres for the horizontal components and 2–3 millimetres for the vertical component were achieved. Helmert transformation of the 2001 results for the markers at the observatory with respect to results from earlier classical geodetic survey and GPS measurements gave residuals on the level of 2–7 millimetres.

1. Introduction

The Onsala Space Observatory was founded mid of last century primarily as radio-astronomical observatory. Geodetic applications and geodetic research were not of first priority. Nevertheless, Onsala participated already 1968 in the first Mark-I geodetic VLBI experiment [9]. In those days the 25 m radio telescope at the observatory was used for VLBI. The 20 m telescope was build in the mid seventies and the first geodetic Mark-III VLBI experiment at Onsala was observed in 1979. Geodetic research became an aspect of increasing importance at the Onsala Space Observatory [8], [2]. Today the 20 m radio telescope at Onsala is a network station for the International VLBI Service for Geodesy and Astrometry (IVS) and contributes regularly to geodetic research by participating in European and International VLBI sessions [4].

A local geodetic survey has been performed in the seventies to connect the two radio-telescopes and the Swedish triangulation point on the observatory site. Later, also the reference marker for Doppler measurements was connected using a classical geodetic survey. A local geodetic control network of reference points and observing pillars has not been constructed, though. A particular difficulty with the 20 m radio-telescope is, that the telescope is enclosed by a radome. Thus, direct observations of its geodetic reference point are impossible from any outside control network.

Equipment for the Global Positioning System was installed late in 1987 at the observatory at a distance of approximately 80 m from the 20 m radio-telescope. Onsala started then to participate in the CIGNET network and soon the GPS station at Onsala became an important contributor to national and international GPS networks. Today Onsala is an important observing site for the International GPS Service (IGS). A couple of geodetic markers have been established in the bedrock around the GPS monument and classical geodetic survey has been performed between the GPS monument and the VLBI telescope in the beginning of the nineties [3]. Also local and regional GPS campaigns have been observed in the beginning of the nineties [3] and in 1992 there was a short-baseline VLBI experiment with the mobile VLBI station MV-2 [7].

With the increasing importance of geodetic research at the observatory and the availability of collocated space geodetic techniques, local geodetic survey becomes more and more important. For both space geodetic techniques, VLBI and GPS, it is of interest to monitor the position of the reference monuments and their reference points with respect to local, regional and global reference systems. The IVS and IGS reference points are the intersection of the azimuth and elevation axis of the VLBI telescope and the phase centre of the choke-ring GPS antenna, respectively. In order to use results from both techniques for the establishment and maintenance of international coordinate systems, as for example the International Terrestrial Reference Frame (ITRF), a precise and accurate knowledge of the local tie between the reference points is of great importance.

Figure 1 gives an overview on all reference points and geodetic markers at the observatory.

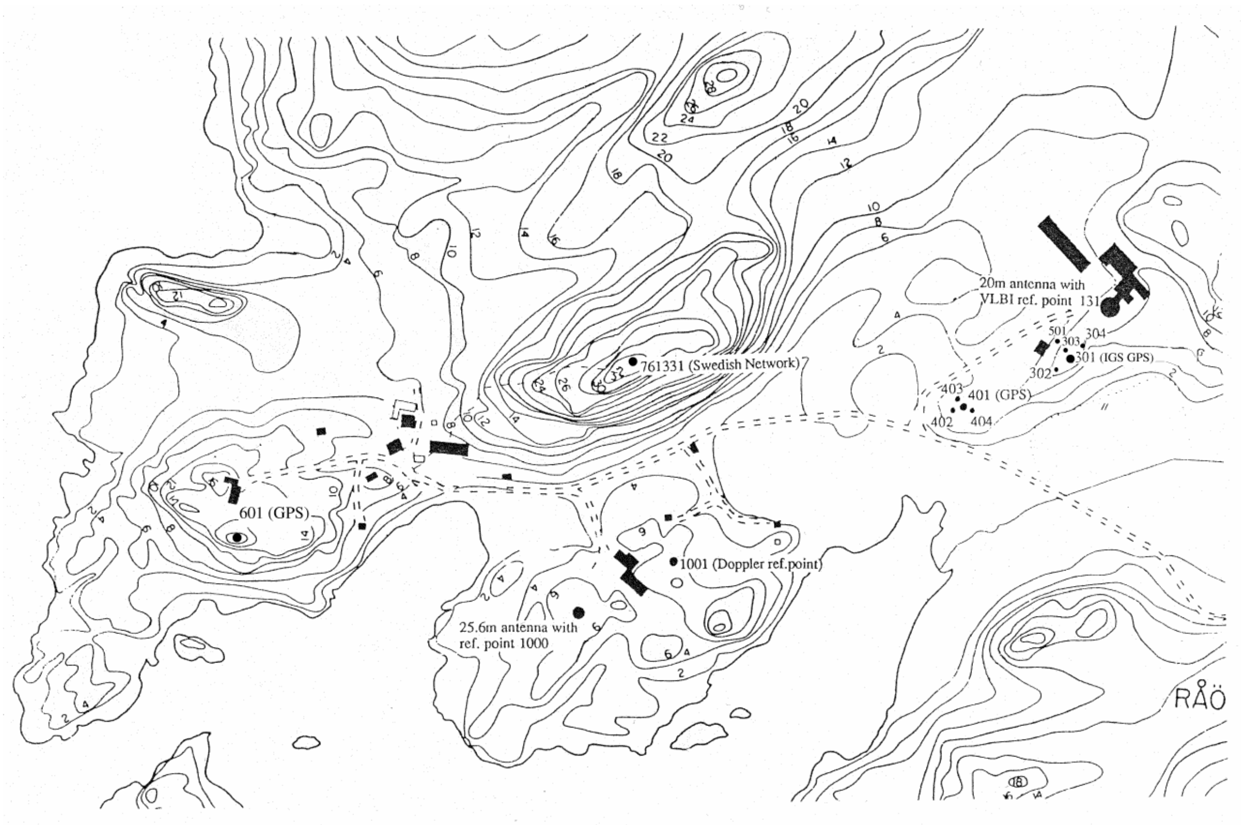

Figure 1. Map of the Onsala Space Observatory and the available geodetic markers: Point 131 and point 301 are the IVS and IGS reference point, respectively. Point 501 is the reference marker for mobile VLBI, point 1001 the reference point for Doppler observations, and point 761331 is the Swedish triangulation marker. All other markers are control markers in bedrock for classical survey and GPS measurements.

2. Monitoring of the local VLBI-GPS tie

In the summer of 1999 we installed a choke-ring GPS antenna permanently on top of the VLBI telescope behind the sub-reflector close to its Apex position. An additional GPS antenna close to the Vertex position of the main reflector has been mounted sporadically. The idea is to monitor the local tie between the IVS and IGS reference monuments on regular intervals. During breaks in the usual astronomical or geodetic observing schedule, the radio telescope is oriented to its zenith position and GPS observations are performed. The installation of the two antennas APEX and VTEX and the necessary equipment, and first results of the analysis of the observations have been described for example in [1].

During the tie-measurement campaigns GPS data are recorded every 30 seconds with the GPS receivers connected to the APEX and VTEX antennas. The data are analysed together with GPS data of the IGS station OSO301 in a small network using the Bernese GPS analysis software package Version 4.2 [5]. The daily positions for APEX and VTEX relative to OSO301 are determined from 24 h of observational data. Figure 2 shows the residuals of the individual daily solutions with respect to a combined solution for APEX and VTEX.

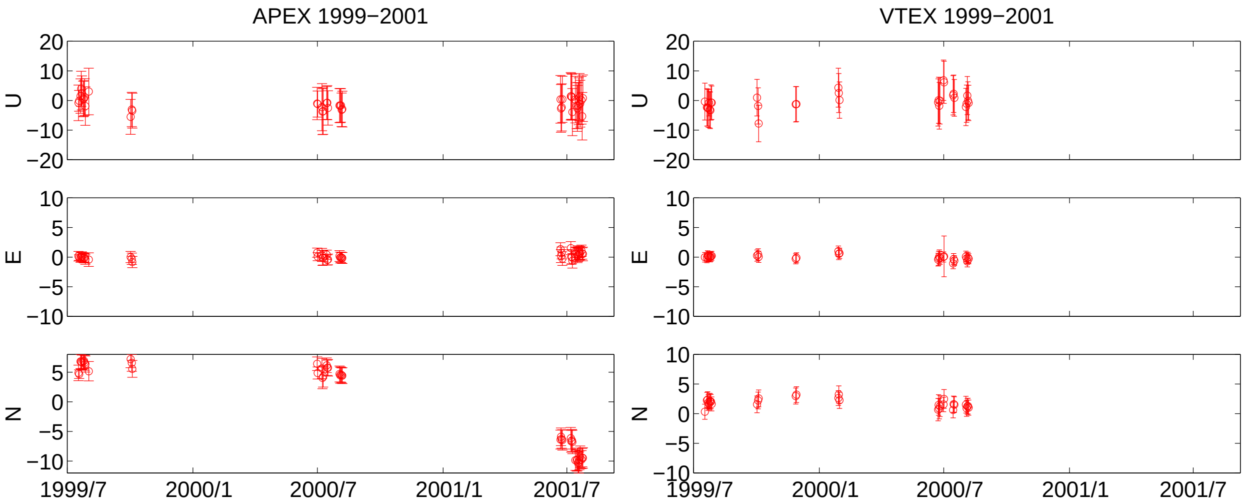

Figure 2. Time series of residuals of daily solutions for APEX and VTEX with respect to a combined solution. Shown are the up (U), east (E) and north (N) component in millimetres.

Unfortunately, the sampling of the observation campaigns is not regular and there are large gaps of several months. This is due to constraints in the telescope availability, but also caused by failing GPS receivers at some occasions. Furthermore, so far we were not able to observe GPS data with VTEX in 2001 and thus have only results for 1999 and 2000. The results for the north component of the position of APEX show a significant deviation for the year 2001 with respect to the years 1999 and 2000. The up and the east component do not show a similar behaviour. We do not have an explanation for this, but we suspect that the reason is that the telescope was not pointed exactly to its zenith position during the campaigns in 2001. This could be related to the usage of different antenna pointing models or no pointing model during the different campaigns. Usually we move the telescope to its zenith position when it is oriented toward azimuth south. Roughly speaking, the 20 m VLBI telescope is situated north of the IGS monument. An elevation of less than 90 degrees will therefore cause a shift in the north component of the antenna APEX, while the up and east component will not be affected significantly. A deviation of 0.05° in elevation will cause a shift in the north component of approximately 12 mm, which corresponds reasonably well to the differences we see between 1999/2000 and 2001. Repeated measurements will help to solve the problem.

Table 1. Repeatabilities in millimetres for APEX and VTEX.

Station	Up	East	North	Station	Up	East	North
APEX 1999-2000	2.3	0.3	1.0	APEX 2001a	1.9	0.2	0.3
VTEX 1999-2000	2.8	0.4	1.9	APEX 2001b	2.2	0.8	0.3

In general, the repeatabilities that can be achieved for the topocentric positions of two GPS antennas on the VLBI telescope are on a level of 2.3 mm, 0.8 mm and 1.0 mm for APEX, and 2.8

mm, 0.4 mm and 1.9 mm for VTEX, respectively, see Table 1. If one does not separate APEX into the three individual sites APEX 1999–2000, APEX 2001a and APEX 2001b, the repeatabilities change to 2.4 mm, 0.5 mm and 7.0 mm for the up, east, and north component. This indicates clearly, that only the north component has a problem, which, as described above, could be related to inconsistent elevation of the telescope for the different observation campaigns.

3. The spring 2001 footprint measurements

In spring 2001 we performed a local and regional GPS campaign at the observatory and the surrounding region in west-Sweden. The seven geodetic markers OSO302, OSO304, OSO761331, OSO401, OSO501, OSO601 and OSO1001 at the observatory itself (see Fig.1) and additionally three sites outside the observatory area have been occupied with choke-ring GPS antennas and equipped with GPS receivers of Turbo Rogue or Ashtech Z12 type. Additionally, for the data analysis we included data observed with the IGS permanent station OSO301 at Onsala and the three closest SWEPOS sites Hässleholm, Borås and Vänersborg. Figure 3 gives an overview of all sites involved in the campaign.

Since we did not have the necessary number of antenna/receivers combinations to occupy all sites simultaneously, we had to move some GPS equipment from the inner network at the observatory itself to the outer network after some time. The equipment at OSO304 was moved to Bua vattentorn and the equipment at OSO302 was moved to Tjolöholm Slott after approximately two weeks. Unfortunately, the site Tjolöholm Slott does not have any power supply and the battery driven GPS receiver recorded only data for less than 48 hours. Failing power supply at the site OSO761331 reduced the amount of usable data for this marker to 10 days only. The equipment was then moved to Landvetter Flygplats, but here the receiver failed completely after only 12 hours, so this site later has been excluded from the data analysis.

The data were analysed using the Bernese GPS software package Version 4.2 [5], determining coordinates of all participating sites with respect to OSO301, the IGS site at Onsala. Figure 4 shows daily residuals for the three dimensional station positions with respect to the combined solution. The repeatabilities for the sites are given in Table 2. For nearly all stations the repeatabilities are on the level of 1–2 millimetres for the horizontal components and 2–3 millimetres for the vertical component. The exceptions are the two sites Bua Vattentorn and Tjolöholm slott. Bua Vattentorn is affected by disturbances due to close by transmitters for mobile telephone, and Tjolöholm slott recorded data for less than 48 hours, thus explaining the low performance.

Table 2. Repeatabilites in millimetres during the spring 2001 footprint campaign.

Station	Up	East	North	Station	Up	East	North
Borås	2.4	0.8	0.7	OSO302	2.2	0.4	0.9
Vänersborg	2.9	0.6	1.5	OSO304	3.5	0.9	1.3
Hässleholm	3.0	1.2	2.3	OSO401	2.4	0.4	0.7
Bua vattentorn	10.4	1.1	1.3	OSO501	2.7	0.3	0.8
Tjolöholm slott	5.5	0.1	0.6	OSO601	2.2	0.3	0.5
OSO761331	2.8	0.4	1.6	OSO1001	2.3	0.4	0.6

Coordinates in ITRF90 for markers at the observatory, based on EUREF GPS observations and local geodetic survey, have been presented in [3]. Thus, coordinates for those sites are available for two epochs. We performed a seven parameter Helmert transformation regarding both coordinate sets as random variables [6] and determined the transformation parameters. We detected that the site Bua vattentorn was not the same marker in the two measurements campaigns. The earlier measurements had been taken at a different marker in approximately eight metre distance to the

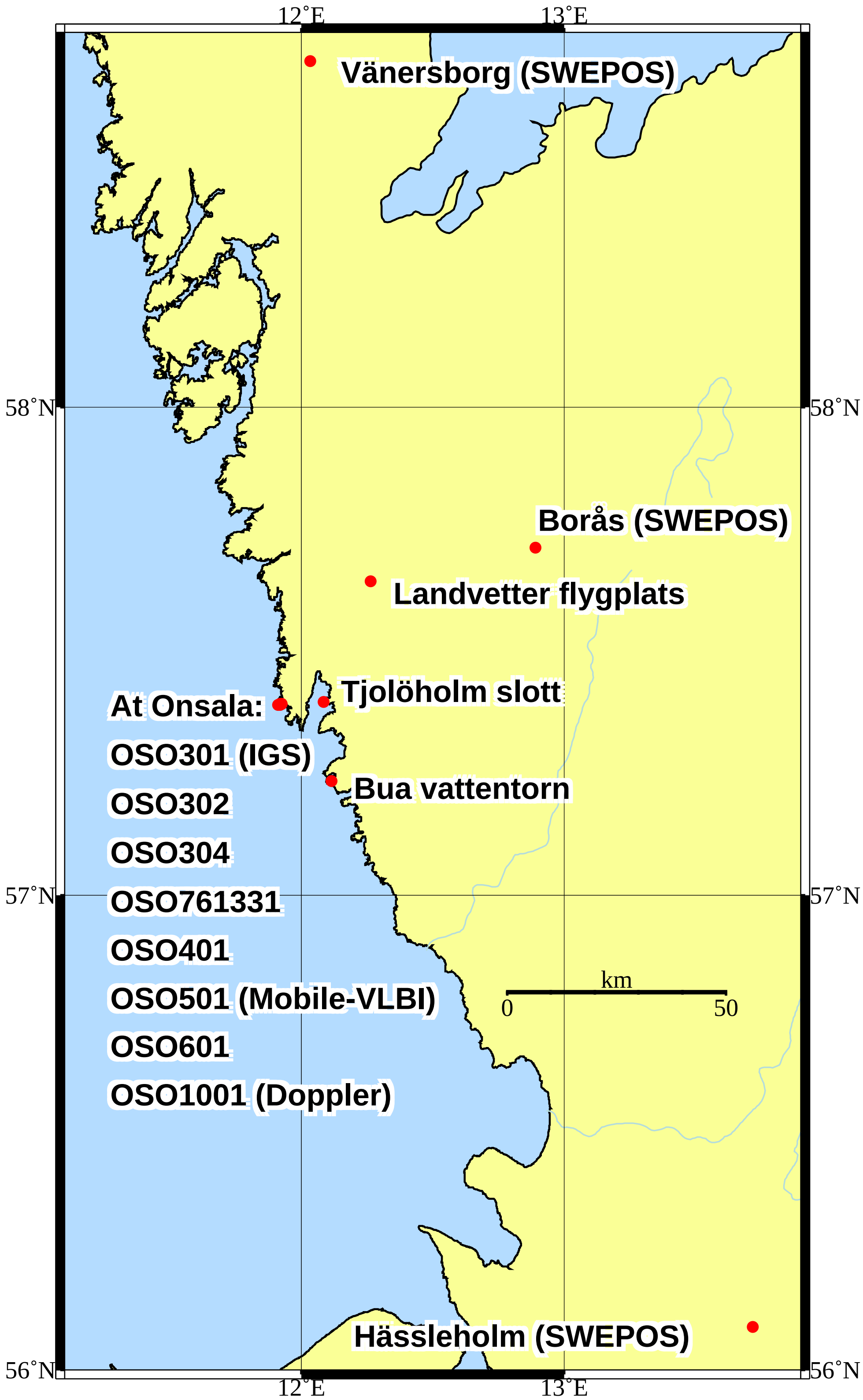

Figure 3. The network of the spring 2001 footprint measurements.

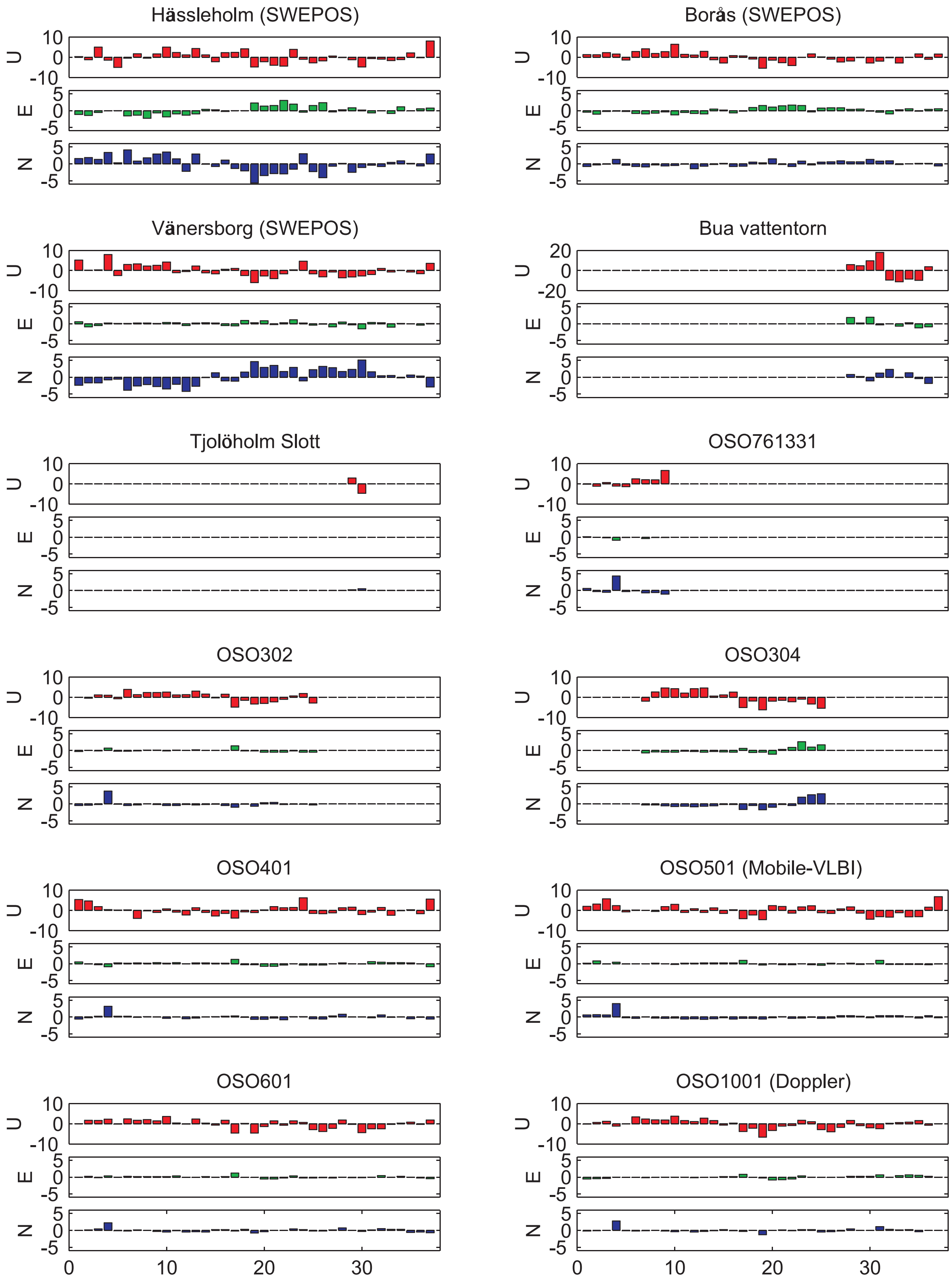

Figure 4. Time series of the residuals of daily solutions for the topocentric up (U), east (E) and north (N) station components in millimetres with respect to the combined solution.

marker we used for the spring 2001 campaign. Figure 5 shows the residuals for the coordinate sets of the six remaining identical points after estimation of the transformation parameters.

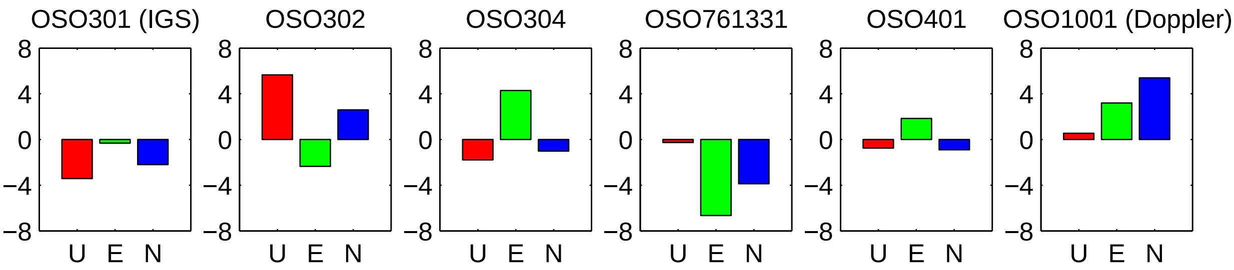

Figure 5. Residuals for markers at the observatory between two the epochs after estimation of the parameters of a 7 parameter Helmert transformation.

The two markers OSO761331 and OSO1001 show large residuals for the horizontal components. These markers are holes in the bedrock and thus the exact positioning of the GPS antennas at these markers is extremely difficult. Furthermore, point OSO761331 was only observed for 10 days. The residuals on the level of several millimetres in the horizontal components can be explained by these difficulties. Also the marker OSO302 shows considerably large residuals. Here we do not have a plausible explanation. We do not suspect a real change in the position, but rather suspect also here a problem in exact positioning of the GPS antenna. Repeated measurements have to be performed to clarify this discrepancy. Regarding the achieved repeatabilities during our campaign, none of the markers can be regarded as being significantly displaced. The observatory site appears to be stable on the level of accuracy of campaign type GPS measurements.

4. Discussion and outlook

The analysis of the GPS-VLBI tie-measurements using APEX and VTEX indicates the importance of regular measurements under same conditions. The detected shift in the north component of APEX between the 1999–2000 and 2001 campaigns is most probable due to non-identical elevation of the radio-telescope during the different campaigns, maybe due to the usage of different or no pointing models. This problem has to be investigated and further measurement campaigns on more regular intervals have to be and will be performed. With optimised setup of the campaigns, the measurements should allow the monitoring of the three-dimensional tie on a millimetre level.

The spring 2001 footprint measurements show that the local network at the observatory is stable on the accuracy of campaign type GPS measurements. No obvious displacement of any marker has been detected from the comparison of measurements taken in the late eighties / early nineties and spring 2001. Re-measurement of the local and regional footprint at the observatory using GPS is planned to be performed on regular intervals of about two to three years.

For spring 2002 we plan a classical geodetic survey at the observatory focusing on the determination of the IVS reference point in a local and a global reference frame. The survey work will include the installation of a network of survey pillars on the foundation of the radome.

References

[1] Bergstrand, S., Haas, R., and Johansson, J.M., "A new GPS-VLBI Tie at the Onsala Space Observatory", In: N.R. Vandenberg and K.D. Baver (eds.): *Proc. of the First IVS General Meeting*, 128–132, **NASA/CP-2000-209893**, Goddard Space Flight Center, Greenbelt, MD 20771 USA, 2000.

[2] Elgered, G. and Haas, R., "VLBI in the Service of Geodesy 1968–2000: An Onsala perspective", In:

J.E. Conway, A.G. Polatidis, R.S. Booth, and Y. Pihlström (eds.): *Proc. of the 5'th European VLBI Network Symposium*, 209–216, Chalmers University of Technology, Onsala Space Observatory, 2000.

[3] Johansson, J.M., Elgered, G., and Rönnäng, B.O., "The Space Geodetic Laboratory at the Onsala Observatory: Site Information", In: Johansson, J.M., A Study of Precise Position Measurements Using Space Geodetic Systems, Ph.D. Thesis, paper A, A1–A16, Chalmers University of Technology, *Techn. Rep.*, **229**, 1992.

[4] Haas R., Elgered G., and Scherneck, H.-G., "Onsala Space Observatory - IVS Network Station", In: N.R. Vandenberg (ed.): *International VLBI Service for Geodesy and Astrometry, 1999 Annual Report*, 90–93, **NASA/TP-1999-209243**, Goddard Space Flight Center, Greenbelt, MD 20771 USA, 1999.

[5] Hugentobler, U., Schaer, S., Fridez, P., (eds.), "Bernese GPS Software Version 4.2", 515 pp., Astronomical Institute University of Berne, 2001.

[6] Koch, K.R., Fröhlich, H., and Böker, G., "Transformation räumlicher variabler Koordinaten", *Allgemeine Vermessungs-Nachrichten*, **107**, 293–295, 2000.

[7] Potash, R., "Accurate VLBI Geodetic Tie from Onsala VLBI Reference Point to Ground", Report, Interferometrics/GSFC, Nov. 31, 1992.

[8] Scherneck, H.-G., Elgered, G., Johansson, J.M, and Rönnäng, B.O., "Space Geodetic Activities at the Onsala Space Observatory: 25 years in Service of Plate Tectonics", *Phys. Chem. Earth*, **23(7–9)**, 811–823, 1998.

[9] Whitney, A.,R., "Precision Geodesy and Astrometry via Very Long Baseline Interferometry", Ph.D. thesis, Dept. of Electrical Engineering, MIT, Cambridge, MA, 1974.

Session 5

Reference Frames and Astrometric Results

Chopo Ma: Extension of the ICRF, Proceedings of the 15th Working Meeting on European VLBI for Geodesy and Astrometry, p.187–193
http://www.ieec.fcr.es/hosted/15wmevga/proceedings/cma

Extension of the ICRF

Chopo Ma

NASA Goddard Space Flight Center
e-mail: cma@virgo.gsfc.nasa.gov

Abstract

The ICRF is the current defining celestial reference frame and is a catalog of positions of extragalactic objects measured with VLBI. It was derived in 1995 and came into effect on 1 January 1998. Since then two additional catalogs have been produced. ICRF-Ext.1 includes additional data through April 1999 with 59 new sources. The VLBA Calibrator Survey, carried out 1994-1997, has an additional catalog of 1298 dual-frequency and 34 X-band only positions. Because of the atypical observing profile, the analysis of the VLBA survey was different from ICRF and ICRF-Ext.1, and unique systematic errors may be present. Observing and analysis activities to support the extension and refinement of the ICRF are continuing.

1. International Celestial Reference Frame (ICRF)

The ICRF became the defining celestial reference frame on 1 January 1998. It differs from the previous realization FK5 in several fundamental ways, most importantly in using extragalactic radio sources and by assigning the pole and right ascension origin independently of the equator and ecliptic. To provide continuity, however, the pole and origin of the ICRF agree with FK5 within the errors of the latter. There are some small quirks arising from the method used to define the origin and orientation of the predecessor IERS catalog that are seen in the ICRF because of the much smaller errors achieved by modern astrometric measurements. The mean pole modeled by the current IAU 1980 nutation theory is not exactly aligned with the ICRF pole at the reference epoch J2000.0 but is separated by a rotation of $\sim$5 mas about the ICRF x-axis and a rotation of $\sim$17 mas about the ICRF y-axis. The pole position modeled by the new IAU 2000 nutation theory will include these offsets to give correct pole values with respect to the ICRF. Similarly the dynamical equinox of J2000.0 is eastward from the x-axis or origin of the ICRF by $\sim$80 mas. Future fundamental celestial reference frames, whether radio or optical, will also rely on extragalactic objects. The orientation of successive frames will be maintained by a statistical no-net-rotation condition of objects in common. The motion of the equator, ecliptic and equinox are then measured quantities relative to a fixed, quasi-inertial frame currently specified by the measured positions of 212 ICRF defining objects.

The positions of the ICRF objects were derived from dual-frequency VLBI observations and analyzed with state-of-the-art models and estimation methods as of mid 1995. The temporal distribution of data is shown in Fig. 1. It can be seen that substantially more observations were made in the later time intervals. It should also be noted that the sources were observed very nonuniformly. As can be seen in Fig. 2, most sources were observed infrequently while $\sim$100 have the bulk of the observations. This disparity arises from the fact that 95% of the data were from geodetic sessions, which used the strongest compact sources available. Figures 3-7 show the sources in the time intervals in which they were first observed. The fainter dots show the cumulative sources up to the particular period. The ICRF analysis determined the positions of 608 extragalactic sources using $\sim$ 1.6 million observations from 2549 sessions, most of 24-hr duration. The accuracy of individual positions is estimated to be 0.25 mas and the orientation of the coordinate axes is good at the 0.020 mas level. Details of the analysis and results are given in Ma et al. (1998) [1].

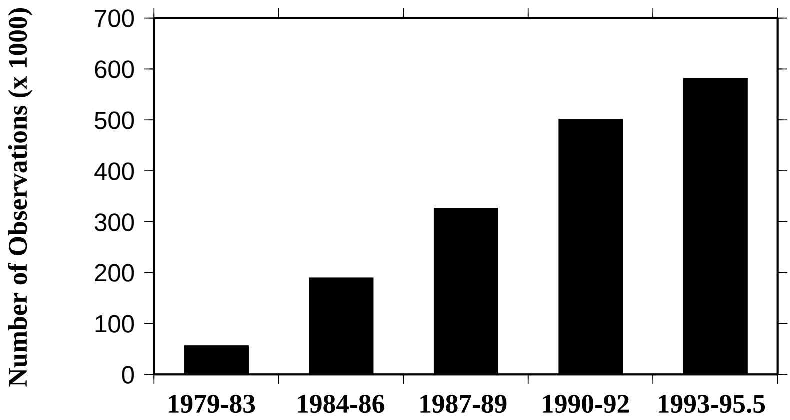

Figure 1. Temporal distribution of observations.

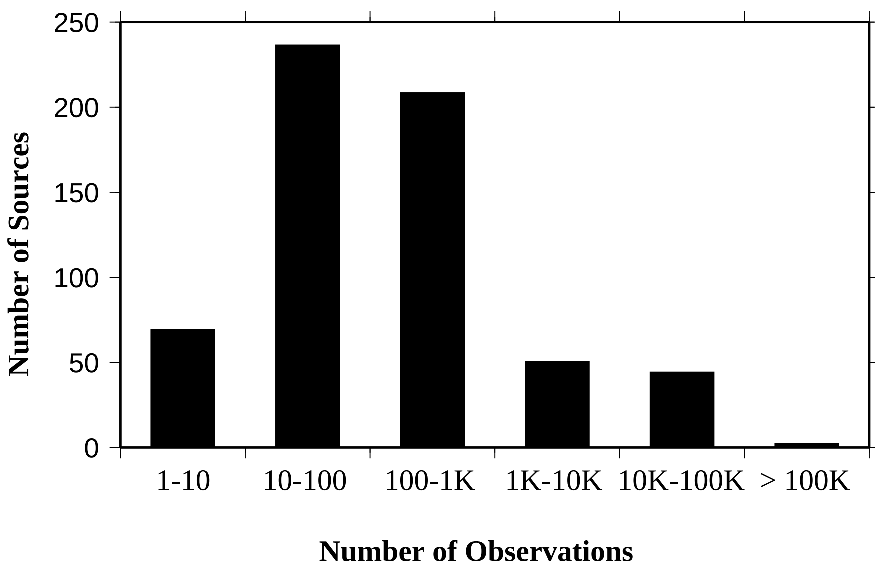

Figure 2. Distribution of observations over sources.

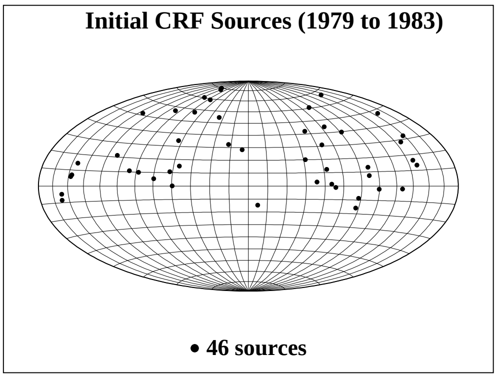

Figure 3. Sources first observed in 1979-83.

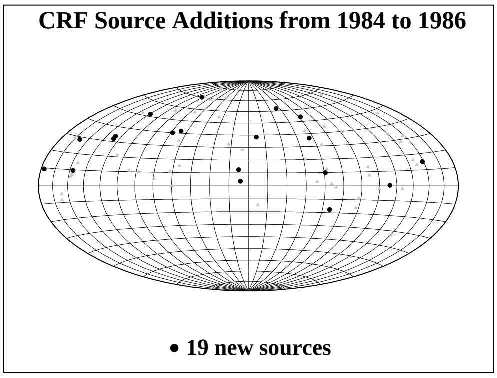

Figure 4. Sources first observed in 1984-86.

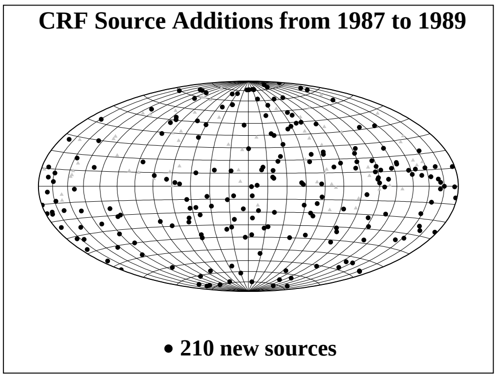

Figure 5. Sources first observed in 1987-89.

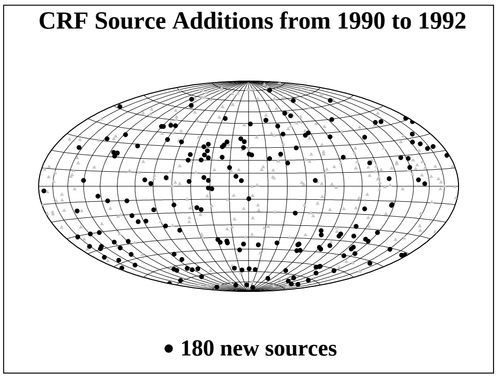

Figure 6. Sources first observed in 1990-92.

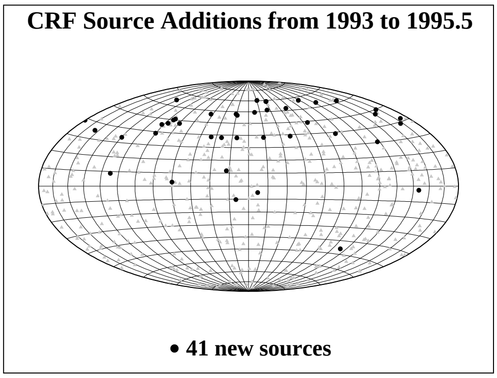

Figure 7. Sources first observed in 1993-95.5.

2. ICRF-Ext.1

VLBI data continued to accumulate for both geodetic and astrometric purposes, and the first extension of the ICRF was assembled in 1999. This extension included data from August 1995 through April 1999, ~600k observations in 461 sessions, and added 59 new sources, shown in Figure 8. The guiding principle of analysis in extending the ICRF is to maintain consistency within the originally stated errors. Thus some limited improvements in analysis were applied but changes that would have introduced systematic differences in the positions of non-defining sources were set aside. The ICRF is defined formally by the positions of the 212 defining sources, so these positions and errors are not changed in the catalog of ICRF-Ext.1. The analysis differences are shown in Table 1. The solution included both the original ICRF observations as well as the later sessions. In passing, it should be mentioned that not all data in the 1995-1999 interval were used. Sessions that included the VLBA and other, mostly geodetic stations were withheld because of some indication of systematic differences with non-VLBA data. These sessions were processed at the VLBA correlator and fringed with AIPS, while the vast majority of the ICRF data were processed at Mark III correlators and fringed with FOURFIT. Considerable progress has been made in understanding the differences, and these sessions most likely will be included in the next ICRF extension.

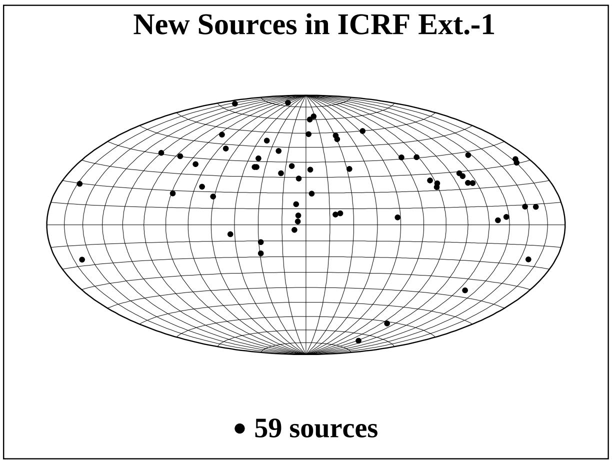

Figure 8. Sources added in ICRF-Ext.1.

Table 1. Comparison of ICRF and ICRF-Ext.1.

Differences:	ICRF	ICRF-Ext.1
troposphere interval	60 min	20 min
high frequency EOP	27 UT1, 36 PM	41 UT1, 57 PM
axis offsets	global	by session
troposphere mapping function	MTT	NMF

3. VLBA Calibrator Survey

A group led by A. Beasley carried out a very different astrometric program to provide better positions of radio sources for phase referencing. In each of ten dual-frequency sessions between 1994-1997 a particular declination belt was scanned as shown in Table 2. Other sources were observed at intervals of ~1 hr to provide clock and troposphere calibration. In total there were ~150k good observations of the 1811 sources attempted. Most target sources were observed in one or two scans. The astrometric analysis was done by the Goddard VLBI group.

Table 2. VLBA Calibrator Surveys

session		declination	
		south limit	north limit
1	$94AUG12XW	50	62
2	$95APR19XW	60	80
3	$95JUL15XW	0	13
4	$96MAR13XW	12	25
5	$96MAY15XW	24	35
6	$96JUN07XW	34	45
7	$96AUG10XW	43	52
8	$97MAY07XW	-15	0
9	$97JUL02XW	-27	-14
10	$97AUG27XW	-29	-17

The observing geometry of the calibrator survey was quite different from usual geodetic and astrometric sessions. Geodetic sessions attempt to observe uniformly the entire mutually visible sky as well as the local sky at each station. In the calibrator sessions these conditions were not met, and it is possible that the systematic errors are rather different. For this reason the astrometric analysis of the calibrator survey was somewhat modified from ICRF-Ext.1. The positions of sources with small errors in ICRF-Ext.1 were held fixed. Sources not in ICRF-Ext.1 and sources with large errors in ICRF-Ext.1 were adjusted. The time interval for troposphere parameters was extended to one hour. To provide the most complete information for phase referencing, a second solution using only X-band data was made to estimate positions of 34 sources that had no successful S-band observations. In addition there were three close pairs whose data were not usable because the fringe processing locked onto different centroids at different observing geometries. The new sources (1298 dual-frequency and 34 only X-band) are shown in Figure 9. The distribution of the semi-major axes of the position error ellipses is given in Figure 10. Figure 11 shows the density of the new calibrator sources. The grey scale indicates the number of sources in a disk of 5 degrees radius.

4. ICRF activities

Ongoing ICRF activities include both observation programs and analysis. The current weakness of the ICRF in the Southern Hemisphere is being ameliorated by a mapping and astrometric program using Australian and Asia-Pacific stations. The mapping program observes with S2 equipment at X-band while the astrometry program records standard dual-frequency using Mark IV. In the north 50 new sources have been successfully observed using the EVN to fill specific gaps, and another 100 sources are planned. A small portion of certain geodetic sessions is used to observe ICRF sources so that each ICRF source, except in the far south, is observed recurrently.

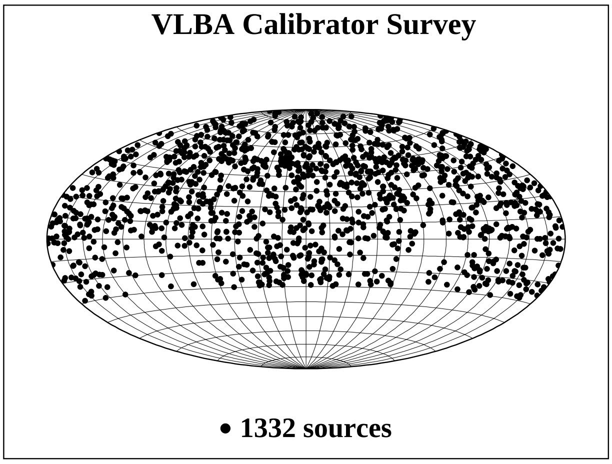

Figure 9. Sources with new positions from the VLBA Calibrator Survey.

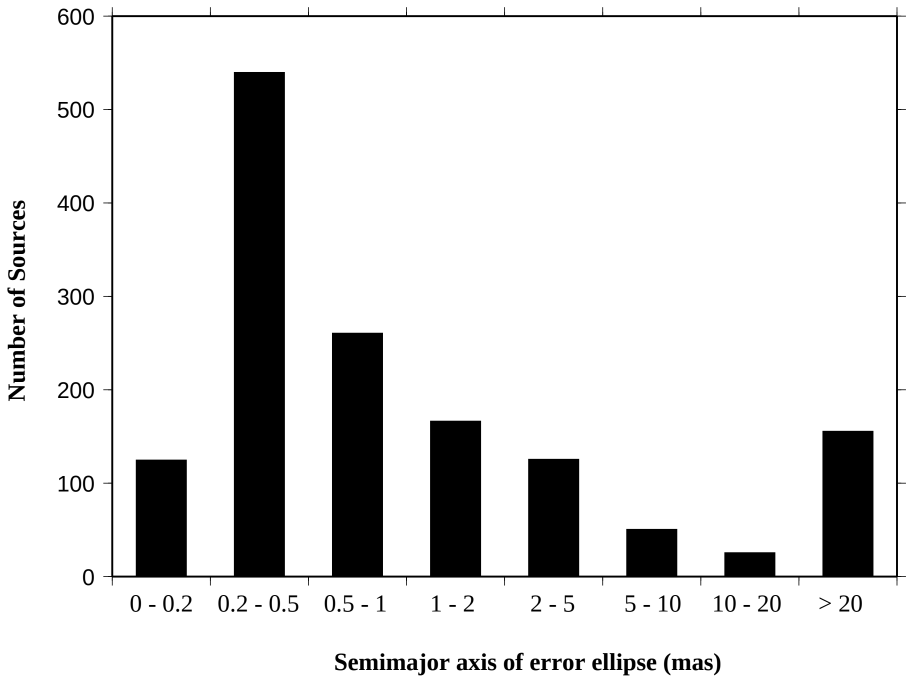

Figure 10. Distribution of errors of new VLBA Calibrator Survey positions. The error is the semi-major axis of the position error ellipse.

The current analysis efforts are directed both to further extensions of the ICRF and also to changes that will cause the next ICRF realization to be substantially better. These changes include modeling, particularly for the troposphere, editing and data weighting. The effect of source structure on astrometric stability is being studied although its general application in the ICRF is uncertain. An overall goal of VLBI analysis is to integrate the generation of TRF, CRF and EOP results in a single solution with minimal differences with results from solutions optimized separately for each type of output.

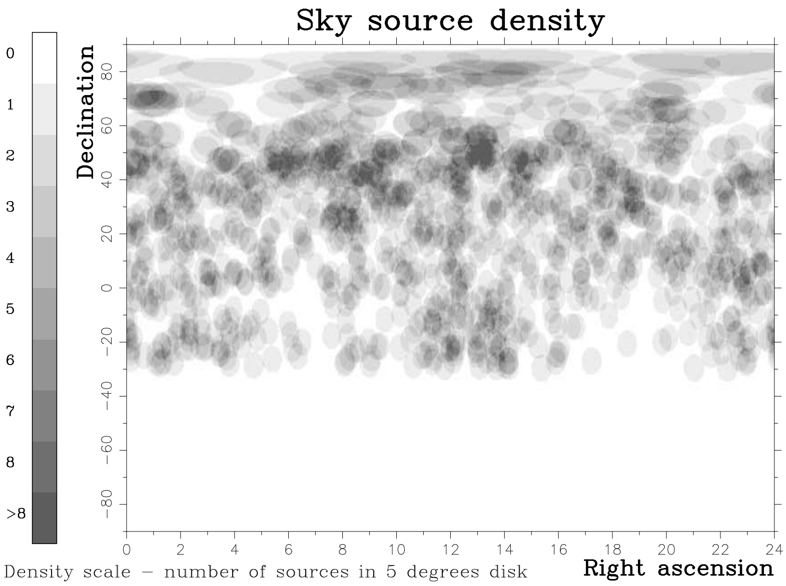

Figure 11. Density of sources in the VLBA Calibrator Survey. Grey scale shows the number of sources within a disk of 5 degrees radius.

References

[1] Ma, C, Arias, E.F., Eubanks, T.M., Fey, A.L., Gontier, A.-M., Jacobs, C.S., Archinal, B.A., and Charlot, P., "The International Celestial Reference Frame as Realized by Very Long Baseline Interferometry", Astron. J., 116, 516-546, 1998.

Patrick Charlot et al.: ITRF2000 Positions of Non-geodetic Telescopes in the European VLBI Network, Proceedings of the 15th Working Meeting on European VLBI for Geodesy and Astrometry, p.194–200
http://www.ieec.fcr.es/hosted/15wmevga/proceedings/charlot

ITRF2000 Positions of Non-geodetic Telescopes in the European VLBI Network

Patrick Charlot [1], *Robert Campbell* [2], *Walter Alef* [3], *Kazimierz Borkowski* [4], *John Conway* [5], *Anthony Foley* [6], *Simon Garrington* [7], *Alexander Kraus* [3], *Axel Nothnagel* [8],*Ojars Sovers* [9],*Corrado Trigilio* [10],*Tiziana Venturi* [11],*Huang Xinyong* [12]

1) *Observatoire de Bordeaux – CNRS/UMR 5804*
2) *Joint Institute for VLBI in Europe*
3) *Max-Planck-Institut für Radioastronomie*
4) *Nicolaus Copernicus University, Torun Centre for Astronomy*
5) *Onsala Space Observatory*
6) *Netherlands Foundation for Research in Astronomy*
7) *MERLIN/VLBI National Facility, Jodrell Bank Observatory*
8) *Geodetic Institute of the University of Bonn*
9) *Remote Sensing Analysis Systems, Inc. – Jet Propulsion Laboratory*
10) *Instituto di Radioastronomia, Stazione VLBI Noto*
11) *Instituto di Radioastronomia, CNR*
12) *Shanghai Observatory, Chinese Academy of Sciences*

Contact author: Patrick Charlot, e-mail: `charlot@observ.u-bordeaux.fr`

Abstract

The European VLBI Network (EVN) has conducted a dedicated non-standard geodetic VLBI experiment in November 2000 with the goal of improving the positions of three non-geodetic EVN telescopes (Jodrell Bank, Torun, Westerbork). The positions of these telescopes were previously known to a few meters only, which is not sufficient for accurate processing of VLBI experiments conducted in phase-referencing mode. The observing frequency was 5 GHz, the highest common frequency available at all telescopes. Observations and data analysis are discussed with special emphasis on the effects of the ionosphere, the dominating error source in this single-frequency experiment. Assessment of the quality of the results indicates that the new estimated telescope positions are accurate to about 5 cm.

1. Introduction

The European VLBI Network (EVN) is an array of radio telescopes[1] spread throughout Europe and Asia, which conducts VLBI observations of radio sources, generally for astrophysical purposes. Some of these telescopes also participate regularly in dual-frequency (S- and X-band) geodetic campaigns [1], and thus have highly-accurate geodetic positions. By contrast, some other EVN telescopes, not equipped with S/X radio receivers, have poorly known positions because they have never participated in such campaigns. The major telescopes in the latter category are located at Jodrell Bank (United Kingdom), Torun (Poland) and Westerbork (Netherlands).

Inaccuracy in the terrestrial coordinates of the above antennas has been a major limitation for EVN observations with the phase-referencing technique. This technique, now commonly used for imaging weak radio sources, alternates observations between a target source and a nearby calibrator, and requires accurate knowledge of the VLBI geometrical model to be successful [2]. To overcome this situation, a dedicated geodetic VLBI experiment was carried out by the EVN in November 2000, with the aim of improving those poorly known telescope positions. The following sections present the design of this non-standard geodetic experiment, the data analysis scheme,

[1] see the list of telescopes at http://www.jive.nl/jive/evn/network/network.html

and the results of these observations. The accuracy of the new estimated telescope positions is discussed in Section 5.

2. Experiment design and observations

Observations were carried out during a 24-hour period starting at 9:30 UT on November 23, 2000, with a network consisting of four geodetic telescopes (Effelsberg, Medicina, Noto, Shanghai) and five non-geodetic telescopes located at Cambridge, Jodrell Bank, Onsala, Torun, and Westerbork. An additional geodetic antenna (Urumqi) was scheduled but could not observe because of technical problems. At Jodrell Bank, the Mk2 telescope was used, while at Onsala, the 25 m antenna (Onsala85) was employed. The option of observing with a single telescope (antenna 7) at Westerbork was preferred to using the phased-array because the effective phase centre of the array (and therefore the geodetic position) might vary when the array configuration is changed, for example if some antennas are switched in or out of the array.

Unlike standard dual-frequency geodetic observations, this experiment was carried out at the single frequency of 5 GHz, the highest frequency available at all observing telescopes. A specific bandwidth synthesis scheme recording 8 frequency channels, each 8 MHz-wide, spread over 108 MHz was designed for this experiment. This bandwidth was chosen based on the common frequency range between telescope receivers which was about 120 MHz. The individual channel frequencies were 4906.99, 4909.99, 4918.99, 4936.99, 4969.99, 4993.99, 5008.99 and 5014.99 MHz. Data from the MERLIN telescope at Cambridge were recorded at Jodrell Bank via a 200-km 28-MHz microwave link and thus had only a limited bandwidth. Due to this mode of transmission, path length variations between Cambridge and Jodrell Bank could not be measured and removed from the VLBI data in the standard automatic way.

Scheduling was carried out with the NASA SKED program in order to optimize the sky coverage at each telescope as in standard geodetic experiments. A total of 20 strong sources selected from the International Celestial Reference frame (ICRF) catalog [3], well spread in right ascension and between $-25°$ and $80°$ declination, was observed for this purpose with generally 5 to 15 scans on each of them. Integration times ranged from 1 to 6 min and were set to obtain signal to noise ratios larger than 100. Low elevation observations ($< 10°$) were avoided to limit systematic errors caused by the ionosphere.

3. Data analysis and modeling

The raw data bits were correlated with the Mark IV data processor in Bonn, Germany, and exported through a geodetic data base file. Further analysis of the bandwidth synthesis delay and delay rate was conducted with the MODEST software [4] after converting the data into NGS format. The overall analysis strategy aimed at fixing all "known" parameters of the VLBI model to limit possible biases and systematic errors caused by improper knowledge of the ionosphere, which is the dominant error at this relatively low observing frequency.

Following this scheme, the coordinates of all extragalactic sources were held fixed at their ICRF values. Similarly, the coordinates of the geodetic telescopes were held fixed at their values in the International Terrestrial Reference Frame, namely the ITRF2000[2]. The coordinates of the non-geodetic antenna Onsala85 were derived from those of the nearby geodetic antenna Onsala60 using a local tie measured with X-band VLBI in the early 1980's [5] and were also held fixed. The Earth orientation parameters were adopted from the IERS combined series C04[3], which is consistent at the sub-centimeter level with the above terrestrial and celestial reference frames. In all, only clocks

[2]ITRF2000 coordinates are available at http://lareg.ensg.ign.fr/ITRF/

[3]IERS combined Earth orientation parameters are available at http://hpiers.obspm.fr/eop-pc/

(using a time-linear model with breaks when needed), tropospheric zenith delays (see below), and the coordinates of the non-geodetic telescopes (except Onsala85) were estimated.

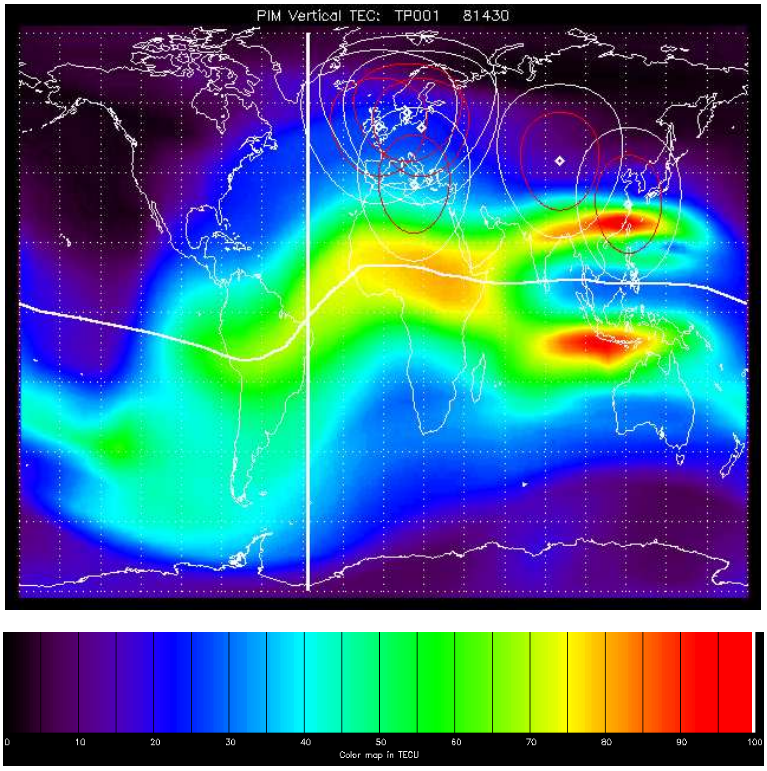

Figure 1. Global ionospheric map showing the vertical TEC calculated by PIM at 14:30 UT on November 23, 2000, with color scale in TEC units (1 TECU=10^{16}electrons/m^2). The thick vertical line indicates the longitude of the Sun, while the line orientated East-West represents the magnetic equator. “Circles” around selected stations show intersections of constant-elevation lines of sight (0° for white circles, 30° for red circles) with an altitude of 500 km, representing a maximal value for the height of the F_2-layer peak.

The troposphere was modeled using the Niell mapping function [6], estimating one zenith tropospheric delay per station for the whole 24-hour period with a priori values derived from meteorological measurements. This scheme differs from that used in standard geodetic experiments where new zenith tropospheric delays are estimated at much shorter time intervals, but was preferred for this specific dataset to limit the number of estimated parameters. The ionosphere was modeled using the Parameterized Ionospheric Model (PIM), which is a theoretical model of ionospheric climatology developed at USAF Phillips Laboratory [7] and freely available. This model determines the electron density at a given point of the ionosphere (defined by latitude, longitude and height) as a function of local time, latitude, season, solar activity, geomagnetic activity, and interplanetary magnetic-field direction. Integration along a given direction then provides the total electron content (TEC), which serves as the basis to calculate the ionospheric delay. For our analysis, ionospheric delays were determined directly along the lines of sight between the stations/observed sources using a specific version of PIM developed for application to VLBI astrometry [8], and added afterwards to the ionospheric-free VLBI model implemented in MODEST. Figure 1 shows a global map of vertical TEC, representative of the ionospheric morphology at 14:30 UT on the day of our observations. Examination of similar maps at various times during the experiment revealed that the ionosphere was relatively stable over Europe on that day, but was significantly disturbed over the eastern part of China where the Shanghai telescope is located (see Fig. 1).

4. New telescope positions

Based on the above analysis and modeling, the post-fit rms residuals were 292 ps for delay with a χ^2 per degree of freedom of 1.03, and 230 fs/s for delay rate with a χ^2 per degree of freedom of 1.05. The data from two telescopes, Shanghai and Cambridge, have not been used in the analysis. All baselines to Shanghai showed larger residuals, most probably caused by ionospheric disturbances improperly modeled by PIM (see above). It was also decided to discard the observations from Cambridge because this telescope had usable data in only one frequency channel. This was, however, not a major inconvenience for the project, since the coordinates of Cambridge could be derived from those of Jodrell Bank by using estimates of the Cambridge-Jodrell Bank baseline, measured to a few centimeter accuracy from MERLIN observations of source pairs. Figure 2 shows the rms delay residuals as a function of baseline length with a least-squares linear fit to the data. There is a statistically-significant trend indicating an increase of the residuals with baseline length, which is expected if the ionosphere is the dominating error in the model. For short baselines, mismodeling is attenuated because ionospheric variations are correlated at nearby stations and partially cancel out when calculating the differential delay contribution.

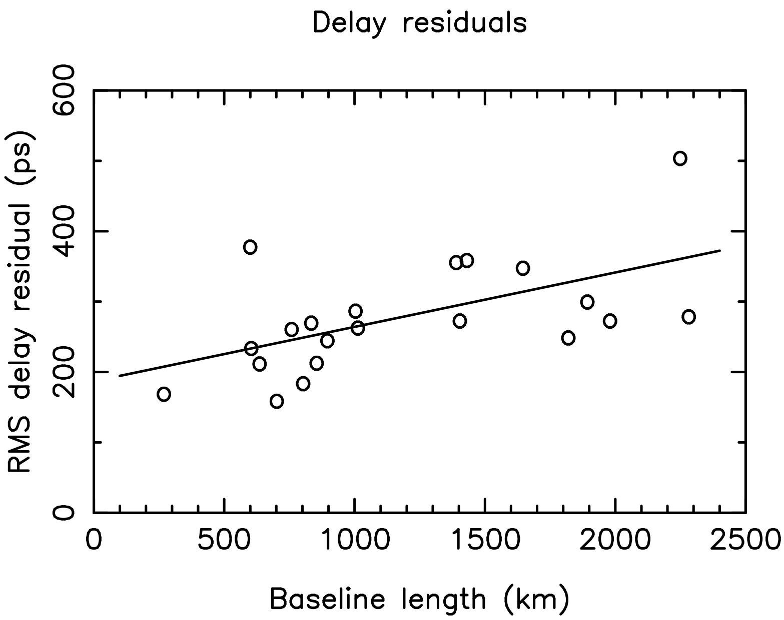

Figure 2. Rms delay residuals (in ps) as a function of baseline length (excluding baselines to Shanghai).

The estimated geodetic positions of Jodrell Bank, Torun, and Westerbork derived from this analysis, are given in Table 1 together with the shifts to the original coordinates (as previously available from the station catalog of the SCHED scheduling software). These shifts are listed for each telescope on the line immediately following its estimated coordinates. For completeness, the coordinates and shifts of the non-geodetic antenna Onsala85 are also listed, although these were not estimated in the analysis (see above). One notes that the corrections to the original coordinates of the four telescopes are as large as several meters. Uncertainties in the individual coordinates (one-sigma error derived from the least-squares fit) range from 1 to 3 cm, which is relatively small for such single-frequency observations. To determine whether these are realistic, alternate analyses estimating "known" parameters have been carried out, as described below.

Table 1. Coordinates of four EVN telescopes in ITRF2000 (epoch 1997.0) and shifts to original values.

Telescope	X (m)	Y (m)	Z (m)
Jodrell Bank	3822846.76 ± 0.02	-153802.28 ± 0.01	5086285.90 ± 0.02
	4.10 ± 0.02	-2.15 ± 0.01	-1.32 ± 0.02
Torun	3638558.51 ± 0.02	1221969.72 ± 0.01	5077036.76 ± 0.03
	0.51 ± 0.02	2.72 ± 0.01	-4.24 ± 0.03
Westerbork	3828651.29 ± 0.02	443447.48 ± 0.01	5064921.57 ± 0.02
	4.11 ± 0.02	-2.54 ± 0.01	-1.51 ± 0.02
Onsala85	3370966.126 –	711465.954 –	5349664.023 –
	-2.055 –	1.037 –	-0.090 –

5. Assessment of accuracy

Validation of our analysis and results was first considered by estimating the coordinates of the geodetic telescopes. For this purpose, four alternate analyses, each estimating in turn the coordinates of one of the geodetic telescopes (including Onsala85) in addition to those of the non-geodetic telescopes, have been carried out. Results are given in Table 2 in terms of corrections to ITRF2000 coordinates. Since these coordinates are known to sub-centimeter accuracy, any significant correction would have to be attributed to deficiencies of our analysis. Table 2 shows that this is not the case since all estimated corrections are within one-sigma error. This is an indication that our derived uncertainties, although relatively small, are probably realistic.

Table 2. Estimated corrections to ITRF2000 coordinates of EVN telescopes at geodetic sites.

Telescope	ΔX (m)	ΔY (m)	ΔZ (m)
Effelsberg	0.00 ± 0.02	0.00 ± 0.01	-0.01 ± 0.03
Medicina	-0.02 ± 0.03	0.01 ± 0.01	0.03 ± 0.03
Noto	-0.01 ± 0.03	0.00 ± 0.01	-0.02 ± 0.02
Onsala85	0.00 ± 0.02	-0.01 ± 0.01	-0.03 ± 0.03

An additional test consisted in estimating the telescope axis offsets. Again, these should be known to centimeter accuracy and no significant deviations should be found. For this test, a single analysis estimating the axis offsets of all telescopes together with the coordinates of the non-geodetic telescopes, was performed. The axis offset corrections derived from this analysis are given in Table 3, also including antenna types and a priori values for completeness. The results in Table 3 show that the estimated corrections are not significant for six of the telescopes, confirming the previous indication that parameter uncertainties derived from our analysis appears to be realistic. For Jodrell Bank, however, a correction significant at the 3-sigma level (-0.19 ± 0.06 m) is found. It is not yet understood whether this correction might be real or whether it is an artefact from our data. When estimating this parameter, the X and Z coordinates of Jodrell Bank shift by 15 to 20 cm, which is larger than the uncertainties given in Table 1. These coordinates are thus subject to caution (at such a level of accuracy) until the origin of the axis offset correction is understood.

Finally, a qualitative evaluation of our results was accomplished by comparing phase-referenced maps made with the original and newly-derived telescope coordinates. For this comparison, we used data from a 6-cm phase-reference test experiment consisting of 1-hour of interleaved observations on the close pair 3C345/J1635+380 (separation of 2.25°). Figure 3 shows the maps of J1635+3808

Table 3. Antenna types, a priori axis offsets and estimated corrections.

Telescope	Antenna type	Axis offset (m)	Correction (m)
Effelsberg	AZEL	0.00	0.01 ± 0.02
Jodrell Bank	AZEL	0.458	-0.19 ± 0.06
Medicina	AZEL	1.83	-0.01 ± 0.03
Noto	AZEL	1.83	0.00 ± 0.02
Onsala85	EQU	2.15	0.01 ± 0.01
Torun	AZEL	0.00	-0.02 ± 0.06
Westerbork	EQU	4.95	0.02 ± 0.02

AZEL = azimuth-elevation mount, EQU = equatorial mount

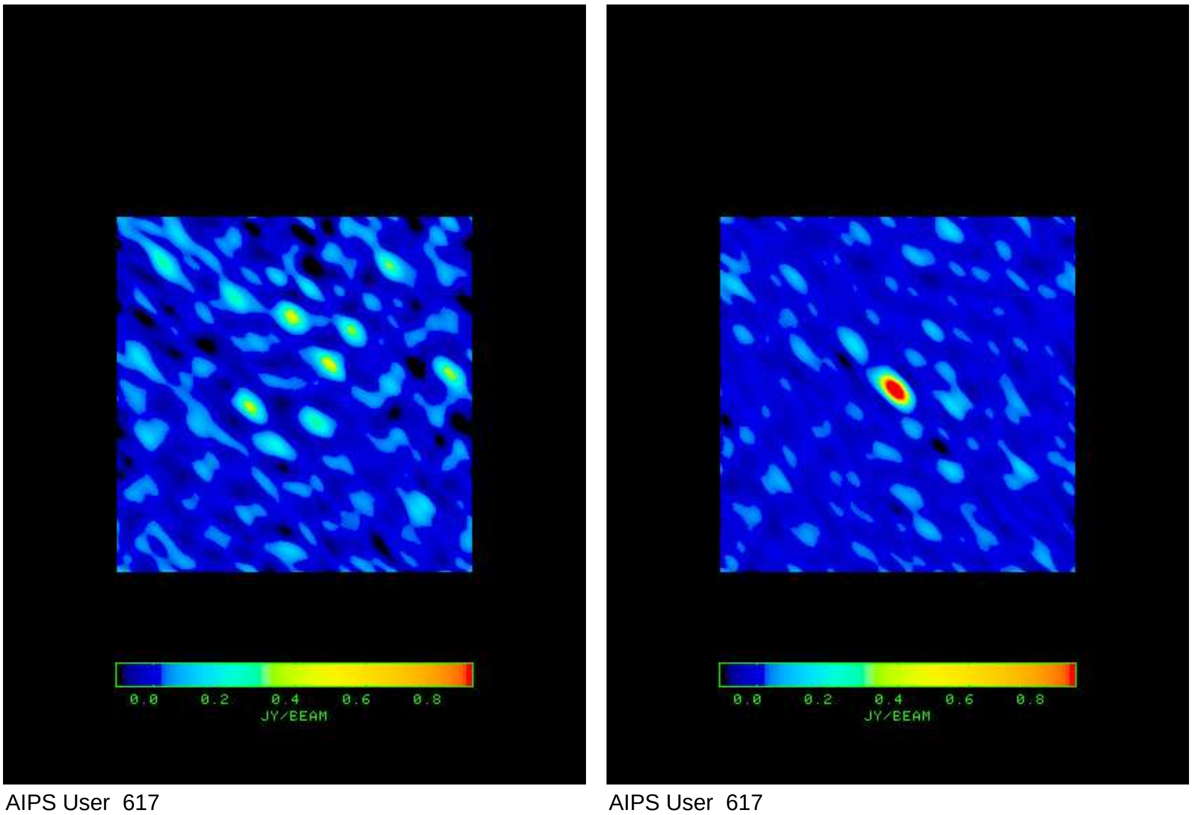

Figure 3. Phase-referenced maps of J1635+380 using 3C345 as phase calibrator. *Left:* image made using the original telescope coordinates. Peak flux is 0.49 Jy/beam. *Right:* image made using the newly-derived telescope coordinates in Table 1. Peak flux is 1.55 Jy/beam. Both images are plotted with the same color scale, ranging from -0.1 to 0.9 Jy/beam.

for the two cases. The problems with the phase-reference map using the original telescope positions are evident, as is the improvement in focusing the flux into the source and the reduction of the off-source noise when the newly-derived positions are used. This decisive test validates definitively our estimated telescope positions, and alternately demonstrates that phase-referencing can only be successful if an accurate geometrical VLBI model is available.

6. Conclusion

Based on a non-standard 5 GHz geodetic experiment conducted in November 2000, improved coordinates of three non-geodetic EVN telescopes have been obtained. These newly-derived positions are accurate to about 5 cm, a factor of 100 improvement over previous values. Such improved coordinates will be largely of benefit to VLBI observations with the EVN, especially those conducted with the phase-referencing technique. The new telescope positions, and others derived from these via local ties, have been made available to the EVN users[4] and VLBI correlators that regularly process data from EVN telescopes. Further investigation will continue, in particular to determine the as-yet-unidentified origin of the Jodrell Bank axis offset correction, but also more generally to evaluate the influence of the ionosphere, troposphere and clock modeling on these results.

Acknowledgements

We are indebted to a number of people who have indirectly contributed to the success of this project. Nancy Vandenberg provided us with a version of SKED that can deal with single-frequency setups and made useful suggestions regarding the design of this experiment. Chris Jacobs, Chopo Ma and Dave Shaffer also helped in the initial stages of the experiment design, while Ed Himwich answered last-minute critical questions. The data were exported to a geodetic data base file with help from Arno Müskens and Izabela Rottmann. Special thanks are due to Richard Porcas for stimulating discussions and to Huib Jan van Langevelde for continued interest in this project. The observations and analysis presented in this report were carried out for the benefit of the EVN with support from the European Commission's IHP programme Access to Research Infrastructures under contract No. HPRI-CT-1999-00045.

References

[1] Campbell, J., Nothnagel, A.: 2000, European VLBI for Crustal Dynamics, J. of Geodynamics, Vol. 30, p. 321.

[2] Beasley, A. J., Conway, J. E.: 1995, VLBI Phase-Referencing, Very Long baseline Interferometry and the VLBA, J. A. Zensus, P. J. Diamond, and P. J. Napier (eds.), ASP Conf. Ser., Vol. 82, p. 327.

[3] Ma, C., Arias, E. F., Eubanks, T. M., Fey, A. L., Gontier, A.-M., Jacobs, C. S., Sovers, O. J., Archinal, B. A., Charlot, P.: 1998, The International Celestial Reference Frame as Realized by Very Long Baseline Interferometry, AJ, 116, 516.

[4] Sovers, O. J., Jacobs, C. S.: 1996, Observation Model and Parameter Partials for the JPL VLBI Parameter Estimation Software "MODEST"–1996, JPL Publication 83-39, Rev. 6, August 1996.

[5] Lundqvist, G.: 1982, Precision Surveying at the 1-mm level using radio interferometry, Proceedings of Symposium No. 5–IAG, NOAA Technical Report NOS 95 NGS 24, p. 99.

[6] Niell, A. E.: 1996, Global mapping functions for the atmosphere delay at radio wavelengths, JGR, 101, 3227.

[7] Daniell, R. E., Brown, L. D., Anderson, D. N., Fox, M. W., Doherty, P. H., Decker, D. T., Sojka, J. J., Schunk, R. W.: 1995, Parameterized ionospheric model: A global ionospheric parameterization based on first principles models, Radio Sci, 30, 1499.

[8] Campbell, R. M.: 1999, Ionospheric corrections via PIM and real-time data, New Astronomy Reviews, 43, 617.

[4] a recipe for incorporating station coordinate improvements into AIPS analysis of already-correlated data is also available at http://www.jive.nl/jive/evn/user_guide/stapos.html

Richard W. Porcas: Finding astrometric reference sources using the NVSS Survey, Proceedings of the 15th Working Meeting on European VLBI for Geodesy and Astrometry, p.201–207
http://www.ieec.fcr.es/hosted/15wmevga/proceedings/porcas2

Finding astrometric reference sources using the NVSS Survey

Richard W. Porcas

Max-Planck-Institut fuer Radioastronomie
e-mail: `porcas@mpifr-bonn.mpg.de`

Abstract

The technique of phase-reference mapping can be used both for mapping faint radio sources and for relative astrometry measurements. One astrophysically interesting application of the latter is the registration of source maps made at different frequencies; for this the "reference" source should itself be achromatic. Here I describe a case study where the "target" source (the gravitational lens system B0218+357) is strong, so that phase-reference maps of the achromatic reference sources can be made, using the target source phase. This permits the use of relatively weak reference sources. I describe the selection of suitable sources from the NVSS survey, and MERLIN and EVN investigations of their compactness.

1. Introduction

Studies of the frequency-dependence of radio source structures can play an important role in astrophysical investigations. However, the use of VLBI *hybrid* maps, which are made using phase self-calibration, limits such studies because the structures at difference frequencies can only be registered using intelligent guess-work. The "standard" solution is to make *phase-reference* maps instead, which preserve the relative astrometry with respect to a phase calibrator, whose structure is assumed achromatic (see Porcas and Rioja, 1996). This assumption may be wrong, especially since many compact radio sources have asymmetric, and frequency-dependent, core-jet structures at the mas-level (see Porcas and Patnaik, 1995; Porcas and Rioja, 1997).

The astrometric registration of weak sources requires the reference source to be strong, since it must act as a phase, as well as an astrometric, reference. If the source being studied is strong, however, the *target* and *reference* roles can be reversed for the phase-referencing; phases are determined on the strong source, allowing a phase-reference map of the astrometric reference to be made. This procedure permits use of weak reference sources, with a number of attendant advantages: **(a)** There are many more weak sources than strong ones, allowing choice of a reference much closer to the target, and thus reducing errors in the relative phase arising from deficiencies in the correlator model. **(b)** It easily accommodates use of multiple reference sources, reducing the impact of any frequency-dependent structures which they may have. **(c)** Weaker sources may well be smaller and less active, resulting in structures which may have less frequency and temporal dependence.

The gravitational lens system B0218+357 is a relatively strong radio source whose frequency-dependent properties are of considerable astrophysical interest (Porcas and Patnaik, 1995). In preparation for a multi-frequency VLBI investigation, therefore, I have been searching the lists of known, weak radio sources, in order to select suitable astrometric reference candidates. Desireable properties are compactness, a flat radio spectrum, and closeness on the sky to B0218+357. In the following sections I describe the source selection process and follow-up MERLIN and EVN investigations of their compactness.

2. Selecting the candidates

The basis for the reference source search was the NRAO VLA Sky Survey(NVSS; Condon et al, 1998) which lists 2 million sources north of declination –40° stronger than 2.5 mJy at 1.4 GHz. Within 2° of 0218+357 there are 122 sources stronger than 15 mJy, of which 68 are unresolved by the 45" NVSS beam. The Westerbork Northern Sky Survey (WENSS: Rengelink et al, 1997), which lists sources stronger than 18 mJy at 325 MHz, was then used to select out those sources with spectral indices flatter than –0.47, resulting in a preliminary list of 14 sources. Additional flux densities were obtained at 5 GHz from the NRAO GB6 survey (Gregory et al, 1996) and at 8.4 GHz from the CLASS gravitational lens search project (Browne et al, 2001). On the basis of these, 3 of the 14 sources were excluded from further consideration. The remaining candidate reference sources are listed in Table 1, together with positions from the NVSS (accuracy ca. 1 arcsec), angular separation from B0218+357, flux densities and WWW survey references.

Table 1. Candidate reference source list from the NVSS Survey

SOURCE (1950)	RA (2000)	DEC (2000)	SEP deg	FLUX DENSITIES (mJy) 0.3	1.4	5.0	8.4 (GHz)
0210+366	02 13 48.24	+36 52 34.8	1.74	56	32	41	131
0212+344	02 15 49.41	+34 43 04.6	1.62	213	151	114	120
0213+340	02 16 12.47	+34 18 15.5	1.91	20	19		
0215+364	02 18 50.04	+36 40 42.8	.87	156	129	102	89
0216+357	02 19 42.31	+35 37 43.9	.42	48	42	19	
0219+372	02 22 15.48	+37 31 16.0	1.60	144	109	121	90
0220+371	02 23 34.77	+37 20 46.7	1.49	23	19		
0222+369	02 25 27.29	+37 10 27.9	1.52	373	196	137	170
0223+361	02 26 49.02	+36 22 56.7	1.24	24	35	42	36
0224+359	02 27 48.89	+36 11 28.1	1.38	61	46	45	38
0224+343	02 27 59.90	+34 32 41.2	1.98	50	41		40

Flux density references:

0.3 GHz WENSS http://www.strw.LeidenUniv.nl/%7Edpf/wenss/
1.4 GHz NVSS http://www.cv.nrao.edu/nvss/
5.0 GHz GB6 http://www.cv.nrao.edu/~jcondon/gb6ftp.html
8.4 GHz CLASS http://www.jb.man.ac.uk/~njj/glens/class.html

3. MERLIN observations

Observations were made at 5 GHz with the 6-station MERLIN array on 29 April 2001. Each of the 11 candidate reference sources (and 0218+357) was observed for 11 scans, each nominally 4 mins, and the phase-reference source 0233+359 was observed for 2 mins every 6. Visibility amplitudes were calibrated with respect to 3C286, assuming a flux density of 7.09 Jy (which takes account of 3 percent resolution by MERLIN).

Phase-reference maps of all candidates were made using the AIPS package, with uniform weighting, a pixel size of 10 mas, and a circular CLEAN restoring beam of 40 mas. These are presented in Fig. 1. All sources are essentially point-like to MERLIN; the maps indicate the errors in the NVSS positions. Hybrid maps of all sources (using a few iterations of phase self-calibration) were also made, where possible; these recover typically a further 5 - 10 percent of flux. Both 0218+357 and the calibrator 0233+359 are resolved; hybrid maps of these are also shown in Fig 1.

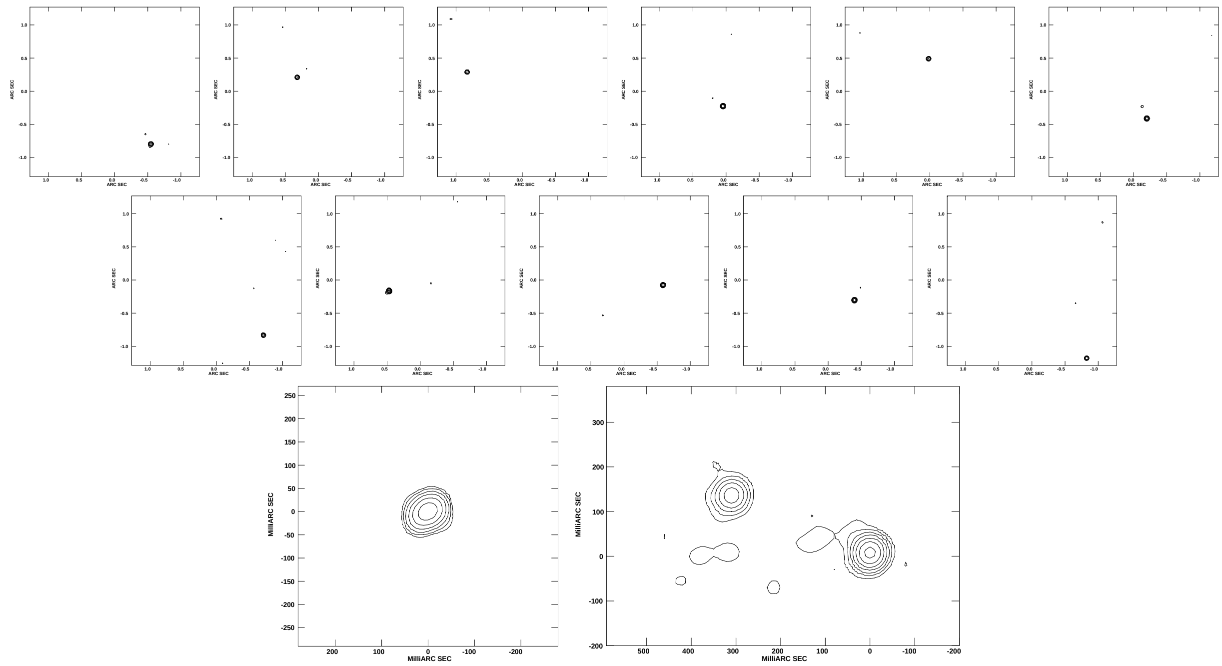

Figure 1. **MERLIN** maps:
Top: Phase-ref. maps of sources **0210+366, 0212+244, 0213+340, 0215+364, 0216+357, 0219+372**
Middle: Phase-ref. maps of sources **0220+371, 0222+369, 0223+361, 0224+359, 0224+343**
Bottom: Hybrid maps of calibrator **0233+359** and gravitational lens **0218+357**
.

The AIPS task JMFIT was used to estimate peak and integrated flux densities (from phase-ref. and hybrid maps), deconvolved source sizes, and corrected positions; these are presented in Table 2. The new MERLIN positions are believed to be accurate to about 10 mas. The spectral index (1.4 to 5 GHz) is also given. The sources 0213+340, 0216+357 and 0220+371 proved too weak for MERLIN self-calibration. Two show steep spectra, and the other is relatively distant from B0218+357, so all 3 were excluded from further consideration.

4. EVN observations

EVN "short observations" were made at 5 GHz on 6th June 2001, from UT 04h–08h, using 9 antennas (Eb, Wb, Jb, On, Mc, Nt, Tr, Ur, Sh) which provide baselines up to 140 million wavelengths. The 8 remaining reference candidates, and the strong fringe-finder source 0234+285, were each observed for 5 scans, of length 3 or 7 minutes, depending on strength. One scan on the MERLIN calibrator 0233+359 was also included. Recording mode 128-8-1 was used, with dual circular polarisations each of total bandwidth 32 MHz. The recordings were correlated at the MPIfR-BKG MKIV correlator in Bonn, with an output integration time of 4s and 32 delay steps. A new task, MK4IN, was used to read the data into AIPS for further analysis.

Analysis of only the LHC polarisation data is described here. Initial amplitude calibration was made using telescope and system data provided by the individual observatories but considerable adjustments proved necessary later. Phase alignment between the 4 "IF" channels was determined from the strong calibrator 0234+285, and residual phases, rates and delays were determined by global fringe-fitting of each scan using AIPS task FRING. All 8 candidate reference sources were detected on even the longest baselines, indicating that they all have compact components within their structures. A plot of the residual (multi-band) delay on the baseline Effelsberg-Shanghai for these 8 is presented in Fig 2, where the zero point is set by the IF calibration scan on 0234+285.

Table 2. Source parameters from MERLIN 5 GHz observations

SOURCE (1950)	RA(1950) hh mm ss	DEC(1950) dd '' ""	FLUX (P.Ref) Peak (mJy/b)	FLUX (P.Ref) Int. (mJy)	FLUX (SELF-Cal) Peak (mJy/b)	FLUX (SELF-Cal) Int. (mJy)	FLUX (SELF-Cal) err (mJy)	MAJxMIN,PA (mas, deg)	SP.I 1.4/5 (GHz)
0210+366	02 10 47.2059	36 38 34.306	98.6	107.8	122.3	128.9	1.0	< 20	+1.09
0212+344	02 12 50.1874	34 29 09.991	125.5	131.9	160.6	169.7	1.1	< 20	+0.09
0213+340	02 13 13.6165	34 04 21.906	10.1	11.3		(12.2	.6)	< 20	-0.35
0215+364	02 15 48.3462	36 26 55.068	82.0	89.2	90.5	97.6	.8	< 20	-0.22
0216+357	02 16 41.5185	35 23 59.052	15.2	16.3		(17.5	.7)	< 20	-0.69
0219+372	02 19 12.2714	37 17 36.589	77.5	82.8	85.1	90.6	.6	< 20	-0.15
0220+371	02 20 31.4653	37 07 10.210	8.0	8.6		(9.2	.5)	< 20	-0.57
0222+369	02 22 23.9316	36 56 56.865	156.6	174.3	171.2	190.2	1.4	< 20	-0.02
0223+361	02 23 46.1806	36 09 29.277	28.5	30.3	30.5	31.7	.4	< 20	-0.08
0224+359	02 24 46.0985	35 58 03.041	31.7	35.0	33.7	37.3	.5	< 20	-0.16
0224+343	02 24 58.7584	34 19 15.771	24.5	25.2	34.0	34.8	.5	< 20	-0.13
0233+359	02 33 34.0175	35 59 39.046			162.6	212.5	.5	32x9,123	
0218+357A	02 18 04.1290	35 42 31.833	570.2	619.4	658.1	707.7	4.6	< 20	
0218+357B	02 18 04.1545	35 42 31.965	143.6	206.4	195.9	240.8	5.0	21x18,153	

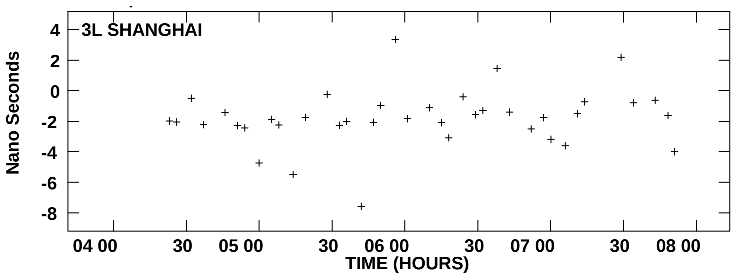

Figure 2. **EVN** multi-band delay fringe-fit residuals on baseline Effelsberg-Shanghai.

The low scatter of ca. 1 nsec confirms the high accuracy (better than 10 mas) of the positions derived from the MERLIN observations.

Plots of the calibrated, scan-averaged visibility amplitudes against u-v distance are given in Fig. 3. All 8 candidate sources show a good fraction of their short-baseline flux-densities on the longest baselines at 140 M-wavelengths. In 4 cases (0210+266, 0215+364, 0219+372, 0222+369) this fraction is ca. 60 percent. Regrettably, the very high uncertainty in the *a priori* amplitude calibration results in a large uncertainty in this fraction; the true fractional visibility at high resolutions may be considerably higher.

Fig. 4 shows the closure-phase on 3 selected baseline-triangles for all 8 candidate reference sources. This quantity is independent of the amplitude and phase calibration and would be zero for an unresolved source. There is little evidence for any significant resolved, asymmetric structure in any of the sources, even on long baselines.

Hybrid maps were made for all sources, using a pixel size of 0.3 mas and a CLEAN restoring beam of 1 mas; they are presented in Fig. 5. Uniform grid weighting and equal station weights were used, in order to emphasize the longest baselines and thus highlight compactness. All 8 candidate reference sources are seen to be dominated by a single, compact component. The poor

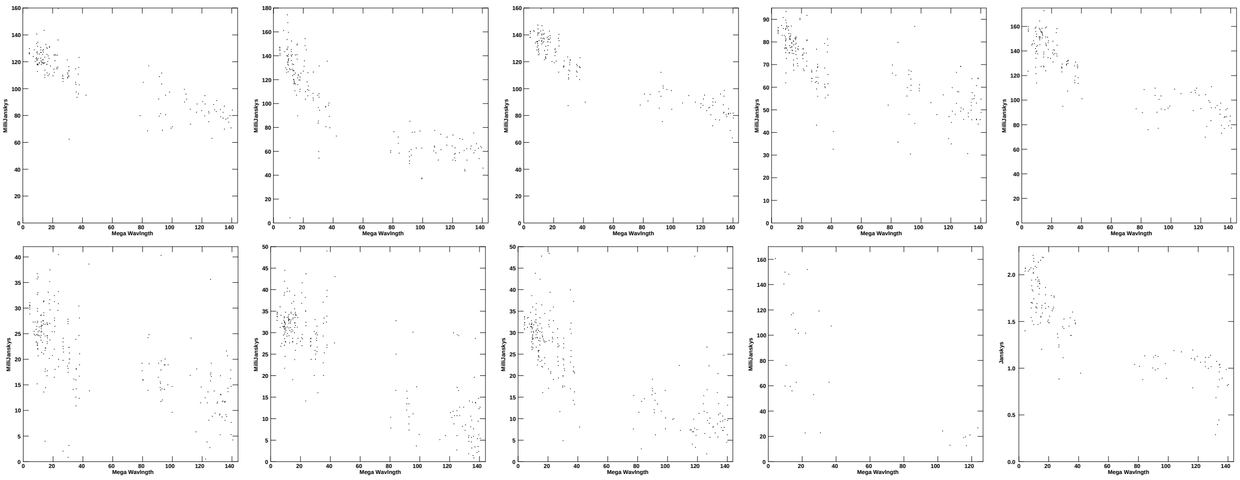

Figure 3. **EVN** visibility plots:
Top: Candidate sources: **0210+366, 0212+344, 0215+364, 0219+372, 0222+369**
Bottom: Candidate sources: **0223+361, 0224+359, 0224+343**, calibrators **0233+359, 0234+285**

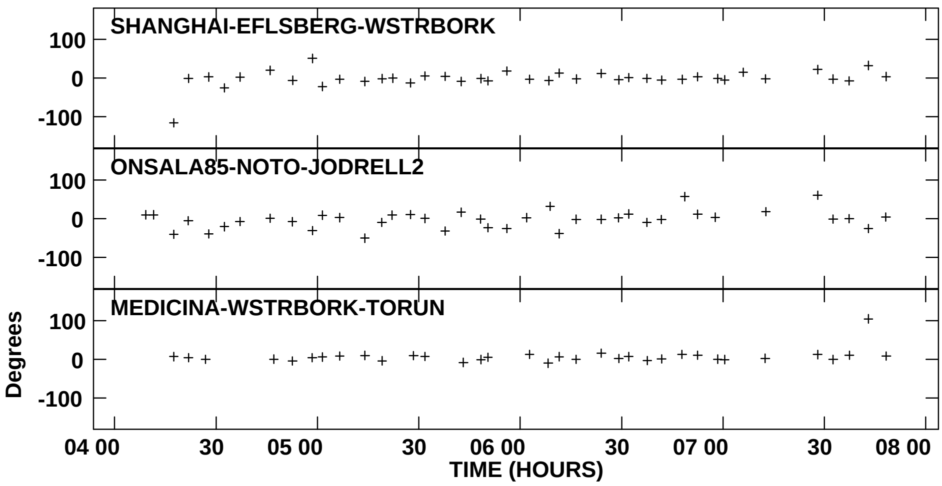

Figure 4. **EVN** closure-phase plots for the 8 candidate reference source

u,v coverage and amplitude calibration of these observations does not allow much information on their extended structures to be obtained.

In order to quantify the "compactness" of each source, two approaches were taken; the results are presented in Table 3. First, the ratio of the correlated flux on the shortest EVN baseline, Effelsberg-Westerbork (S-EW) was compared with the peak flux in the MERLIN hybrid map. The resulting visibility ratio (EW/PK.MERLIN) is close to unity for most sources, verifying the basic EVN flux density scale adopted, and confirming that many sources are unresolved with MERLIN. The relatively strong source 0215+364 has clearly increased in flux by 50 percent in the 5 weeks between the MERLIN and EVN observations. The correlated flux density on the long Effelsberg-Shanghai baseline (S-ES) was then compared with S-EW and the ratio (ES/EW) formed as a measure of high-resolution compactness. The 4 compact sources mentioned above have values ranging from 0.60 to 0.66. Note that the VLBI calibrator 0234+285 has a value of 0.46; its map (Fig. 4) indicates a jet-like feature extending to the North, which is confirmed by other maps of this source. The MERLIN calibrator 0233+359 is heavily resolved. Its EVN map reveals it to be a double, in a PA close to that deduced from the MERLIN data.

For the second approach, the AIPS task JMFIT was used to fit a single, elliptical gaussian

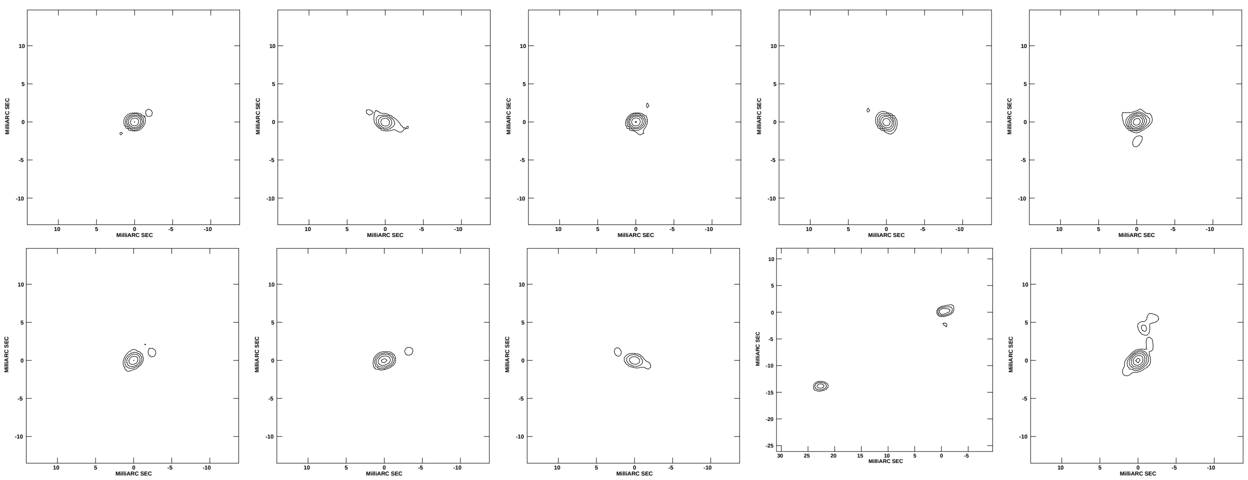

Figure 5. **EVN** hybrid maps:
Top: Candidate sources: **0210+366, 0212+344, 0215+364, 0219+372, 0222+369**
Bottom: Candidate sources: **0223+361, 0224+359, 0224+343**, calibrators **0233+359, 0234+285**

Table 3. Source parameters from 5 GHz EVN observations

SOURCE (1950)	S-EW mJy	S-ES mJy	EW/PK. MERLIN	ES/EW		PEAK mJy	INT. mJy	MAJ x MIN mas x mas	PA deg	SEP mas	PA deg
0210+366	127	85	1.04	0.66		96	112	0.5 x 0.2	93		
0212+344	144	62	0.90	0.42		74	109	1.0 x 0.4	67		
0215+364	140	86	1.55	0.61		100	118	0.6 x 0.3	97		
0219+372	85	51	1.00	0.60		56	71	0.7 x 0.3	47		
0222+369	151	91	0.88	0.61		103	129	0.7 x 0.3	117		
0223+361	31	12	1.02	0.39		15	22	0.9 x 0.4	123		
0224+359	34	6	1.01	0.18		19	30	1.1 x 0.4	107		
0224+343	32	8	0.94	0.26		14	25	1.3 x 0.5	74		
0233+359	161	13	0.99	0.08	SE	27	57	1.7 x 0.4	93		
					NW	36	91	1.8 x 0.7	114	26.8	122
0234+285	2059	957		0.46		1129	1586	0.9 x 0.4	132		

function to the source response in the map. The peak and integrated flux densities are also given in Table 3, along with estimates of the major and minor axis sizes and PA. Because of the poor amplitude calibration, however, these size estimates must be considered unreliable. For 0233+359, two components were fitted.

5. Conclusions

Using the NVSS survey as a starting point, and the WENSS survey and other lists to provide spectral data, 11 candidate reference sources within 2 ° of the strong gravitational lens B0218+357 were found, with flux densities above 15 mJy and flat spectra. Observations with MERLIN established that all these sources were compact on intermediate baselines, although the 3 weakest sources were eliminated as unsuitable. The 4-hour observation with the EVN confirmed that the remaining 8 sources show a high percentage of their flux in a single compact component, even on baselines of 140 million wavelengths; unfortunately, the exact fraction is unclear, due to poor EVN amplitude calibration. The small scatter in the delay deterninations on the longest baselines indicate that the MERLIN positions are accurate to better than 10 mas.

Four of the candidate reference sources with the highest "compactness" fulfill the initial aims of the project - to select compact, hopefully achromatic, astrometric reference points for multi-frequency, phase-reference observations of B0218+357. The lack of any obvious asymmetry, as indicated by their compactness and the closure-phase data, suggests that mas-scale jets are not prominent in these sources, and they are therefore unlikely to have a strong frequency-dependence in their positions. Extrapolation of this "success rate" suggests that there are about 1000 sources per steradian with equal compactness, and hence around 13,000 in the whole sky.

Of the 4 very-compact sources, 0215+364 is only 52 arcmins away from B0218+357. The evidence of strong variability in this source is worrying, however, since such activity may cause temporal "jitter" in its position.

Acknowledgements

I am grateful to Simon Garrington and Peter Thomasson for granting ad hoc MERLIN time and providing calibrated data, and to Simon Garrington and Rolf Schwartz for granting EVN short observations. I thank Walter Alef for his assistance at the Bonn MKIV correlator; he, Dave Graham and Colin Lonsdale deserve special mention for their collaborative production of the AIPS task MK4IN used during this analysis.

References

[1] Browne, I.W.A. et al, *Gravitational lensing: recent progress and future goals*, ed. Brainerd and Kochanek, ASP Conf. Series 237, p15 (2001)

[2] Condon, J. J. et al, A.J., 115, 1693 (1998)

[3] Gregory, P.C. et al, Ap.J.Supp, 103, 427 (1996)

[4] Porcas, R. W. and Patnaik, A.R., *Proc. of the 10th Working Meeting on European VLBI for Geodesy and Astrometry*, ed. R. Lanotte and G. Bianco, Matera, p188 (1995)

[5] Porcas, R.W and Rioja, M. J., *Proc. of the 11th Working Meeting on European VLBI for Geodesy and Astrometry*, ed. G. Elgered, Goteborg, p209 (1996)

[6] Porcas, R.W and Rioja, M. J., *Proc. of the 12th Working Meeting on European VLBI for Geodesy and Astrometry*, ed. B. Pettersen, Honefoss, p133 (1997)

[7] Rengelink, R.B. et al, A+A Supp., 124, 259 (1997)

Eduardo Ros and Andrei P. Lobanov: Opacity in the Jet of 3C 309.1, Proceedings of the 15th Working Meeting on European VLBI for Geodesy and Astrometry, p.208–215
http://www.ieec.fcr.es/hosted/15wmevga/proceedings/ros

Opacity in the Jet of 3C 309.1

Eduardo Ros, Andrei P. Lobanov

Max-Planck-Institut für Radioastronomie
Contact author: Eduardo Ros, e-mail: `ros@mpifr-bonn.mpg.de`

Abstract

The "core" of a radio source is believed to mark the frequency-dependent location where the optical depth to synchrotron self–absorption $\tau_s \approx 1$. The frequency dependence can be used for derive physical conditions of the radio emitting region and the ambient environment near the central engine of the radio source. In order to test and improve the models to derive this information, we made multi-frequency dual-polarization observations of 3C 309.1 in 1998.6, phase-referenced to the QSOs S5 1448+76 and 4C 72.20 (S5 1520+72) (4°26′ and 1°49′ away, respectively). We present here preliminary results from these observations: total and polarized intensity maps, spectral information deduced from these images, and the relative position of 3C 309.1 with respect to S5 1448+76 at different frequencies. Finally, we discuss briefly the observed shift of the core position.

1. Introduction

Opacity in pc-scale jets The unresolved "core" of a compact extragalactic radio source is believed to mark the location where the optical depth to synchrotron self absorption $\tau_s \approx 1$. This position changes with observing frequency as $R_{\rm core} \propto \nu^{-1/k_r}$ [1]. The power index k_r depends on the shape of the electron energy spectrum and on the magnetic field and particle density distributions in the ultra-compact jet. Hence, by studying variations at k_r as a function of frequency, we may study the detailed physical conditions of the radio emitting region and the ambient environment of the source very near the central engine. Following [2] we can estimate basic physical parameters of the jet including luminosity, maximum brightness temperature, magnetic field in the jet, particle density, and the geometrical properties of the jet (i.e., the core location respect to the jet origin).

To measure k_r a knowledge of the absolute position of the core (or at least the core offset between different frequencies) is needed. Hybrid maps in VLBI lack this positional information due to the use of closure-phase in the imaging process. The rigorous alignment of hybrid maps can be made by astrometric phase-referencing (e.g. [3, 4, 5, 6]). In sources with extended structure, an optically thin component can be used to align maps at different frequencies and then estimate the position of the core.

The QSO 3C 309.1 The QSO 3C 309.1 (V=16.78, z=0.905[1]) is one of the most prominent compact steep spectrum (CSS) radio sources [7, 8]. Many of the CSS sources display polarized emission at cm-wavelengths. The ionized gas surrounding the jet disrupts its flow and is responsible of the complexity of the radio structures seen. There is evidence suggesting that 3C 309.1 is located at the center of a very massive cooling flow with $\dot{M} > 1000\,{\rm M}_\odot\,{\rm yr}^{-1}$ within a radius of $11.5\,{\rm h}^{-1}$ kpc [9].

VLBA observations of 3C 309.1 at 6 frequencies were used for determining the behavior of k_r between 1.6 and 22 GHz [2]. To improve and extend this determination to higher frequencies, we observed 3C 309.1 using the VLBA at eight frequencies with dual polarization. In this contribution, we present a preliminary analysis of the new observations.

[1]This redshift corresponds to a linear scale of $5.60\,h^{-1}$ pc mas^{-1} for H_0=75 h km s^{-1} Mpc^{-1} and q_0=0.5.

2. Mapping analysis

VLBA Observations We carried out VLBA multi-frequency, dual-polarization observations of 3C 309.1 on July 19th and 23rd 1998 using all 10 VLBA antennas and observing at 1.5, 1.6, 2.3, 5, 8.4, 15, 22, and 43 GHz. The data were correlated at the NRAO[2] and processed using AIPS[3] and DIFMAP [13]. DIFMAP was used for mapping the total intensity emission. The polarized intensity mapping and the phase-referencing analysis were carried out in AIPS. The 43 GHz data had to be discarded due to calibration and coherence problems.

Total intensity mapping We applied the CLEAN algorithm and self-calibration in DIFMAP to obtain the total intensity maps presented in Fig. 1 and described in Table 1. The resulting images show a structure very similar to the reported in earlier works (see [10] and references therein). The source shows a core-jet structure first oriented southward and turning later to the East at about 60 mas from the core.

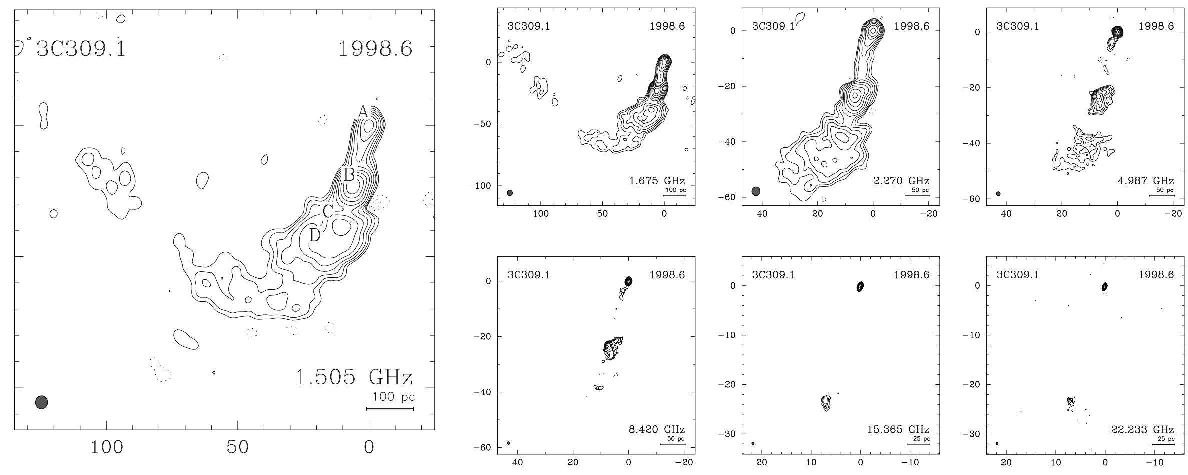

Figure 1. VLBA total intensity images of 3C 309.1. The synthesized interferometric beams are represented at the bottom left corner of each image. Contour levels are drawn at $\sqrt{2}$ intervals. The left image follows the labelling convention from [12]. Map parameters (beam, total flux density, peak of brightness, lowest contour in map) are given in Table 1.

Table 1. Total intensity map parameters (Figs. 1 & 4)

	— **3C 309.1** —					— **4C 72.20** —					— **S5 1448+76** —				
ν [Hz]	Beam size [mas]	P.A. [°]	$S_{\rm peak}$ [Jy/b]	$S_{\rm min}$ (a) [mJy/b]	$S_{\rm tot}$ (b) [Jy]	Beam size [mas]	P.A. [°]	$S_{\rm peak}$ [Jy/b]	$S_{\rm min}$ (a) [mJy/b]	$S_{\rm tot}$ (b) [Jy]	Beam size [mas]	P.A. [°]	$S_{\rm peak}$ [Jy/b]	$S_{\rm min}$ (a) [mJy/b]	$S_{\rm tot}$ (b) [Jy]
1.505	5.00×4.60	−7.5	0.972[c]	2.0	3.424	6.47×5.96	−5.5	0.053	0.5	0.055	6.49×6.21	1.7	0.145	0.6	0.171
1.675	4.50×4.10	−4.3	0.819[c]	2.0	3.181	5.83×5.34	−4.5	0.050	0.4	0.052	5.77×5.50	−3.3	0.149	0.6	0.174
2.270	3.19×2.90	−10.5	0.604[c]	2.0	2.699	4.09×3.68	−8.4	0.083	0.8	0.085	4.11×3.74	−13.8	0.225	0.8	0.253
4.987	1.40×1.35	8.5	0.675[d]	2.0	1.797	1.90×1.82	−13.6	0.053	0.4	0.065	1.88×1.79	−24.8	0.263	0.6	0.313
8.420	0.95×0.85	−5.0	0.646[d]	2.0	1.326	1.08×0.99	−6.7	0.056	0.8	0.057	1.10×1.02	−11.0	0.216	0.8	0.303
15.365	0.47×0.45	−17.8	0.492[d]	3.0	0.921	0.58×0.56	−14.8	0.100	0.8	0.101	0.59×0.58	4.7	0.156	1.1	0.244
22.233	0.41×0.33	−14.8	0.430[d]	3.0	0.712	0.54×0.45	−0.2	0.195	1.5	0.205	0.55×0.45	−6.6	0.211	1.6	0.241

[a] Minimum contour level in the figure. [b] Total flux density recovered in the map model. [c] Corresponds to the B component. [d] Corresponds to the A component.

[2]VLBA correlator, Array Operations Center, National Radio Astronomy Observatory (NRAO), Socorro, NM.
[3]Astronomical Image Processing System, developed and maintained by the NRAO.

Polarized intensity maps We applied the instrumental polarization calibration from the total intensity maps using the AIPS task LPCAL as described in [14]. We imaged the Stokes Q and U and produced images of the linearly polarized emission and the electric vector position angle. An exhaustive description of these results will be published elsewhere. We show an image of the linear polarization distribution at 1.5 GHz in Fig. 2. The core is unpolarized as in many QSOs. In the region South of B the electric vector is radial, suggesting a toroidal magnetic field viewed edge-on. The degree of polarization is higher at the outer parts of the jet.

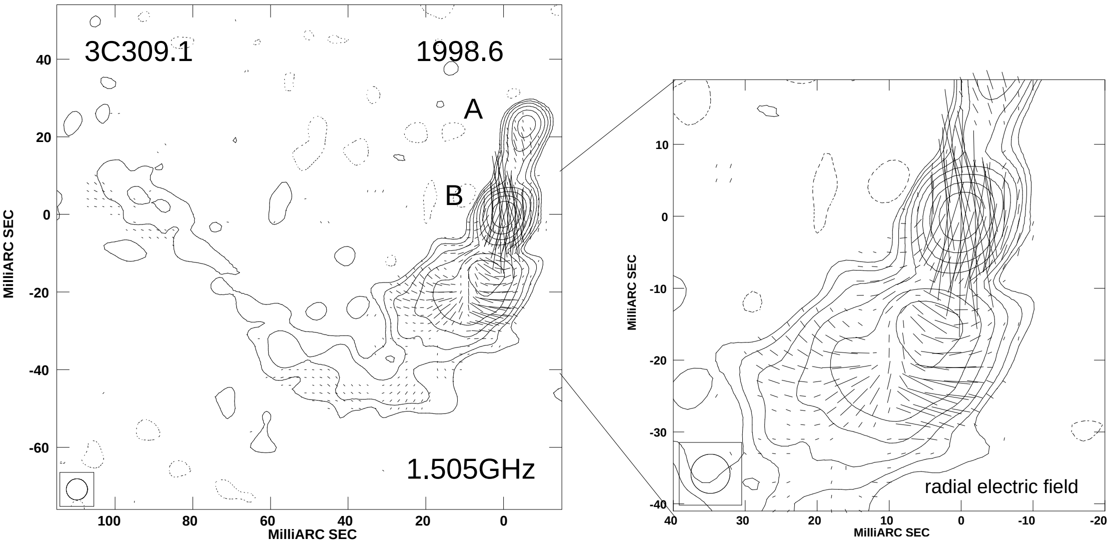

Figure 2. Polarized intensity image of 3C 309.1 at 1.505 GHz (λ 21cm). Electric field vectors are shown.

Spectral analysis The overall spectral index of 3C309.1 is -0.57 ± 0.01. This result is obtained by adding together emission from all of the radio source structure which may have very different physical properties.

To study spectral properties at different parts of the source, we mapped the radio source at all frequencies using natural weighting and very strong tapering (Gaussian function with half maximum at a distance of 33 Mλ). We convolved the CLEAN components with a circular beam of 4 mas in size, aligning the images on the peak-of-brightness of component A. We show these images in Fig. 3 together with the spectra of components A and B and the total spectrum of the VLBI emission. The turnover frequency for A is around 8.4 GHz, and is below 1.4 GHz for B. A linear regression to the points for B provides an overall spectral index of -0.67 ± 0.04.

3. Phase-referencing analysis

The calibrators We used two position calibrators for 3C 309.1:

- 4C 72.20 is a QSO with z=0.799 and V=16.5, 1°49′ East of the target source. It is a point-like source with an inverted spectrum. The imaging results are presented in Fig. 4.
- S5 1448+76 is a flat spectrum, compact radio source with z=0.899 and V=20.0. It is 4°26′ to the NW of 3C 309.1. It shows a faint jet to the NE at the lower frequencies, and it is also elongated in the East-West direction at the higher frequencies. The hybrid maps are shown in Fig. 4.

The analysis We carried out the phase-referencing analysis in AIPS. We solved for the phase, delay and phase-rate for 3C 309.1, using the total intensity maps as input (dividing the (u, v)-data

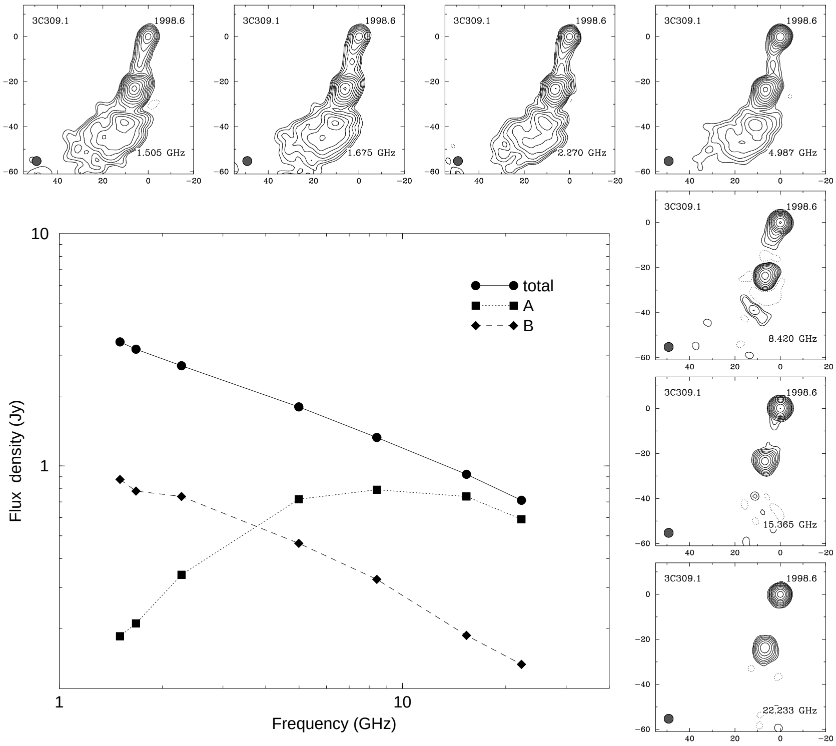

Figure 3. Maps of 3C 309.1 at 4 mas resolution, obtained using the natural weighting and Gaussian tapering with the half maximum at 33 Mλ. The contour levels are drawn at $\sqrt{3}$ intervals. The lowest level is of 3 mJy/beam

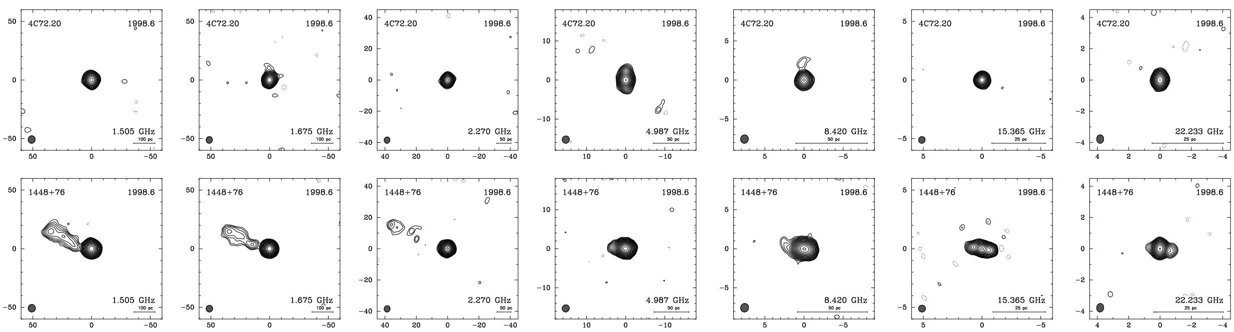

Figure 4. Hybrid maps of the position calibrator sources 4C 72.20 (top) and S5 1448+76 (bottom). The map parameters are described in Table 1.

by the CLEAN model) and thus removing the effect of the source structure. We then interpolated the values fitted using the task CLCAL for the fainter phase-reference calibrators, S5 1442+76 and 4C 72.20 (S5 1520+76).

After editing the data, we mapped the radio sources using the AIPS task IMAGR with the same parameters as were used for the hybrid imaging in DIFMAP. The phase-referenced maps are shown in Fig. 5 and the corresponding map parameters are given in Table 2. We measured the positions of the brightness peaks, whose offsets from the coordinate origin correspond to the offsets from the nominal position of 3C 309.1 relative to the calibrators. The relative positions deduced from this procedure are presented in Table 3.

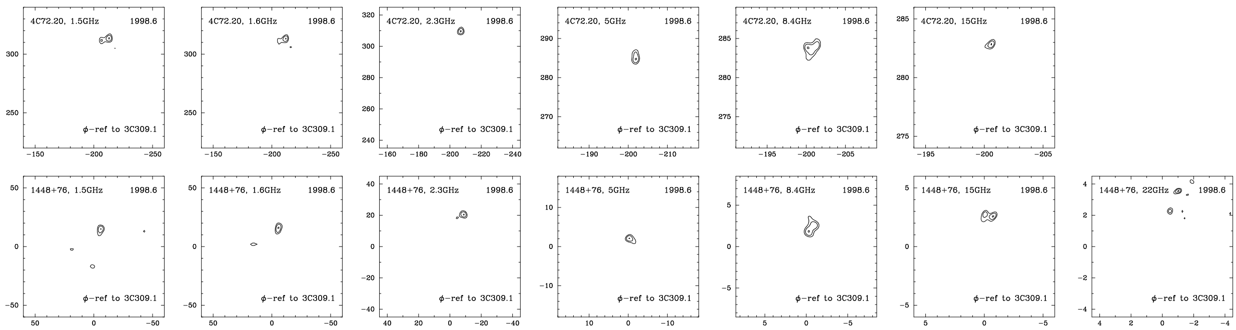

Figure 5. Phase-reference maps of 4C 72.20 and S5 1448+76 obtained using the phase, delay and phase-rate solutions for 3C 309.1 as described in the text. The contours are 49, 69 and 98% of the peak of brightness for each map. The values of the brightness peaks and their ratio (in percentage) with respect to their peaks in the hybrid maps (Fig. 4) are given in Table 2.

Table 2. Phase-referenced map parameters for 4C 72.20 and S5 1448+76 (Fig. 5)

	— **4C 72.20** —			— **S5 1448+76** —		
ν	$S_{\rm max}^{\phi-\rm ref}$	$S_{\rm max}^{\rm hybrid}$	$\frac{S_{\rm max}^{\phi-\rm ref}}{S_{\rm max}^{\rm hybrid}}$	$S_{\rm max}^{\phi-\rm ref}$	$S_{\rm max}^{\rm hybrid}$	$\frac{S_{\rm max}^{\phi-\rm ref}}{S_{\rm max}^{\rm hybrid}}$
[GHz]	[mJy/beam]	[mJy/beam]	[%]	[mJy/beam]	[mJy/beam]	[%]
1.505	13.6	53.3	25.5	29.2	145.2	20.1
1.675	14.8	49.7	29.8	33.3	148.7	22.4
2.270	30.0	82.3	36.5	82.4	225.3	36.6
4.987	19.0	52.8	36.0	143.7	263.2	54.6
8.420	7.1	55.3	12.8	55.3	216.3	25.6
15.365	4.7	100.4	4.7	22.2	155.8	14.2
22.233		—		11.9	211.3	5.6

Table 3. Relative right ascensions and declinations in J2000.0 coordinates of 3C 309.1 with respect to 4C 72.20, and S5 1448+76, obtained via AIPS phase-referencing. Biases have not been corrected.

	— **4C 72.20** —		— **S5 1448+76** —	
ν [GHz]	$\Delta\alpha_{(\rm 3C\,309.1\ -\ 4C\,72.20)}$	$\Delta\delta_{(\rm 3C\,309.1\ -\ 4C\,72.20)}$	$\Delta\alpha_{(\rm 3C\,309.1\ -\ S5\,1448+76)}$	$\Delta\delta_{(\rm 3C\,309.1\ -\ S5\,1448+76)}$
1.505	$-0^{h}21^{m}40^{s}.0554\pm0^{s}.0015$	$-0^{\circ}44'45''.712\pm0''.007$	$0^{h}10^{m}38^{s}.805\ \pm0^{s}.002$	$-4^{\circ}20'51''.721\ \pm0''.006$
1.675	$-0^{h}21^{m}40^{s}.0557\pm0^{s}.0015$	$-0^{\circ}44'45''.712\pm0''.007$	$0^{h}10^{m}38^{s}.8045\ \pm0^{s}.0014$	$-4^{\circ}20'51''.722\ \pm0''.005$
2.270	$-0^{h}21^{m}40^{s}.0568\pm0^{s}.0014$	$-0^{\circ}44'45''.708\pm0''.006$	$0^{h}10^{m}38^{s}.8053\ \pm0^{s}.0007$	$-4^{\circ}20'51''.726\ \pm0''.003$
4.987	$-0^{h}21^{m}40^{s}.0565\pm0^{s}.0014$	$-0^{\circ}44'45''.707\pm0''.006$	$0^{h}10^{m}30^{s}.80476\pm0^{s}.00017$	$-4^{\circ}20'51''.7313\pm0''.0006$
8.420	$-0^{h}21^{m}40^{s}.0569\pm0^{s}.0014$	$-0^{\circ}44'45''.706\pm0''.006$	$0^{h}10^{m}30^{s}.80482\pm0^{s}.00009$	$-4^{\circ}20'51''.7320\pm0''.0003$
15.365	$-0^{h}21^{m}40^{s}.0568\pm0^{s}.0014$	$-0^{\circ}44'45''.705\pm0''.006$	$0^{h}10^{m}30^{s}.80489\pm0^{s}.00008$	$-4^{\circ}20'51''.7318\pm0''.0003$
22.233	—[a]	—[a]	$0^{h}10^{m}30^{s}.80482\pm0^{s}.00007$	$-4^{\circ}20'51''.7315\pm0''.0003$

[a] No phase-referencing detection.

The catalogue position of 4C 72.20 used at the correlator in error of +200 in α and –280 mas in δ. This translates into an estimated uncertainty of $\sim$6 mas, in our preliminary position determination at each frequency, making this fraction of the data unusable for our purposes. A proper analysis, correcting for the wrong position of 4C 72.20 will be published elsewhere. No ionosphere corrections have been applied in the data analysis. At frequencies lower than 8.4 GHz, the ionospheric dispersion may severely bias our results. The tropospheric delay, especially the wet part, affects the phase for the highest frequencies, where the size of the water particles in the atmosphere is comparable to the wavelength.

Notice that the ratio between the peaks of brightness of the phase-referenced maps and the hybrid maps ($4^{\rm th}$ and $7^{\rm th}$ columns in Table 2) is the highest at the intermediate frequencies, where the compromise between the ionospheric and the tropospheric effects is found. Even when the *a priori* position of 4C 72.20 is in error, its ratios are similar to the ones in S5 1448+76, probably because the former is $\sim$3 times closer to 3C 309.1 than the latter.

The error budget in the positions (uncertainties in Table 3) includes the following error terms: a priori coordinates of the source, determination of peak-of-brightness in the maps, polar motion (estimated error of 1 mas), UT1–UTC (10^{-4}s), station coordinates (5 cm), troposphere, ionosphere ($\propto \nu^{-2}$), and problems in the AIPS phase connection. This constitutes a conservative estimate of the uncertainty. We consider thus the phase-referencing results with S5 1448+76 at the highest frequencies as correct (central panel of Fig. 6).

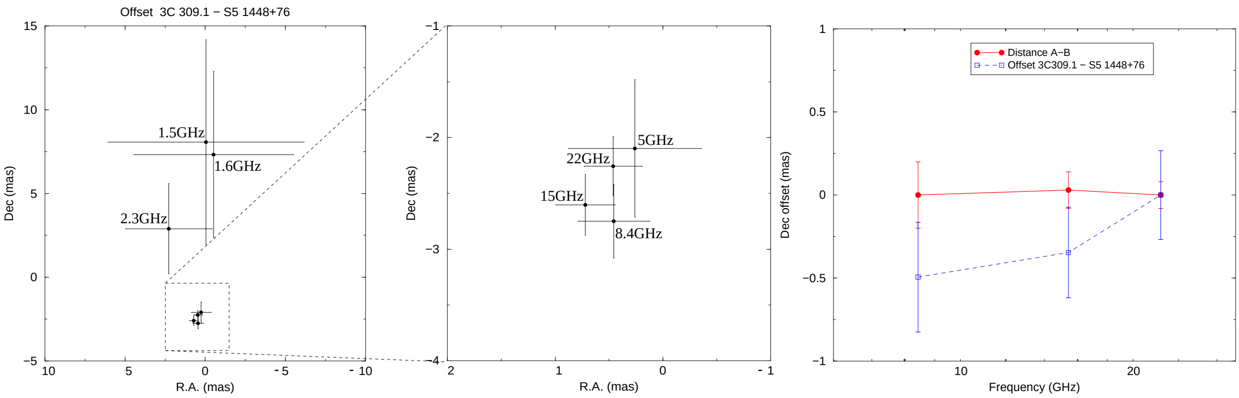

Figure 6. **Left and central panel:** Relative position of 3C 309.1 with respect to S5 1448+76, obtained via AIPS phase-referencing as described in the text. The data at the lowest frequencies are dominated by the ionospheric effect and are invalid for our purposes. **Right panel:** Comparison between the two different methods presented in the text to determine the core offset at 8.4, 15 and 22 GHz: the distance A-B with respect to the phase referencing results. The values at 22 GHz are set as zero reference. The A-B offset is biased due to beam effects in the L-shaped B component. The astrometric results are biased by the unmodelled ionosphere and a simplistic model for the troposphere.

The core position We assign the peak offset in α to S5 1448+76 and in δ to 3C 309.1. The declination offsets in 3C 309.1 between contiguous frequencies are shown in Table 4. The relative offsets are also plotted in Fig. 6, where the value at 22 GHz has been set to be zero.

An alternative way to measure the core offset is to assume that the B component in the maps from Section 2 is optically thin and its peak is at the same position for all frequencies. These values are also presented in Table 4, and in the right panel of Fig. 6.

The trend in the dependence of the core position with the frequency is different in both methods. The A–B separation measurements is apparently frequency-independent: the difference at the beams at different frequencies may bias this result, since the structure of the B component is L-shaped and in the declination coordinate it is more extended to the South. Our preliminary

Table 4. Core shift in **declination** for 3C 309.1 at the higher frequencies (see right panel in Fig. 6).

Frequencies	Distance A-B in maps	AIPS phase-referencing
15 – 8.4 GHz	–130±140 μas	150±430 μas
22 – 15 GHz	130±140 μas	350±380 μas

positional results from the AIPS astrometry at 8.4, 15 and 22 GHz (but not at 5 GHz) suggest that the peak-of-brigthness of the maps shifts closer to the jet basis (core at infinite frequency) at higher frequencies, being this jet basis to the North of the A feature. This would be the expected opacity shift produced by the synchrotron self-absorption in the jet. Assuming that k_r=1 (self-absorbed core, [15]) at 8.4 GHz and that $R_{\rm core} \propto \nu^{-1/k_r}$, the astrometric results provide values of k_r=1.1±0.5 at 15 GHz and k_r=0.9±0.6 at 22 GHz. The big uncertainties do not permit to draw any conclusions about the physical parameters of the jet from k_r at the present status of the analysis. A detailed analysis with the final, unbiased astrometric results will be published elsewhere.

4. Summary

We have presented preliminary results from a detailed multi-frequency study of the QSO 3C 309.1 based on the VLBA observations made in mid 1998. We find a curved jet extending up to 100 mas to the East at low frequencies with two main components, A and B. The A component has a turnover frequency around 8.4 GHz and the B component is optically thin. The polarized intensity map at 1.5 GHz shows that the core is un polarized. In the region southern to B the electric field has a radial structure. The external parts of the jet have a high degree of polarization. A preliminary astrometric analysis provides a determination of the core position at different frequencies by phase-referencing to a nearby radio source QSO S5 1448+76. The changes at the core position with frequency suggest high opacity close to the core caused by synchrotron self-absorption. Due to the big uncertainties we cannot make any assert about the value of k_r at high frequencies. An exhaustive analysis including ionospheric and tropospheric bias removal and physical modeling of the source will be presented in a forthcoming paper.

Acknowledgements

We acknowledge Dr. Scott E. Aaron for his support during the data collection and Dr. Richard W. Porcas for his critical reading of the manuscript. The National Radio Astronomy Observatory is a facility of the National Science Foundation operated under cooperative agreement by Associated Universities, Inc.

References

[1] Königl, A. 1981, AJ 243, 700

[2] Lobanov, A. P. 1998, A&A 330, 79

[3] Lebach, D. E., Ransom, R. R., Ratner, M. I., Shapiro, I. I., Bartel, N., Bietenholz, M. F., Lestrade, J.-F., 2001, in "Galaxies and their Constituents at the Highest Angular Resolution", IAU Symp. 205, p. 59

[4] Brisken, W. F., Benson, J. M., Beasley, A. J., Fomalont, E. B., Goss, W. M., Thorsett, S. E., 2000, ApJ 541, 959

[5] Pérez-Torres, M. A., Marcaide, J. M., Guirado, J. C., Ros, E., Shapiro, I. I., Ratner, M. I., Sardón, E., 2000, A&A 360, 161

[6] Ros, E., Marcaide, J. M., Guirado, J. C., Ratner, M. I., Shapiro, I. I., Krichbaum, T. P., Witzel, A., Preston, R. A., 1999, A&A 348, 381

[7] van Breugel, W., Miley, G., Heckman, T., 1984, AJ 89, 5

[8] Fanti, C., Fanti, R., Parma, P., Schilizzi, R. T., van Breugel, W. J. M. 1985, A&A 143, 292

[9] Forbes, D. A., Crawford, C. S., Fabian, A. C., Johnstone, R. M. 1990, MNRAS 244, 680

[10] Aaron. S. E., 1996, PhD Thesis, Brandeis University, MA, US

[11] Aaron, S. E., Wardle, J. F. C., Roberts, D. H. 1997, Vistas in Astronomy 41, 225

[12] Kus, A. J., Wilkinson, P. N., Pearson, T. J., Readhead, A. C. S. 1990, in: Parsec-Scale Radio Jets, ed. J.A. Zensus, T.J. Pearson, Cambridge University Press, 161

[13] Shepherd, M. C., Pearson, T. J., Taylor, G. B. 1995, BAAS 26, 987

[14] Leppänen, K. J., Zensus, J. A., Diamond, P. J. 1995, AJ 100, 2479

[15] Blandford, R. D., Königl, A. 1979, ApJ 232, 34

Splinter Meeting

IVS Working Group 2

Harald Schuh et al.: IVS Working Group 2 for Product Specification and Observing Programs - Final Report (1st of November 2001), Proceedings of the 15th Working Meeting on European VLBI for Geodesy and Astrometry, p.219–247
http://www.ieec.fcr.es/hosted/15wmevga/proceedings/ivs˙wg2

IVS Working Group 2 for Product Specification and Observing Programs - Final Report (1st of November 2001)

Harald Schuh [1], *Patrick Charlot* [2], *Hayo Hase* [3], *Ed Himwich* [4], *Kerry Kingham* [5], *Calvin Klatt* [6], *Chopo Ma* [7], *Zinovy Malkin* [8], *Arthur Niell* [9], *Axel Nothnagel* [10], *Wolfgang Schlüter* [3], *Kazuhiro Takashima* [11], *Nancy Vandenberg* [4]

1) *Institute of Geodesy and Geophysics, Vienna University of Technology, Vienna, Austria*
2) *Observatoire de Bordeaux, Floirac, France*
3) *Bundesamt für Kartographie und Geodäsie, Fundamentalstation Wettzell, Kötzting, Germany*
4) *NVI Inc., Goddard Space Flight Center, Greenbelt, MD, USA*
5) *U.S. Naval Observatory, EO Department, Washington, D.C., USA*
6) *Geodetic Survey Division, Natural Resources Canada, Ottawa, Canada*
7) *NASA Goddard Space Flight Center, Greenbelt, MD, USA*
8) *Institute of Applied Astronomy, St. Petersberg, Russia*
9) *MIT Haystack Observatory, Westford, MA, USA*
10) *Geodetic Institute of the University of Bonn, Bonn, Germany*
11) *Geographical Survey Institute, Tsukuba, Japan*

Contact author: Harald Schuh, e-mail: `hschuh@luna.tuwien.ac.at`

Abstract

After the scientific rationale is given in the introduction the Terms of Reference and the proceeding of IVS Working Group 2 are presented. Then the present status and future goals of all international activities within IVS are described. In particular the current products of IVS are described in terms of accuracy, reliability, frequency of observing sessions, temporal resolution of the parameters estimated by VLBI data analysis, time delay from observing to product, i.e. time which has passed after the end of the last session included in the VLBI solution till availability of the final products and frequency of solution (in the case of “global solutions”, when all existing or a high number of VLBI sessions are used to determine so-called global parameters). All IVS products and their potential users are covered in the report. This includes the Earth orientation parameters (EOP), the reference frames (TRF and CRF), geodynamical and geophysical parameters and physical parameters. Measures which should be taken within IVS to meet the goals defined in the first steps are presented. As most of the measures are related to the observing programs, these are the main focus for improving the current status of IVS products. The report shows that due to various requirements of the different users of IVS products the following aspects must be accomplished:

- significant improvement of the accuracy of VLBI products,
- shorter time delay from observation to availability of results,
- almost continuous temporal coverage by VLBI sessions.

A first scenario of the IVS observing program for 2002 and 2003 considers an increase of observing time by about 30%–40% and includes sessions carried out by S2 and K4 technology. The midterm observing program for the next 4–5 years seems to be rather ambitious. However, it appears feasible if all efforts are concentrated and the necessary resources are made available.

Executive Summary

For all present-day Earth and space science, high precision reference frames are an essential prerequisite. The most important reference frames are the International Celestial Reference Frame (ICRF) realized by some hundreds of extragalactic radio sources and the International Terrestrial Reference Frame (ITRF) established by globally distributed observing stations. For the transformation between these two reference frames the Earth orientation parameters (EOP) have to be known with high precision. Temporal variations of EOP on different time scales allow the investigation of interactions of components of system Earth. All space techniques have their particular strengths, and VLBI gets its outstanding importance through being the only technique for establishing and maintaining the ICRF and the direct tie of the ITRF to the ICRF by monitoring the time dependent EOP.

An important part of the efforts of IVS is to provide the best ICRF, ITRF, and EOP products for the user community and to optimize the use of available global resources in making these products. The charter of IVS Working Group 2 was to review current products, recommend goals, and suggest observing programs. Users of the IVS products include the International Earth Rotation Service (IERS) for all products; individual scientist users for EOP; all geodetic activities for the TRF; the astrometric and astrophysical community for CRF.

Products can be described in terms of accuracy and reliability, frequency of observing sessions, temporal resolution of the parameters estimated by the VLBI data analysis, time delay from observing to final product, and frequency of solutions. Presently, the accuracy of EOP from 24-hour sessions is 5 μsec for UT1 and 100–200 microarcsec for the pole, observed $\approx$3 days per week. The EOP are released with a time delay of one week to several months. A goal of improving the accuracy by a factor of 2 to 4 should be feasible over the next few years, along with observing 7 days per week and a time delay of less than five days. Comparable accuracy in both x_p and y_p is another goal. Observing should take place every day to avoid any jumps, bias, or inconsistency. The network offset problem (offsets between EOP results obtained by simultaneously observing VLBI networks) needs a solution because strictly consistent reference frames are a strong requirement. A particular strength of VLBI is its contribution to the scale of the ITRF. Present accuracy is 5–20 mm for the TRF time series (single sessions) and 1–4 mm for global solutions. More stations in the southern hemisphere are needed. For the CRF, VLBI is the unique technique. More analysis centers should provide solutions, and an improved sky distribution is needed. Besides TRF, CRF, and EOP products, IVS should provide EOP rates, and regular solutions of geodynamical parameters (solid Earth tides, ocean loading, and atmospheric loading) and physical parameters (tropospheric and ionospheric parameters, relativity parameters).

Measures that need to be taken to meet these goals depend on new technology plus a commitment from IVS member organizations for strong support of the observing program. Improvements in accuracy are expected based on technology improvements, better analysis, better observing geometry, more observables taken by more stations, and improved station reliability. The time delay from observing to final product can be reduced by assigning high priority to operational sessions and more automation. Temporal continuity and resolution can be improved by denser and longer observing sessions. Redundancy requirements emphasize more analysis centers, different software packages, plus some parallel observing networks.

IVS as a service needs to carry out regular programs, in order to deliver its products as reliably and precisely as possible, consistent with available resources. The proposed IVS observing program tries to meet the goals by extending and updating existing programs while maintaining continuity with existing time series. Features of the proposed program include combining the requirements of

various users, including all techniques and new technologies (Mk4/Mk5, K4, S2), including R&D sessions, and improving global coverage.

The accuracy goal can be achieved by the above-mentioned measures that will be supported by studying results of special R&D sessions. The timeliness goal can be addressed initially through setting up a fast and routine procedure for shipping recorded media to the correlator, and ultimately through support of broadband communication links. The competitiveness of VLBI products would be significantly increased by contributing to such important tasks as:

- Support prediction of EOP.
- Allow reaction to episodic events in near real-time.
- Support atmospheric and ionospheric investigations.
- Guarantee the availability of the results in case of emergency.

The goal of daily VLBI sessions will rely on gradual augmentation of resources for station observing time, correlator capacity, and recording media and data transmission facilities. The main arguments for continuous VLBI measurements are:

- Contribute to the proposed IAG project IGGOS.
- Provide a permanent comparison and control of results of other techniques.
- Resolve the smaller tidal terms in solid Earth tides, ocean loading, and ocean tidal excitation of the EOP.
- Determine the amplitudes of the many short period nutation terms.
- Catch episodic events both on Earth and on extragalactic sources.
- Increase the accuracy of the results by increasing the number of observations.

For 2002 the proposed IVS program includes two 6-station rapid-turnaround sessions per week, a monthly R&D session, a monthly 9-station TRF session, a 14-day continuous session, and four short-duration one-baseline sessions per week with at least one of these sessions having independent observing. The program includes participation by S2 and K4 networks and correlators. The proposed years 2003–2005 have a gradual increase in network size, number of observing days and recording media usage. By 2005 continuous observing is possible if the projected shortfall in resources can be overcome.

Geodetic VLBI plays an essential role in geodesy and astrometry due to its uniqueness in observing UT1-UTC and the precession/nutation angles unbiased over a time span longer than a few days. It is also necessary for the ICRF and contributes to the generation of the ITRF. Due to various requirements of different users of IVS products the following aspects must be accomplished:

- Significant improvement of the accuracy of VLBI products,
- Shorter time delay from observation to availability of results,
- Almost continuous temporal coverage by VLBI sessions.

The proposed observing program to accomplish these goals increases observing time by 30–40% over the next two years and includes sessions carried out using S2 and K4 technology. This observing program is rather ambitious but it is feasible if efforts of the IVS components are concentrated and the necessary resources become available.

1. Introduction

For all present-day Earth and space sciences high-precision reference frames are an essential prerequisite, e.g. for positioning and navigation on the Earth, Earth observation by satellites and space navigation. The most important reference frames are in space the International Celestial Reference Frame (ICRF) realized by several hundred extragalactic radio sources and on Earth the International Terrestrial Reference Frame (ITRF) established by globally distributed observing stations.

For the transformation between those two reference frames the Earth orientation parameters (EOP) have to be known with high precision. Temporal variations of the EOP on different time scales allow us to investigate the interactions of the various components of system Earth, i.e. between the solid Earth, the atmosphere, the hydrosphere and the cryosphere. Motions of these geophysical fluids also influence the Earth's gravity field, which can be precisely monitored by the upcoming geodynamical satellite missions CHAMP, GRACE, GOCE and others. Both variations of the EOP and of the gravity field are an important source for modeling the Earth's interior and for determining the parameters of Earth models.

In the last two decades different space geodetic techniques have been developed for measuring the EOP and realizing the above-mentioned reference frames. While each of the different space techniques has its particular strengths and merits, VLBI earns its outstanding importance from being the unique technique for the establishment and maintenance of the ICRF and the direct tie of the ITRF to the ICRF by monitoring the time dependent Earth orientation parameters that relate the ITRF to the ICRF. In particular VLBI is unique in observing the UT1-UTC parameters that correspond to the rotational speed of the Earth and the direction of the rotation axis of the Earth in space expressed by the precession/nutation angles ($\Delta\varepsilon$, $\Delta\Psi$). This has been recognized by the International Astronomical Union (IAU) at its XXIVth General Assembly in Manchester in Resolutions B1.1 and B1.6 approved in August 2000.

The International Association of Geodesy (IAG) which presented a plan for reorganization at its recent Scientific Assembly in Budapest (Sept. 2001) demonstrates the importance of the new space geodetic techniques by assigning the international services representing these techniques to the same level as the four scientific Commissions (Beutler et al. 2001). In the proposed internationally organized long-term project IGGOS (Integrated Global Geodetic Observing System) the IAG will combine the fundamental areas of geodetic research into one integrated global observation and analysis system for Earth sciences. This requires in particular the combination of modern space geodetic techniques into a joint system (Rummel et al., 2001). As redundancy and independent control are the strongest requirements for the IGGOS, an essential aspect of IGGOS is that the different techniques observe on all time scales with a global network as dense as possible. The need for regular and simultaneous observations by all space geodetic techniques, as recognized by IAG, alone justifies the extension of the present international VLBI activities within IVS: more stations globally distributed should carry out continuous measurements. Furthermore this will yield results of highest relevance for the Earth sciences by monitoring parameters describing global geodynamics needed to model effects such as global plate motion, earthquakes or postglacial rebound.

An important part of the IVS efforts is to provide the best products for the user community and to optimize the use of available global resources. During the 5th IVS Directing Board meeting on February 15th, 2001 the IVS products and related programs were discussed with respect to the general goals described above. It was decided to set up an IVS Working Group (WG2) for Product Specification and Observing Programs. Members of WG2 were chosen among experts in the field of geodetic/astrometric VLBI. The Terms of Reference (ToR) of WG2 are to

- review the usefulness and appropriateness of the current definition of IVS products and suggest modifications,
- recommend guidelines for accuracy, timeliness, and redundancy of products,
- review the quality and appropriateness of existing observing programs with respect to the desired products,
- suggest a realistic set of observing programs which should result in achieving the desired products, taking into account existing agency programs,
- set goals for improvements in IVS products and suggest how these may possibly be achieved in the future,
- present a written report to the IVS Directing Board at its next meeting.

An overview of the activities of Working Group 2 and the results achieved are presented in this report.

2. Proceeding of the Working Group

During the first weeks after its establishment, the procedure for how to achieve the Terms of Reference was thoroughly discussed. It was decided to proceed step by step:

Step 1: Description of the present status of international VLBI activities within the IVS

In particular the current products of IVS should be described in terms of

- accuracy;
- temporal resolution of the parameters estimated by the VLBI data analysis;
- time delay from observing to product, i.e. time which has passed after the end of the last session included in the VLBI solution until availability of the final products;
- frequency of observing sessions;
- frequency of solution (in the case of "global solutions", when all existing or a high number of VLBI sessions are used to determine so-called global parameters);
- reliability of the IVS products (for details see below).

All these features are essential for comparing the products delivered by IVS to those provided by other space geodetic techniques and their international services. Another very important criterion is the reliability of the IVS products which can be assessed by the measures that are taken to independently check the IVS results provided to the users. As for the reliability criterion, any external checks, i.e. comparison with other space geodetic techniques, were not considered here because they are beyond the scope covered by IVS. There are also several IVS products that cannot even be estimated by other techniques because VLBI is unique for the respective parameters. The reliability was specified by the following rating scheme:

1. reliability does not exist, e.g. results were obtained by only one IVS Analysis Center using one software package;

2. reliability almost does not exist, e.g. results were obtained by different IVS Analysis Centers, but using the same software package;
3. reliability clearly exists, e.g. results were obtained by different Analysis Centers which used different software packages, but only from sessions of one network;
4. strongly redundant, same as 3 but results were obtained from sessions of several VLBI networks, partly running in parallel.

In parallel with presenting the IVS products, their various users were also described (see section 4).

Step 2: Description of the goals for future IVS products

In this step the requests from the users' point of view should be described because the most important factor for activities of IVS should be the needs and wishes of the users of the products. The goals should be defined according to the same criteria as given above. For instance it would not be very useful to increase the temporal resolution of a particular parameter down to a couple of hours when an accepted theory shows that the periodic variations and other temporal changes of that parameter occur on time scales never shorter than one month. The required accuracy also strongly depends on the magnitude of the effect that is going to be investigated. An important basis for these considerations was a memo by Benjamin F. Chao on "Global science enabled by Earth rotation observations" (Word document vlbicore.doc at http://ivscc.gsfc.nasa.gov/mhonarc/corepanel/msg00030.html 2001) and a very thorough examination of the present accuracy of IVS products by Richard S. Gross (http://ivscc.gsfc.nasa.gov/mhonarc/core-panel/msg00038.html 2001). Sometimes step 2 also includes some "vision" of the VLBI experts, i.e. what could be done within the IVS without considering the limited resources.

Step 3: Definition of future observing programs, technological improvements and further changes

In this step the goals defined above were matched to the real world with its limited resources in funding and manpower and its many organisational restrictions. The highest priority should be given to all VLBI products that are unique compared to other techniques. Thus, the task was to develop ideas for VLBI observing schemes that allowed achieving the goals defined in the previous step without considerably increasing the present resources and efforts. The different interests of all users of VLBI products should be equally considered. First, the existing observing programs carried out by various agencies and organizations within IVS (see tables in section 4) had to be reviewed with respect to the desired products. The central role of VLBI in geodesy and astrometry is clearly described in a memo by W. Cannon (http://giub.geod.uni-bonn.de/vlbi/IVS-AC/divers/cannon.html 2001):

- the establishment and maintenance of the International Celestial Reference Frame (ICRF);
- the direct tie of the International Terrestrial Reference Frame (ITRF) to the ICRF;
- the monitoring of the time dependent Earth orientation parameters (EOP) that relate the ITRF to
- the ICRF especially the UT1-UTC and precession/nutation angles ($\Delta\varepsilon$, $\Delta\Psi$) which are uniquely determined by VLBI.

Step 4: Final Report

The results obtained from the considerations described above shall be summarized and presented in a written report to the IVS Directing Board as well as to the international VLBI community and its sponsoring agencies. The recommendations presented in that report should be used for further discussions of future observing programs and analysis strategies and should consequently become the basis for the future of geodetic and astrometric VLBI within IVS in the next five to ten years.

3. Present status and future goals

The international VLBI activities within the IVS are comprehensively represented in tables 1a,b,c. The left part of tables 1a,b,c shows the present status, the right part the future goals. In subsections 3.1-3.5 the tables will be discussed in more details.

3.1. Earth orientation parameters (EOP)

At present, the Earth orientation parameters are usually observed in three 24h sessions per week (NEOS, CORE, IRIS-S, ...). In addition, so-called intensive sessions of 60min (INTENSIVE) take place on a single baseline with a long east-west extension (Wettzell - Kokee Park) four times per week. The latter can only be used to determine UT1-UTC. It should be noted that the accuracy obtained from the 24h sessions is worse for the xp than for the yp component of polar motion (200 microarcsec versus 100 microarcsec), due to the unfavourable geometry of most of the networks. Concerning the time delay from observing to product of these sessions it should be pointed out that the results of the NEOS program normally become available between one and four weeks after the session, whereas the data of the other programs are usually not correlated and analysed before one to even four months after the session. This generally too long time delay from observing to product is a clear disadvantage with respect to other space geodetic techniques. The EOP rates, i.e. dUT1/dt and dx_p/dt, dy_p/dt, are geophysically very interesting because they can be directly connected to atmospheric and oceanic excitation. Thus, EOP rates will be needed in the future as another product of IVS; so far VLBI has obtained only preliminary results.

Concerning the goals given on the right hand side of tables 1a,b,c a further improvement of the accuracies by a factor of 2 to 4 seems feasible, e.g. UT1-UTC should be determined to $\pm 2 - 3$ microsec and the pole position to $\pm 25 - 50$ microarcsec in both components. In particular for the x_p component of the pole, this requires an improved network geometry. The same holds for the precession/nutation angles. All measures for improving the accuracy of the IVS products will be dealt with in sections 5 and 6.2.1. As VLBI is unique for the unambiguous determination of UT1-UTC and of nutation (with periods as short as 2 days), the VLBI sessions should take place every day, i.e. continuously 7 days per week, to avoid any jump, bias or other inconsistency. One of the main problems which still has to be solved within the IVS are the offsets and drifts between results obtained by different VLBI networks. Strictly consistent reference frames are a prerequisite for solving this problem.

Short period variations of the EOP occur with periods of a few days, of one day (diurnal variations due to ocean tides) and of half a day (semidiurnal variations due to ocean tides). To resolve the 11 main ocean tidal terms requires a time resolution of at least 1h which can already be achieved with the presently available VLBI data. In order to get the whole picture of ocean tides induced

Table 1a: Present status and future goals of geodetic and astrometric VLBI within IVS - single session products (EOP and TRF)

		Present status					**Goals**						
	IVS data products	***accuracy***	***frequency of session / solution***	***reso-lution***	***delay from observing to product***	***reliability by indep. checking****	***accuracy (per 24h)* in 2005**	***frequency of session* in 2005**	***resolution*** 2002	2005	***timeli-ness ***** 2002	2005	***reliability by indep. checking****
EOP	***UT1 from 24h sessions :***	5 microsec	~3d/week	1d	NEOS: 1-4 weeks other 24h ses-sions: 1-4 months	24h sessions: 3	2-3 microsec	7d/week (continuous)	1h	10 min	3-4d	1d	4
	from 60min intensive ses-sions :	20microsec	~4d/week	1d	intensives: 1 week	intensives: 2	5-7 microsec		-	-			
	dUT1/dt (lod) from 24h ses-sions	only pre-liminary results	~3d/week	-	-	-	0.3-0.5 micro-sec/day	7d/week	1h	10 min	-	-	4
	x_p, y_p	for x_p: 200 microarcsec for y_p: 100 microarcsec	~3d/week	1d	NEOS: 1-4 weeks other 24h ses-sions: 1-4 months	3	25-50 micro-arc-sec (for xp, yp)	7d/week	2002: 1h	2005: 10 min	2002: 3-4d	2005: 1d	4
	dx_p/dt, dy_p/dt from 24h ses-sions	only pre-liminary results	~3d/week	-	-	-	8-10 microarc-sec/day	7d/week			-	-	4
	$\Delta\varepsilon$, $\Delta\psi$	100-400 microarcsec	~3d/week	1d	NEOS: 1-4 weeks other 24h ses-sions: 1-4 months	3	25-50 micro-arc-sec	7d/week	1d		2002: 3-4d	2005: 1d	4
TRF (single sessions)	***time series (one solution per session) x, y, z (b, h, v)***	5-20 mm	~3d/week	1d	3-4 months	2	2-5 mm	7d/week	1d		2002: 3-4d	2005: 1d	3
	episodic events (also in EOP)	(10 mm)	to be investigated				2-3 mm	7d/week	1h		2002: 3-4d	2005: 1d	4

** timeliness starts at the end of the last session used for the solution
b - baseline length, h - horizontal component, v - vertical component

Table 1b: Present status and future goals of geodetic and astrometric VLBI within IVS multi-session products (TRF and CRF)

		Present status					**Goals**							
	IVS data products	***accuracy***	***freq. of solution***	***reso-lution***	***delay from observing to product***	***reliability by indep. checking****	***accuracy*** **in 2005**	***freq. of solution*** **in 2005**		***resolution***		***timeli-ness *****		***reliability by indep. checking****
								2002	2005	2002	2005	2002	2005	
TRF (multi sessions)	***annual solutions (all sessions used) coordinates: velocities:***	1-4 mm 0.1-1 mm/y	1y	-	3-6 months	2	improved distribution of stations, 1-2 mm 0.1-0.3 mm/y	1y		-		3m	1m	3
	non-linear changes (e.g. periodic variations or irregular changes)	(10 mm)	to be investigated				2-3 mm	1y		sufficient sessions per year to detect annual and semiannual periodic variations		3m		3
CRF	***α, δ***	0.25-3 mas	1y	-	3-6 months	3	0.25 mas for as many sources as possible + improved sky distribution	1y		-		3m	1m	4
+	***time series of α, δ***	variable	-	-	3-6 months	1	0.5mas	1y	1m	1m		3m	1m	4
astro-phy-sics	***source structure***	-	2m	2m	2-3 years	1	-	2m	1m	2m	1m	1y	3m	2
	flux density	-	irregular	6h - 6d	1-2 years	1	-	7d/w	7d/w	6h	1h	3-4d	in real time	2

** timeliness starts at the end of the last session used for the solution

Table 1c: Present status and future goals of geodetic and astrometric VLBI within IVS - geodynamical and physical parameters

		Present status					**Goals**				
	IVS data products	***accuracy or uncer-tainety***	***frequency of solution***	***resolution***	***delay from observing to product***	***reliability by indep. checking****	***accuracy or uncer-tainety***	***freq. of solution***	***reso-lu-tion***	***timeli-ness***	***reliability by indep. checking****
geodyn-amical param-ters	***solid Earth tides h,l (frequency and site de-pendent)***	5-10%	1-3y	-	1year	1-2	0.1%	1y	1y	1m	3
	ocean load-ing A, φ (site dependent)	10-20%	1-3y	-	1year	1	1%	1y	1y	1m	3
	atmospheric loading (site de-pendent)	30-40%	1-3y	-	1year	1	10%	1y	1y	1m	3
physical parame-ters	***tropospheric parameters: zenith delays gradients***	4-8 mm 1-2 mm	~3d/week ~3d/week	1h 6h	1w-4m 1w-4m	1 1	1-2 mm .3-0.5mm	7d/week 7d/week	10min 2h	1d 1d	3 3
	ionospheric mapping	1-5 TEC-units	~3d/week	1h	1w-4m	1	0.5 TEC-units	7d/week	1h	1d	3
	light deflec-tion para-meter γ	0.3%	1-3y	-	1y	1	0.1%	1y	all sessions used	1m	2

[*] **rating scheme for ‘reliability‘ in tables 1a,b,c**

1 - not existing (only one Analysis Center using one software package) (present status) / not important (required)

2 - almost not existing (different Analysis Centers, but using the same software package) (“ “) / desired (“)

3 - clearly exists (different Analysis Centers use different software packages; but only sessions from one network) (“ “) / important (“)

4 - strongly redundant (as 3, but several VLBI networks, partly running in parallel) (“ “) / very important (“)

EOP variations at least several hundreds of smaller terms in the near-by side bands should be determined, too. Only then would the full information become available on resonance effects close to the K_1-tide and on the so-called effective load Love number k'. A separation of *all* the ocean tidal terms in the EOP is only possible from VLBI observing sessions which cover at least 18.6 years continuously using a well adjusted TRF. In that respect it should be mentioned that in the period range of diurnal and semi-diurnal terms most of the satellite techniques suffer from resonances with the satellite orbital periods, a problem that does not occur in VLBI. Thus, GPS is not able to resolve several of the diurnal periods of the EOP, e.g. K_1, S_1, and Ψ_1 due to resonances with the orbital period.

From recent Fourier and wavelet analyses of the EOP observed by GPS, variations with sub-semidiurnal periods (8h, 6h, 4.8h, 4h, ...) were found. It is still an open question whether these periods really exist and are due either to higher harmonics of the ocean tides or to atmospheric tones. Other explanations could be that they appear in the spectra due to some asymmetry of a 24h quasi-sinusoidal wave or just that it is a pure artefact caused by resonances with GPS satellite orbits. The ratio of the higher harmonics of a solar day plays an important role as for instance in recordings of various geophysical phenomena the S_7 (period 3.43h) is usually stronger than the S_5, S_6 and S_8. Anyhow, some resonances or modes of the Earth might affect Earth rotation on very short time scales, too, and scientists hope to catch episodic events, caused by earthquakes, volcanoes or strong typhoons. As these many open questions need to be investigated from independent EOP measurements by VLBI, almost continuous VLBI sessions and a temporal resolution of 10min are highly desirable by 2005. This becomes in particular important if VLBI is required to control not only satellite techniques (GPS, Glonass, ...) but also new observation technologies such as laser gyros which are designed to observe the rotation of the Earth almost continuously.

A timeliness of 3 to 4 days (one or two days for tape transport, one day for correlation, one day for data analysis) could be achieved with the present VLBI technology although this is a rather challenging goal. The 1-day timeliness, which is given as the goal for 2005, can only be achieved if tape transport is replaced by broadband communication links allowing real-time correlation of the signals. Direct connection between radiotelescopes and the correlators have been under discussion for several years (e.g. Proceedings of the Real-Time VLBI Forum, MIT Haystack Observatory, 1998) and were successfully demonstrated by Japanese VLBI groups within the Key Stone Project (see various TDC News of the CRL, http://www.crl.go.jp/ka/radioastro/).

The reliability of the EOP (which are one of the most important products of IVS) is in rating class 3, i.e. there is a redundancy because different analysis centers use different software packages for data analysis. However, in the future the redundancy should still be improved to rating class 4 by using several VLBI networks that partly run in parallel to allow an independent checking of the IVS results.

It was already mentioned in sections 1 and 2 that VLBI is a unique technique for unbiased monitoring of the precession/nutation angles $\Delta\varepsilon$, $\Delta\Psi$. New theoretical models were developed in nutation theory during the last 10 years and also a semi-empirical model was derived recently by Mathews et al. (2001). This model was adopted by the International Astronomical Union (IAU) at its XXIVth General Assembly in Manchester in Resolution B1.6 approved in August 2000, which will be the future standard for many applications in geodesy and astronomy.

Comparing nutation models with VLBI observations is important for various reasons that were described in detail in a comprehensive paper by Dehant et al. (1999) and also by Mathews at al. (2001). The modeling of nutation involves a frequency-dependent transfer function and the rigid

Earth nutation amplitudes. The transfer function is different for each nutation term because of the existence of resonances, because of the mantle inelasticity and of the ocean loading effects. The transfer functions for individual nutation terms deviate from a value computed from a mean frequency-dependent transfer function (Mathews et al., 2001). A small error in the transfer function can only be seen in the largest nutations. The others are very small and so they are less sensitive to changes in the transfer function. For instance, for a small nutation amplitude of 1 milliarcsec, a one percent error in the transfer function would give a 1 μarcsec error in the nutation; while a large nutation of 100 milliarcsec would have a 1 milliarcsec error. So the observation of the 100 milliarcsec nutation, if the rigid nutation is "perfectly" known, at a precision of 20 muarcsec in the observation, will provide constraints on the transfer function at the 10^{-5} level. This is in particular the case for the 13.66 day nutation term with a mean amplitude of 91 milliarcsec. From the other short period nutations according to the new model mentioned above (Mathews et al., 2001) the following terms are of particular importance for the determination of the transfer function (the mean amplitudes are in parentheses): 31.81 days (3 milliarcsec), 27.55 days (15 milliarcsec), 23.94 days (1 milliarcsec), 14.77 days (1 milliarcsec), 13.78 days (1 milliarcsec), 9.56 days (2 milliarcsec), 9.13 days (12 milliarcsec), 7.10 days (1 milliarcsec), 6.86 days (1 milliarcsec).

Also the question arises how long do we have to observe by VLBI to monitor the Free Core Nutation (FCN) at about 430 days, the annual and semi-annual nutation terms and the longer nutation periods? For obtaining geophysical information from the nutation measurements, it is necessary to observe the following long periods: 386.00 days, 365.26 days, 346.64 days, 182.62 days, 121.75 days. In order to be able to separate those terms and the longer periods of 9 years (3399.19 days), 18.66 years (6798.38 days), and precession, at least two times the 18.66 year period should be covered by VLBI observations.

Based on these requirements, there is a great need for monitoring the precession/nutation angles regularly. The main arguments are summarized, below:

- The amplitude of the retrograde Free Core Nutation (FCN) at $\approx$ 430 days cannot be predicted and is therefore not contained in the new astronomical nutation models; the attenuation of the FCN amplitudes requires a regular and frequent monitoring of the nutation angles by VLBI; the same holds for the prograde Free Inner Core Nutation (FICN) with a predicted period of 1025 days which has not been observed so far.
- There are seasonal (annual and semi-annual) influences of the atmosphere and the oceans on nutation which also have to be monitored.
- The shortest nutation period which is of greater interest for astronomers and geophysicists is at 13.66 days; to recover that period by VLBI needs precise observations at least every 3.4 days considering the Nyquist frequency and prograde and retrograde terms. If the period at 6.86 days has to be resolved, too, VLBI observations every 1.7 days would be necessary.

It should be mentioned here, that the need for *regularly* monitoring precession/nutation angles by VLBI was explicitly encouraged in the IAU resolution referred to above.

3.2. Terrestrial reference frame (TRF)

The TRF determined from single session solutions or from a global solution is another very important IVS product because this is an essential part for creating the ITRF by the corresponding IERS Product Center. A particular strength of VLBI is its contribution to the scale of the ITRF.

Usually the TRF is computed from the same 24h sessions that are dedicated to observing the EOP. However, only a few analysis centers provide TRF single session solutions and these are not released as official IVS products. In addition, the TRF global solution in the past has been published by only one IVS analysis center (GSFC) using the Global SOLVE software. Other global solutions exist (by GIUB/BKG and Shanghai Observatory) but all of them were obtained by program SOLVE. Thus, the TRF received a rating of 2 for redundancy. A combined IVS TRF solution in terms of individual time series and also of global station positions and velocities should be established as soon as possible based on individual solutions of various analysis centers using different software. Another important aspect is the distribution of VLBI stations on the Earth, which should be generally improved. There is a need for having more stations in the southern hemisphere, with at least two stations on each main tectonic plate. Episodic events and non-linear changes of the baseline components are aspects that are mainly interesting for geophysicists and seismologists. Such effects might be detectable by the still rapidly increasing accuracy of space geodetic techniques. Thus, it is important that the temporal continuity of VLBI sessions should be sufficient to detect such effects. A successful detection of non-linear changes of baseline rates was reported in August 2000 by the Japanese Key Stone Project (KSP) (http://ksp.crl.go.jp/).

3.3. Celestial reference frame (CRF)

For the ICRF realized by extragalactic radio sources VLBI is again the only technique. Thus, the ICRF can be seen as another very important IVS product. This has been explicitly recognized by the International Astronomical Union (IAU) at its XXIVth General Assembly in Manchester in Resolution B1.1 approved in August 2000. For the ICRF, again, a lack of redundancy of the results can be noticed because the ICRF and its extension were produced only by a single analysis center of the IVS. (It should be noted, however, that using the results of a single solution was the consensus of the IAU subgroup that generated the ICRF). Additional CRF solutions by other IVS analysis centers for detailed comparison are highly desirable. The idea of deriving a combined IVS CRF solution should be investigated in cooperation with the IAU Working Group on Celestial Reference Systems.

Rather than improving the current ICRF source position accuracy, it is felt that finding new sources to improve the overall sky distribution is more important for the immediate future. If the ICRF will be used as a catalog of calibrators for phase-referencing VLBI observations (most of the VLBI experiments with astrophysical goals are of this type now), then a reference source (calibrator) every few degrees on the sky is needed. For geodesy and astrometry, better observing schedules can be made if there is a more dense distribution of sources available. In this respect, the ICRF suffers from a deficit of sources with an average of only one source per $8^\circ \times 8^\circ$ on the sky. Moreover, the distribution of the ICRF sources is found to be largely non-uniform. For example, the distance to the nearest ICRF source for any randomly-chosen sky locations can be up to 13° in the northern sky and up to 15° in the southern sky. Charlot et al. (2000) showed that adding 150 new sources at specific location in the northern sky would reduce this distance to about 6°, and progress is being made towards this goal. An even larger effort is required for the southern sky since most of the sources far in the south have only a limited number of observations because of the lack of VLBI stations in the southern hemisphere.

The temporal variations of the source positions should also be investigated by solving for time series of source coordinates since these may be affected by source structure variations. Maps of the source structures can be derived from geodetic VLBI sessions if the number of observing stations is large enough, as are total flux density variations. Just recently, Koyama et al. (2001) showed that flux density variations of compact radio sources could be monitored within the Key Stone Project. The real-time property of that VLBI network even enables on-line monitoring of rapid flux density variations. Such monitoring is necessary to optimize observing schedules but is also useful to study source physics.

In the longer term the accuracy and precision of the ICRF will be improved with the goal of generating refined realizations for adoption by the IAU. The IVS will work together with the IERS and the IAU Working Group on Celestial Reference Systems in this matter. The current level of accuracy is ≈ 0.25 mas. A VLBI frame that is better by at least an order of magnitude is needed to match the projected precision of some planned astrometric satellite programs. To improve the current level requires reduction of systematic errors through better modeling and analysis as well as reduction of random errors through further observations of all ICRF sources. Routine non-CRF observing programs should allot a small portion of the time to cycling through the extended ICRF catalog. The ultimate accuracy of the VLBI reference frame may be set by variations in radio source structure or gravitational microlensing, so these effects require study by the IVS analysis centers and other researchers.

3.4. Geodynamical parameters

In the last decades VLBI has proved to be a very powerful technique for the determination of various geodynamical parameters. These are Love and Shida numbers used in the model of the solid Earth tides deformations, site-dependent amplitudes and phases of the ocean loading models, and site-dependent deformations due to atmospheric pressure variations (atmospheric loading). All the relevant parameters could be determined with an accuracy sufficiently high to detect and verify the particular effect (Schuh and Haas, 1998; Haas et al., 2001). However, the modelers also want to use the VLBI results to validate and possibly to improve their models. This is only possible if the present accuracies are increased by another factor of 5 to 50 and if the VLBI results are more reliable in terms of consistency and redundancy. Thus, it is highly recommended that the parameters described above are determined on a regular basis (e.g. once per year) and published as an IVS research product. The solutions should be carried out by several IVS analysis centers to increase the redundancy. As a mid-term goal for 2005 the individual results should be combined and be published as the "official" IVS product. Considering the hundreds of closely-spaced tidal terms which are contained in the models for solid Earth tides and for ocean loading, an unambiguous and uncorrelated determination will only be possible when almost continuous observations over 18.6 years are available. The problem gets even more difficult when complex Love numbers corresponding to anelasticity of the Earth's crust and latitude dependent Love numbers are to be derived. Again, continuous 18.6 years of VLBI observations are needed, by stations distributed all over the Earth.

3.5. Physical parameters

Lately, tropospheric and ionospheric parameters have been determined by IVS analysis centers not just within the standard EOP or TRF solutions but to specifically investigate the troposphere and/or ionosphere. As so far only preliminary results exist, that field could be clearly extended by further investigations. A need in this context is a continuous monitoring, i.e. 7 days per week, and the availability of the results with a very short time delay. Only then can the IVS results be useful for comparison with other space geodetic techniques and for meteorological purposes such as climate studies. The improvement in accuracy of the tropospheric and ionospheric parameters results indirectly from the goals set for the other IVS major products like EOP. Additional research in this area is necessary to study the degree of usefulness of such by-products.

There are other physical parameters which can be estimated from VLBI data, e.g. the so-called light deflection factor γ of the theory of general relativity. This parameter was determined for the Sun several years ago. Regular re-estimates are desirable as well as investigation of other relativistic effects. These and other activities should be organized under the umbrella of IVS. Thus, the IVS should be open for new observing sessions dedicated to special research tasks, e.g. for observing parameters of special or general relativity or for VLBI observation of spacecraft to investigate solar system dynamics.

4. Users of VLBI products

The users of VLBI products can be divided into different categories according to different IVS products (table 2):

Table 2: IVS products and their users

IVS products	users and their tasks
operational EOP	IERS Rapid Service and Prediction Product Center for predicting the EOP, other EOP prediction centers
EOP	IERS for generating final EOP series; individual users for precise positioning and navigation on Earth and in space (by interplanetary spacecrafts) and for geophysical studies
TRF	IERS for determination of ITRF, many users of ITRF which is a basis for almost all geodetic activities
TRF series	individual users for geodynamical studies
ICRF	geodesists, astronomers and astrophysicists, users in space research
source structure and other astrophysical parameters	astrophysicists
tropospheric and ionospheric parameters	meteorologists, climatologists and geodesists
geodynamical parameters	scientists in Earth dynamics and geophysics
relativistic parameters	physicists, scientists in cosmology and relativity

5. Measures to meet the goals for IVS products

Table 3 gives a short overview of the measures which should be taken within IVS to meet the goals defined in tables 1a,b,c. As most of the measures are related to the observing programs, these are the main focus for improving the current status of IVS products. Thus, new observing programs will be proposed in the next section.

Table 3: Measures to be taken in order to improve important criteria

Improvement of	Measures
accuracy	- technological improvement (higher data rates, digital Mk5 recording systems, …) - more precise models in data analysis - more observables taken by more stations with a stronger geometry (distribution of stations on the Earth and of sources in the sky) - surveying of local parameters at antennas - improvements in station performance (better reliability, improved sensitivity, faster slewing)
time delay from observing to products	- strict organization of observing programs (tape or disc transport, correlation ...) - broadband communication - acceleration of correlation procedure - acceleration and automation of data analysis
temporal continuity	- denser observing programs
temporal resolution	- observing programs (networks, schedules, …) - improve stochastic model of data analysis
redundancy	- data analysis by different analysis centers - data analysis using different software - more than one VLBI network in parallel
coverage of Earth by VLBI stations	- more stations on southern hemisphere, e.g. by use of mobile stations
coverage of sky by radio sources	- more sources, especially in the southern sky
regular releases of: ICRF and TRF, geodynamical parameters	- release official IVS products once per year with timeliness of one month
availability and distribution of: physical parameters (e.g. tropospheric and ionospheric mapping), source structure and other astrophysical parameters	- regular release as IVS products

6. Proposed observing programs

6.1. Overview of existing programs

IVS currently has no observing program of its own for the generation of IVS products; only existing observing programs have been used so far. The NEOS, CORE and INTENSIVE programs established and coordinated by USNO and/or NASA are the basis for observing the EOP. The same VLBI sessions are used for determining the TRF. Additional observing programs coordinated by other organizations, e.g. by FGS (German Research Group on Satellite Geodesy) and GSI (Japan), have been established for specific research purposes such as the EOP and/or the TRF. Only very few programs are dedicated to observing the CRF. Some extended programs have been organized by NASA for special R&D requirements. Only NEOS and INTENSIVE sessions are strictly organized to optimize timeliness, i.e. the time from observation to availability of final products is kept as short as possible.

The observing programs for the year 2001 (as of mid August) are summarized in table 4. A total of 968 observing days per year ("station days") are planned for 2001, approximately equivalent to 2.9 observing days per week for the typical network size of 6 stations; this does not include the INTENSIVE sessions. The table shows the type of program, the responsible Operation Center (OC) and Correlator (CO), and the average time delay for sessions already correlated. Table 5 lists the number of observing days for each Network Station (NS) in 2001, plans for 2002 and goals for several years in the future.

6.2. Requirements and recommendations for new observing programs

Now the question arises how the existing observing programs can be extended to match the goals defined in tables 1a,b,c. There are three main areas which need to be improved considerably within IVS:

1. accuracy of results (see 6.2.1),
2. time delay from observation to final product (see 6.2.2),
3. frequency of sessions in order to achieve a more continuous time series (see 6.2.3).

For the scientific requirements, the temporal resolution and the accuracy of the products have to be increased to be able to detect many of the effects mentioned in sections 3.1 and 3.2. Individual local information and local measurements such as permanent surveying of the shape of the antennas and in particular of motions of the VLBI reference point have to be provided additionally.

Requirements for extending and upgrading the existing IVS products are:

- improve the coverage of the week towards a continuous service,
- decrease time delay in order to improve timeliness,
- improve reliability of IVS products by independent checking,
- increase the accuracy and temporal resolution,
- develop networks that increase the accuracy of x_p up to the level of y_p.

Recommendations for updating existing programs and establishing new ones for the IVS are:

- combine the requirements of various users,
- include all techniques (Mk4/Mk5, K4 and S2),
- include R&D programs to explore and extend the full capacity of geodetic VLBI,
- improve global coverage of VLBI stations,
- include CRF observing programs,
- maintain continuity with the existing time series, mainly NEOS, INTENSIVE, and existing CORE,
- incorporate new VLBI technologies.

Table 4: Observing Programs for 2001, OC-Operation Center, CO-Correlator, NS-Network Station

Day of Week	Start UT	Dur hrs	Type	Purpose	OC	CO	Number/year	#NS	#station days days	Tapes/station	Time Delay days
Monday											
	8:00	24	SYOWA	TRF	JARE	Mitaka	5	3	15		90
	12:00	24	EUROPE	Vertical	Bonn	Bonn	2	8	16	1	60
	14:00	24	C-OHIG	TRF	Bonn	Bonn	2	5	10	1	60
	14:00	24	C-IRIS-S	EOP	Bonn	Bonn	12	6	72	1	60
	14:00	24	RDV	TRF/CRF	NASA	VLBA	6	20	120	3	45
	16:00	24	APSG	TRF	NASA	WACO	2	6	12	1	60
	17:30	24	CORE-1	EOP	NASA	Hays	12	6	72	2	100
	17:30	24	CORE-B	EOP	NASA	WACO	4	6	24	1	90
	17:30	24	CORE-C	EOP	NASA	WACO	7	6	42	1	90
	17:30	24	CONTM	EOP	NASA	WACO	2	6	12	1	80
	18:30	1	NEOS-INT	UT1	USNO	WACO	52	2	4.3		5
Total Monday 24h sessions				54	(some sessions are actually on Thursday)						
Tuesday											
	18:00	24	NEOS	EOP	USNO	WACO	52	6	312	1	17
	18:00	24	CONTM	EOP	NASA	WACO	1	6	6	1	80
Total Tuesday 24h sessions				53							
Wednesday											
	18:30	24	CONTM	EOP	NASA	WACO	2	6	12	1	80
	18:30	24	CRF	CRF	USNO	WACO	4	7	28	1	60
	18:30	24	CORE-3	EOP	NASA	Hays/Bonn	34	6	204	2	100
	18:30	1	NEOS-INT	UT1	USNO	WACO	52	2	4.3		5
Total Wednesday 24h sess.				40							
Thursday											
	19:00	24	SURVEY				2	3	6		90
	18:30	1	NEOS-INT	UT1	USNO	WACO	52	2	4.3		5
Total Thursday 24h sessions				1							
Friday											
	18:30	1	NEOS-INT	UT1	USNO	WACO	52	2	4.3		5
Total Friday 24h sessions				0							
Saturday, Sunday											
			no programs								
Total number of station days									**968**		
Total number of 24-hr sessions							**149**				
Total number of 1-hr sessions							**156**				
Avg days/week covered by 24-hr sessions							**2.9**				
Avg tapes/session										**1.3**	
Avg time delay											**60.0**

Table 5: Number of observing days for each network station

Geodetic Station Usage				
Station Name	Code	2001 Actual	2002 Plan	2005 Goal
Algonquin	Ap	64	76	208
Effelsberg	Ef	1	1	1
Fortaleza	Ft	79	79	208
Gilmore Creek	Gc	101	110	208
GGAO/MV3	Gg	3	4	4
HartRAO	Hh	59	52	108
Hobart	Ho	23	40	104
Kokee	Kk	101	104	208
Kashima	Ka	3		
Matera	Ma	37	104	208
Medicina	Mc	26	52	52
Ny Alesund	Ny	82	83	208
Noto	No	5	5	52
Onsala	On	24	26	52
O'Higgins	Oh	7	7	12
Seshan	Se	16	12	12
Simeiz	Sm	6	6	12
Syowa	Sy	7	6	6
TIGO	Ti	8	52	208
Tsukuba	Ts	32	32	208
Urumqi	Ur	6	6	12
Westford	Wf	72	72	72
Wettzell	Wz	112	112	208
Yebes	Yb	6	12	12
Yellowknife	Ye	13	13	12
DSS15	15	3	15	26
DSS45	45	6	15	26
DSS65	65	6	6	6
VLBA (10 antennas)	Va	60	60	60
Total		968	1162	2517

6.2.1. Accuracy of Results

Achieving the accuracies listed in the goals of table 1 can mainly be achieved through further technological improvements, e.g. by extending the observing program to higher data rates, and by improved operational reliability. Also the models used for data analysis can still be improved following the most recent scientific research in various fields such as solid Earth tides, atmospheric and ocean loading and tropospheric refraction. This can be complemented by incorporating local survey done at the antennas. Special efforts should be devoted to use more stations in each network and to design new networks to achieve the best possible EOP and TRF measurement accuracy. In particular, networks should be designed so that x_p and y_p results are of comparable accuracy. Station performance is critical to the accuracy of results, too. Stations should be encouraged to aim for the highest possible standards for high quality, reliable recorded data.

Special R&D sessions should be scheduled depending on scientific requirements and to further develop VLBI accuracy and time resolution. Following the extremely successful CONT94 and CONT96 sessions, such special CONT-type sessions should be carried out once or twice per year, if possible for a continuous 14 days to investigate the full capacity of geodetic VLBI. As many stations as could be correlated in one correlator pass (8-12) should participate and the highest standards of technical excellence must be used. Such special R&D sessions might be less critical with respect to timeliness.

The offsets and drifts between EOP series determined by different VLBI networks, demonstrated by the CORE-A/NEOS sessions, represent the current accuracy of results. Additional R&D sessions should be devoted to studies of the offset problem. To detect and remove the reasons for the problems described above partially concurrent observing sessions are proposed which overlap by a couple of hours. In addition, at least two identical stations should observe in successive networks.

6.2.2. Timeliness

As long as global transmission of observed data cannot be realized via the Internet, magnetic tapes or discs will have to be shipped between stations and correlators. One of the objectives of the IVS observing program is to set up a fast and routine procedure to ship the recorded media immediately after the sessions to the correlator. Assuming that shipping tapes will start instantly after each session, 1 or 2 days will be needed for transportation, 1 day for correlation and 1 day for data analysis and providing the products. This roughly means a minimum delay of at least 3 to 4 days, longer from stations that are not located near convenient transportation hubs.

Besides faster shipping of tapes to the correlator, we recommend that the correlators give priority to processing certain types of sessions, as is the current practice for the NEOS sessions. A second regular session should receive similar priority attention so that regular results will be available with a short time delay.

The research and development on broadband communication links for geodetic and astrometric VLBI should be strongly supported within IVS, as well as the development of a more rapid data analysis by faster processing and automation. Direct links between the components of a VLBI system (radio telescopes, correlators, analysis centers) would not only improve the data flow but is the only chance to considerably improve the timeliness of IVS products because it will allow the IVS to provide final products in near real-time. In May 1998 a forum on Real-Time VLBI was held at MIT Haystack Observatory (Proceedings ed. by J. Ray and A.R. Whitney, 1998) where the various aspects of direct broadband communication links were discussed. As the data transmission rates have increased significantly since 1998 with steadily decreasing costs, real-time VLBI seems to be feasible and affordable in the near future. The K4 system has demonstrated that reliable, sustained daily VLBI operations can be accomplished with minimal time delays of less than one day, if use is made of near real time data transmission, automated correlation procedures, and automated analysis.

The competitiveness of VLBI products would be significantly increased by contributing to such important tasks as:

- Support prediction of EOP by IERS Rapid Service and Prediction Product Center and other EOP prediction centers.
- Allow reaction to episodic events in near real-time (both geophysical phenomena on Earth and astrophysical phenomena on extragalactic sources).
- Support atmospheric and ionospheric investigations.
- Guarantee the availability of the results (in particular of rapid UT1-UTC) in case of emergency, e.g. if air traffic is stopped.

6.2.3. Frequency of Sessions

The justification for daily, continuous VLBI sessions was given in several sections of the report. The main arguments for continuous VLBI measurements are repeated here:

- Contribute to the proposed IAG project IGGOS that can only be realized by regular, if possible continuous, contributions of *all* space geodetic techniques; VLBI is essential as it plays a unique role (from those diurnal tidal terms that cannot be observed by GPS to short and long period nutation parameters).
- Provide a *permanent* comparison and control of results of other techniques, such as GPS, SLR, absolute gravity and ringlaser systems.
- Resolve the smaller tidal terms in solid Earth tides, ocean loading, and ocean tidal excitation of the EOP.
- Determine the amplitudes of the many short period nutation terms; this allows the investigation of the transfer functions, in particular how each term deviates from a mean frequency-dependent transfer function.
- Catch episodic events both on Earth and on extragalactic sources.
- Increase the accuracy of the results by increasing the number of observations.

Continuous VLBI sessions can only be achieved in gradual steps as we augment resources available for the observing programs. It is recommended that we carry on and extend the existing types of regular observing programs, such as CORE and NEOS, in order to maintain continuity with existing time series. As a next step we recommend establishment of a regular weekly 24-hour session in addition to the weekly NEOS. Also, a regular weekly or monthly session could be observed by including S2 and K4 components. In future years, Saturday and Sunday observations should be considered. This may be a staff and budget problem, but it should be considered nevertheless. We should support development of new technologies and control systems that will enable unattended observing.

A strong demand exists for INTENSIVE type experiments to determine UT1-UTC, one of the most important parameters provided by IVS due to the unique capability of VLBI. Daily INTENSIVE measurements with very small delay (3-4 days with tape recording and less than one day in case of broadband data transmission, see sub-section 6.2.2) would be desirable in order to provide reliable UT1 predictions and a high-frequency UT1 series for geophysical studies. As many days as possible should include a short-duration one-baseline session optimized for UT1 measurement. Additional independent observations on a second baseline would be highly desirable in order to provide independent control and robustness, i.e. if one session should fail there would be another available.

6.3. Resources

A realistic observing program requires careful balancing of available resources. Within the geodetic VLBI community there are three types of resources:

1. Station observing time,
2. Correlator capacity,
3. Recording media and data transmission facilities.

At various times in the past years, each of these types of resources has taken its turn as the least available resource. In recent years correlator time was in the shortest supply, but now the efficiency of the Mk4 correlators is improving rapidly, and the observing programs will probably be limited by availability of tapes in 2002. If we improve the tape shipping procedures, and if the correlator efficiency continues to improve, we may be limited by availability of station observing days by 2003. The estimated resources that will be available for the next few years are shown in table 6.

The most-used stations observe up to two or three 24-hour sessions per week on average; many stations observe only once per month. A continuous program of 6-station networks will require 2190 station days per year, more than double the current resource availability. For 8-station networks, nearly 3000 station days are required annually. Besides additional observing burdens in sheer numbers, continuous observing also means that stations will be observing on weekends.

It is anticipated that the efficiency of the Mk4 correlators will continue to increase, doubling their 2001 efficiency so that by 2005 they can process one day of observing in one day of correlator time: a processing factor of one. The correlator capacity is shown in the table as the number of sessions that can be processed, taking into account the expected Mk4 processing factors. The calculations assume that the number of supported correlator operational days for each of the three Mk4 correlators remains the same throughout the period (Haystack 50, Washington 200, and Bonn 110 days). The anticipated availability of the S2 and K4 correlators is shown as increasing over the next years.

The number of required tapes depends on the recording technology (Mk4, S2, or K4), the recording data rate, and on the average time delay between observing and export of data from the correlator. Each recording technology uses a different type of tape. The Mk4 tapes are 1-in wide and loaded on 14-in glass reels; tape capacity is ≈ 4.7 Tb. At a recording rate of 128 or 256 Mb/s one station uses typically two tapes in a 24-hr session. There are 468 Mk4 tapes in the geodesy pool; no further purchases are planned because of the imminent deployment of the disc-based Mk5 recording systems. S2 tapes are standard VCR tapes and are counted in “boxes” of eight cassettes each. The capacity of one box is ≈ 1.8 Tb; a station uses 3-4 boxes for a 24-hr session recorded at 128

Table 6: Estimated resource availability for the years 2000-2005

		2000	2001	2002	2003	2004	2005
Observing Time (station days)							
		834	968	1162	1500	1800	2517
Correlator Capacity (sessions)							
	Mk4	103	144	171	180	180	180
	S2			12	26	52	52
	K4				12	12	12
	VLBA	6	6	6	6	6	6
	Total	109	150	189	224	250	250
Recording media (equivalent Mk4 tapes)							
	Mk4	363	468	468	468	468	468
	S2			75	100	200	200
	K4				50	50	50
	Mk5			50	100	200	200
	Total	363	468	593	718	918	918

Mb/s. Requirements for S2 tapes are expected to be met from the existing Space-VLBI/geodesy supply. K4 tapes are D1 type cassettes used in the commercial VCR business. One tape has a capacity of ≈ 0.6 Tb, and typically a station uses 6-7 tapes of the size usually used for VLBI in a 24-hr 64 Mb/s session. Additional K4 tapes would need to be purchased to support a monthly K4 network session. The Mk5 will record on a set of 16 100-GB discs for a capacity of ≈ 12.8 Tb per set. One set of discs per station will be needed for a 256 Mb/s 24-hr session. The numbers of recording media in table 6 are shown in equivalent Mk4 tape capacity, so that the totals can be used in table 7.

6.4. Proposed IVS observing programs for 2002-2005

IVS as a service needs to carry out regular programs, in order to deliver its products as reliably and precisely as possible with respect to the available resources. Special R&D programs will have to be scheduled, too, to support scientific research and improvement of the VLBI technique.

Table 7 outlines a proposed IVS observing program for the years 2002-2005, including 2001 as a reference point. Each section of the table shows one year's program in columns giving the type of session, number of stations, number of sessions, number of tapes, and time delay in days. At the bottom various statistics and totals show the resource usage (station days, correlator time, tapes), estimated resource availability for that year (from table 6), and resource shortfall (or excess, shown as negative numbers). The table shows 24-hr sessions, short INTENSIVE-type sessions, and R&D sessions. The IVS Coordinating Center will implement the details of the program, table 7 gives the outline and overview.

Highlights of the proposal for each year are:

- 2002: The proposed program moves the current NEOS session from Tuesday to Monday with the new name IVS-R1, and adds a second weekly rapid-turnaround session on Thursday

Proposed IVS Observing Program

	2001					2002					2003					2004					2005				
	Type	# stn	# sess	tap	delay	Type	# stn	# sess	tap	delay	Type	# stn	# sess	tap	delay	Type	# stn	# sess	tap	delay	Type	# stn	# sess	tap	delay
Monday																									
	CORE-1	6	12	38	90	IVS-R1	6	52	88	15	IVS-R1	8	52	87	10	IVS-R1	8	52	89	10	IVS-R1	8	52	94	10
	C-IRIS-S	7	12	35	60																				
	INT	2			5																				
	Other	6	30	100	100																				
Tuesday						Other	6	18	54	60	Other	6	12	35	60										
						IVS-INT1	2			5	IVS-INT1	2			5	IVS-INT1	2			5	IVS-INT1	2			5
	NEOS	6	52	81	17	IVS-T2	7	12	42	60	IVS-T2	7	0	0	30	IVS-T2	7	26	64	30	IVS-T2	8	52	129	20
Wednesday											Science	8	12	46	60	Science	8	12	53	60	Science	8	12	61	60
	CORE-3	6	34	114	100	R&D	8	12	48	60	R&D	8	26	66	30	R&D	8	26	73	30	R&D	8	26	64	20
						IVS-E3	8	12	34	30	IVS-E3	8	26	66	30	IVS-E3	8	26	73	30	IVS-E3	8	26	64	20
	INT	2			5	IVS-INT1	2			5	IVS-INT1	2			5	IVS-INT1	2			5	IVS-INT1	2			5
	Other	6	8	27	100	CONT02	8	15	216	90	CONT03	8	15	240	60	CONT04	8	12	53	60	R&D	8	12	61	60
Thursday						IVS-CRF	6	4	12	60	IVS-CRF	6	4	12	60	IVS-CRF	6	4	12	60	IVS-CRF	6	4	12	60
	CRF	6	4	13	90	IVS-INT1	2			5	IVS-INT1	2			5	IVS-INT1	2			5	IVS-INT1	2			5
	RDV	10	6		45	RDV	10	6		45	RDV	10	6		45	RDV	10	6		45	RDV	10	6		45
	INT	2			5	IVS-R4	6	52	88	15	IVS-R4	8	52	87	10	IVS-R4	8	52	89	10	IVS-R4	8	52	94	10
Friday						IVS-INT1	2			5	IVS-INT1	2			5	IVS-INT1	2			5	IVS-INT1	2			5
						IVS-INT2	2			5	IVS-INT2	2			5	IVS-C5	6	26	55	30	IVS-C5	8	52	129	20
Saturday																									
																IVS-C6	6	26	48	20	IVS-C6	8	52	129	20
Sunday																									
											IVS-C7	6	26	50	30	IVS-C7	6	52	109	30	IVS-C7	8	52	129	20

	2001	2002	2003	2004	2005
Days/ week observed:	3.0	3.5	4.4	6.2	7.7
Average Session Parameters (fixed)					
avg ship to stn (weeks):	8	6	4	3	2.5
avg tapes/session:	1.3	1.8	2	2.5	3
Resource usage					
sessions to be correlated:	158	183	231	320	398
station days used:	984	1212	1776	1862	3188
recording media:	407	583	689	718	966
Resource availability					
correlatable sessions:	150	215	270	310	430
station days:	968	1162	1500	1800	2313
recording media:	468	468	468	500	500
Resource shortfall					
correlator:	8	-32	-39	10	-32
station days:	16	50	276	62	875
recording media:	-61	115	221	218	466

named IVS-R4. This provides continuity with the current NEOS and concentrates resources currently used for CORE sessions into a second weekly session. (The R in the name stands for Rapid.) The monthly IVS-E3 will emphasize EOP and will use S2-technology. A 14-day continuous session named CONT02 is proposed. A monthly R&D session should be used for technique improvement studies. The RDV (Research and Development VLBA) sessions would continue to serve as the main source of data for the CRF; other CRF sessions are proposed for observing southern sources not visible to the VLBA. The "other", mainly regional, sessions continue. The IRIS-S sessions are renamed IVS-T2 for TRF emphasis. INTENSIVE sessions would be on Tuesday, Wednesday, Thursday and Friday and at least one of these days would have a second independent session for robustness and independent control, e.g. by K4. Real-time data transfer for the INTENSIVES should be investigated. Testing and initial deployment of Mk5 units should be carefully coordinated.

- 2003: The two rapid-turnaround sessions are increased to 8 stations. A weekend day observing is added on a bi-weekly basis. It will probably take at least all of year 2002 to figure out how to support weekend observing. A monthly session is available for proposal-based scientific experiments. Deployment of additional Mk5 units should be done this year.
- 2004: The first weekend day is made weekly this year, and a second bi-weekly session on the weekend is added.
- 2005: This year shows the full 7-day observing program. There are serious shortfalls in resource usage of stations days, correlator time, and tapes. This program may not be realistic unless we can find significant new resources, but it is shown for completeness. It is possible that some real-time facilities for data transmission might be in place by this time, but it is difficult to estimate either the time scale or resources needed.

7. Recommendations

It is recommended that IVS components devote the resources necessary to accomplish the observing program proposed in the previous section, with special emphasis on the following points:

- Network stations should commit to shipping tapes more efficiently to the correlators so that the time delays in the plan can be accomplished. The correlators should commit to assign priority to certain sessions.
- It is strongly recommended for the success of the proposed plan that initially the S2 correlator support one day per month of observations, rising to one day per week in the future. Likewise, it is strongly recommended that the K4 correlator support one INTENSIVE observing session per week, with more days coming in the future.
- Unattended operations should be considered by each Network Station during 2002 so that weekend observing by a network can begin in 2003.
- Some R&D sessions should be devoted to studying the network offset problem.
- The 14-day R&D continuous sessions will require additional station resources and planning for the high tape usage.
- The CRF and RDV sessions should be used to expand the source catalog used for regular geodetic sessions. Inclusion of new, weaker sources will fill in gaps in sky coverage and facilitate better schedules.

- A vigorous R&D program should be part of every year's observing program to study methods for technique improvement, identify and eliminate instrumental effects, and study other systematic error sources.

Recommendations concerning the VLBI data analysis within IVS:

- Increase the EOP time resolution to 1h in 2002 with a goal of 10min in 2005.
- Determine EOP rates as another IVS product.
- Establish a combined TRF solution (time series or global solution of station positions and velocities) as an IVS product on a regular basis.
- Encourage additional CRF solutions for detailed comparison.
- Investigate the idea of a combined ICRF solution.
- Continue investigation of temporal variations of source positions and of monitoring source structures and encourage investigation of source structure delay corrections.
- Determine regularly geodynamical parameters such as solid Earth tides Love numbers and oceanic and atmospheric loading coefficients with clearly increased accuracy to be published as IVS research products.
- Continue investigation of tropospheric parameters and ionospheric mapping by VLBI.
- Incorporate local surveying results done at the antennas.
- Encourage development of partially automated data analysis.
- Encourage data analysis by more analysis centers using different software packages.
- Improve models used for data analysis wherever possible.

Recommendations on technological upgrades and developments:

- All stations that are Mk3 should be upgraded to Mk4 capability as soon as possible so that they can participate in higher data rate sessions and use Mk4 recording modes.
- Deployment of geodetic S2 and K4 systems at more stations is encouraged so that good geodetic networks can be designed that use these systems and be integrated into the international geodetic observing program.
- Additional media equivalent to the capacity of at least 100 Mk4 tapes will be necessary to carry IVS through the proposed program.
- Improved technologies should be strongly pursued because higher data rates, advanced data transmission techniques, and automated observing and processing methods lead to increased accuracy, timeliness, reliability, and efficient use of resources.

Recommendations concerning IVS organization:

- IVS should establish and publicize procedures for submitting and reviewing proposals with R&D, technique improvement, technique validation, and/or scientific goals.
- IVS should establish a permanent Program Committee (PC) to advise the Coordinating Center in implementing the observing program. The PC would review proposals, discuss and recommend the observing program, and carry out policies related to the observing program as determined by the Directing Board.

8. Conclusions

Geodetic VLBI plays an essential role in geodesy and astrometry due to its uniqueness in observing UT1-UTC and the precession/nutation angles unbiased over a time span longer than a few days. It is also needed for the establishment of the ICRF and contributes extensively to the generation of the ITRF. The report shows that due to various requirements of the different users of IVS products the following aspects must be accomplished:

- significant improvement of the accuracy of VLBI products,
- shorter time delay from observation to availability of results,
- almost continuous temporal coverage by VLBI sessions.

A first scenario of the IVS observing program for 2002 and 2003 considers an increase of observing time by about 30%-40% and includes sessions carried out by S2 and K4 technology. The midterm observing program for the next 4-5 years seems to be rather ambitious, although it is feasible if all efforts are concentrated and the necessary resources become available.

9. References

Beutler, G. et al., 2001: The IAG-REVIEW 2000-2001 Executive Summary. Presented at the IAG Scientific Assembly, Budapest, 2.-6. September 2001.

Cannon, W.: Comments on VLBI as a Fundamental Geodetic Positioning Technique and IVS Combined VLBI Products. http://giub.geod.uni-bonn.de/vlbi/IVS-AC/divers/cannon.html , 2001.

Chao, B.F.: Global science enabled by Earth rotation observations, document vlbicore.doc at http://ivscc.gsfc.nasa.gov/mhonarc/core-panel/msg00030.html , 2001.

Charlot, P. et al.: A proposed astrometric observing program for densifying the ICRF in the northern hemisphere. IVS 2000 General Meeting Proceedings, ed. by N.R. Vandenberg and K.D. Baver, NASA/CP-2000-209893, 168-172, 2000.

Dehant, V. et al.: Considerations Concerning the Non-Rigid Earth Nutation Theory. Celestial Mechanics and Dynamical Astronomy, No. 72, 245-310, 1999.

Gross, R.S.: Accuracy of VLBI and GPS Polar Motion Measurements, http://ivscc.gsfc.nasa.gov/-mhonarc/core-panel/msg00038.html , 2001.

Haas et al. : Report of the IAG/ETC/WG6/1 (VLBI). Bulletin Marées Terrestres, No. 134, Observatoire Royal de Belgique, Brussels (in press) 2001.

IAU resolutions : International Astronomical Union Information Bulletin, No. 88, 15-22, http://-www.iau.org/IAU/Activities/publications/bulletin/, 2000.

Keystone Project: http://ksp.crl.go.jp/

Koyama, Y., T. Kondo, and N. Kurihara: Microwave flux density variations of compact radio sources monitored by real-time very long baseline interferometry. Radio Science, Vol. 31, No. 2, 223-235, 2001.

Mathews, P.M., T.A. Herring, and B.A. Buffett. Modeling of nutation-precession: new nutation series for non-rigid Earth, and insights into the Earth's interior. JGR, in press, 2001.

Real-Time VLBI Forum: Proceedings of a Discussion held at MIT Haystack Observatory, 3. May 1998, ed. by J. Ray and A.R. Whitney, 1998.

Rummel, R., H. Drewes, and G. Beutler: Integrated Global Geodetic Observing System (IGGOS): A Candidate IAG Project. Presented at the IAG Scientific Assembly, Budapest, 2.-6. September 2001.

Schuh, H. and R. Haas: Earth Tides in VLBI Observations. 13th International Symposium on Earth Tides. ed. by B. Ducarme and P. Paquet, Observatoire Royal de Belgique, Série Géophysique, 111-120, 1998.

Acknowledgements

The authors want to express their thanks to James Campbell, Rüdiger Haas, Veronique Dehant and all other colleagues who have actively contributed to the report.

Affiliations of the members of IVS Working Group 2

Harald Schuh (chairman)
Institute of Geodesy and Geophysics
Vienna University of Technology
Gusshausstr. 27-29
A-1040 Wien
Austria

Patrick Charlot
Observatoire de Bordeaux
CNRS/UMR 5804
2 Avenue de l'Observatoire, BP 89
33270 Floirac
France

Hayo Hase
Bundesamt für Kartographie und Geodäsie
Fundamentalstation Wettzell
Sackenrieder Str. 25
D-93444 Kötzting
Germany

Ed Himwich
NVI, Inc./Goddard Space Flight Center
Code 920.1
Greenbelt, MD 20771
USA

Kerry Kingham
U. S. Naval Observatory
EO Department
3450 Massachusetts Ave.
Washington, D.C. 20392-5420
USA

Calvin Klatt
Geodetic Survey Division, Natural Resources Canada
615 Booth Street
Ottawa, Ontario
Canada

Chopo Ma
NASA Goddard Space Flight Center
Code 926
Greenbelt, MD 20771
USA

Zinovy Malkin
Institute of Applied Astronomy
nab. Kutuzova, 10
St. Petersburg, 191187
Russia

Arthur Niell
MIT Haystack Observatory
Westford, MA 01886
USA

Axel Nothnagel
Geodetic Institute of the University of Bonn
Nussallee 17
D-53115 Bonn
Germany

Wolfgang Schlüter
Bundesamt für Kartographie und Geodäsie
Fundamentalstation Wettzell
Sackenrieder Str. 25
D-93444 Kötzting
Germany

Kazuhiro Takashima
Geographical Survey Institute
Kitasato-1
Tsukuba-Shi
Ibaraki-Ken, 305-0811
Japan

Nancy Vandenberg
NVI, Inc./Goddard Space Flight Center
Code 920.1
Greenbelt, MD 20771
USA

Annex

List of Participants

Programme

Participants of the 15th European VLBI Meeting, Proceedings of the 15th Working Meeting on European VLBI for Geodesy and Astrometry, p.251–251
http://www.ieec.fcr.es/hosted/15wmevga/proceedings/participants

Participants of the 15th European VLBI Meeting

Name	Institution	Country	E-mail
Alef, Walter	MPIfR Bonn	Germany	walef@mpifr-bonn.mpg.de
Behrend, Dirk	IEEC Barcelona	Spain	behrend@ieec.fcr.es
Böhm, Johannes	TU Vienna	Austria	jboehm@luna.tuwien.ac.at
Campbell, Bob	JIVE Dwingeloo	Netherlands	campbell@jive.nl
Campbell, James	Univ Bonn	Germany	campbell@sn-geod-1.geod.uni-bonn.de
Charlot, Patrick	Obs de Bordeaux	France	charlot@observ.u-bordeaux.fr
Colomer, Francisco	OAN Yebes	Spain	colomer@oan.es
Gerald, Engelhardt	BKG Leipzig	Germany	engelhardt@leipzig.ifag.de
García-Miró, Cristina	MDSCC Robledo	Spain	cgmiro@lrid.mdscc.nasa.gov
Gueguen, Erwan	ITIS-CNR	Italy	gueguen@itis.mt.cnr.it
Haas, Rüdiger	Onsala Space Obs	Sweden	haas@oso.chalmers.se
Himwich, Ed	NVI/GSFC	USA	weh@ivscc.gsfc.nasa.gov
Kingham, Kerry	U.S.N.O.	USA	kak@cygx3.usno.navy.mil
Koyama, Yasuhiro	CRL Kashima	Japan	koyama@crl.go.jp
Lanotte, Roberto	ASI/Telespazio	Italy	roberto.lanotte@asi.it
Ma, Chopo	GSFC	USA	cma@virgo.gsfc.nasa.gov
Mantovani, Franco	IRA-CNR	Italy	fmantova@ira.bo.cnr.it
Matsuzaka, Shigeru	Geograph Surv Inst	Japan	shigeru@gsi-mc.go.jp
Müskens, Arno	MPIfR Bonn	Germany	mueskens@mpifr-bonn.mpg.de
Niell, Arthur	MIT Haystack Obs	USA	aniell@haystack.mit.edu
Nothnagel, Axel	Univ Bonn	Germany	nothnagel@uni-bonn.de
Plag, Hans-Peter	NMA	Norway	plag@statkart.no
Porcas, Richard	MPIfR Bonn	Germany	porcas@mpifr-bonn.mpg.de
Ribó, Marc	Univ Barcelona	Spain	mribo@am.ub.es
Rioja, María	OAN Yebes	Spain	rioja@oan.es
Rius, Antonio	IEEC/CSIC	Spain	rius@ieec.fcr.es
Ros, Eduardo	MPIfR Bonn	Germany	ros@mpifr-bonn.mpg.de
Sarti, Pierguido	ITIS-CNR	Italy	pierguido.sarti@itis.mt.cnr.it
Schlüter, Wolfgang	BKG-FS Wettzell	Germany	schlueter@wettzell.ifag.de
Schuh, Harald	TU Vienna	Austria	hschuh@luna.tuwien.ac.at
Schwegmann, Wolfgang	Univ Bonn	Germany	schwegma@chagall.geod.uni-bonn.de
Sorgente, Mauro	IRA-CNR	Italy	msorgente@hotmail.com
Sovers, Ojars	RSA Systems/JPL	USA	ojars@rsasys.com
Tesmer, Volkmer	DGFI Munich	Germany	tesmer@dgfi.badw-muenchen.de
Thorandt, Volkmar	BKG Leipzig	Germany	vt@leipzig.ifag.de
Tomasi, Paolo	IRA-CNR	Italy	tomasi@ira.bo.cnr.it
Vandenberg, Nancy	NSV/GSFC	USA	nrv@gemini.gsfc.nasa.gov
Walter, Hans-Georg	ARI Heidelberg	Germany	walter@ari.uni-heidelberg.de
Whitney, Alan	MIT Haystack Obs	USA	awhitney@haystack.mit.edu
Zeitlhöfler, Reinhard	TU Munich	Germany	zeitlhoefler@wettzell.ifag.de

Programme of the 15th European VLBI Meeting, Proceedings of the 15th Working Meeting on European VLBI for Geodesy and Astrometry, p.252–255
http://www.ieec.fcr.es/hosted/15wmevga/proceedings/programme

Programme of the 15th European VLBI Meeting

Friday, 7th September 2001

Session 1: IVS and Facility Reports

Chair: James Campbell

09:00–09:30	Welcome addresses
09:30–09:50	H. SCHUH IVS working group 2 for product specification and observing programs – status report of the chairman
09:50–10:00	C. STEINFORTH, A. NOTHNAGEL Combination of VLBI EOP within the IVS
10:00–10:10	V. THORANDT, D. ULLRICH, R. WOJDZIAK, G. ENGELHARDT Technological processes at BKG data and analysis center
10:10–10:25	G. ENGELHARDT, V. THORANDT, D. ULLRICH The current status of the IVS analysis center at BKG
10:25–10:35	C. GARCIA-MIRO, J. GOMEZ, D. BEHREND, A. RIUS, A. ALBERDI, E. JIMENEZ BAILON, I. DE GREGORIO MONSALO Radio astronomy at the NASA Madrid deep space communications complex: status report
10:35–10:40	R. PORCAS Effelsberg station report
10:40–10:50	F. COLOMER Activities of the IGN/OAN at Yebes
10:50–10:55	G. COLUCCI, R. LANOTTE Operational VLBI activities at Matera
10:55–11:25	**COFFEE BREAK**
11:25–11:40	B. CAMPBELL Status report on the EVN MkIV data processor at JIVE
11:40–11:50	W. ALEF MPIfR/BKG correlator report
11:50–12:00	A. MUESKENS Improvements of the Geodesy MK4 correlation progress in the last year

Session 2: Data Analysis and New Developments

Chair: Harald Schuh

12:00–12:20	A. NOTHNAGEL, O. BROMORZKI, J. CAMPBELL, A. MUESKENS, H. ROTTMANN, I. ROTTMANN Comparisons of Mark III and Mark IV correlation results
12:20–12:40	J. CAMPBELL, B. RICHTER Towards a stable European vertical velocity reference system using VLBI, GPS and absolute gravity measurements
12:40–13:00	W. SCHWEGMANN Automatic VLBI data analysis using CALC/Solve and a knowledge-based system
13:00–15:00	**LUNCH BREAK**
15:00–15:20	V. TESMER, H. KUTTERER, H. SCHUH, H. SCHMITZ-HUEBSCH, B. RICHTER Reassessment of the quality of Earth orientation parameters with high resolution determined by VLBI
15:20–15:40	Y. KOYAMA, T. KONDO, J. NAKAJIMA, M. SEKIDO, M. KIMURA Internet VLBI system and 1 Gbps VLBI system based on the VSI
15:40–16:00	E. GUEGUEN, P. TOMASI, H.-G. SCHERNECK, R. HAAS, J. CAMPBELL Recent crustal movements: geological meaning of European geodetic VLBI network observations
16:00–16:20	M. BOS, R. HAAS Observing the long period tides in gravity and VLBI observations on Ny-Alesund, Spitsbergen
16:20–16:50	**COFFEE BREAK**

Session 3: Atmospheric Modelling
Chair: Antonio Rius

16:50–17:10	A. NIELL An apriori hydrostatic gradient model
17:10–17:30	A. NOTHNAGEL On the effect of solution types on atmospheric zenith path delay results
17:30–17:50	J. BOEHM, H. SCHUH Spherical harmonics as a supplement to global tropospheric mapping functions and horizontal gradients
17:50–18:10	M.J. RIOJA, P. TOMASI Combined geodetic techniques
20:30–23:00	**WORKSHOP DINNER**

Saturday, 8th September 2001

Session 4: Local Surveys
Chair: Paolo Tomasi

09:00–09:20	L. VITTUARI, P. SARTI, P. TOMASI 2001 GPS and classical survey at Medicina obsevatory: local tie and VLBI antenna's reference point determination
09:20–09:40	A. NOTHNAGEL, C. STEINFORTH, B. BINNENBRUCK, L. GRIMSTVEIT, L. BOCKMANN Results of the 2000 Ny-Alesund Local Survey
09:40–09:50	R. HAAS, M. KIRCHNER The spring 2001 footprint measurements at the Onsala Space Observatory

Session 5: Reference Frames and Astrometric Results
Chair: Paolo Tomasi

09:50–10:10	C. MA Extension of the ICRF
10:10–10:30	P. CHARLOT ITRF2000 positions of non-geodetic telescopes in the European VLBI network
10:30–10:50	R. PORCAS Finding phase and astrometric reference sources using the NVSS survey
10:50–11:10	E. ROS, A.P. LOBANOV Phase-referencing and opacity in the jet of 3C309.1

11:10–11:40 **COFFEE BREAK**

Closing Session
Chairs: James Campbell and Antonio Rius

11:40–13:00 General discussion

13:00 **OFFICIAL END OF MEETING**

Contributions without Presentation

Session 1: IVS and Facility Reports

H. HASE:
Status of the TIGO-Project in Concepción

Z. MALKIN:
On computation of combined IVS EOP series

Session 2: Data Analysis and New Developments

Z. MALKIN, N. PANAFIDINA, E. SKURIKHINA:
Length variations of European baselines derived from VLBI and GPS observations

E. SKURIKHINA:
On computation of antenna thermal deformation in VLBI data processing

Session 3: Atmospheric Modelling

A.A. STOTSKII, I.M. STOTSKAYA:
Structure analysis of wet path delays in IRIS-S experiments